AN EXAMINATION OF THE TOXICITY AND INFLAMMATORY POTENTIAL OF MULTI-WALLED CARBON NANOTUBES *IN VITRO* AND *IN VIVO*

KARL ALEXANDER STERNAD

A thesis submitted in fulfilment of the requirements of the degree of Doctor of philosophy awarded by the University of Edinburgh

Centre for inflammation research
University of Edinburgh
2010

To study a subject best, understand it thoroughly before you start.
Anon.

I hereby declare that this thesis was written by me and that all of the work contained therein was performed by me except where otherwise indicated.

Karl Alexander Sternad

This thesis is dedicated to my parents without whose encouragement it might not have been started and to Jennifer, without whom it might not have been finished.

Acknowledgements

The author wishes to thank a number of individuals for their time, contributions and advice given generously during the researching and writing of this project. In particular I am indebted to my advisor, Professor Ken Donaldson for his time, patience, expertise, and guidance throughout this work, also Dr. Roger Duffin for his patience, contributions and support and technical expertise, I would to thank Craig A. Poland for his contributions and generous help (in particular for assistance with S.E.M and T.E.M. and *in vivo* work) and advice and Irene McGuinness for her help and support. I wish to acknowledge the generous technical assistance of Shonna Johnston with confocal microscopy, Danny McClure with Electron spin resonance and Steve Clark (of the institute of occupational medicine) with scanning electron microscopy. I would also like to thank Dr. Ellen Drost for her support and advice. I wish to thank the institute of occupational medicine for the use of the scanning electron microscope and their gift of asbestos samples used during this work. In addition I wish to gratefully acknowledge the University of Edinburgh centre for cardiovascular science for use of the electron spin resonance spectrometer. The generous gift of ultrafine carbon (Printex 90) black from Napier University, Edinburgh is gratefully acknowledged. This work was supported by the University of Edinburgh/MRC.

Abstract

The rise of nanotechnology industries has led to the design and production of new nano-scaled materials such as quantum dots, nano-metals, carbon nanotubes, fullerenes and a myriad of functionalised derivatives. Extensive work concerning well characterised pathogenic fibres has led to the development of a fibre paradigm that suggests respirable fibres vary in their ability to cause disease based on length and pulmonary bio-persistence. Induction of oxidative stress is also a central plank of the mechanism used to explain inflammatory, fibrotic and carcinogenic effects of fibres. The toxicity of different particle types has consistently been shown to depend upon particle size and surface area, reactive surface molecular groups, metal content, organic content and the presence of endotoxins. A growing body of work has begun to examine the potential pathogenicity of carbon nanotubes to the pulmonary system as a consequence of superficial similarities to known pathogenic particle and fibres. The aim of this thesis was to investigate the potential toxicity of two commercially manufactured multi-walled carbon nanotubes (MWCNT) compared to a panel of low and high toxicity particles and fibres. The pro-inflammatory nature of MWCNT was examined *in vitro* and *in vivo* to determine the effects they may exert in the pulmonary system.

In aqueous solutions of phosphate buffered saline, saline and cell culture medium (with or without foetal calf serum supplementation) MWCNT were found to exist as tight aggregates even after sonication. Analysis of metal content of MWCNT by ICP-AES revealed the presence of a low percentage of non extractable residual iron. From analysis of MWCNT by electron spin resonance (ESR) the CNT were found to be ready producers of a free radical species, despite this MWCNT were not able to cleave plasmid DNA. Upon incubation with the alveolar epithelial cell line A549 MWCNTs did not cause noticeable toxicity but did dose dependently deplete total glutathione levels. No increase in production of the pro-inflammatory cytokine IL-8 could be detected at the level of protein or at the level of mRNA. Analysis of the levels (protein and mRNA) of the pro-fibrotic mediator TGF-β did not indicate induction of a fibrotic response to MWCNT. Neither were MWCNTs found to consistently activate the pro-inflammatory associated transcription factor nuclear factor kappa B (NF-κB). Upon instillation into the peritoneal cavity of mice MWCNT failed to induce a pro-inflammatory response in contrast to long amosite asbestos that induced an extensive inflammatory reaction. Analysis of the diaphragms of exposed animals revealed the induction by MWCNT of an apparent foreign body type reaction.

Overall with limited processing and dispersion MWCNT were morphologically more akin to particles than fibres. Although apparently able to spontaneously generate ROS in aqueous solution this did not translate into a capacity to cause toxicity or a capacity to induce inflammation either *in vitro* or *in vivo*.

Summary and Aims

The structure and function of the pulmonary system renders it vulnerable to insult by a growing body engineered particles and fibres whose dimensions are ever decreasing. The pathogenicity of particles and fibres has been investigated resulting in the view that a combination of physical characteristics (e.g. size and surface area), chemical characteristics (reactive surface functional groups and numbers of atoms at the surface) and associated transition metals and organic compounds explain the cellular and tissue damage observed in biological systems in response to certain materials. Carbon nanotubes are one of a growing number of new materials; their superficial resemblance to known pathogenic fibres such as asbestos combined with their meeting the criteria for many pathogenic particles has prompted increasing concerns. This is compounded by a general ignorance about the properties and chemistry of CNT and how this is dictated by their nano dimensions. Although there is a growing community probing the potential toxicity of CNT there is little agreement as to its level, the mechanisms involved or the materials characteristics that may be responsible. One commonality has been the presence of metals associated with, and defects in the structure of CNT that may lead to the generation of free radicals. Based on work with better characterised pathogenic particles a role for free radical generation, oxidative stress and activation of oxidative stress responsive pathways such as NF-κB have been investigated as potential mechanisms through which CNT may exert damaging effects.

This thesis focuses on an investigation of the intrinsic free radical generating potential of MWCNT, their ability to induce oxidative stress and their pro-inflammatory effects *in vitro* and *in vivo*. Particles are known to interact with

pulmonary epithelial cells and stimulate them to initiate inflammatory responses; as a result most of the work reported here was carried out using an alveolar type II epithelial cell line – A549. For assessing the effects of MWCNT *in vivo* the peritoneal cavity of mice was chosen, this region has been found to have a particular sensitivity to long fibres. This *in vivo* model was thus deemed particularly useful for determining whether MWCNT without application of significant dispersive techniques would behave as a fibre or particle and the level of inflammation it would induce compared to known pathogenic fibres.

The aims of this work were to investigate the toxicity of two MWCNT differing from each other only in their lengths in a relatively un-adulterated state without use of harsh dispersive techniques compared with known pathogenic and non-pathogenic particles. Also, to investigate how a nominally fibrous material that was morphologically more particulate in nature would interact with biological systems to gain an understanding of the comparative level of pathogenicity MWCNT.

ALI	Acute lung injury
AM	Alveolar Macrophage
ANOVA	Analysis of variance
AP-1	Activator protein 1
ARE	Antioxidant response element
AT I/II	Alveolar epithelial type I/type II cell
ATP	Adenosine triphosphate
BAL	Bronchiolar alveolar lavage
BALF	Bronchiolar alveolar lavage fluid
BSA	Bovine serum albumin
C_{60}	Buckminster Fullerene
Ca^{2+}	Calcium
cAMP	Cyclic adenosine mono phosphate
CB	Carbon black
cDNA	Complementary deoxyribose nucleic acid
CHO	Chinese hamster overy cells
CNT	Carbon nanotube
Co	Cobalt
Cr	Chromium
CVD	Catalytic/Chemical vapour deposition
Cu	Copper
Cu, Zn SOD	Copper, Zinc superoxide dismutase
DCF	2',7' dichlorofluorescein
DCFH-DA	dichlorohydrofluorescein diacetate
DEP	Diesel exhaust particle
DEPC	Diethyl procarbonate
DMEM	Dulbecco's modified eagle medium
DMSO	Dimethyl sulfoxide
DMTU	Dimethyl urea
DNA	Deoxyribonucleic acid
dNTP/s	Di-nucleotide triphosphate/s
DPPC	Dipalmitoyl Phophatidylcholine
DQ12	Quartz - Dioxosilane (O_2Si)
DWCNT	Double wall carbon nanotube
e-	eletron
EAD	Eletric arc discharge
ECM	Extra-cellular matrix
EC-SOD	Extra-cellular superoxide dismutase
EDTA	Ethylene diamine tetra acetic acid
EGF	Epidermal growth factor
EGFR	Epidermal growth factor receptor
ELF	Epithelial lining fluid
ELISA	Enzyme linked immunosorbant assay
EPR	Electron paramagnetic resonance
ERK	Epidermal signal related kinase
ERK 1/2	Epidermal growth factor receptor 1/2
ESR	Electron spin resonance
FBS	Foetal bovine serum
FCS	Foetal calf serum
Fe	Iron

Fe^{2+}	Ferrous iron
Fe^{3+}	Ferric iron
FITC	Fluorescein Isothiocyanate
GAPDH	Glyceraldehyde -3-phosphate dehydrogenase
γ-GCS	γ-glutamylcysteine synthase
GI	Gastro intestinal
GM-CSF	Granulocyte macrophage - colony stimulating factor
GS	Glutathione synthase
GR	Glutathione reductase
GSH	L-γ glutamyl-L-cysteinyl glycine (reduced form)
GPx	Glutathione peroxidase
GSSG	L-γ glutamyl-L-cysteinyl glycine (oxidsed form)
GST	Glutathione -s- transferase
HARN	High aspect ratio nanoparticles
HEK	Human epidermal keratinocytes
HiPco CNT	High pressure carbon monoxide disproportionate carbon nanotubes
4-HNE	4 - hydroxy nonenal
H_2O_2	Hydrogen peroxide
HOCL	Hypochlorous acid
ICAM-1	Intracellular adhesion molecule-1
ICP-MS	Inductvely coupled plasma mass spectroscopy
ICP-AES	Inductively coupled plasma Adsorption/emission spectroscopy
Ig	Immunoglobulin (e.g. IgE, IgG)
IκB	Inhibitory kappa B
IKK	IκB Kinase
IL -	Interleukin (e.g. IL-8, Interleukin - 8)
I.P.	Intra peritoneal lavage
IPF	Idiopathic pulmonary fibrosis
JAK	Janus activated kinase
JNK	c-jun N-terminal kinase
KPE	Potassium phosphate buffer
L	Lymphatics
LAb	Laser ablation
LLF	Lung lining fluid
LC	lymphatic lacunae
LFA	Long fibre amosite asbestos
LDH	Lactate dehydrogenase
LMWCNT	Long multi walled carbon nanotube
LMWe	Long multi wall extract
LPS	Lipopolysaccharide
MAPK	Mitogen activated protein kinase
MCP-1	Monocyte chemotctic protein-1
MDA	Malondialdehyde
MEK	MAPK Kinase
MEKK	MAPK Kinase kinase
MIP-2	Macrophage inflammatory protein 2
MMP	Matrix metalloproteinase
MMVF	Man made vitreous fibre
MnSOD	Manganses superoxide dismutase
mRNA	Messenger ribonucleic acid

MTT	(3-(4,5-dimethylthiazol-2-yl)-2,5-diphenyl tetrazoliumbromide
MSL	Mesothelium/Mesothelial cells
MWCNT	Multi walled carbon nanotubes
NAC	N-acetyl-L-cysteine
NAD	β-Nicotinamide adenine dinucleotide (oxidised form)
NADH	β-Nicotinamide adenine dinucleotide (reduced form)
NADPH	β-Nicotinamide adenine dinucelotide phophate (reduced form)
NADP+	β-Nicotinamide adenine dinucelotide phophate (oxidsied form)
NF-κB	Nuclear protein kappa B
Ni	Nickel
NIK	NFκB Inducing protein
NLS	Nuclear localisation signal
NO	Nitric oxide
NOS	Nitric oxide Synthase
NT	Nanotube
$^1O_2$	Singlet oxygen
O_2	Oxygen
O_2^-	Superoxide anion
OD	Optical density
$^{\cdot}OH$	Hydroxyl radical
$ONOO^-$	Peroxynitrite
8-oxo-dG	8-oxo-7,8-dihydro-2-deoxyguanosine
PAF	Platelet activating factor
PAH	Poly aromatic hydrocarbons
PBS	Phosphate buffered saline
PCR	Polymerase chain reaction
PDGF	Platelet derived growth factor
PDTC	Pyrollidine dithiocarbamate
PKC	Protein kinase C
PL	Peritoneal lavage
PM	Particulate matter
PM_{10}	PM with a mean aerodynamic diameter <10μm
PMN	Poly morphonucleocyte
rCNT	Raw carbon nanotube
Redox	Reduction-Oxidation
RNA	Ribonucleic acid
ROFA	Residual oil fly ash
ROS	Reactive oxygen species
RNS	Reactive nitrogen species
RT-PCR	Reverse transcriptase polymerase chain reaction
S	Stomata
SBP	Soy bean peroxidase
SDF	Stromal derived cell factor
SDS	Sodium dodecyl sulphate
SFA	Short fibre amosite asbestos
SEM	Scanning electron microscopy
Si	Silicon
SMWCNT	Short multi walled carbon nanotube
SMWe	Short multi wall extract
SOD	Superoxide dismutase

SP	Surfactant protein
STAT	Signal transduction and activators of transcription
TBE	Tris-tracetate EDTA
TE	Tris-EDTA
TEMPONE-H	1-hydroxy-2,2,6,6-tetramethyl-4-oxo-piperidine
TGFα	Transforming growth factor alpha
TGFβ	Tranforming growth factor beta
TiO_2	Titantium dioxide
TNFR	Tumour necrosis factor receptor
TRAF	TNF receptor associated factor
uf	Ultrafine
ufCB	Ultrafine carbon black
V	Vanadium
VCAM	Vascular cell adhesion molecule
VEGF	Vascular endothelial growth factor
Zn	Zinc

Chapter 1

Introduction

1.1 Lung anatomy and physiology

The respiratory system is divisible into upper and lower regions structurally, and conducting and gas exchange portions functionally. The conducting portion of the lung consists of a series of interconnected cavities and tubes that funnels air into the lungs, the respiratory portion is made up of tissues where gas exchange occurs and includes respiratory bronchioles, alveolar ducts, alveolar sacs and alveoli. The lungs almost fill the thoracic cavity, they are both enclosed and protected by pleural membranes whose superficial layers line the walls of the thoracic cavity (parietal pleura) and whose deep layers (Visceral pleura) cover the lungs themselves. Between the two layers of the pleural membranes is a fluid filled cavity called the pleural cavity, the small amount of lubricating fluid it contains allows the parietal and visceral membranes to easily slide over each other. Blood vessels, lymphatic vessels, nerves and the bronchi enter and exit the lungs at the hilus. Each lung is divided by fissures into lobes each of which receives its own secondary bronchus that sub-divides into ten tertiary bronchi in each lung. Each tertiary bronchus supplies a bronchopulmonary segment that is divided into lobules (a portion of lung wrapped in elastic connective tissue and contains a lymphatic vessel), an arteriole, a venule and a branch from a terminal bronchiole. Terminal bronchioles divide into microscopic respiratory bronchioles whose lining epithelium changes from simple cuboidal to simple squamous as they penetrate more deeply into the lungs. Each respiratory bronchiole sub-divides into alveolar ducts (from trachea to alveolar ducts there are about 25 orders of branching). Surrounding each alveolar duct are alveoli and alveolar sacs. Alveoli are cups of simple squamous epithelium growing over a thin elastic basement membrane; an alveolar sac is a group of two or more alveoli

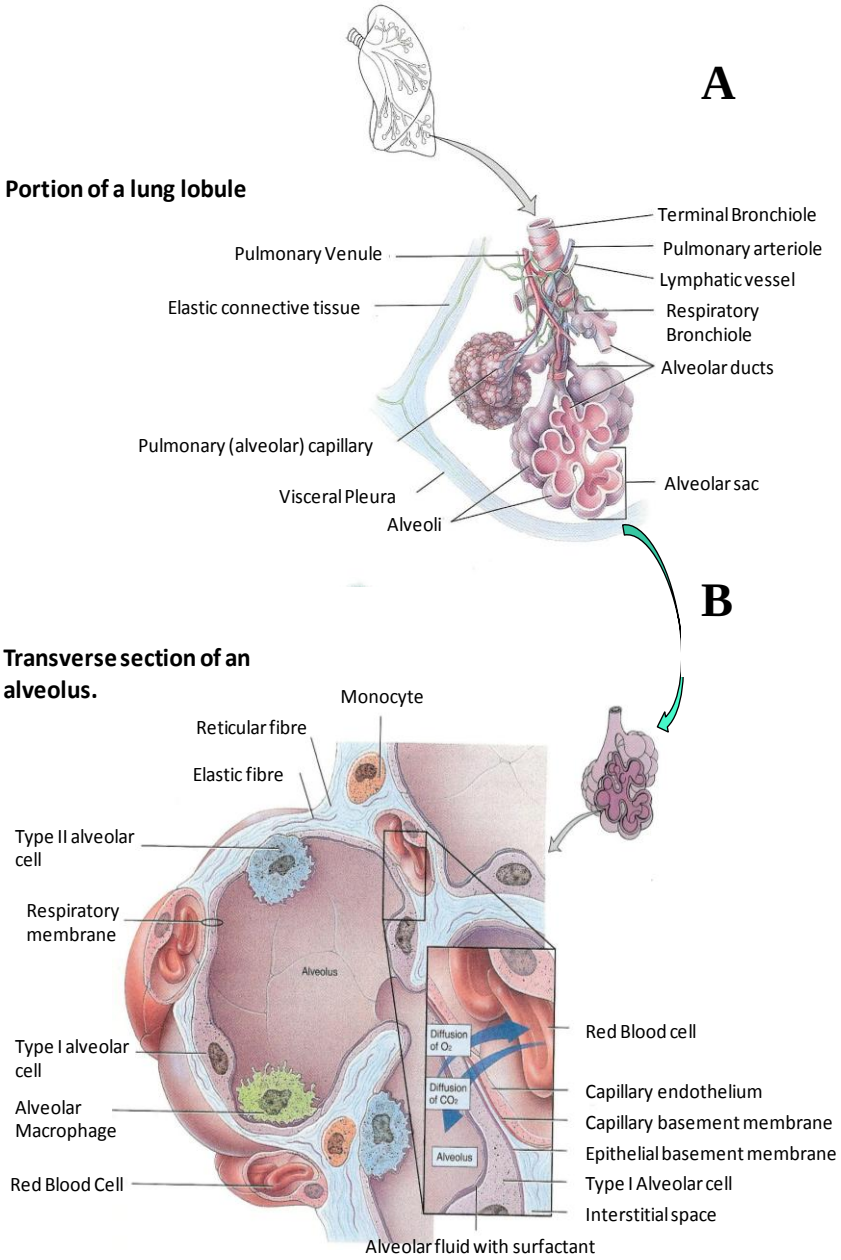

Figure 1.2. A) Diagram of a portion of a lobule of the lung. Lobules are sub-divisions of bronchopulmonary segments that are wrapped in elastic connective tissue and contain a lymphatic vessel, an arteriole, a venule and a branch from terminal bronchiole. Terminal bronchioles sub-divide into microscopic respiratory bronchioles that in turn sub-divide into alveolar ducts. **(B) A diagram of an individual alveolus with cellular components.** Around the circumference of each alveolar duct are numerous alveoli and alveolar sacs (two or more alveoli that share a common opening. The walls of alveoli are composed of simple squamous epithelial cells (Type I cells) across which gas exchange occurs that form an almost continuous lining interrupted by cuboidal epithelial cells (Type II cells). Adapted from Tortora and Grabowski 2000.

sharing the same opening. Alveoli are lined by two types of cell, type I alveolar epithelium that are simple squamous cells that form an almost continuous lining of the alveolar wall and are the main points of gas exchange and type II alveolar epithelial cells that interrupt that lining. Type II cells are cuboidal with microvilli on their free surfaces, they secrete a thin film of liquid (alveolar fluid) that contains surfactant (a detergent consisting of lipoproteins and phospholipids) to lower the surface tension of the alveolar fluid. Moving over the alveolar wall are phagocytic alveolar macrophages that remove dust particles and other debris. Found in the alveolar wall are fibroblasts that produce reticular and elastic fibres that are the structural scaffold for the type I alveolar epithelial cells. Gas exchange occurs in the alveolar space by diffusion across four layers; 1) the alveolar epithelium, 2) the epithelial basement membrane, 3) the capillary basement membrane, and 4) capillary endothelial cells, a distance of only 0.5μm (Tortora and Grabowski 2000,Weihel 2009).

1.2 Pulmonary Epithelial cells

The 2^{21} – 2^{23} branches of the human bronchial tree are covered by a continuous epithelial sheet (Crystal et al 2008). The cellular composition varies along its length (Thompson et al1995, Crystal et al 2008) and includes ciliated, columnar, un-differentiated, and secretory and basal cells (Crystal et al 2008). The epithelial sheet acts as a unit and interacts with endothelial, mesenchymal and immune cells and the matrix of the bronchial wall (Crystal et al 2008). In the airways the epithelium acts to protect the air spaces through a number of mechanisms; as a barrier made tight by junction complexes and a luminal surface impervious to macro-molecules and pathogens (Thompson et al 1995), also as a result of coordinated secretion of mucus and ciliary action that clears mucus bound particles (Thompson et al 1995, Crystal et

al 2008). Clearance is assisted by secretion of surfactant from Clara and type II epithelial cells that changes the surface charge of inhaled particles making them less sticky (Thompson et al 1995). Finally, protection is provided as a result of epithelium producing pro and anti inflammatory molecules that modulate the course of inflammatory reactions (Thompson et al 1995, Herzog et al 2008). By releasing chemo-attractants epithelial cells can recruit and regulate inflammatory cells. These include the powerful neutrophil chemo-attractant from the CXC family of chemokines, interleukin-8 whose production is negligible under resting conditions but can be up-regulated in response to appropriate stimuli. In addition to molecules that promote inflammation, airway epithelial cells secrete anti-inflammatory molecules including Transforming growth factor-β (TGF-β) (that has been detected in epithelial lining fluid) (Thompson et al 1995).

As a result of its constant exposure to an oxygen rich environment airway epithelium contains a high concentration of the antioxidant molecule glutathione and antioxidant enzymes Superoxide dismutase (SOD) and catalase. A glutathione redox cycle maintains a high ratio of reduced glutathione (GSH) to oxidised glutathione (GSSG) whose high intracellular concentration and ubiquitous cellular distribution points to its importance. Extracellular epithelial lining fluid is also rich in anti-oxidants, largely serum derived but including the epithelial produced metal binding protein lactoferrin and the anti-oxidant and opsonin surfactant protein-A (SP-A) (Thompson et al 1995). In the alveoli epithelial cells are either type I (ATI) (covering 95% of the alveolar surface) or type II cells (ATII) (covering only 5% of the alveolar surface but making up 15% of the total cells in the lung) (Herzog et al 2008). Whilst ATI cells are specialised for gas exchange ATII cells for fill a more complicated role.

Sitting in the corner of the alveolus they produce, secrete and recycle pulmonary surfactant, their Na^+/K^+ ATPases help keep the alveoli free of fluid whilst their ability to produce and secrete cytokines and chemokines enables them to regulate the activities of immune cells (Thompson et al 1995, Herzog et al 2008). Finally in response to injury or death of ATI cells, hyperplasic ATII cells cover the basement membrane and differentiate into ATI cells maintaining the integrity of the alveolus (Herzog et al 2008).

1.3 Neutrophil

Of all the granulocytes found in the blood, neutrophils (polymorphonuclear leukocytes, PMNs) are the most common subtype with critical roles in anti-bacterial and anti-fungal defence (Simon 2003). They spend a few hours in the blood stream prior to being recruited towards inflammatory districts where they survive for one to two days before undergoing apoptosis (Donà et al 2003). When activated, neutrophils are specialised for rapid changes in phenotype and function including adhesion, migration, phagocytosis, synthesis of biologically active lipids, generation of ROS and degranulation of stored inflammatory peptides. Factors released by neutrophils are displayed on their surfaces and mediate local response to infection and injury and provide cues that conduct involvement of the active immune system (Lindermann et al 2004). Neutrophils are terminally differentiated immune effectors that migrate from the blood to sites of tissue damage and inflammation early in the acute phase of the response eliminating pathogens intracellulary or extracellularly by releasing toxic mediators (a process that causes varying degrees of collateral tissue damage) (Simon 2003, Lum et al 2005). Many neutrophil activation responses do not involve altered gene expression or new protein synthesis and so the cells were

believed not to be capable of regulated production of new gene products after leaving the marrow. It is now clear that in response to specific stimuli they can produce specific proteins (Lindermann et al 2004). Release of cytokines by neutrophils amplifies the initial inflammatory response so that the cells act as both effectors and regulators of inflammation (Simon 2003). Neutrophils are produced largely in the bone marrow and constitutively released into circulation, this constitutive production and release can be enhanced in response to chemotaxins produced at the sites of inflammation such as TNFα. Neutrophils released to circulation have two possible fates: either migration to tissues to participate in inflammatory responses or senescence (Lum et al 2005), to resolve inflammation neutrophils must be removed and this is accomplished in part by apoptosis (Simon 2003). The life span of neutrophils summoned to sites of inflammation is extended as a result of resistance to Fas- and TNF- induced apoptosis brought about by anti-apoptotic effects of molecules such as Granulocyte colony stimulating factor (GM-CSF) as well as the mechanism of neutrophil movement into tissues that appears to down regulate pro-apoptotic regulators (Lum et al 2005). Eventually at the site of inflammation neutrophils undergo apoptosis and are phagocytised by macrophages (Lum et al 2003) in a process associated with the release of anti-inflammatory mediators. Neutrophil apoptosis controls the duration of an inflammatory response and thus the extent of the neutrophil mediated tissue damage (Simon 2003). Neutrophils not entering the tissues and participating in an inflammatory response become senescent after about six hours and express CXCR4 on their surfaces becoming chemotactic towards stromal cell derived factor 1(SDF-1) and migrating to areas of its production such as the bone marrow, in the bone marrow senescent

neutrophils undergo apoptosis (Lum et al 2005). Despite their protective role neutrophils are also at the heart of tissue injury in a diverse range of diseases including sepsis, inflammatory lung, bowel, and joint diseases, acute coronary syndromes, atherosclerosis and various other deregulated inflammatory disorders (Lindermann et al 2004).

1.4 Macrophages

Macrophages are one of the principal cells of the chronic inflammatory response. If not resident at the site of inflammation they develop from circulating inactive monocytes that migrate to and are converted into functioning macrophages by γ-interferon. With activation macrophage morphology changes and they develop the machinery necessary for protein synthesis, in their activated state macrophages have both secretory and phagocytic capacity. Secretions from macrophages include mediators of acute inflammation such as platelet activating factor (PAF), arachidonic acid metabolites, ROS, proteases and hydrolytic enzymes, cytokines (IL-1 and TNFα – that stimulate fibroblast proliferation and the laying down of collagen), and growth factors that stimulate blood vessel growth, division and migration of fibroblasts (Stevens and Lowe 2000). Macrophages release over 100 substances ranging in activity from induction of cell growth and proliferation to cytotoxicity. Macrophages are a highly phagocytic part of pulmonary defence, following exposure to inhaled or blood borne antigens alveolar macrophages release factors that recruit and activate other inflammatory lung cells, their capacity to recruit large numbers of inflammatory cells and release secretory products hints at their being significant mediators of pulmonary tissue damage (Laskin & Pendino 1995). In addition to phagocytosing invading micro-organisms macrophages also phagocytose infiltrating

neutrophils that have undergone apoptosis. Clearance of neutrophils is necessary for the resolution of acute inflammation as their ingestion prevents the lytic release of their damaging contents. Macrophages may also initiate apoptosis of neutrophils (Meszaros et al 2000). Macrophage activation in the face of toxic insults (such as ozone) to the respiratory system results in the release of ROS and RNS, IL-1, TNFα, and fibronectin, it is the exaggerated release of oxidants and cytokines that is thought to result in lung injury. Human pulmonary diseases with macrophage associated inflammatory components include fibrosis, asbestosis, mesothelioma, and bronchogenic carcinoma. These diseases are in part caused by macrophage activation and release of pro-inflammatory mediators. Failure of macrophage mediated phagocytosis and clearance results in damage and death of the cells with leakage of oxidants and proteolytic enzymes as well as chemo-attractants resulting in massive neutrophil recruitment and the induction of acute inflammation. Macrophages attraction of fibroblasts and their capacity with that of type II epithelial cells to stimulate the release growth factors is thought to account for their contribution to fibrotic lung diseases (Laskin & Pendino 1995).

1.5 Free radicals and reactive species

A free radical can be defined as any atom or molecule with one or more unpaired electrons such as hydrogen atoms, oxygen molecules and most transition metals (Halliwell & Guteridge 1984, Yu et al 1994). Reactive species is a looser term describing atoms or molecules with a strong ability to oxidise or reduce other molecules. The terms free radicals and reactive species encompasses reactive oxygen species (ROS) that are oxygen ions or molecules formed from the incomplete one electron reduction of oxygen (Jin-Shui et al 2009). In cellular metabolism oxygen

typically undergoes a four electron reduction to water (Halliwell & Gtteridge 1984). The single electron reduction of oxygen generates the superoxide anion (Fridovich 1983, Halliwell & Gutteridge 1984):

$O_2 + e^- \rightarrow O_2^{\bullet -}$

Addition of a second electron to the superoxide anion generates the peroxide ion (O_2^{2-}). At physiological pH peroxide ions protonate to hydrogen peroxide, production of hydrogen peroxide is also accomplished by dismutation of superoxide ions:

$2O_2^- + 2H^+ \rightarrow H_2O_2 + O_2$

Although not particularly reactive hydrogen peroxide can serve as the progenitor of the highly reactive hydroxyl radical (OH•), this can occur as a result of hydrogen peroxides reaction with an iron (II) salt in process named the Fenton reaction or Fenton chemistry:

$Fe^{2+} + H_2O_2 \rightarrow Fe^{3+} + {}^{\cdot}OH + OH^-$

Iron (III) can be reduced back to iron (II) by further reactions with hydrogen peroxide:

$Fe^{3+} + H_2O_2 \rightarrow Fe^{2+} + O_2^- + H^+$

Further reactions are also possible:

$2{}^{\cdot}OH + H_2O_2 \rightarrow + 4H^+ + 2O_2^-$

$O_2^- + Fe^{3+} \rightarrow Fe^{2+} + O_2$

${}^{\cdot}OH + Fe^{2+} \rightarrow Fe^{3+} + OH^-$

In these reactions iron is acting as a catalyst, other transition metals such as copper can also catalyse the production of hydroxyl radicals from hydrogen peroxide (Halliwell & Gutteridge 1984).

1.6 Pulmonary antioxidant defence

Present in excess in tissues free radicals and ROS damage proteins, lipids and DNA resulting in inflammation, reduced or compromised tissue function, enhanced susceptibility to infection and exacerbation of existing diseases (Ciencewicki et al 2008). It has become understood that the lungs are susceptible to damage by ROS (Johnson et al 1981, Sandblom et al 1983) and that a multi-layered system of defence has evolved in response (Fridovich & Freeman 1986).

The first layer of defence involves limiting the scope for production of ROS through the arrangement of the enzymes of the respiratory chain in mitochondria and by the chelation of free metal ions by the proteins ferritin, transferrin and ceruloplasmin (Sies 1993, 1997). A second enzyme based layer of defence then exists. Components include superoxide dismutase that is found in both the cytosol and mitochondria and catalyses the dismutation of superoxide anion to hydrogen peroxide, also the haem centred peroxisomal enzyme catalase that catalyses the reduction of hydrogen peroxide to water. Hydrogen peroxide can also eliminated by peroxidases such as glutathione peroxidase using the tripeptide glutathione (GSH) at the cost of a molecule of the coenzyme nicotinamide adenine dinucleotide phosphate (NADPH) (REF!). The third line of pulmonary oxidant defence consists of a host of scavenger molecules distributed throughout cells. One of the most abundant is glutathione, a tripeptide of glutamic acid, cysteine and glycine. The cysteine molecule provides a nucleophilic sulphydryl group enabling the molecule to react with electrophiles (Timbrell 2002) including superoxide, hydroxyl radicals and hydrogen peroxide. Other important examples include the hydrophobic membrane portioned α-tocopherol that halts the propagation of chain propagating fatty acid

radicals generated by lipid peroxidation (Fridovich & Freeman 1986), also hydrophilic ascorbic acid that can react directly with and neutralise superoxide anions, hydroxyl and lipid hydroperoxide radicals and uric acid that quenches hydroxyl radicals' intra and extracellularly (Pal Yu et al 1994). These antioxidant molecules and enzymes do not work in isolation from each other but interact to maintain a balanced oxidation – reduction (redox) environment in the lung. The layering of defence means that upon expenditure of one antioxidant another is available (Jacob 1995). Antioxidant defences also form an important component of epithelial lining fluid (ELF), a layer of surfactant and antioxidant that interfaces between the external environment and respiratory tract epithelial cells (Cross et al 1994, Putman et al 1997). The principal antioxidants of the human ELF include ascorbic acid, uric acid and GSH with lesser amounts of vitamin E, metal binding proteins, antioxidant enzymes, sacrificial proteins and unsaturated lipids (Putman et al 1997). Ascorbic acid scavenges neutrophil derived oxidants and reduces oxidised vitamin E that protects lipids in aqueous dispersions and membranes from peroxidation. Oxidative damage caused by particulate matter (PM) appears to be ameliorated by antioxidants found in ELF, for instance vitamin E protects against the effects of hypoxia (Jacobson et al 1990) whilst sub optimal levels of vitamin E have been shown to heighten lung responsiveness to oxidant injury (Cross et al 1994, Reddy et al 1998).

1.7 Oxidative stress

Free radicals are generated in tissues as a result of cellular respiration, inflammatory response (during the respiratory burst) and by peroxisomal oxidases and cytochrome

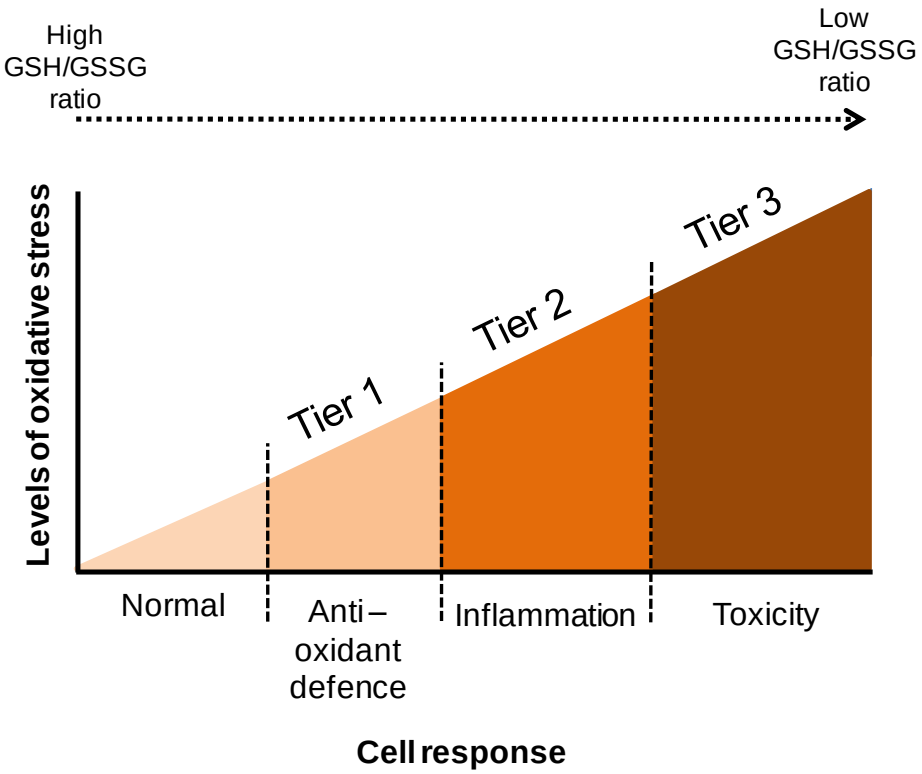

Figure 1.3. The response to oxidative stress. This diagram shows a stratified cellular response to oxidative stress, cells first response to oxidative stress is through its anti-oxidant defence (such as glutathione – GSH)). As levels of cellular anti-oxidants decline the level of oxidative stress is allowed to increase producing progressively more severe responses in the cell such as initiation of an inflammatory response followed (if the source of the oxidative stress is not removed) by toxicity and cell death. Adapted from Nel et al 2003.

P450 enzymes (Kopáni et al 2006). Production of ROS may lead to cycles of oxidation and reduction that deplete intracellular antioxidants such as GSH and NADPH (Timbrell 2002) tipping the cellular redox balance in favour of oxidising conditions and an environment where additional free radicals can be produced without challenge.

Superoxide anions are only cytotoxic under aerobic conditions and only reactive in hydrophobic conditions. Superoxide's hazardous nature largely arises from its dismutation to hydrogen peroxide (Bandypadhyaya et al 1999). Hydrogen peroxide has been shown to inflict cytotoxicity in type II epithelial cells and deplete levels of non protein thiols (Mulier et al 1998) and induce apoptosis in tracheobronchial epithelial cells (Goldkron et al 1998). It had been thought that enzymic removal of hydrogen peroxide and the consequent oxidation of redox active cofactors (such as NADPH) would adversely affect membrane calcium ion pumps causing cytosolic calcium ion concentrations to increase leading to cell death (Bellomo et al 1982, Moore et al 1985, Farber 1994). Although such changes in calcium homeostasis may have a detrimental impact what is now clear is that they can often be uncoupled from cell death (Starke et al 1986, Sakaida et al 1991, Farber et al 1994). A major cause of oxidative injury is increasingly thought to be production from hydrogen peroxide of more reactive species as a result of interactions with transition metals (Fenton chemistry) (Starke et al 1986, Sakaida et al 1991). The sources of intracellular metals and the process of their mobilisation are uncertain (Farber 1994), species such as superoxide anions can release iron from iron binding proteins such as ferritin (Biemond et al 1986, Biemond et al 1987, Farber et al 1994) and the

existence of a non protein bound iron pool has also been proposed (Stäubli & Boelsterli 1998).

Unchecked ROS would damage macromolecules integral to the structure and function of cells. Their reaction with lipids (lipid peroxidation) generates lipid peroxy radicals in a self perpetuating chain reaction that significantly damages cell membranes by altering their fluidity, permeability and metabolic function (Bandyppadhyay et al 1999), other toxic by products such as 4-hydroxynanenal or malondialdehyde can damage bio-molecules (Hardy & Aust 1994). Lipid peroxidation has also been linked to the activation of the pro-inflammatory transcription factors (Bowie et al 1997). This chain reaction is thought to be initiated by hydroxyl radicals or iron oxygen complexes (perferryl or ferryl complexes) (Schafer et al 2000). Nuclear and mitochondrial (Shokolenko et al 2009) DNA is susceptible to oxidative damage including base modification (8-oxo-7, 8 dehydro-2'-deoxyguanosine, 2,6-diamino-4-hydroxy-5-formaminodipyrimadine, 8-OH-adenine, 2-OH-adenine and thymine glycol), deoxyribose oxidation, strand breakages, DNA protein cross linking and mutagenic alterations (Bandyyppadhyay et al 1999). Oxidative damage to DNA can also lead to depletion of adenosine triphosphate (ATP) and nicotinamide adenine dinucleotide (NAD) as a result of poly-ADP-ribose and synthetase activation resulting in cell death (Schraufstatter et al 1986, Szabó et al 1996, Chatterjee et al 1999). Reactive oxygen species can cause global damage to proteins resulting in their aggregation and fragmentation or local damage with no gross structural modifications. Changes to protein conformation can cause them to become vulnerable to degradation (Bandyppadhyay et al 1999).

1.8 Signalling pathways & Transcription factors

NF-κB is a transcription responsible upon stimulation for initiating and controlling the production of pro-inflammatory molecules such as interleukin-8 (IL-8). It is a homo or heterodimer of p50, p52, p65, cRel and Rel B proteins that at rest is anchored in the cytoplasm by inhibitory proteins IκBα, IκBβ, IκBε, BCL-3, p100 and p105 (Wang et al 2002, Scheidercit 2006). NF-κB is activated through a classical or an alternative pathway. Classical activation is brought about by cytokines such as TNFα and involves rapid phosphorylation of IκBα and p105 by IκB Kinase (IKK), a complex of kinase subunits (IKKα and IKKβ) and the regulatory NF-κB essential modifier (NEMO). Phosphorylation targets IκB for ubiquitination and proteosomal degradation freeing NF-κB to migrate into the nucleus (Scheidercit 2006, Yates & Górecki 2006, Hoffmann & Baltimore 2006) where it regulates inflammation, proliferation and apoptosis (Hoffmann & Baltimore 2006). Activation of the alternative pathway is brought about by lymphotoxin β, B-cell activating factor, receptor activator of NF-κB (RANK) or by IKKα interaction with NF-κB binding kinase (NIK) (Yates & Górecki 2006). Numerous pathways lead to the activation of NF-κB largely but not solely through IKK activation and IκB degradation (Hayden & Ghosh 2004). Diverse stimuli including cytokines, mitogens, environmental and occupational particles, toxic metals, intracellular stresses, viral or bacterial products and UV light all activate NF-κB (Chen & Shi 2002).

AP-1(activator protein 1) is a second transcription factor family associated with regulation of cell growth, differentiation, neuronal excitation and cellular stress consisting of Fos and Jun homo/heterodimers (Galter et al 1994, Rahman & MacNee 1998). The dimer of the two proteins form the active transcription factor, referred to

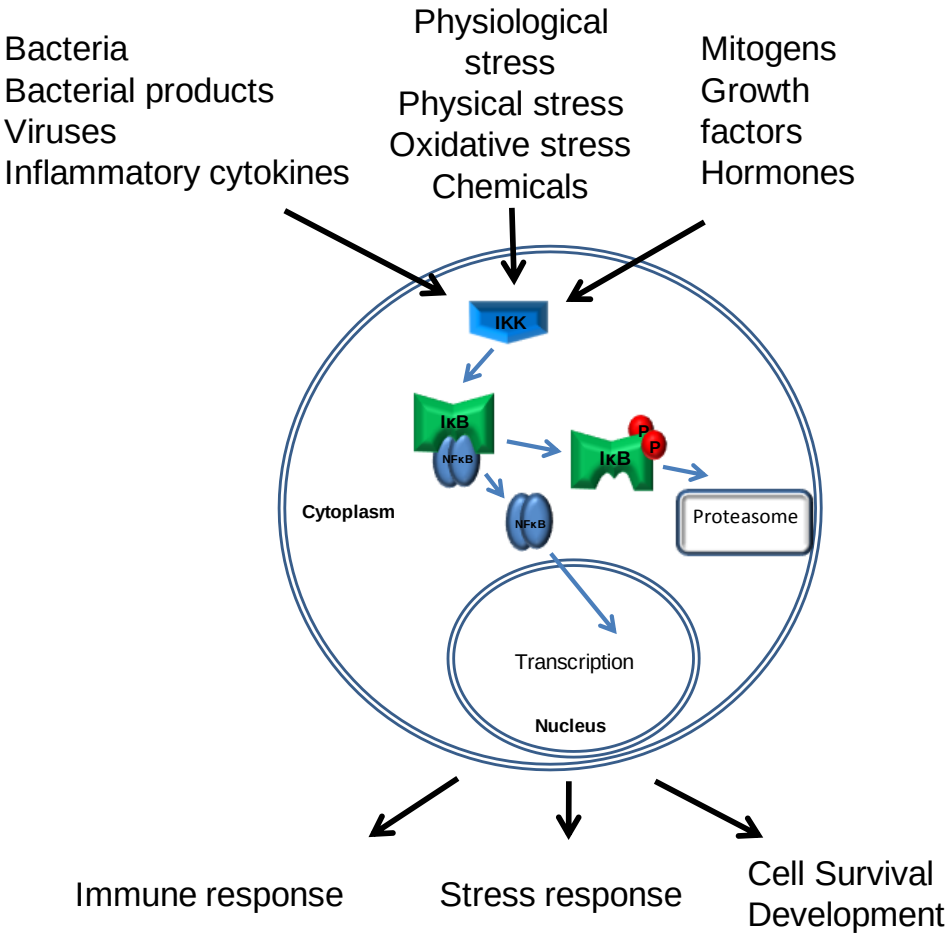

Figure 1.4. Stimuli of the activation of transcription factor nuclear factor kappa B (NF-κB). Shown above the cell diagram are various stimuli capable of activating NF-κB. The transcription factor (blue ovals) is held in the cytoplasm by IκB (Green) and released upon appropriate stimulation by phosphorylation of IκB by IκB kinase (IKK) (Blue) where upon NF-κB migrates to and enters the nucleus initiating transcription of target genes. This process triggers a variety of cellular responses including Immune responses, stress and survival responses or developmental changes. Adapted from Li & Stark 2002.

as activator protein 1 (AP-1). Dimerization is a pre-requisite for DNA binding although only heterodimers of fos-jun can interact with DNA in such a way to activate AP-1 mediated transcription.

Reactive oxygen species can overwhelm cellular antioxidant defences resulting in oxidative stress (Martindale & Holbrook 2002, Surh et al 2005) activating stress signalling pathways that terminate at transcription factors including NF-κB and AP-1. Their activity is therefore said to be 'redox sensitive' (Anderson et al 1994, Ginn-Pease et al 1996, Rahman & MacNee 2000). This redox sensitivity may be exerted through modulation of up-stream kinases to directly activate the transcription factor or by a change in the activity of a mediator protein (Saitoh et al 1998, Adler 1999, Haddad 2004, Storz et al 2004, Gloire et al 2006). Reactive oxygen species such as hydrogen peroxide may act as cell specific mediators of NF-κB activation (Flohé et al 1997, Zhang & Chen 2004), or may mediate cross talk between signalling pathways for example in tumour necrosis factor α (TNF-α) stimulation of NF-κB (Zheng & Chen 2004, Gloire et al 2006).

The direct reaction of reactive species with reduced glutathione (GSH) can result in its oxidation (GSSG). If the rate of GSH oxidation to GSSG is greater than the rate of GSSG reduction back to GSH then GSSG is exported out of the cell and lost, depleting overall the cellular levels of glutathione (Timbrell 2002). Changes in the GSH:GSSG ratio appears to affect the activity and DNA binding capacity of NFκB and AP-1(Ginn-Pease & Whisler 1996). Accumulation of GSSG appears to activate NFκB in an effect mitigated by antioxidants or GSH replenishment (Flohé et al 1997, Li & Karin 1999, Manna et al 1999, Rahman & MacNee 2000, Storz et al 2004), this control by glutathione over NFκB activity may be mediated through

redox sensitive ubiquitinases (Obin et al 1998, Manna et al 1999) and proteolytic degradation of IκBα (Obin et al 1998, Li & Karin 1999). In addition the ability of NFκB to bind DNA appears to be sensitive to levels of the endogenous redox active molecule thioredoxin (Hirota et al 1999). The ratio of GSH:GSSG may also effect the DNA binding capacity of the c-jun subunit of the AP-1 transcription factor (Klatt et al 1999).

Endogenously or exogenously produced ROS and oxidative stress may act directly upon transcription factors to modulate their activity. ROS appear to act through the JNK pathway to phosphorylate c-Jun (Yvonne et al 1996) and induce transcription of c-Jun and c-fos of AP-1 (Wilhelm et al 1997). ROS may also act upon the downstream regulators of transcription factor activity inhibiting their ability to switch them off and prolonging their working lifetime (Enesa et al 2008).

It is not entirely clear how ROS or other non specific reactive molecules can modulate well coordinated signalling pathways (Storz & Toker 2003), transcription factor activation by ROS can have multiple explanations and should not be considered as pointing to a ROS requiring step (Bowie & O'Niell 2000). Much evidence for ROS activation of transcription factors is based on antioxidant attenuation of this ability however antioxidants can have multiple points of activity (Li & Karin 1999) and inhibition of transcription factor activation may be unrelated to their antioxidant capacity (Hayakawa et al 2003). Paradoxically whilst ROS appear to activate NF-κB they simultaneously reduce its DNA binding capacity and thus its ability to mediate transcription of pro-inflammatory molecules in response. Also, in the case of toxic metals chromium (VI) is a much stronger producer of ROS than arsenic (III) however the latter in a much greater inducer of NF-κB making it

unclear if ROS are crucial mediators of NF-κB activation or are just coincidentally present (Chen & Shi 2002). These considerations are equally applicable to particles and fibres where ROS are implicated in transcription factor activation.

1.9 Cytokines and inflammation

Inflammation is the evolved acute response of tissue to injury characterised by increased blood flow, vascular permeability and oedema. Soluble cell derived polypeptides activate local and immune cells regulating their activity and proliferation, cytokines form part of this array of polypeptides (Lakhani et al 1993, Toews et al 2001).

1.10 Tumour Necrosis Factor-α

Tumour necrosis factor – α (TNF-α) is a pro-inflammatory cytokine produced from cells including mast cells, leukocytes and epithelial cells, it binds the receptors tumour necrosis factor receptor 1 and 2 (TNFR1 and TNFR2) found on virtually all cell types. TNFR1 initiates the majority of biological functions of TNF-α (Ka ming Chan et al 2000) that (for the purposes of this introduction) principally include immune stimulation and initiation of inflammatory responses. Binding of TNF-α to TNFR1 activates a host of secondary proteins on the cytoplasmic aspect of the membrane in a cascade reaction that ends with receptor interacting protein (RIP) (Micheau & Tschopp 2003, Li & Lin 2008). RIP activates IKK that in turn activates NF-κB or AP-1 by alternative signalling routes (Devin et al 2000, Devin et al 2001, Chen & Goeddel 2002, Bonif et al 2006, Li & Lin 2006, Li & Lin 2008) resulting in the production of IL-1β, IL-6, IL-10 and TNFα (Haddad 2002). This process is switched off in an auto regulatory step due to NF-κB induced expression of IκBα and

the protein A20 (Lee et al 2000) that interferes with RIPs interactions with other proteins (Li and Lin 2008).

1.11 Interleukin-8 (IL-8)

IL-8 is a hallmark of the inflammatory response (Baldwin et al 1991) mediating leukocyte transmigration into the inflamed tissues, re-organisation and changes in avidity of neutrophil and endothelial surface receptors for adhesion and migration. It stimulates leukocyte degranulation and the respiratory burst and is also chemotactic for basophils, eosinophils and indirectly for T-cells (Mukaida 2003). Transcription of IL-8 is controlled in a large part by NF-κB but sites for AP-1 and CAAT/enhancer binding protein (C/EBP) are also present in the IL-8 promoter sequence. These latter two are necessary for maximal gene expression (Holtmann et al 1999, Hoffmann et al 2002, Jijon et al 2002).

1.12 Transforming Growth Factor-β (TGF-β)

Transforming growth factor – β (TGF-β) is a growth factor released by epithelial cells, T-cells, platelets and monocytes as an inactive precursor (Sheppard 2006, Verrecchia & Mauviel 2007). TGF-β binds receptors TβRI or TβRII resulting in activation of smad protein complexes that translocate to the nucleus where either directly or in combination with DNA binding proteins they act as transcription factors (Verrecchia & Mauviel 2007) to control the cellular response. The major effects of TGFβ include chemo attraction, inhibition of epithelial proliferation, expression of genes encoding components of the ECM and inhibition of matrix metalloprotease (MMP) genes. Human recombinant TGFβ is redox- sensitive possibly facilitating its role in inflammation, where cell- derived oxidants could abrogate the requirement for proteolytic activation (Barcellos-Hoff & Dix 1996,

Nath et al 1998, Feghali & Wright 1997). Epithelial cell-derived TGFβ release is also stimulated by ROS and RNS possibly through AP-1 (Jin Kim et al 1989, Bellocq et al 1999) or as a result of oxidant-mediated release from storage sites (Bellocq et al 1999).

1.13 Pulmonary inflammation and disease

Tissue damage results in inflammation with cytokine, histamine, eicosanoids, proteases and chemokines released from local cells causing local vasodilatation, extravasation of fluid, migration, activation of leukocytes in the affected area, increased adhesive properties of endothelium and neutrophil degranulation and respiratory burst. An acute inflammatory response should be transient and halted by a series of brakes and stop signals with a switch at late stage inflammation from tissue damaging to a tissue regeneration mode (reviewed by Nathan 2002).

Pulmonary injury induced by hypoxia (Sarada et al 2008), LPS (Szarka et al 1997, O'Grady et al 2004) or pathogenic particles (Albrecht et al 2004) or fibres (Bissonnette & Rola-pleszczynshi 1989) results in a progressive cellular influx into the affected area. In the early phase this is characterised by neutrophils (O'Grady et al 2001, Albrecht 2004) that may remain present for much longer periods of time should the injurious conditions or insult remain (Albrecht et al 2004). Following injury local cells (epithelial cells or alveolar macrophages) (Albrecht et al 2004) release soluble mediators as a result of direct cellular damage and/or activation of signalling cascades terminating in the nuclear translocation of a pro-inflammatory transcription factors (i.e. NF-κB) (Sarada et al 2008) and resulting in the production of acute phase mediators such as TNF-α, IL-1, IL-6, IL-8, MIP-1 and MCP-1 (O'Grady et al 2001). This may also occur in response to oxidative stress (Albrecht

Et al 2004, Sarada et al 2008) and transcription factor activation may persist (Albrecht et al 2004, Enesa et al 2008). Pro-inflammatory mediators (TNF-α, IL-1, histamine) induce expression of adhesion molecules (ICAM-1, VCAM-1 and selectins) on local capillary endothelial cells enabling the migration of neutrophils from the blood to the site of injury (Lakhani et al 1993, Sarada et al 2008). Recruitment of neutrophils to the site of injury coincides with heightened levels of IL-8 although other chemo-attractants and trophic factors may maintain their presence (O'Grady et al 2001). Neutrophils alter the inflammatory milieu and provide links between innate and adaptive immunity (Lindermann et al 2004), they also mediate damaging pulmonary responses as demonstrated in models of acute lung injury (ALI) Yang et al 2003). In later stages a shift in chemokine and cytokine profile results in the influx of monocytes (Hurst et al 2001, O'Grady et al 2001, Marin et al 2001, Kaplanski et al 2003). This may be mediated by IL-6 and its soluble receptor and IL-8 released from neutrophils and endothelial cells (Modur et al 1997, Romano et al 1997, Lindermann et al 2004).

Persistent or chronic pulmonary inflammation is considered a key factor in the development of pulmonary fibrosis and carcinogenesis. Persistence of the inflammatory insult is necessary for maintenance of the inflammatory response. A specialised form of chronic inflammation is granulomatous inflammation a state characterised by the presence of macrophages, secretory epithelial cells and multi-nucleated giant cells aggregated into demarcated focal lesions called granulomas. Lymphocytes, plasma cells and fibroblasts may also be present (Williams & Williams 1983). Granulomas are thought to be a means of protection against

persistent irritants (Williams & Williams 1983), walling off and reabsorbing unwanted material (Diaz et al 2000).

Pulmonary fibrosis is a condition linked to chronic inflammation where inflammation and tissue remodelling and repair occur simultaneously (Wynn 2008) resulting in excessive fibroblast proliferation and extra cellular matrix (ECM) deposition (Atamas 2002). The condition idiopathic fibrosis has been linked to oxidative stress and chronic inflammation where excessive ECM deposition is driven by cytokine/chemokine paracrine interactions between macrophages and epithelial cells. Cytokines including IL-4, 6, 11, 13, TGFβ, macrophage chemo-attractant protein, macrophage inflammatory protein and growth factors such as connective tissue growth factor and platelet derived growth factor are considered inducers of fibrosis with many being up regulated in the lungs of patients with scleroderma and pulmonary fibrosis (Atamas 2002, Atamas & White 2003, Wynn 2008). Over expression of TGFβ results in significant tissue remodelling without inflammation (Gauldie et al 2007) but no sustained fibrosis (Strieter 2008). TGFβ can be activated by ROS and can activate NADPH oxidase in fibroblasts potentially adding to the oxidant levels in a damaged region (Kinnula et al 2005). It should be noted however that fibrosis driven by TGFβ may be the result of aberrant repair process rather than inflammation (Atamas 2002, Gauldie et al 2007, Stramer et al 2007).

1.14 Factors influencing particle/fibre pathogenicity

Nano derives from the Greek nanos meaning dwarf and it is being used as a prefix to an increasing number of words (e.g. nanotechnology, nanoparticle, nanotube, and nanoscience). A nanometre equates to a one billionth of a metre. A nanomaterial is defined as a material with at least one dimension of less than 1000nm (1μm) that can

be amorphous or crystalline and due to unique properties should perhaps be considered a distinct state of matter (Buzea et al 2007). The consequences of matter being nanosized include a tendency to bond differently and to have different electronic structures, crystalline shapes and behaviours.

1.15 Size, surface area, & surface reactivity

To exert a detrimental pulmonary effect a particle or fibre must be inhaled. Assuming the penetration of a particle into the pulmonary airways it may be deposited by (depending on its characteristics) interception, impaction, sedimentation, diffusion, or electrostatic repulsion (Lippmann et al 1980). Particle parameters that contribute to determining the site and mechanism of deposition include size, shape density, hydroscopicity and electric charge (Stuart 1976). Interception is particularly important for particles and fibres and occurs when their trajectory brings them close enough to an airway wall to make contact (Lippmann et al 1980). Impaction is a function of inertia, despite changes in airflow direction a particles momentum will cause it to continue along its original path to collide with an airway wall (Stuart 1976, Lippmann et al 1980). For particles reaching the small airways and alveolar spaces sedimentation (particle settling due to gravity) is important for deposition (Stuart 1976, Lipmann et al 1980). The movement of sub micron particles is reliant upon Brownian motion (increasingly so with decreasing particle diameter). Other factors affecting deposition include respiratory and flow factors (air velocity, laminar nature of air flow and tidal volume), anatomical factors (airway diameter and breathing patterns), physiological factors (thickness of the lining mucus layer) and the presence or absence of chronic lung diseases (Lippmnn et al 1980). Airway structure has a particular importance in effecting particle

deposition. Parameters such as airway segment length, diameter, inclination towards gravity, and branching angles all have an influence (Stuart 1976, Yeh et al 1976). The compartment of the lungs in which a particle deposits depends on its size, for a spherical particle, particle size may be defined by its geometrical diameter, for a non spherical particle size can be defined by aerodynamic diameter. This is the diameter of a unit density ($1g/cm^3$) sphere that has the same terminal settling velocity (the point at which gravity and air resistance of a falling particle balance) as the subject particle (Stuart 1976, Yeh et al 1976). Of inhaled particles 100nm in diameter 50% will enter the alveoli (Maynard & Kuempel 2005). For pulmonary toxicologists a fibre is particle with a length greater than 5μm and a diameter of less than 3μm with an aspect ratio (length/diameter) of 3:1. As fibre inhalation depends upon aerodynamic diameter which is not greatly affected by length even very long fibres can reach the lungs as long as they are thin (Donaldson & Lang 2005). Particles and fibres reaching the alveoli are deposited on lung lining fluid (LLF) through which they must be displaced to contact the underlying cell layer and resident macrophages (Gehr et al 2003, Gehr et al, Schurch et al 1999, Win & Feng 2005, Ye et al 1999).

Particle size influences recognition by and interaction with cells, affecting the mechanisms and efficiency of uptake in non phagocytic cells (Win & Feng 2005, Rejman et al 2004, Zauner et al 2000). For ultrafine particles aggregates are more likely to be internalised than individual particles (Stearns et al 2001). Internalisation is important as it allows particles access to various compartments of the cell. Decreasing particle size also increases the particle number and total surface area of a material for a given mass dose (Donaldson & Stone 2003) and the proportion of atoms displayed at the materials surface raising the likelihood of kinetic or

thermodynamic reactions with bio-molecules (Jefferson 2000). Fibre length is an important influence upon interactions with cells; length dependant cytostasis was observed after Chinese hamster ovary (CHO) cells were exposed to Man-made vitreous fibres (MMVF) (Hart et al 1994) and length dependant NF-κB activation, TNFα secretion and superoxide production was reported in RAW 264.7 macrophages following fibre exposure (Ohyama et al 2001).

Ultra-fine particles appear to be more toxic with greater inflammatory potential than fine particles at the same mass dose (Brown et al 2001, Brown et al 2000, Renwick et al 2004, Oberdorster 2000) indicating surface area is a major driver of inflammatory responses to inhaled particles. Surfaces of nano sized structures differ from those of bulk materials by accommodating poorly coordinated atoms or local centres of reactivity (Fubini et al 1997). Small particles have much more surface on a mass basis so can harbour more reactive groups per unit mass. The pathogenicity of silica for example is linked to silicon-oxygen surface bound radicals and reactive groups (Albrecht et al 2005) generating hydrogen peroxide and hydroxyl radicals in solution (Donaldson & Borm 1998, Fubini 2003, Razzaboni & Bolsaitis 1990) and damaging cell membranes (Nash et al 1966, Summerton et al 1977, Fubini 1998, Donaldson & Borm 1998). Surface characteristics may change as particles age and can be modified by adsorption, chemical or thermal treatments (Guthrie 1997). Modification of quartz's surface was found to diminish its pathogenicity (Albrecht et al 2005, Dick et al 2003).

Ultrafine carbon black (ufCB) is an aggregated arrangement of spherical particles composed of stacked turbostratic graphite (Ungar et al 2002, Muller et al 2006, Vorob'ev-Desyastovlii et al 2006) with an ability to generate free radicals ((Wilson

et al 2002, Dick et al 2003, Brown et al 2004). As with quartz this property may be due to surface reactive groups (Dick et al 2003, Brown et al 2004). Turbostatic carbons can be considered macro-stable radicals (Vorob'ev-Desyastovlii et al 2006) with reactive 'dangling' bonds at their edges (Ungar 2002, Kang & Wang 1997). This imparts chemical reactivity which is utilised in graphite-based heterogenous catalysis (Sanchez-Cortezon 2002) and has been compared to the role of iron in Fenton chemistry (Lucking et al 1998).

A particle or fibres pathogenicity is often the sum of a range of characteristics including but not limited to size, surface area and surface reactivity. Also important are the ways in which a particle or fibre interacts with the tissue into which it is deposited and how the tissue responds to its presence. This will be considered below.

1.16 Compound Particles

Transition metals are important in the toxicity of combustion derived nanoparticles and asbestos due to their ability to react with oxygen and generate oxygen radicals (Fubini 1997, Miller et al 1990, Pierre & Fontecave 1999). Ferrous and ferric iron salts were both found to enhance the extent of ROS production, the amount of oxidative stress and the level of neutrophil influx in the lungs of rats induced by carbon black (Wilson et al 2002) whilst iron in PM_{10} dose dependently activated NFκB (Jimenez et al 2000). Metals may also directly interact with bio-molecules for example vanadium binds and inactivates phosphotyrosine phosphatase whilst iron activates src kinases resulting in activation of pro-inflammatory transcription factors (Aust et al 2002).

The metal component of particles and fibres may also be mobilised into solution from coal, oil fly ash, diesel particles, PM_{10}, crustal dusts and asbestos (Aust et al 2002, Hutchison et al 2005). Water soluble extracts from pollution particles have been found to stimulate hydrogen peroxide production by endothelial cells (Li et al 2006). Mobilised metals can cause oxidative damage, the limiting factor is the ease with which a metal can be mobilised (Aust et al 2002).

Particles and fibres may also contain or carry biological and organic molecules, for example endotoxin may contribute to pathogenicity of PM10 (Donaldson et al 2003) resulting in IL-6 and IL-8 release from mononuclear phagocytes (Monn and Becker 1998). Particle surfaces can also adsorb organic molecules such as poly aromatic hydrocarbons (PAH) like Benzo-[a]-pyrene (Donaldson et al 2003) causing mutagenicity and DNA adduct formation (Binkova et al 2003). The inflammatory effect of Benzo-[a]-pyrene when adsorbed to a particles surface possibly results from its increased retention and availability in the lungs (Garcon et al 2001).

1.17 Inherent Redox capacities

The ability of particles or fibres to engage in redox reactions contributes to pathogenicity. Crocidolite and amosite may provide a continuous source of electrons for reduction of bio-molecules and free radical formation (Fubini 1997). Redox processes are strongly controlled by crystal structure and for asbestos by the availability of redox active surface iron (Hardy & Aust 1994, Guthrie 1997). Electron transfer from a crystal can occur from surface to the environment and from interior to surface during mineral catalysed redox reactions (Fubini 1997). The need to maintain charge balance may cause release of surface iron, driving Fenton reactions, whilst transfer of electrons from the interior to the surface enables chronic

free radical production. Electron transfer from mineral surfaces has been implicated in increased free radical formation by freshly fractured quartz compared to aged samples; such free radical activity diminishes as surface radicals equilibrate (Anpo et al 1999). Diesel exhaust particles (DEP) have a surface associated redox capacity probably due to surface associated semi – quinone groups enabling production of reactive oxygen species (Pan et al 2004). Carbon black induced lung injury and cytotoxicity towards immortalized human lung cells (A549) also appears to be due to their ability to produce ROS (Dick et al 2003, Garza et al 2008). The source of these ROS may be the edges of the graphene fragments that form CB particles (Garza et al 2008). Ultrafine nickel, titanium dioxide, cobalt and copper are also able to generate free radicals (Dick et al 2003); in some cases there may be a synergistic interaction between metal oxides and chemisorbed organic species (such as polychlorinated dibenzofurans) to generate free radicals and ROS (Balakrishna et al 2009). A redox activity has also been described for CNT, in some cases this has been specifically attributed to semi-conducting type CNT (Zheng & Diner 2004). However redox activity of CNT has also been ascribed to the presence of residual transition metals resident in the cavities or tips of CNT (Kim & Sigmund 2004). Removal of these residual metals has been found to be difficult (Jurkschat et al 2007). Where metals have been largely removed from CNT this has been found to diminish the ability of nanotubes to generate ROS. Pulskamp et al (2006) found that in comparison to a range of SWCNT and MWCNT containing varying levels of the metals Co, Cu, Ni, Fe and Mo (between 0.009 – 4.2 wt.%), acid treated (to reduce levels of metal catalyst impurities) SWCNT did not produce ROS (as detected by DCF fluorescence in NR8383 cells following 24 hours exposure) or change the mitochondrial

membrane potential of A549 cells. It should be pointed out that acid purification did not completely eliminate metal impurities as acid treated CNT contained 1.3 and 1.2 wt.% CNT of Co and Ni respectively. This suggests that rather than a difference in total metal content between CNT samples being important for toxicity the critical parameter is the level of bio-available or bio-soluble metals.

1.18 Adsorption and surface modification

Adsorption of molecules to a particle or fibre surface can alter the properties of both the surface and the adsorbed material. Protein binding depends on its orientation to the surface as well as the amount of surface available; kinetics of binding depends on protein charge. High surface occupancies force protein to adopt specific conformations to become bound (Valenti et al 2007); this is affected by pH (Song et al 2006). Adsorption of a protein can alter its conformation leading to exposure of new epitopes, perturbation of function, and reduction or abolition of activity (Cederwall et al 2007). Adsorption of chicken egg lysozyme to silica nanoparticles resulted in its denaturation, this effect was nullified at smaller particle sizes possibly due to the higher surface curvature of smaller particles promoting retention of native protein structure or as a result of a decrease (with increasing curvature) in lateral interactions (between adjacent protein molecules adsorbed on a curved surface) that can damage proteins (Kane & Strook 2007). As particle size decreases and surface curvature increases efficient close packing of proteins becomes more difficult reducing the level of protein coverage. Protein adsorption and activity (upon adsorption) depends not only on particle size and surface characteristics but also on protein identity (Cedarwell et al 2007) for example the activity of α-Chymotrypsin was reduced to 1% of normal following adsorption to SWCNT whilst soybean

peroxidase (SBP) retained 28% activity. Retention of activity also seems to be loading – dependent increasing with surface coverage (Karajanagi et al 2004), protein adsorption may stabilise its structure (Asuri et al 2006). Many proteins appear to form transient complexes with nanoparticles in a process of competitive binding; those that do bind become part of the identity of the particle. Thus protein adsorption depends not only on particle size and surface characteristics but also on protein identity (Cedarwall et al 2007).

Adsorption can alter toxicity of respirable particles for example clay adsorption to quartz particles suppresses toxicity (Wallace et al) whilst vitronectin coating of chrysotile and crocidolite enhances their phagocytosis (Wu et al 2000), a process considered to be an important part of their toxicity to mesothelial cells (Boylan et al 1995). Adsorption by nanotubes of components of the classical complement pathway (a diverse family of proteins activated that increase vascular permeability, chemotaxis of immune cells, opsonisation of pathogens and direct lysis of organisms) dose dependently resulted in its activation potentially triggering an inflammatory response (Salvador-Morales et al 2006).

1.19 Particle interactions with lung lining fluid & Cells.

Particles depositing in airways interact with an aqueous/gel lining consisting of water, ions, sugars, proteins, proteoglycans and lipids that over lies the epithelium (Schurch et al 1999) in a two phase system of a thinner sol phase over laid by a viscous mucus layer. Separating and lubricating the two is a phospholipid surfactant layer (Gehr et al 1993) that is continuous from the alveoli throughout the airways (Geiser et al 2003). The surfactant reduces the surface tension of this lining further facilitating re-inflation of the alveoli. Additional functions include aiding transport

of inhaled matter from the alveoli to the ciliated airways and displacing inhaled particles towards the airway epithelium (Gehr et al 1993, Schurch et al 1999, Gehr et al 2000, Geiser et al 2003). Surfactant may also be responsible for displacement of particles towards underlying epithelium (Gehr et al 1993). Particles depositing on the lining layer become wetted and are displaced towards the underlying epithelium by capillary forces (Gehr & Schurch 1992) in a process whose extent depends on the surface tension of the surfactant film as well as particle shape and surface chemistry (Schurch et al 1999, Gehr et al 2000). This process has been found to occur to a greater extent for particles that are smaller or have higher surface free energy than for larger particles or particles with lower free energy (reviewed by Schurch et al 1999, Gehr et al 2000). The coating of particles upon their deposition in the airways by surfactant (Gehr et al 1993) may determine whether they are removed (either free or in macrophages) or are transported into tissues (Gehr et al 2000).

Fibre deposition on a liquid surface is more complicated than that of spherical particles as a result of the multiple ways a fibre can hit a liquid surface due to orientation, variability of dimensions (whether fibres are straight or curved), heterogeneity of surface chemistry and adsorption of impurities (that lower the free energy of materials) (Geiser et al 2003).

Lung lining fluid acts as a buffer through which a particle or fibre must pass to interact with the underlying epithelium. During passage, components of lung lining fluid can become adsorbed to surfaces leading to their conditioning, for example in the short term DPPC attenuates quartz cytotoxicity (Schimmelpfeng et al 1992, Wallace et al 2006). The amount of DPPC in ELF however has been found to be too low to protect macrophages from the effects of DQ12 or chrysotile asbestos

(Schimmelpteng et al 1992). Quartz binds DPPC by hydrogen bonding unlike kaolin that covalently binds DPPC (Yuan et al 1995, Murray et al 2005). The nature of the bonding of the surfactant coat to the particle determines the ease of its removal by enzymes such as phopholipase A2 (Hill et al 1995) thus surfactant coatings may only delay toxicity (Murray et al 2005). The protective character of surfactants may also be a result of antioxidant abilities as demonstrated by the synthetic surfactant Exosurf (Ghio et al 1994) and DPPC, also DPPC has been shown to inhibit the respiratory burst of macrophages (Tonks et al 2001).

Surfactant proteins (SP) constitute a fraction (8-10%) of pulmonary surfactant and are divided into four groups; SP-A, SP-B, SP-C, and SP-D. Of the four the two principal constituents are generally considered to be SP-A and SP-D. These are multimeric proteins possessing both collagen and globular domains enabling them to bind sugars, lipids, calcium and pathogens (the latter as part of their role in innate immune defence). Present to a lesser extent are the hydrophobic proteins SP-B and SP-C that appear to modulate the surface and bio-physical properties of the surfactant film (SP-A is increasingly being considered in this role also). Equally important roles for these proteins includes transferring phospholipids from the hypophase (fluid phase between epithelial cells and the surfactant layer) to the interface (the air – water boundary) and stabilising the surfactant film as it comes under compression during expiration (reviewed by Pèrez-Gil 2002). Levels of these proteins appear to be modulated by inflammatory agents for example quantities of SP-A and B where increased in the lungs of silicotic sheep (Lesur et al 1993). Both SP-A and D were found to protect silica challenged macrophages (Spech et al 2000) in what may be an antioxidant effect (Bridges et al 2000).

1.20 Bio-persistence

Bio-persistence is the ability of a particle or fibre to remain intact in the lung despite physiological clearance mechanisms including the mucociliary escalator, phagocytosis by alveolar macrophages (AM), dissolution or disintegration. The efficacy of these processes is dependent on the characteristics of the particle or fibre (Muhle & Bellman 1997).

The bio-persistence of a fibre is a function of its length (Maxim 2006) and bio-durability (Muhle & Bellmann 1995), whilst retention kinetics depends on composition, length distribution and duration of exposure (Muhle & Bellmann 1995). A bio-persistent particle must be resistant to dissolution and be able to avoid or escape from cellular clearance mechanisms (Muhle & Bellmann 1995). Exposed to a heterogeneous range of pulmonary conditions a particle of fibres chemical stability will depend on its environment (Muhle et al 1994). Fibres of Wollastonite and xonotlite are not bio-persistent as they dissolve (Bellmann et al 1987); similarly the magnesium component of chrysotile asbestos fibres is subject to dissolution in dilute acids leaving a silica skeleton behind whose slower rate of dissolution determines the length of time of pulmonary residence (Hume & Rimstidt 1992, Langer & Nolan 1994). This leaching of magnesium decreases chrysotile's surface charge and diminishes its haemolytic potential (Bellmann et al 1987). Unlike chrysotile asbestos crocidolite asbestos is resistant to dissolution and is therefore bio-persistent. Partial dissolution can structurally weaken fibres and make them subject to disintegration due to the development of weak points (Archer & Dixon 1979, Muhle & Bellmann 1994, Muhle & Bellmann 1997). Uniquely, chrysotile asbestos undergoes longitudinal splitting into fibrils in the lung (Hume & Rimstidt 1992).

1.21 Clearance

Clearance of particles from the respiratory system begins with the onset of exposure (Sorokin & Brian 1974) with the method of clearance determined by where the particle deposits (reviewed by Stuart 1984), its size, physiochemical properties and cytotoxicity (Davis et al 1994). Understanding clearance is important as the risk posed by a hazardous inhaled material can't be assessed without knowing how much is deposited in a specific region and how much remains after clearance (Stuart 1984). Rapid clearance of particles is associated with deposition in the upper airways and delayed clearance with deposition in the alveoli (Lee et al 1985, Davis et al 1994), the rate of the clearance response to particle exposure will increase with the level of challenge (Vincent et al 1987). Clearance involves three regions of the respiratory tract; the nasopharynx, the conducting airways and the gas exchange regions (reviewed by Stuart 1984). It is a multi phase process involving rapid removal of tracheobronchially deposited particles followed by slower clearance of the alveoli (Langenback et al 1990). The three regions of the respiratory tract are served to varying degrees by clearance of material to the gastrointestinal (G.I.) tract by mucociliary escalator, to the blood via pulmonary vasculature or to the lymphatics (Sorokin & Brian 1974, reviewed by Stuart 1984). Particles depositing on the airway walls between the trachea and terminal bronchioles will land upon a mucus layer that serves as a device for trapping and conveying (by the coordinated beating of cilia) material towards the oropharynx (reviewed by Stuart 1984, van der Schans 2007). The number of ciliated cells decreases from the peripheral to the central airways; this is compensated for by the faster beating of cilia in the central airways and the takeover by airflow as the principal means of mucus transport (reviewed by

van der Schans 2007). Ciliary action and higher up in the airways airflow sweeps mucus and its cargo towards the glottis.

Particles reaching the alveoli are removed by dissolution or endocytosis (including phagocytosis) by alveolar macrophages. The ease (and rate) of particle clearance by macrophages is dependent on the amount of material deposited; cell motility can be inhibited when the cell becomes overloaded with material (Stuart 1984, Davis 1994). Upon deposition of material in the alveoli the number of macrophages present may increase as a result monocyte (immature macrophages) immigration from the blood (Stuart 1984). The dimension of the material deposited is also important (Morgan et al 1982), for example where as short fibrous particles can be entirely engulfed long fibres can penetrate the macrophage membrane upon ingestion affecting their mobility and survival (Stuart 1984). The inability of a macrophage to successfully engage and engulf a particle or fibre has been termed frustrated phagocytosis. Je et al (1999) demonstrated using the murine macrophage cell line RAW 264.7 an inability of the cells to completely engulf glass fibres of 17μm opposed to their successful ingestion of fibre 7μm long. The threshold between long bio-persistent fibres and short more easily cleared fibres is defined by the size of the alveolar macrophage (Maxim et al 2006). The size limitation placed upon macrophage phagocytosis may be the amount of cell surface membrane available to push around their target (Cannon & Swanson 1992). The inability to clear long fibres from the airways and alveoli results in an increasing lung burden with continued exposure (Yu et al 1996). Particle laden macrophages may migrate from the alveoli (to the ciliated airways) by one of or several mechanisms including by random migration, along a

chemotactic gradient, through the interstitium or by being drawn towards ciliated airways on a continuously moving fluid film (Stuart 1984, Lehnert 1992).

Inhaled deposited particles may be cleared through the pulmonary lymphatic systems either in macrophages or as free entities (Sorkin & Brian 1974, Stuart 1984, Lee et al 1985, Lehnert 1992). Work by Harmsen et al (1985) found that coloured micron sized beads instilled into dogs when found in tracheobronchial lymph nodes were almost always observed in macrophages. Harmsen et al (1985) interpreted their results to suggest particle laden alveolar macrophages where capable of migrating to regional lymph nodes. The relative toxicity of material (Stuart 1984) as well as the quantity of deposited material (a threshold level may exist) (Vincent et al 1987) appears to have a bearing on whether material is cleared to the lymph nodes. Vincent et al (1987) determined that the rate of material cleared from the deep lung to the lymph nodes was approximately proportional to the amount of material in the deep lung in excess of the threshold. Dendritic cells (antigen presenting cells located on the basal lamina below the epithelial cell layer) may also have a hand in transporting deposited particles to regional lymph nodes (Rothen-Rutishauser 2005).

Particles of sufficiently small size may translocate into the interstitium; in rats 24% of inhaled ultrafine titanium dioxide particles were found to breach the epithelial cell barrier and penetrate the micro vasculature (Geiser et al 2005). Work in rats has indicated that fibres can translocate throughout the body regardless of their initial site of penetration (Monchaux et al 1982) however movement of fibres into the lymph nodes appears to be limited to those of shorter lengths (Drew et al 1987, Le Bouffant et al 1987).

1.22 Particle and fibre toxicology.

1.22a Asbestos

Asbestos is a family of naturally occurring hydrated silicate fibres divisible into serpentine and amphibole types (Kamp & Weitzman 1999). Prolonged cumulative exposure results in diseases including pulmonary fibrosis (asbestosis), pleural diseases (pleural plaques and effusion), bronchogenic carcinoma and malignant mesothelioma often after 15-40 years latency (Kamp & Weitzman 1999).

Length has been identified as critical to asbestos toxicity; Archer (1979) proposed that in attempting to engulf fibres longer than their diameter (frustrated phagocytosis) substantial amounts of ROS would leak from neutrophils and macrophages, damaging surrounding tissue. This was demonstrated with different lengths of glass fibres in RAW 264.7 macrophages by Ye et al (1999) and by the milling of chrysotile asbestos that reduced its length and corresponding toxicity (Hesterberg & Barrett 1984).

Fibre length affects clearance. In rats phagocytosis and clearance of glass fibres became impaired as their lengths reached 30μm (Morgan et al 1982), it has been proposed that cell sensitivity to long fibres is the result the cells orientation with respect to the fibre during internalisation (Ohyama et al 2001). Long, unlike short, amosite fibres were found to cause rapid detachment of cells from their substratum independent of oxidant generation suggesting their length was of importance (Donaldson et al 1993). The effect a deposited fibre has on a cell layer may be enhanced (*in vivo*) by pulmonary tidal stretching indicating a physical interaction between fibres and cells (Tsuda et al 1999). Unlike length, width has not been associated with the cytotoxicity (Hesterberg & Barrett 1984, Ohyama et al 2001).

The toxicity of some asbestos fibres is contributed to by their high bio-durability indicated by the low dissolution constants for crocidolite and chrysotile asbestos (Scholze & Conradt 1987). To a large extent the solubility of fibres is controlled by the proportion of constituent alkaline earth metals (Bellman et al 1987). For example the magnesium hydroxide constituent of chrysotile asbestos undergoes rapid dissolution leaving a less degradable silica skeleton that controls the clearance half time of the fibre (Hume & Rimstidt 1992).

All asbestos fibres contain iron as part of their crystal structure, substitute cation, or as surface contaminants. The iron content of amosite and crocidolite is 27% compared to 1-6% found in chrysotile asbestos (reviewed by Kamp et al 1992 & Hardy & Aust 1994). The importance of iron to asbestos toxicity is its ability to generate ROS by Fenton chemistry and augment the catalytic ability of some materials through its coordination state (Kamp et al 1992). Amosite and crocidolite have been shown to cleave DNA by Fenton reaction-derived oxidants (Donaldson et al 1996), confirmed by Oterp Aeán et al (2001) although only in the presence of a reductant or hydrogen peroxide. Leaching of iron from fibres may be more important than direct ROS generation for toxicity although this requires a chelator (Kamp et al 1992, Hardy & Aust 1995) and mobilisation may alter fibre surface charge also affecting toxicity (Light & Wei 1977). The ability of iron to generate ROS depends on its electronic environment and the quantity of it in a redox available state at the surface of a fibre (Kamp et al 1992, Hardy & Aust 1994).

There are various hypotheses concerning the mechanisms by which asbestos fibres destructively interact with pulmonary cells and ultimately result in pathogenic outcomes such as carcinoma. One is that inhaled deposited fibres chronically

generate ROS (and induce prolonged oxidative stress) that damage DNA resulting in mutations in oncogenes, tumour suppressor and growth regulatory genes (reviewed by Kane 1996, Upadhyay & Kamp 2003). The capacity for asbestos fibres to produce ROS was introduced above. Asbestos activation of macrophages and neutrophils can intensify ROS production (Kamp & Weitzman 1999) enhancing cytotoxicity towards alveolar epithelial cells (Kamp et al 1994) and mesothelial cells (Kinnula et al 1995). This could the result of mitochondrial depolarisation, frustrated phagocytosis and/or fibre activation of ROS producing enzymes including NADPH oxidase (Sesko et al 1990, Kamp & Weitzman 1999). Reactive nitrogen species (RNS) may also be important modulators of asbestos pathogenicity. Peroxynitrile production was noted in mice instilled with crocidolite (Dörger et al 2002) and nitric oxide radical production was observed in rat alveolar macrophages following inhalation of crocidolite or chrysotile (Quinlan et al 1998).

An alternative hypothesis is fibres can physically interfere with cell division. This requires first that fibres are internalised. Internalisation by phagocytosis has been demonstrated in mesothelial cells (Liu et al 2000), however internalised fibres have been found to be contained within phagolysosomes preventing any direct contact (i.e. by adsorption) with chromosomes (reviewed by Kane1996). Mechanisms proposed to explain asbestos fibres interference with cell division have therefore focused upon their possible disruption of the microfilaments segregating chromosomes during mitosis and the spindle apparatus (Dopp et al 1995, reviewed by Kane 1996, Levresse et al 1997).

According to a third hypothesis asbestos fibres stimulate the proliferation of cells. Proliferation is important as it fixes mutations induced by exposure to genotoxic

agents. Levresse et al (1997) found that crocidolite and chrysotile asbestos acted both as DNA damaging agents and disruptors of the cell cycle. They suggested that as a result of this preferential activation of DNA repair over apoptosis DNA lesions unsuccessfully repaired could become fixed. Apoptosis serves to help balance proliferation (and thus the extensive fixation of mutations that could lead to carcinogenesis in cell populations) thus its induction by asbestos fibres in relation to the fibres carcinogenic potential may seem counter intuitive. However asbestos induced apoptosis may trigger compensatory proliferation of adjacent non apoptotic cells harbouring DNA damage (Albrecht et al 2004). Asbestos induced apoptosis appears to be mediated through various mechanisms that are not mutually exclusive. In asbestos exposed T-lymphocytes for example apoptosis was mediated through the Fas-Fas L system whilst more generally asbestos induced apoptosis has been found to be associated with mitochondrial disruption and dysfunction instigated by the presence of the fibre (Janssen et al 1998, Kamp et al 2002, Panduri et al 2003). Asbestos induced apoptosis may also be the result of stimulation of intracellular signalling pathways. For example the interaction of crocidolite with EGFR might trigger ERK1/2 activation resulting in c-fos transcription and AP-1 activation leading to changes in proliferation and eventually cell apoptosis (Jimenez et al 1997, Zanella et al 1999, Kamata et al 2000, Albrecht et al 2004, Baldys & Aust 2005). It is thought activation of ERK1/2 linked apoptosis could be an important step in the induction of carcinogenesis. Thus asbestos induced carcinogenesis may be the result of compensatory proliferation associated with asbestos induced apoptosis.

Asbestos induced proliferation may also be the result of compensatory proliferation in response to direct toxicity of the fibre (reviewed by Kane 1996). This leads on to

another principal hypothesis to explain asbestos induced toxicity; that asbestos fibres induce chronic inflammatory reactions resulting in prolonged ROS production, activation of transcription factors and release of cytokines and growth factors (reviewed by Kane 1996). Macrophages are the initial target of asbestos deposited in the lungs. Engagement of asbestos fibres by macrophages results in ROS production (Kamp et al 1994) in addition to release of inflammatory mediators that initiate a local inflammatory (reviewed by Kane 1996) response and the infiltration of neutrophils. Activation of macrophages and neutrophils can intensify ROS production (Kamp & Weitzman 1999) enhancing cytotoxicity towards alveolar epithelial cells (Kamp et al 1994) and mesothelial cells (Kinnula et al 1995). This may be the result of mitochondrial depolarisation, frustrated phagocytosis and/or fibre activation of ROS producing enzymes including NADPH oxidase (Sesko et al 1990, Kamp & Weitzman 1999). Asbestos- induced cellular activation (resulting in the production of inflammatory mediators) can occur internally (Baldys & Aust 2006) or extra-cellularly (Swain et al 2003). In mesothelial cells and rat tracheal epithelial cells probably as a result of oxidative stress crocidolite caused p65 nuclear translocation (Janssen et al 1997) and increased p65/50 binding to the NF-κB consensus sequences respectively. Similarly in rat type II epithelial and A549 cells exposure to crocidolite resulted in NF-κB activation (Simeonova et al 1997, Driscoll et al 1998, Luster & Simenonova 1998). The role of oxidative stress is supported by anti-oxidant inhibition of NF-κB nuclear translocation following exposure of epithelial cells to amosite (Brown et al 1999). The time required for fibres to contact cells, or to generate a threshold level of oxidants and the limited diffusion capacity of some oxidising species may all be factors in determining the rapidity and extent of

transcription factor activation (Janssen et al 1995, Janssen et al 1997). Activation of pro-inflammatory transcription factors from macrophages and epithelial cells results in the release of pro-inflammatory mediators (cytokines and chemokines) amplifying the initial response. Persistent release of these substances may lead to tissue damage (in addition to that caused by free radicals and oxidative stress), fibrosis and cell proliferation resulting in pathological effects such as asbestosis and carcinomas (reviewed by Kane 1996). The latency between asbestos exposure and the appearance of pathological conditions associated with it indicates these are long term processes. For example despite significant DNA damage, amosite and chrysotile induced no mesothelial cell proliferation after only 24 hours and no loss of contact inhibition after two months (Bertino et al 2007). Significant mutagenicity was observed in transgenic rats following amosite exposure but only after 12 weeks (Topinka et al 2004) indicating that this may be the result of long term exposure.

1.22b Silica

Silica (silicon dioxide) comprises a family of seven recognised crystalline minerals (DQ12 Quartz, Cristobalite, Moganite, Tridymite, Melanphlogite, Coesite and Stishovite) of which □ □ quartz (here afterreferred to as quartz) is by far the most important in occupational disease terms. Quartz comprises chiefly of silicon and oxygen (SiO_2) with varying amounts of trace metals including aluminium, iron, manganese, magnesium, sodium and calcium. It is found ubiquitously in the earth's crust and miners and quarries etc are exposed to quartz in a respirable form. Amorphous silica is a less toxic, non-crystalline form of the mineral. Inhalation exposure to quartz is associated with the development of a variety of pathologically

and clinically distinct inflammatory and fibrotic diseases generically called silicosis (Mossman & Churg 1998).

The pathogenicity of crystalline silica is governed extensively by its reactive surface (Elias et al 2000), additional factors such as atomic packing density of its surface structure may also be important (Mossman & Churg 1998), but crystallinity appears to have no bearing on toxicity. (Elias et al 2000). Quartz is cytostatic, mitogenic and cytotoxic interacting with cells through surface reactive functional groups including silanol groups, surface silica radicals and free radicals from trace iron (Elias et al 2000).

Inhaled quartz particles (<5μm) reach and deposit in the alveoli and are phagocytosed by AMs resulting in their incorporation into phagosomes and later phagolysosomes. After several hours the phago-lysosome membranes are thought to disintegrate releasing silica particles and the digestive enzymic contents of the phago-lysosome into the cytosol where it destroys the metabolic and structural apparatus of the cell. Degradation of phagolysosomal cell membranes is thought to result from abstraction of membrane phospholipids or proteins (Nash et a 1966). With the resultant cell- death, silica particles are released back into the lung to be phagocytosed by other AM (Summerton et al 1977). In this manner silica may persist in the lung.

Deposited silica particles interact externally and internally with alveolar epithelial cells exposing them to free radicals and ROS inducing oxidative stress and DNA damage (Shi et al 1994, Deshpande et al 2002, Fanizza et al 2007). They may also bind DNA strands potentially bringing reactive oxygen species to within a few Angstroms of the double helix (Saffiotti et al 1994). Short term exposure potentially

results in ROS mediated activation of NF-κB although this does not appear to require the internalisation of particles (Desaki et al 2000, Øvrevik et al 2006). Exposure results in the persistent production of the pro-inflammatory neutrophil chemo-attractant IL-8 (Schins et al 2000, Desaki et al 2000) and activation of other inflammation-associated pathways including MAPK p38 and ERK1/2 that appear to link to IL-8 production possibly through AP-1 (Ding et al 1999, Øvrevik et al 2004) or post-translationally regulate its production (Jijon et al 2002, Li et al 2002). The neutrophilic influx responding to pro-inflammatory signals is associated with increased epithelial cell DNA damage (Knaapen et al 2002) possibly due in part to the initiation of the oxidative burst (Albrecht et al 2005). The combined effect of silica's bio-persistence, its pro-inflammatory effect and resultant damage to surrounding cells conspires to induce carcinogenic and fibrotic outcomes. No single clear mechanism to explain silica carcinogenicity exists, it activation of AP-1 (a mediator in tumour progression) (Ding et al 1999), either by oxidative stress or stimulated release of TNFα or other mediators from surrounding cells (Rahman et al 2002) stimulating proliferative responses (Saffiotti et al 1994) may be part of the mechanism.

1.22c Carbon black (CB)

Carbon black particles are combustion-derived particles that are manufactured by incomplete combustion or thermal decomposition of natural gas or petroleum and are composed of graphite. Different carbon blacks including channel black, impingement black, furnace black and thermal black have different characteristics such as varying particle sizes. Commercial CB particle sizes range from 10-400nm and can be associated with poly-aromatic hydrocarbons (Rausch et al 2004). The

constituent units of CB particles include graphite that is chemically reactive and is reported to undergo a reaction similar to Fenton chemistry (Lücking et al 1998). The oxidative capacity of CB has been found to be proportional to its surface area (Koike and Kobayashi 2006). This may have to do with the decreasing size and increasing curvature of the constituent stacked graphenes that increases their surface area as well as the number of their reactive edges (Ungár et al 2002, Müller et al 2006). Factors such as these may help explain the variation in toxicity of different CB that appears to be related to particle surface area.

Ultrafine carbon black (mean diameter 14.3nm) has been found to reduce the metabolic competence of A549 cells and reduce GSH content after 48 hours. In an acellular assay it was also observed to cleave DNA (Stone et al 1998), whilst in alveolar epithelial cells DNA adduct formation was observed after ufCB exposure (Jacobsen et al 1997). The inability of fine CB (mean diameter 260nm) to demonstrate these activities (Stone et al 1998) suggested a surface area effect. This was supported by the observation that printex-90 CB, a nanoparticle form with a surface area of $300m^2/g$, significantly increased the occurrence of 8-oxo-dG DNA adduct in rat lungs compared to larger Sterling V CB with a surface area of 37m2/g (Gallagher et al 2003).

The ufCB ability to activate IL-8 gene expression was also found to be surface area dependent and surface area was found to be the main driver of this response amongst otherwise different particles (Barlow et al 2005). Exposure has also been associated with increased TNFα and VEGF synthesis in an antioxidant- inhibited manner, hinting at an oxidative component to toxicity (Chang et al 2005).

Surface area as a property is not a cause of free radical generation, but for a surface free radical generating activity, a given mass of NP will have a greater oxidative capacity (than fine particles) due to their greater surface area/unit mass. ICP-MS detected iron in CB and ufCB (50 and 100ng/mg respectively) although leachates failed to induce pulmonary inflammation in rats or effect intracellular calcium signalling (that modulates inflammatory gene expression) in MM6 cells (Brown et al 2000). Particle Iron levels were judged insufficient to account for their pro-inflammatory affects strengthening the possibility that CB generated ROS originate from dangling bonds at the reactive edges of the constituent graphite plates.

Despite its apparent inflammatory potential little evidence of human CB toxicity has been gathered. Neither Barlow et al (2005) or Monteiller et al (2007) found evidence of significant CB induced cytotoxicity despite its ability to generate ROS. In addition many of the CB induced effects observed in rats have been attributed to particle (Gallager et al 2003, Rausch et al 2004) overload although one study showed modest pro-inflammatory effects at an exposure that was much lower than overload levels (Gilmour et al 2004). In humans the effect of CB exposure appears limited. A two-fold greater incidence of cancer in German CB workers compared to the general population from 1976-1998 (not explained by selection, smoking or other occupational risk factors) could not be linked to CB exposure (Wellmann et al 2008). In fact pulmonary effects of CB exposure have been down-graded over successive decades with effects attributed to CB exposure now explained by non-specific irritant effects combined with dust retention, most genotoxicity tests of CB have proved negative (Rausch et al 2004).

1.22d Carbon nanotubes (CNT)

Carbon nanotubes are carbon macromolecules composed of single or multiple graphene (individual graphite layers) sheets rolled into tubes and capped at each end by half a fullerene molecule. Nanotubes formed from a single graphene sheet are designated single walled carbon nanotubes (SWCNT) whilst a concentric arrangement of multiple graphene sheets are multi walled carbon nanotubes (MWCNT) (Balasubramanian et al 2005, Lin et al 2003). Individual SWCNT have diameters in the range 1-2nm (Huczko et al 2006, Balasubramanian & Burghard 2005) while those of MWCNT range from 2-100nm (Ajayan 1999, Balasubramanian & Burghard 2005). Nanotube lengths may range from <10μm to many hundreds of microns (Tasis et al 2006) giving these molecules extremely high aspect ratios and making them almost one dimensional structures. Individual tubes self assemble into ropes arranged in a crystalline triagonal lattice (Ajayan 1999). The structure of nanotubes contain numerous topological defects, rehybridisation defects and incomplete bonding defects (Ebbesen & Takada 1995, Banerjee et al 2002, Balasubramanian & Burghard 2005, Lu & Chen 2005) that originate from their synthesis and purification (Mawwhinney et al 2000, Hirsch 2002).

Carbon nanotubes are synthesised by three main processes (all of which result in the manufacture of CNT with unsorted structures) (Huczko 2002) that includes electric arc discharge (EAD) (Ajayan 1999, Fonseca et al 1998, Terrones 2003, Huczko 2002, Avouris 2004) , laser ablation (LAb) (Huczko 2002, Terrones 2003) and chemical/catalytic vapour deposition (CVD). Nanotubes are generated from the vaporisation of graphite targets (EAD, LAb) or by passing a carbon containing vapour over supported metal catalyst nanoparticles in a furnace (CVD). Metal

catalyst particles may be of single elements (Co, Ni, Fe, Gd, Pt or Pd) or mixtures (Co-Pt, Co-Ru, Ni-Y, Rh-Pt or Co-Fe-Ce). Their use in EAD and LAb results in the synthesis of SWCNT. In each synthesis procedure CNT are produced as aggregates with different diameters, lengths, chiralities, and levels of defect (Hircsh 2002, O'Connell et al 2005) although variability of length and diameter can be tuned to a degree by control of the growth conditions (Ajayan 1999). At the end of synthesis in addition to CNT, amorphous carbon, fullerenes, graphitic particles and residual metal catalyst contaminants are present (Monthioux et al 2000, Thien-Nga et al 2002, Jurkschat et al 2006) and have to be removed. Commonly used harsh mineral acid purification leads to functionalization of the CNT sidewalls with oxygen groups and can result in the break-up of the nanotube into 100-200nm fragments (Balasubramanian et al 2005, Hirsch 2002, Huczko 2002, Niyogi et al 2002, Zhang et al 2003).

The chemistry of CNT is partly due to their nanoscale and partly due to the chemistry of graphene sheets (McEuene et al 2002). Nanotubes possess distinct regions of chemical reactivity that are the end caps and sidewalls (Balasubramanian et al 2005). The curvature of the side wall forces a triagonal carbon – carbon bond arrangement into a tetrahedral alignment inducing bond strain and chemical reactivity (Srivastava et al 1999, Niyogi et al 2002, Banerjee et al 2005). This effect is intensified at the end caps (lin et al 2005) making them susceptible to addition chemistry. The chemical reactivity of CNT is also a result of bond misalignment and the presence of dangling bonds at vacancies and un-capped ends of CNT (Ebbessen & Takada 1995, Kang & Wang 1997, Mijata et al 2006).

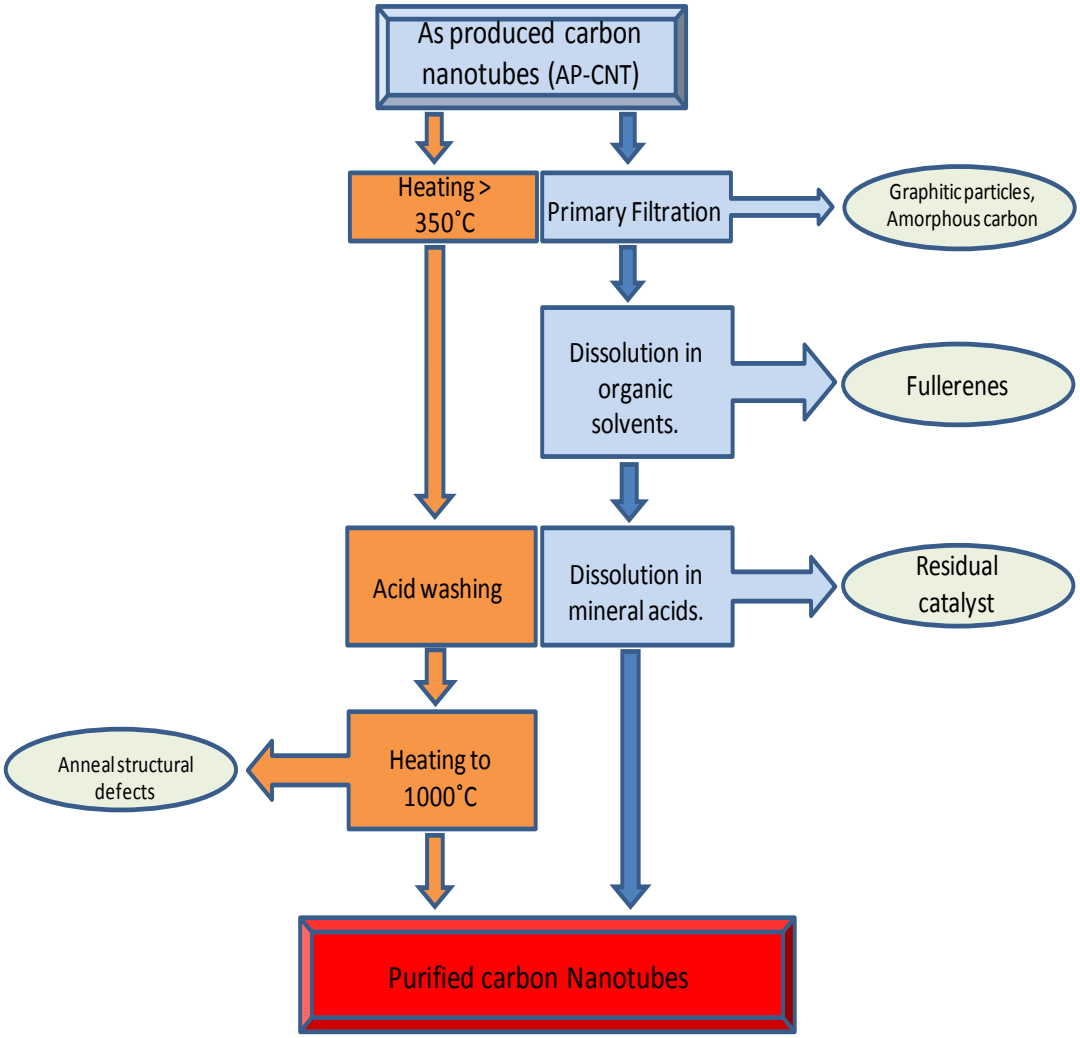

Figure 1.13. Simplified scheme of two purification procedures (Orange and blue) for un-purified as produced carbon nanotubes with the by-products removed at each of the stages (Green ovals) (Ajayan 1999, Monthioux et al 2000, Huczko 2002, Zhang et al 2003, Balasubramanian & Burghard 2005).

Strong hydrophobicity and van der waals' attractions between CNT cause them to aggregate in aqueous solutions (Tosis et al 2003). Dispersion of CNT in aqueous solutions can be achieved by physical modification (adsorption of molecules to the surface) or chemical modification (covalent addition of polar molecules to the surface) of nanotube surfaces with polar molecules (Vaisman et al 2007). Typically dispersion involves sonication of CNTs (functionalised or in a surfactant solution) (Huang et al 2002, Bandyopadhyaya et al 2002, Strano et al 2003, Paredes & Burghard 2004) producing gaps or spaces at the ends of CNT ropes into which surfactants diffuse, adsorb and increasingly separate bundled CNTs into isolated tubes (Strano et al 2003,Vaisman et al 2007). Surfactant effectiveness depends on their structure, molecular size, charge, presence of charged groups, hydrophilic tail length or branching and size of adsorbed hydrophobic region (Islam et al 2003, Schaefer et al 2003, Jiang et al 2003, Wenseleers et al 2004) (For a list of surfactants and solvents used with CNT see appendix I).

Carbon nanotubes combination of size, structure and topography endows CNT with high stability, strength, stiffness combined with a low density and elastic deformability (Ajayan & Zhou 2001). The commercial attractiveness of CNT springs from their properties, with 10-50 times the tensile strength of steel, five times electrical and five times the thermal conductivity of copper (Sherman 2008). Currently use of MWCNT is concentrated in the automotive industries for example in the manufacture of static dissipative fuel handling components and conductive body panels and bumpers for electrostatic painting. Roles for MWCNT are also envisioned in anti static films for packaging electronic components and EMI shielding for computers and cell phone housings, MWCNT are also being

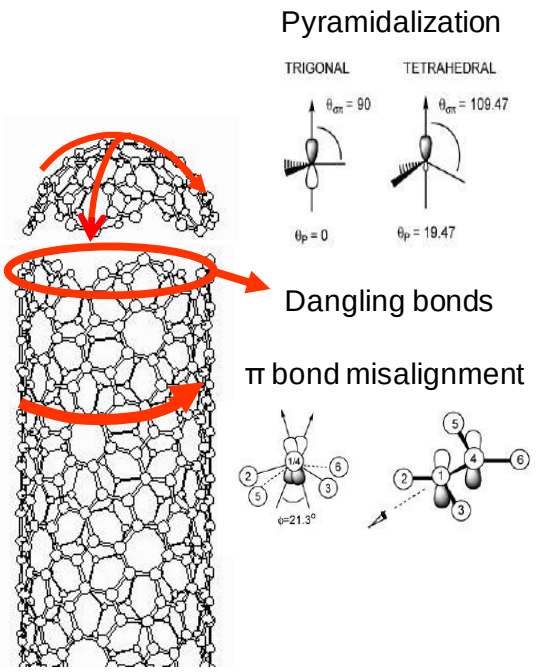

Figure 1.13. The chemistry of carbon nanotubes. The spherical geometry of CNT end caps places great strain on carbon – carbon bonds. Although sp^2 hybridized and thus triagonal the hemi spherical shape of the end caps forces the bond angles into something closer to a tetrahedral arrangement. Conversion of the trivalent carbons into tetravalent carbons by chemical reaction would relieve bond strain. Holes (vacancies) or open ends in the CNT structure are regions of incomplete bonding and thus reactive dangling bonds may be present. The curvature of the CNT walls induces pyramidalisation and misalignment of π bonds increasing the reactivity of constituent carbon atoms. Adapted from Niyogi et al 2002.

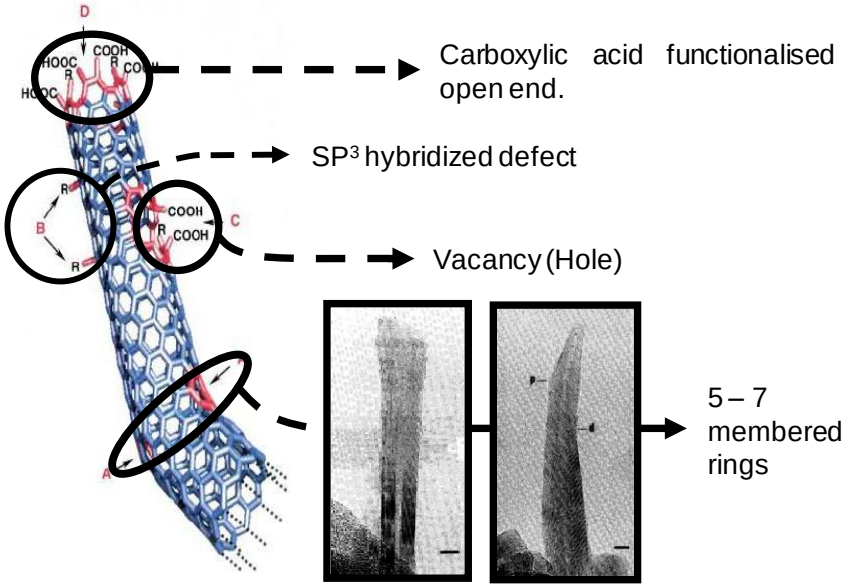

Figure 1.14. Typical defects in carbon nanotubes. From top to bottom of the picture; **(A)** open ends on CNT are often formed following acid purification and become oxidised and terminate with COOH groups. Other terminal groups can also be found including NO_2, OH, H and =O. **(B)** SP^3 hybridized defects can be found where a C – H or C – OH has been formed and the carbon atoms have moved from a triagonal to a tetrahedral arrangement. **(C)** As a result of synthesis or purification holes (Vacancies) can be left in carbon frameworks that act as local centres of reactivity. **(D)** The inclusion of 5 or 7 membered rings in the carbon hexagon framework causes the CNT to bend. The effect upon actual MWCNT is illustrated by two photographs. Adapted from Ebbesen & Takada 1995 and Hirsch 2002.

incorporated into polymers to enhance their mechanical properties (Sherman 2008). Other areas where MWCNT are expected to have a significant commercial impact are the aerospace industry and defence industries in the manufacture of body armour. The potential uses of SWCNT range from transparent electrodes in displays, flexible clear conductive films (for use in touch screens), computer hard drives, coatings, cathode ray lighting elements and for protection of telecom networks, sealed bearings and gaskets for semi conductors, automotive and aerospace fuel systems, molecular wiring, biosensors, drug delivery and semi-conductors (Thayer 2007). The potential applications of CNT also extend into the medical and biomedical worlds such as in radiation oncology and use in biopharmaceuticals, in particular drug delivery with CNT envisioned by attaching proteins and nucleic acids to the outside of nanotubes enabling transport into cells (Pantarotto et al 2004, Shi kam & Dai 2005).

1.22e CNT toxicity *in vitro*

As a result of superficial similarities to asbestos increasing effort is being made to characterise possible threats to human health posed by carbon nanotubes.

In studies conducted in 2005 Murr et al and Soto et al found comparable toxicity between ropes of iron contaminated SWCNT, bundles of MWCNT and chrysotile asbestos towards murine macrophages. At face value these studies alarmingly implied an equivalent level of toxicity between CNT and an asbestiform fibre. However the significance of the findings was diminished by the group's comparisons of fibrous particles of widely differing weights and surface area to mass ratios using a dose metric (mass/volume) that took none of these variables into account. The potential contribution of bio-available metals was also not considered as a toxicity

factor. Jia et al 2005 assessed and compared the toxicities of metal (iron, yttrium, nickel) containing SWCNT, MWCNT and C_{60}. Unlike Murr et al (2005) or Soto et al (2005), Jia et al (2005) found differential effects between particles with metal contaminated SWCNT inducing the greatest cytotoxicity and impairment on macrophage phagocytic ability. Although metal contamination was recognised as a possible contributing factor the extent of its effect was not investigated in this instance. The role of residual metals has taken on increasing importance in attempting to understand the basis of observed CNT toxicity. Works by Kagan et al (2006), Pulskamp et al (2007) and Schrand et al (2007) appear to have shown that only with a residual metal content can CNT demonstrate redox catalytic ability, cause cell activation, generate free radicals (including hydroxyl radicals), deplete intracellular GSH and reduce mitochondrial membrane integrity. That the level of metal contamination required to generate these effects varied between studies from 26% wt (Kagan et al 2006) to 0.26% wt (Schrand et al 2007) possibly reflecting sample variation. Guo et al (2007) found that the level of chelator mediated iron release from SWCNT and MWCNT varied greatly between samples and did not correlate with total iron content. Guo et al (2007) calculated the fluid accessible amount of iron to be between 1-7% wt and that this could release enough iron to cause single strand DNA breaks in an acellular assay. However what needs to be considered in future work is that metal mobilisation will in part be a function of surface area in addition to iron content and would therefore be affected by CNT aggregation. Different chelators may also be more or less effective at removing residual metals. Neither Kagan et al (2006), Pulskamp et al (2006), or Schrand et al (2007) determined how much of the metal in their samples was bio-available. The

above mentioned studies also disagreed on whether the free radicals generated (perhaps) as a result of the presence of residual metals were inorganic (Kagan et al 2006, Guo et al 2007) or biochemical (Schrand et al 2007) in origin. Other confounding factors not considered included the fact that un-purified CNT contain other residuals (graphitic fragments and fullerenes) that may contribute to toxicity. Sample purification can itself have effects on CNT that may influence toxicity through mechanisms not related to metal content (Guo et al 2007). Thus comparing purified and non purified CNT does not necessary mean that samples vary only in their levels of residual metals.

Although CNT toxicity has been associated with metal contamination, acid cleaning of SWCNT has paradoxically also been found to increase their toxicity. This may be due to incorporation of polar functional groups from acid treatment affecting solubility, material dispersion, distribution and the way the material partitions in biological environment (Guo et al 2007, Bottini et al 2005). Magroz et al (2006) supported this finding with their discovery that the presence of hydroxyl, carboxyl and carbonyl functional groups increased MWCNT cytotoxicity.

Carbon nanotube cytotoxicity towards HaCaT, HeLa and A549 cells and GSH depletion in rat lung epithelial cells has been attributed to ROS (Mann et al 2005, Sharma et al 2007, Schrand et al 2007) that may damage DNA. In mouse embryonic stem cells and HEK293 cells exposed to MWCNT and SWCNT respectively there was found to be increased expression of the tumour suppressor gene p53 and numerous DNA repair enzymes indicative of the occurrence of DNA strand breaks (Cui et al 2005, Zhu et al 2007). Exposure of MCF-7 cells to MWCNT resulted in micronuclei formation which appeared to result from both double strand breaks and

chromosome loss. This effect and the others outlined above may result from ROS production, direct interaction between CNT and DNA or interference of CNT with the apparatus of chromosome segregation (Muller et al 2008). In all of these works a mechanism to explain DNA damage needs to be positively identified. Where metal derived ROS are suggested to be the destructive agent then the level of damage needs to be related to the available (only a fraction of available metal is likely to be active however) metal content of the fibre. The species and origin of ROS responsible also needs to be discovered.

The level of CNT dispersion in aqueous solution is an important component of CNT toxicity as it determines the fraction of total surface area available to engage in damaging reactions. Both Davoren et al (2006) and Wick et al (2007) found that aggregated SWCNT to be more toxic than dispersed material. In a comparison of non-dispersed and MWCNT dispersed in pluronic F27 polymer only non-dispersed MWCNT induced significant cytotoxicity and IL-8 release from keratinocytes (Monteiro-Riviere et al 2005). Similarly aggregates of carboxylated SWCNT reduced smooth muscle cell growth (Raja et al 2007). None of these studies separated out the effect of dispersion from any effect of a protein or polymer coating of the CNT, the effect of surface modification was not considered.

Various works have begun to investigate the effects of CNT on cell activation, proliferation and gene expression. Exposure of human skin fibroblasts to 0.6 and 6μg/ml MWCNT for 48 hours resulted in apoptosis, necrosis and cell proliferation (Ding et al 2006). Apoptotic responses were also observed in human epidermal keratinocytes exposed to 25μg/ml SWCNT for 24 hours (Cui et al 2005). Schrand et al (2007) linked the ability of SWCNT to induce apoptosis to their capacity to

activate matrix protein signals. It should be kept in mind that different CNT types may activate cells by different mechanisms (and the morphological nature of CNT at the time of their exposure needs to be considered as well as the presence of contaminants or covalently bonded functional groups). Induction of stress response pathways and release of pro-inflammatory cytokines has been found to follow CNT exposure. A clear increasing IL-8 dose response was established after HEK treatment with 100-400μg/ml MWCNT for 24 hours. High dose (400μg/ml) exposure of HEK to MWCNT for 24 hours caused disruption of cell growth, development, proliferation, vesicular trafficking, endocytosis and the actin cytoskeleton (Witzman & Monteiro-Riviere 2006). A comparatively lower dose (6μg/ml) of MWCNT was observed by Ding et al (2006) to regulate genes for STAT1, IFN7, p38, ERK MAPK and those associated with induction of apoptosis. Whilst the aggregate of these works suggests CNT induce cellular apoptosis and activate cells to release pro-inflammatory mediators these are studies are difficult compare making general conclusions hard to draw. The studies used widely differing doses; effects at different doses may suggest that different CNT have different potentials to induce cellular effects. However this issue may be difficult to clarify due to the widely differing sources of CNT and their contaminants. Dose levels may also influence the mechanism that contributes to a given response and ideally should represent a level that is physiologically relevant. The significance of the ability of CNT to activate cells needs to be established by comparison (through appropriate dose metrics) with other pathogenic materials.

Any fibre shaped (high aspect ratio) particles raise the spectre of asbestos; there is concern that CNT, which are high aspect ratio nanoparticles (HARN), might have asbestos like pathogenicity.

A comparison of MWCNT, carbon nanofibres, and carbon nanoparticles (minimum aspect ratios of 80, 30 and 1 respectively) revealed by MTT assay at doses of 0.2, 0.02 and 0.002μg/ml for 4 days in H596 lung tumour cells a reduction in viability inversely proportional to their aspect ratios. Carbon particles were concluded to be most toxic due to the greater number of dangling bonds (Magrez et al 2006). This might suggest that for CNT at least a fibrous nature is not predictive of toxicity, a result that could be supported due to their ability to aggregate. However Magrez et al's (2006) work can't be taken at face value. Several parameters were not accounted for; particle size was not expressed in terms of length (important when considering fibre toxicology), materials were not characterised fully, and the dose metric selected may not have been appropriate for the endpoint being examined (i.e. surface area was not considered). Aspect ratio may also not be a good basis for comparison of particle toxicity. Aspect ratio can be used to characterise a material as either a fibrous particle or particulate, however not all fibres are toxic as toxicity is partially dependent upon fibre length. As long as a particle is thin enough it can be relatively short (e.g. although MWCNT can be fibrous they aren't necessarily long according to the ability or inability of a macrophage to phagocytose them) and still have a high aspect ratio. Thus SWCNT can have diameters of 1nm or less but a length of only several hundred nanometres, but this still gives then as aspect ratio of greater than 3:1 and therefore makes them toxicologically speaking a fibre. It could therefore be argued that aspect ratio is not an issue for fibres as thin as CNT

(assuming they exist as dispersed individual fibres) and that length is more important since being too long can hinder phagocytosis (Donaldson & Tran 2004). The aspect ratio of CNT is also likely to vary depending how aggregated they are, aggregation may in any case make the notion of aspect ratio irrelevant as individual fibres are no longer being dealt with. The effect of adsorption of the gelatine dispersant on the toxicity of the materials was not controlled for (this issue crops up in numerous studies). Finally Magrez et al (2006) did not compare the toxicity of CNT against other known pathogenic particles and fibres. This too is an issue for other studies and it makes it difficult to determine the toxicity of and the level of hazard that CNT (with respect to other materials) pose to human health. A comparison of MWCNT 825nm long (designated long) with 220nm long (designated short) to induce TNFα secretion from THP-1 cells revealed very little difference related to size (Sato et al 2007). These fibres however fall far short of definitions of long such as the ability of macrophages to phagocytise them completely often used in the context of fibre paradigm (Donaldson & Tran 2004).

Uptake of CNT can occur in some cells following exposure. Protein functionalised SWCNT passively crossed fibroblast membranes (Bianco et al 2005) and was endocytosed by HL60 cells as a result of SWCNT binding cell surface receptors (Sho Kam & Dai 2005). The destination of a functionalised CNT appears to depend upon its cargo. In mouse 3T3 and human 3T6 fibroblasts, FITC labelled SWCNT accumulated in the cytoplasm whilst protein FITC conjugated SWCNT penetrated the nucleus (Pantarotto et al 2004). Subcutaneous implantation of SWCNT in rats (for one week at 0.1mg) indicated length may determine internal cellular localisation. SWCNT of 220nm were found primarily in macrophage lysosomes

whilst SWCNT of 825nm were aggregated in macrophage cytoplasm (Pulskamp et al 2007). In human epidermal keratinocytes MWCNT were retained in cytoplasmic vacuoles as well as free in the cytoplasm close to the nucleus (Monteiro-Riviere et al 2005).

When examining fibre uptake by cells certain points need to be taken into account. The nature of the material (fibrous or aggregated) may determine how it interacts with a cell membrane and the nature of internalisation that follows. The afore mentioned works all need to determine if the internalisation observed in the cell types used were unique to CNT. If internalisation is the end point under study then the dose may have to be expressed in terms of fibre number with the dose internalised also determined. The relevance of *in vitro* work to *in vivo* has to be thought about in future studies, inhalation will bring fibres into an environment in which they will be modified by surface coatings of endogenous molecules. How this affects fibres abilities to enter cells or be taken up by them needs to be considered.

1.22f Carbon nanotube toxicity *in vivo*

A small but growing body of work has started to examine the effect of CNT *in vivo*. Raw CNT (rCNT), HiPco CNT (hpCNT) and electric discharge CNT (edCNT) dispersed in mouse serum and intratracheally instilled into mouse lungs produced mortality amongst high dose groups but few clinical signs in low dose groups (0.1mg/animal). At 7 and 90 days post exposure the lungs of high dose groups (0.5mg/animal) contained AM harbouring large particle aggregates that had entered the alveolar septa and formed granulomas. This pathologic ability was attributed to CNT structure rather than metal content although some fatalities associated with edCNT may have been linked to the presence of nickel (Lam et al 2003). Pulmonary

exposure of rats to ground or un-ground MWCNT for 60 days dispersed in 1% Tween revealed that the more effectively dispersed ground material caused greater inflammation than un-ground material. However un-ground samples were found to be more bio-persistent and induced greater fibrosis with the amplitude of fibrosis paralleling the fraction of material retained in the lungs. Both MWCNT caused granuloma formation that was localised bronchially for un-ground material (reflecting limited pulmonary dispersion) and interstitially and in alveolar spaces for ground material. *In vivo* both MWCNTs induced TNFα secretion although *in vitro* un-ground MWCNT failed to induce the same effect in cultured macrophages (Muller et al 2005).

Guinea pigs were pulmonary instilled with a single dose (12.5mg/animal) of five different MWCNT. After 90 days animals were found to have suffered perivascular, peribronchial and interstitial infiltration of inflammatory cells, central and peripheral emphysema, atelectasis and alveolar exudates. Granulomas were observed centred on CNT material although these were few, focal and did not appear to be prominent. The observed pathologies appeared to result from a combination of physical structure and total insolubility (Grubek-Jaworksa et al 2006).

Differential effects of instilling or inhaling MWCNT have been studied in mice. MWCNT dispersed in 1% Tween-80 induced inflammation at points of deposition along bronchial wall and structural damage to alveoli after 24 days. Inhaled material had little impact on the bronchial wall but caused thickening of alveolar walls. The large aggregates formed during instillation were deemed to cause the greater severity of response (Li et al 2007). In mice, pharyngeally aspirated SWCNT formed both compact aggregates and dispersed structures, the former being associated with

granulomatous inflammation. Progressive interstitial fibrosis' but no persistent inflammatory response and alveolar wall thickening was observed. There was also dose dependent proliferation of and damage to alveolar type II cells with associated depletion of GSH, a short term peak of pro-inflammatory cytokines and delayed but significant increase in TGF-β (Shvedova et al 2005). In mice deficient in vitamin E, SWCNT instillation caused reduced body weight, depletion of GSH and ascorbate, and accumulation of lipid peroxides. The deficiency accentuated the increase in infiltrating PMNs, elevation of LDH and BAL protein levels and IL-6 and TNFα production with enhancement of TGFβ responses. In normal and deficient mice, after 28 days, granulomatous lesions became the major inflammatory response (Shvedova et al 2007). Sparse fibrotic lesions were observed in rats treated with SWCNT dispersed in pluronic F68 that were distributed through the alveolar region and associated with SWCNT containing AM clusters, no granulomas were described neither was an overt inflammatory response. The SWCNT induced injury was blamed on a combination of metal contamination and high surface area (Magnum et al 2006).

As with all *in vivo* studies of fibre toxicity those examining the toxicity of carbon nanotubes need to examine exposure-dose-response relationships, a maximum tolerated dose also needs to be established (parameters for which needs to be decided). Before introduction of CNT into an animal it should be fully characterised to determine possible physicochemical reasons for toxicity such as the availability of metals (the extent of leaching needs to be determined) and the nature of CNT *in vivo* (i.e. the degree of aggregation). Fibre length and diameter have to be recorded (although it is not entirely clear how appropriate this is when CNT aggregate). It

also has to be considered that any observed effects of instillation/inhalation of CNT (and mechanisms of action underlying these effects) are the result of the physical nature of the material on or as a result of its delivery. The degree of aggregation will affect the extent that CNT disperse in the lungs; this may be exacerbated by instillation possibly placing limitations on data. Some studies have attempted to circumvent this problem by pre-dispersing CNT in a surfactant such as Tween-80 however this may prevent adsorption of endogenous material to CNT *in vivo* altering the nature of toxicity.

Cardiovascular and systemic effects of carbon nanotubes are increasingly being investigated; particular focus has been given to the cardiovascular system. Treatment of ApoE-/- mice with SWCNT (32.61mg/m^3) for 8, 16 and 24 days resulted in pulmonary, aortic and cardio activation of haemoxygenase-1, damage to aortic cell mitochondrial DNA with depletion of GSH, and plaque formation that was significantly increased on a high fat diet. There was also acceleration of atherosclerotic progression with increases in VCAM-1 positive cells and plaque-associated macrophages. Influence of SWCNT upon cardiovascular disease may have occurred directly with SWCNT translocation from the lung into systemic circulation or indirectly as a result hypoxemia or pulmonary mediators from SWCNT exposed lung inflammation (Li et al 2007). In this instance fibre characterisation would be important as translocation depends both on the size and dose of the fibre and thus its likelihood could be assessed. In rabbits dosed intravenously with pluronic F108 dispersed SWCNT no significant temporary accumulation of SWCNT were found in tissue reservoirs including the kidneys, lungs, spinal cord, bone muscle, pancreas, intestine and skin. Only liver

significantly sequestered SWCNT but with no signs of acute toxicity (Cheruki et al 2006). Future studies need to compare the kinetics and effects of dispersed CNT with non dispersed samples of the same material as modification of the CNT by the presence of surfactant may modify their kinetics, retention and toxicity. Mice injected with Yttrium-86 labelled SWCNT concentrated the CNT in kidneys, liver and spleen (McDevitt et al 2006). In the skin granuloma formation was noted in rats subcutaneously injected with Hat stacked carbon nanofibres that after four weeks was replaced by fibrous connective tissue (Yokoyama et al 2005). The meaning of granuloma formation in general and in Yokoyama et al's (2005) work in particular can be difficult to quantify. Yokoyama's (et al 2005) work was uncontrolled in respect to any other particle and it is unclear if what they observed was in response to the presence of a large amount of un-degradable material.

The most common effect of pulmonary exposure appears to be a granulomatous response either in response to a unique pathogenicity factor of CNT or simply as a foreign body response. The meaning of granuloma formation following CNT exposure needs to be established, is it a response that can be tracked over a range of doses or does it occur only in response to an acute high dose exposure? Is it a response for which there is threshold dose? It must be remembered that the affects and their underlying mechanisms at high doses may differ to those occurring at low doses. The relevance of granuloma formation as an endpoint in response to CNT exposure also needs to be established. Does it simply occur in response to aggregate nature of the material? This could be could be established by comparing a dispersed CNT system with an identical aggregated system over a range of doses. On a more limited basis fibrosis was also observed however an acute inflammatory response

does not appear to be key feature of exposure. This would tend to contradict *in vitro* findings which suggest CNT can induce an inflammatory effect thus the effects of CNT *in vitro* need to be linked to those *in vivo*.

1.22g Reports showing low or no toxicity of carbon nanotubes

The toxicity of carbon nanotubes is not straight forward clear cut or universally accepted. A number of studies have failed to find evidence of CNT pathogenicity. The pathogenicity of some particles and fibres has been attributed in part to their generation of free radicals. Dispersed in SDS MWCNT were found not to generate ROS, instead a free radical scavenging capacity was observed that was ascribed to the chemistry of the carbon framework in particular high electron affinity of constituent carbon atoms molecular orbital's. Based upon these findings it was suggested inflammatory responses reported in animals exposed to CNT should be attributed to features other than particle generated free radicals (Fenoglio et al 2005). These results mirror those of Chen et al (2004) who found C_{60} incubated with RAW 264.7 macrophages exhibited antioxidant properties. Other studies have found that a lack of cytotoxicity is associated with CNT exposure. No evidence of membrane damage, apoptosis or necrosis was found after SWCNT or MWCNT treatment of NR8383 macrophages for 72 hours, although intracellular ROS and mitochondrial damage was detected (Pulskamp et al 2007). HeLa cells exposed for up to four hours to SWCNT dispersed in FBS supplemented DMEM demonstrated no cytotoxicity although SWCNT did associate with organelles including the nucleus. Cellular growth rates were unaffected and mitochondrial superoxide production was unchanged (Yehia et al 2007). In a comparison of the cytotoxic potential of graphite, CNT or C60, graphite induced more extensive macrophage activation (Fiorito et al

2007) possibly as a result of the greater number of dangling bonds (Chlopeck et al 2006). Functionalization or incorporation in polymers may modulate CNT toxicity- for example, a MWCNT - hydroxyapatite matrix supported osteoblast growth (Balani et al 2007). Tert-butylphenylene- functionalised ultra- short and purified SWCNT as well as polypropylene fumerate and fumerate diacrylate (PPF/PF-DA) composites of the three were found to be non- toxic and allowed fibroblast attachment (Shi et al 2007). The extent of functionalization influences CNT toxicity. For example Sayes et al (2006) found that the toxicity of SWCNT appeared to decrease proportionally to the extent of functionalization whilst glucosamine functionalization of SWCNT improved their compatibility towards 3T3 fibroblasts possibly as a result of increasing hydrophilicity reducing their potential to interact with cell membranes (Nimmagadda et al 2005).

Conclusions - The potential of particles and fibres to induce inflammation and toxicity appears to depend strongly on their ability to excessively stimulate (e.g. an inflammatory response) or disrupt normal physiological processes (e.g. clearance from the lungs). This is often linked to their physicochemical properties, presence of contaminants (organic or inorganic) and the nature, extent and duration of exposure. Often particle and fibre toxicity and inflammatory potential have been linked to their ability to generate or stimulate production of free radicals and induce a state of oxidative stress in exposed cells and tissues. The ability to generate or stimulate production of chemically reactive species appears to be due either to the physical dimensions of the material (such as during frustrated phagocytosis induced by asbestos fibres) and/or to the presence of reactive functional groups or atoms at the surface of the material (such as the silanol groups found on the surface of DQ12).

As the size of a material decreases and approaches the nanoscale its ability to generate reactive species and induce toxicity appears to increase.

Carbon nanotubes are a relatively new material with nanoscale dimensions that can be either fibrous or particulate in nature and significantly bear superficial resemblances to materials with known toxic potentials. Although the toxic potential of these materials is as yet undetermined they are set to be increasingly used in a broad range of industries as a result of their unique structural and electronic properties. The work presented hear set out to investigate the toxic and inflammatory potential of carbon nanotubes *in vitro* and *in vivo* according to paradigms about what makes a particle or fibre toxic developed from investigating the toxicity of Asbestos and quartz. Thus the ability of carbon nanotubes to generate free radicals, induce oxidative stress and cytotoxicity, and ultimately and an inflammatory response was investigated.

Chapter 2

Materials and methods

2.1 Culture of Human Type II Alveolar epithelial cells (A549)

The human type II alveolar epithelial cell line, A549, was cultured in Dulbecco's modified eagle medium (DMEM) (Sigma, PAA) supplemented with heat inactivated 10% foetal calf serum (FCS or FBS), 2mM glutamate and 100 $IU.ml^{-1}$ streptomycin and penicillin at 37°C in a humidified atmosphere containing 5% CO_2. Cells were cultured to confluent monolayers in $162cm^2$ tissue culture flasks (CoStar, Corning) at which point they were washed in $Ca^{2+/}Mg^{2+}$ free phosphate buffered saline (PBS-CMF) (Sigma, PAA) then harvested by incubation with 3ml Trypsin-EDTA for 5 minutes at 37°C. Trypsin was deactivated by addition of 27ml 10% DMEM and detached cells collected by centrifugation at 1000 rpm for 5 minutes. The cell pellet was re-suspended in fresh media and cells seeded at the appropriate concentration for experiments or further diluted for continuous cell culture. Cells were maintained in culture or used in experiments up to passages 25-30.

2.2 Particles

Two types of multi wall carbon nanotube (MWCNT) were obtained from Nanolab Inc. (Newton, MA, USA), a sample containing MWCNT of lengths 5-20μm and designated long MWCNT (LMWCNT or LMW) and a sample designated short MWCNT that contained MWCNT with lengths in the range 1-5μm (SMWCNT or SMW). The MWCNT were synthesised by Catalytic vapour deposition (CVD) over iron nanoparticles on a ceramic support and purified using hydrochloric (HCL) and hydrofluoric acid (HF) prior to being filtered, neutralised and reground to a powder. Sample purity was given as 95%wt.

Ultra fine carbon black (ufCB) (Printex 90) was generously provided by Napier University (Edinburgh, UK).

Titanium dioxide (TiO_2)

DQ12 Quartz (DQ12)

Diesel Exhaust particles (DEP)

Short Amosite (SFA) – generously provided by the institute of occupational medicine.

Long Amosite (LFA) – generously provided by the institute of occupational medicine.

2.3 Particle Dispersion

For most *in vitro* cellular work particles were suspended in serum free DMEM and ultra-sonically agitated for up to 14 minutes by bath sonicator to achieve an even suspension (judged by eye). In some instances particles were prepared in cell culture medium containing 2% (v/v) FCS that acted as a co-incidental dispersant. The surfactant Tween-80 (Sigma) was used during some a-cellular electron spin resonance (ESR) assays at a 1% (v/v) concentration to achieve a more stable separation and dispersion of samples following sonication. During a single animal study the surfactant DPPC (Sigma) was used to disperse MWCNT and a panel of other particles and fibres in sterile saline prior to peritoneal instillation.

2.4 Particle Characterisation: Scanning Electron Microscopy (SEM)

Both LMWCNT and SMWCNT were characterised by SEM at the Institute of Occupational Medicine (IOM, Edinburgh, UK). Briefly samples were suspended in de ionised distilled water at 1mg/ml and sonicated for 14 minutes with manual shaking to prevent sedimentation. Working concentrations of 10, 50 and 100µg/ml were prepared and 50µl pipetted onto glass cover slips pre-stuck to SEM stubs, cover-slips were dried over night at room temperature (RT) under foil. Samples were then prepared, examined and images taken using SEM equipment at the IOM.

2.5 Particle characterisation: Metals analysis

Samples were prepared for analysis of their metal content using a modification of the OSHA ID121 and analysed by inductively coupled plasma/Atomic emission spectrometry (ICP/AES). A brief description of the process follows, for full details refer to the OSHA ID121 document included. Samples were aspirated into the flame of an atomic emission spectrometer and subjected to nebulisation, desolvation, liquefaction, vaporization, atomization, excitation and ionization. The emission of light during atomization and

excitation stages was measured at the characteristic wavelength for the element/s of interest. For emission spectroscopy samples were introduced into flame, atomized and excited. The light emission from excitation was isolated and measured (the intensity of light emitted being proportional to the concentration of the element present). Samples were analysed for the presence of the following transition metal elements: cadmium, cobalt, chromium, copper, iron, manganese, nickel, titanium, vanadium and zinc.

2.6 Particle Characterisation: Electron Spin Resonance (ESR)

The ability of MWCNT and other particles to generate free radicals was investigated by ESR using the spin trapping agent 1-hydroxy-2, 2, 6, 6-tetramethyl-4-oxo-piperidine (TEMPONE-H) (Alexis biochemicals). ESR detects the spins of un-paired electrons however in aqueous conditions at room temperature the sensitivity of this technique is relatively low and the half life of free radicals is often too short to detect and quantify their presence. Sensitivity is enhanced by spin trapping, a technique in which non paramagnetic spin traps react with free radicals and form semi stable paramagnetic compounds that accumulate until their concentration reaches detectable levels. Spin traps are organic molecules able to form stable radicals by reacting with free radicals and producing a spin trap radical reaction product; with longer half lives these are easier to detect and measure (Rohn & Kroh 2005, Bartosz 2006). Spin traps can be differentiated as specific or non specific. Specific spin traps react with radicals at a double bond producing adducts whose ESR signal is characteristic for the original radical. Unspecific spin traps that include the hydroxylamines generally have higher reaction velocities, better stability and can be used at much lower concentrations (Rohn & Kroh 2005). The hydroxylamine TEMPONE-H has been used for the detection of superoxide and peroxynitrile radicals (Bartosz 2006).

The spin trap TEMPONE-H was dissolved in PBS-CMF containing 10^{-2}M Ethylene diaminetetraacetic acid (EDTA) (Sigma) to chelate contaminating metal ions. Stock aqueous dispersions of reference particles and MWCNT were made up to 1mg/ml in PBS-

CMF or 1% tween-80 (Sigma) PBS-CMF then sonicated for 14 minutes. Assessment of free radical activity was carried out on 1ml working solutions containing 10µg/ml particles and 10µl 10^{-1} M TEMPONE-H/EDTA in PBS-CMF warmed to 37˚C on a heating block, working samples were briefly vortexed and transferred to a 10µl capillary tube. Readings were taken from samples every 15 minutes for one hour. Confirmation of the presence and identity of free radicals was investigated using antioxidants. Working concentrations of particles and TEMPONE-H/EDTA were prepared in antioxidant solutions at concentrations of; 10mM glutathione (Sigma) or 200U Superoxide dismutase (Sigma) made up in PBS-CMF then assayed as previously described. With the exception of TEMPONE-H/EDTA all samples were prepared fresh on the day of assay.

2.7 Treatment of Cultured cells with particles

A549 cells were treated with MWCNT or reference particles in a FCS free (0%) or reduced (2%) FCS DMEM medium. Cells were harvested as previously described and counted by haemocytometer before being seeded into 6, 12 or 24 well plates (Corning) at 150,000 or ~90,000 cells/ml (seeding concentrations titrated as current cell line aged) respectively. Cells were allowed to attach overnight and reach~ 70% confluence in 10% DMEM before being washed with pre-warmed PBS-CMF and the medium replaced with 0% or 2% DMEM for 24 hours (Serum starvation). Starvation medium was removed and cells washed with PBS-CMF before treatments were applied. Treatments were prepared fresh for each experiment in pre-warmed 0% or 2% DMEM at stock concentrations of 1mg/ml and bath sonicated for 14 minutes (with agitation every couple of minutes to prevent sedimentation) prior to working treatment dilutions being prepared (treatments were calculated as µg/cm^2 of well surface) (See table). Treated cells were incubated at 37˚C and 5% CO_2 for times according to the assay being performed.

Assay	Treatment time (hours)	Particles	Concentration (µg/ml)	Concentration (µg/cm^2)
Plasmid Assay	16 hours	LMWCNT, SMWCNT	100, 500	N/A
		ufCB	3.8 - 497	
ESR		LMWCNT, SMWCNT, DQ12, ufCB, TiO_2	10	N/A
LDH cytotoxicity	24	LMWCNT, SMWCNT, DQ12, TiO_2	20 - 200	10.5 - 105.3
Haemolysis		LMWCNT, SMWCNT, DQ12, TiO_2	1000 - 4000	N/A
IL-8 ELISA	6, 24, 48	LMWCNT, SMWCNT	20 - 200	10.5 - 105.5
		DQ12	20 - 80	10.5 - 42.1
Total GSH	24, 48	LMWCNT, SMWCNT, DQ12	100 - 500	10.5 - 52.6
mRNA Extraction	4, 24	LMWCNT, SMWCNT, TiO2, ufCB	100, 500	10.4, 52.6
		DQ12	100	10.4
NFκB Immunocytochemistry	4	LMWCNT, SMWCNT, ufCB, TiO_2, DEP, DQ12	10, 100	5.3, 52.6

Table 2.1. Assays performed *in vitro* and particle concentrations used in µg/ml and µg/cm^2. A table of the assays performed during the course of this work (from the left, column 1), exposure and treatment times (column 2), particles used including; Long multi-walled carbon nanotube (LMWCNT), short multi-walled carbon nanotube (SMWCNT), ultra-fine carbon black (ufCB), quartz (DQ12), titanium dioxide (TiO_2) and diesel exhaust particles (DEP)

2.8 Cell Morphology

A549 cells were seeded onto autoclaved glass cover-slips sterilely placed into six or 12 well plates at concentrations of 150, 000 cell/ml and treated with LMWCNT, SWCNT, DQ12, DEP, ufCB or TiO_2 for four or 24 hours in 0% and 2% DMEM. Treatments were removed and discarded and cells washed twice with PBS-CMF before being fixed and stained by their sequential treatment with 1ml methanol, Eosin and haematoxylin for one minute. Stained cover slips were washed twice with distilled water, allowed to dry and then mounted onto slides with DPX (BDH) for visualisation.

2.9 Assessment of cytotoxicity: Lactose dehydrogenase (LDH) assay

The extent of cell damage and death in response to treatments was assessed by measurement of plasma membrane damage indicated by the release of the stable cytoplasmic enzyme LDH into the cell culture supernatant. Release of LDH was detected using an LDH assay kit (Roche) where enzyme activity is determined in an enzymic test. Briefly, NAD^+ (supplied) is converted to $NADH/H^+$ as LDH in culture medium catalyses the conversion of lactate to pyruvate, H/H^+ from $NADH/H^+$ is catalytically transferred (by supplied diaphorase) to a yellow tetrazolium salt turning it to a red formazan product. Increases in the number of dead or damaged cells results in increased levels and activity of LDH in cell culture supernatant that directly correlates to the amount of red Formazan salt formed in a given period of time. The amount of colour formed (quantified by spectrometry) is directly proportional to the number of damaged cells.

Cells were seeded into 24 well plates at 90 000 cells/ml and cultured over night prior to serum starvation (0 or 2% DMEM) and particulate treatment. Treatments of MWCNT, DQ12 and TiO_2 were applied at least in duplicate and incubated with cells for 24 hours. Assay controls consisted of a medium only back ground control, a low (negative) control from medium alone treated cells and high (positive) controls derived from cells treated with 1% Triton-X100 (Sigma). At the end of the treatment period plates were centrifuged at 250g for 10 minutes and supernatants transferred to labelled eppendorf tubes that were spun down in a micro-centrifuge at 13000rpm for 5 minutes (to sediment out remaining particles that could interfere with the assay). Supernatants were transferred to clean labelled eppendorfs for temporary storage or 96 well plates for assaying. To perform the assay spun treated cell supernatants were placed in triplicate and diluted 1 in 3 in 96 well plates with DMEM (0% or 2% depending on the make-up of the original particle treatments) to a final volume of 100µl. Cytotoxicity LDH assay solution A was diluted 1 in 45 into solution B and 100µl applied to cell supernatants in 96 well plates. Plates were covered to protect them from light

and briefly mixed on a plate shaker before being incubated for a maximum of 30 minutes at RT. Plates were then read on a micro plate reader at 490nm. Cytotoxicity was calculated using the following equation:

$$\text{Cytotoxicity (\%)} = \frac{\text{Experimental value} - \text{Negative control}}{\text{Positive control} - \text{Negative control}} \times 100$$

2.10 LDH Adsorption assay

Extraction of LDH from A549 cells cultured to confluence in 10% DMEM in six well plates was carried out by first removing growth medium and washing cells in PBS-CMF. Cells were then scraped in 1ml PBS-CMF and transferred to 1.5ml sterile eppendorf tubes that were vortexed thoroughly and sonicated in a bath sonicator for 5 minutes with repeated vortexing every minute. Cycles of sonication and vortexing had the effect of mechanically disrupting cellular plasma membranes resulting in lysis and release of intracellular LDH into the PBS. Eppendorfs containing lysed cells were micro-centrifuged for 5 minutes at 13000rpm and supernatants transferred to fresh eppendorf tubes. Stock 1mg/ml suspensions of MWCNT were prepared in PBS or DMEM, sonicated and diluted to create a concentration range from 0 - 200µg/ml. Aliquots of 150µl were transferred from each MWCNT concentration to a 96 well plate in triplicate and mixed with 75µl LDH solution; plates were incubated for one hour at 37˚C and spun at 250g for 10 minutes. Volumes of 33µl of each sample were placed in triplicate into a fresh 96 well plate and diluted 1:3 in PBS or DMEM. Determination of LDH remaining in solution was carried out by LDH cytotoxicity kit (Roche) as previously described. Results were plotted as average optical density for each sample (nm) (y-axis) against MWCNT concentration (x-axis).

2.11 BCA Total protein assay

The protein concentrations of samples were measured using the Bicinchoninic acid (BCA) protein assay. The assay is based upon the biuret reaction, protein in a sample oxidises copper (II) to copper (I) ions each of which is chelated by two BCA molecules forming a purple reaction product that absorbs strongly at 562nm.

A stock solution of Bovine serum albumin (BSA) (Sigma) was prepared at 2mg/ml in PBS and serially diluted in 0.1mg/ml increments to generate standard curve, a volume of 10µl of each standard and sample was added in triplicate to a 96 well plate. Bicinchoninic acid solution was generated by diluting copper (II) sulphate solution 1:50 in to Bicinchoninic acid, 200µl of BCA solution was then added to samples and standards on the 96 well plates. Plates were incubated for 30 minutes at 37˚C and the absorbance read at 570nm on a microplate reader. Linear regression was used to determine the actual protein concentration of samples.

2.12 Assay for the detection of total intracellular glutathione (GSH)

Glutathione (GSH) is an abundant intracellular antioxidant whose concentration is an indicator of oxidative stress; GSH exists in cells in an oxidised sulphydryl (GSSG) or reduced sulphydryl (GSH) form. This assay is designed to spectrographically detect oxidation of GSH by 5,5' –dithiobis[2-nitrobenzoic acid] (DNTB) that forms a yellow derivative 2-nitro-5-thiobenzoic acid in the presence of β-Nicotinamide adenine dinucleotide phosphate (NADPH) following the conversion of GSSG to GSH by glutathione reductase. The rate of formation of the yellow 2-nitro-5-thiobenzoic acid depends on the concentration of total intracellular GSH (GSH+GSSG) within the sample. The actual GSH concentration is determined from a standard curve.

The intracellular glutathione concentration was determined in A549 cells exposed to MWCNT and DQ12 for 24 or 48 hours in 0% or 2% DMEM respectively. Cells were cultured and seeded into six well plates as previously described at concentrations of 150 000

cells/ml. Stock concentrations of MWCNT and DQ12 were prepared in either 0% or 2% DMEM, sonicated and diluted to working concentrations of 10.4μg/cm^2 (100μg/ml), 31.5μg/cm^2 (300μg/ml) and 52.6μg/cm^2 (500μg/ml) in appropriate media. Treatments prepared in 0% DMEM were incubated with cells for 24 hours, treatments prepared in 2% DMEM were incubated with cells 48 hours prior to total GSH assay being performed. To carry out the assay particle-containing media was removed and cells washed twice with 2ml cold PBS-CMF, cells were then scraped in 1ml ice-cold extraction buffer and transferred into 1.5ml eppendorfs. The cell suspension was vortexed and sonicated repeatedly and cell debris collected by centrifugation at 5000 rpm for 5 minutes at 4˚C, pellet and supernatant were then stored on ice prior to analysis of GSH content. A glutathione concentration series was prepared in 0.1M phosphate buffer with 5mM EDTA (KPE), as well as 2mg/3mls DNTB, 2mg/3ml β-NADPH and 40μl/3mls glutathione reductase. To a blank 96 well plate, 20μl GSH standards and 20μl samples were added, equal volumes of DNTB and glutathione reductase solutions were mixed together and 120μl of this solution was added to each well, the plate was then incubated for 30 seconds and the absorbance immediately read at 405nm in a microplate reader. Readings were then taken every 30 seconds for 2 minutes. This process was repeated at least twice more for each sample; the rate of 2-nitro--thiobenzoic acid formation was then calculated (from change in absorbance per minute). Total GSH concentration in samples was then calculated by linear regression from the GSH standard curve, total GSH was expressed as μM/mg protein. Total protein in each sample was calculated by BCA protein assay.

2.13 Glutathione Adsorption assay

The ability of MWCNT to adsorb GSH was tested to indicate possible MWCNT interference with the GSH assay. Particles were made up to 1mg/ml in PBS and sonicated for 14 minutes; a stock of GSH was prepared in PBS and used to dilute particles to concentrations of 100, 300 and 500μg/ml in a final GSH concentration of 25μg/ml. Particles were

incubated in GSH solutions at RT for 1 hour protected from light, a GSH assay was then performed as described above

2.14 ΦX174 plasmid assay

The plasmid assay is a cell free assay used to detect particle surface associated free radical activity. Free radicals can damage the bonds that hold plasmid DNA in a supercoiled compact state causing it to unwind or relax to form a circular DNA molecule. Further attack can linearise circular DNA and continued assaults may cause the DNA molecule to fragment. The extent of this damage can be monitored by DNA agarose gel electrophoresis. Supercoiled DNA forms a tight compact ball or knot that migrates easily through the agarose matrix, relaxed DNA and linear DNA are both impeded becoming entangled by the agarose matrix (but to different extents). The different forms of DNA thus travel though agarose at different rates and are therefore separated from each other in the order (closest to furthest from loading point on the gel); relaxed, linear, supercoiled DNA. The extent of damage to the DNA molecules is detected by monitoring depletion in the intensity of the supercoiled band on the gel. Serial dilutions of MWCNT were prepared from a stock 1mg/ml solution prepared in PBS or 1% PBS/Tween-80. To assess the potential of MWCNT to cause free radical damage dilutions of particles were incubated with 1.16µl (290ng) closed circular superhelical ΦX174 RF1 plasmid DNA (Invitrogen) prepared to a final volume of 20µl. A negative control of un-treated plasmid was prepared as was a linear control by digesting plasmid DNA with 0.5µl of the restriction enzyme PST-1 (*Providenica stuatii*) in 2µl of its corresponding buffer. Some particle samples were spiked by the inclusion of 1mM hydrogen peroxide. Samples were incubated at 37˚C over night on a thermomixer (Eppendorf).

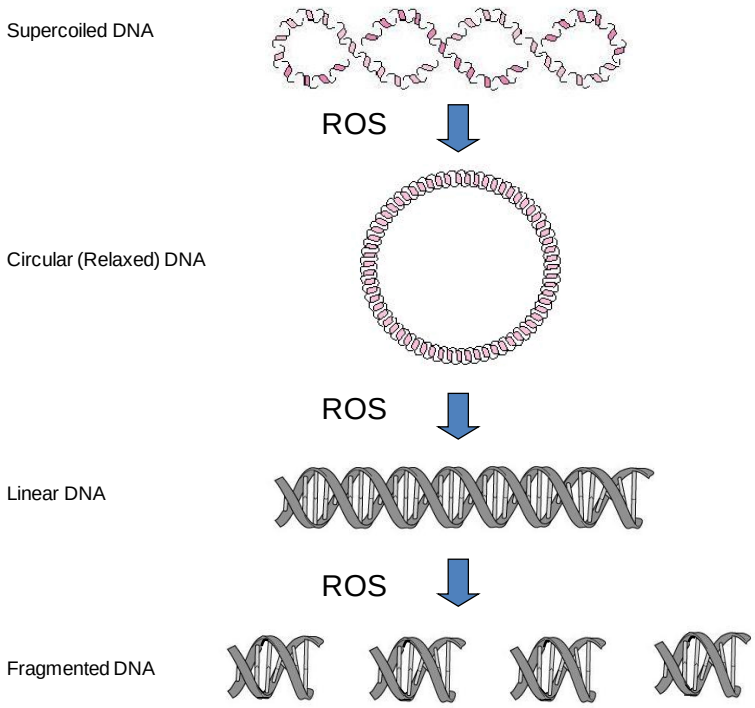

Figure 2.2 The different stages of plasmid DNA cleavage induced by reactive oxygen species (ROS) and the different structural states of DNA that result. Plasmid DNA begins in a supercoiled state but after bond cleavage induced by ROS (the hydroxyl radical) relaxes to an open circular structure described as relaxed. The supercoiled form of the molecule migrates quickly through the agarose, relaxed circular DNA moves most slowly through the gel matrix. Continued free radical attack can cause double strand cleavage resulting in a linear piece of DNA. This migrates through agarose at a velocity intermediate between circular and supercoiled forms. Under extensive free radical insult the DNA strand may fragment with the small segments running off the gel or forming a smear on the gel.

After incubation, 5µl 6x blue/orange loading dye (Promega) was added to each sample. Samples were then run on a 0.8% agarose gel in 1XTBE buffer for one hour at 100V. Following electrophoresis the gel was stained for one hour in 1x TBE containing 0.01% ethidium bromide. Gels were visualised under UV translumination and photographed, the proportion of each of the plasmid forms on the gel was quantified by densitometry. Free

radical damage was expressed as a percentage depletion of supercoiled DNA using the equation:

$$\text{Depletion (\%)} = \left(\frac{\text{Relaxed DNA+ Linear DNA}}{\text{Total DNA}} \right)$$

2.15 Haemolysis assay

Particles including MWCNT, DQ12 and ufCB were weighed out and made up to 5mg/ml in sterile 0.9% saline solution then vortexed and sonicated for five minutes. A stock of red blood cells (RBC) was obtained from fresh human venous blood from healthy donors. A volume of 10ml blood was extracted into 1ml citrate buffer to prevent coagulation then centrifuged for 10 minutes at 2500rpm. Plasma was removed and discarded and the cell pellet re-suspended to original volume in saline and re-spun. This process was repeated twice more before 1ml of RBC suspension was pipetted into sterile 4x 1.5ml eppendorf tubes and centrifuged at 1000rpm for five minutes. The supernatants were removed leaving packed RBCs 100µl of which was aliquoted from each tube and added to 3.6ml 0.9% saline; this preparation was left on ice. In a 96 well plate 150µl of each particle suspension was added in triplicate, negative controls consisted of 150µl saline, whilst the positive control consisted of 150µl 0.1% Triton X-100. To each well containing sample or controls 75µl blood dilution was added and mixed by pipetting. Plates were incubated for 10 minutes at RT with gentle shaking on an orbital plate shaker. Plates were centrifuged at 250g for five minutes and 75µl supernatant carefully removed from each well and transferred to a fresh 96 well plate. Plates were then read on a microplate reader at 540nm. Optical densities were converted to percent haemolysis using the equation:

$X = (y-c)/m$ Where X = percentage haemolysis
Where Y = Optical density
Where C = mean negative control optical density
Where m = (mean positive control optical density) – (mean negative control optical density)/100

2.16 Human Interleukin-8 (IL-8) Enzyme linked immuno-sorbant Assay (ELISA)

Human type II alveolar epithelial cells (A549) were harvested and seeded into 24 well plates as previously described at 90 000 cells/ml and serum starved over night. Stock particle solutions of MWCNT or DQ12 at 1mg/ml were prepared in 0% or 2% DMEM and diluted to desired working concentrations ranging from 10.5 – 105.3μg/cm^2 (20-200μg/ml) (for carbon nanotubes) and 10.5 – 52.6μg/cm^2 (20 - 100μg/ml) for DQ12 in 0% or 2% DMEM for application to cells. Human recombinant TNFα (R&D Systems) was applied to cells at 10ng/ml in 0 or 2% DMEM as a positive control. Cells were treated at~70% confluence for 6, 24 or 48 hours after which plates were centrifuged at 250g for 10 minutes and supernatants transferred to 1.5ml eppendorf tubes, re-centrifuged at 13 000rpm for five minutes and supernatants stored. The ELISA assay was performed using DuoSet® ELISA development system (R&D Systems). Briefly, EIA/RIA 96 well flat-bottomed ELISA plates (CoStar) where coated over night with 100μl IL-8 monoclonal capture antibody (4μg/ml). Plates were washed three times with wash buffer (PBS/0.05% Tween-20) and blocked with 300μl 1% PBS/BSA for one hour, plates were re-washed (x3) and standards (prepared in 0% or 2% DMEM) and samples (100μl) were applied in triplicate then incubated for two hours at RT. After re-washing (x3) plates were coated with 100μl biotinylated, polyclonal detection antibody (made up in reagent diluent) for two hours to form antibody-enzyme conjugates. Plates were re-washed (3x) and 100μl streptavidin-HRP added to each well for 20 minutes. Streptavidin is a specific substrate that binds biotin producing a blue product. After a final wash plates were coated with substrate solution and incubated for 20 minutes in the dark to allow the blue colour to develop, the reaction was stopped by addition of 50μl 2N

sulphuric acid (resulting in a yellow final product) and plates were read on a microplate reader at 450nm. Averages of triplicate readings for each standard were made and used to generate a standard curve. Linear regression was used to determine IL-8 concentration for each sample.

To account for possible IL-8 adsorption to MWCNT a variation of this protocol was adopted. Cells were treated with DQ12 or MWCNT for 6 or 24 hours in 0% DMEM, treatments were then gently washed from the plates with pre-warmed PBS-CMF and medium replaced with fresh 0% DMEM. Cells were re-incubated for a further 24 hours before medium was collected and processed as previously described.

2.17 Isolation of messenger Ribonucleic acid (mRNA)

Seeded into 6 well plates A549 cells were cultured and treated with MWCNT, TiO_2, ufCB, DQ12 (positive particle control) at 10.4μg/cm^2 (100μg/ml), 31.5μg/cm^2 (300μg/ml) and 52.6μg/cm^2 (500μg/ml) or TNFα at 10ng/ml for 4 or 24 hours in 0% DMEM in triplicate. Non-treated controls were also prepared in triplicate. After prescribed treatment periods cells were washed in PBS-CMF and incubated for 10 minutes with 0.75ml TRIzol® reagent (Gibco) before being scraped and the contents of each well transferred to labelled 2ml phase lock gel heavy eppendorf tube (Fischer). Isolation of RNA was then carried out according to the manufacturer's instructions. Briefly, 150μl Bromo-chloro-iodo-propane (BCIP) (Sigma) was added to each tube mixed and allowed to stand; samples were then centrifuged at 13000rpm for 15 minutes at 4˚C. Clear aqueous supernatant was collected from each tube, transferred to fresh eppendorfs, and mixed with 375μl iso-propanol. After 10 minutes standing samples were re-centrifuged as previously described. Supernatant was removed and discarded and the pellet washed with 750μl 75% ethanol by brief vortexing. Samples were then centrifuged at 13000rpm for 10 minutes at 4˚C and the supernatant removed and the pellet allowed to air dry. The pellets (now of RNA) were then re-suspended in 100μl diethylpyrocarbonate (DPEC) treated water, repeat samples were then pooled and heated to

55˚C for 15 minutes to ensure RNA was completely in solution. Samples were aliquoted and stored at -80˚C until use. The concentration of RNA obtained was determined by spectroscopy and later by microplate assay. For spectroscopic determination of RNA concentration 4µl RNA sample was added to 996µl Tris-EDTA (TE) buffer (Sigma) and the absorbance read at 260nm and 280nm. The ratio of $A_{260/280}$ was calculated for each sample with values of 1.6 or greater sought. Concentration of RNA was calculated by the equation:

$$\text{RNA}\mu\text{g/ml} = \frac{A_{260}}{0.025} \quad \text{X dilution factor}$$

Alternatively 2µl RNA sample was diluted into 498µl TE buffer and 100µl transferred in triplicate to a UV transparent 96 well plate where samples were read at 260 and 280 on a microplate reader with the ratio of $A_{260/280}$ calculated.

2.18 Preparation of complementary DNA (cDNA)

Complementary DNA (cDNA) is a single stranded DNA molecule complementary to an RNA molecule. To generate cDNA from cellular RNA extracts 2µg RNA from each sample were added to sterile eppendorf tubes and made up to a final volume of 25µl with DEPC H_2O. A reaction mix containing 5xM-MLV reaction buffer (Promega), 100mM Dithiothreitol (DTT) (Promega, Sigma), 100µg/ml oligo(dT) Primer (Promega), 10mM deoxy tri-nucleotides (dNTP) (Promega), Rnasin (Promega), and M-MLV reverse transcriptase (Promega) was prepared and 25µl added to each 2µg RNA sample. Samples were then incubated for 90 minutes on a heat block set at 37˚C for DNA synthesis, the reaction was stopped by increasing the incubation temperature to 90˚C for 10 minutes.

2.19 Polymerase Chain reaction (PCR)

Reverse transcriptase polymerase chain reaction was used to determine IL-8 and TGFβ-1 RNA levels from treated cells. The genes tested for included Interleukin-8 (IL-8), Tissue

growth factor β (TGFβ-1) and the house keeping gene glyceraldehyde-3-phosphate dehydrogenase (GAPDH). Primer oligonucleotides for these genes were designed and purchased from MWG-Biotech. The following primer pairs were used:

IL-8, sense 5'- AGATGTCAGTGCATAAAGACA-3'

IL-8, antisense 5'- TGAATTCTCAGCCCTCTTCAAAAA-3'

TGFβ1, sense 5' - GAAACCCACAACGAAATCTAT-3'

TGFβ1, antisense 5' – CCTCCACGGCTCAACCAC-3'

GAPDH, sense 5' - CCACCCATGGCAAATTCCATGGCA-3'

GAPDH, antisense 5' – TCTAGACGGCAGGTCAGGTCCACC-3'

Primers were diluted to 100pg/ml in DEPC water. For each PCR reaction 5µl (or 3µl for detection of house-keeping gene) sample cDNA was added to 40µl of a PCR reaction mix consisting of 5x storage buffer (Promega), Magnesium Chloride ($MgCl_2$) at a final concentration of 2.5mM, dNTP at a final concentration of 2mM, forward and reverse primers (100pmol/µl) and sterile nuclease free water. Each sample was loaded with 0.25µl GoTaq DNA polymerase (Promega) and thermal cycling performed. The resulting amplified DNA fragments were separated by electrophoresis through a 1.5% agarose gel for 90 minutes at 60V stained with Gel Red nucleic acid stain. Bands where visualised and scanned by UV transilluminator and quantified by densitometry.

2.20 Antibody staining and Confocal microscope imaging of NF-κB

The transcription factor NF-κB is found in resting cells in the cytoplasm anchored there by IκB inhibitory proteins. Upon cellular activation, IκB is removed and degraded allowing NF-κB to translocate to the nucleus (Scheidercit 2006) and stimulate the expression of genes

including IL-8 (Holtmann et al 1999, Hofmann et al 2002). This translocation can be monitored by immunocytochemistry.

Cells were cultured in 24 well plates on sterile glass coverslips and treated with MWCNT, ufCB, DQ12, and TiO_2 for 4 hours. A positive control consisting of cells treated with TNFα and an untreated control were also prepared. Following treatment cells were washed twice in PBS-CMF then fixed in 1ml 3% formaldehyde (made up in PBS) for 20 minutes. Cells were washed (x3 PBS) and incubated for 10 minutes with 50mM Ammonium chloride (made up in distilled water) after which supernatants were removed and cells made permeable by incubation with 1ml 0.1% Triton X-100/PBS for 4 minutes. Cells were washed and plates blocked (3x PBS, 3x 0.2% BSA, 3x PBS) prior to 1 hour incubation with 200µl rabbit polyclonal anti-NF-κB p50 subunit primary antibody, diluted 1:200 in 0.2% BSA. Cells were rewashed (3x PBS, 3x 0.2% BSA, 3x PBS) and incubated with 200µl FITC labelled anti-rabbit IgG secondary antibody diluted to 1:500 in 0.2% BSA and incubated in the dark for 1 hour. After a final wash (3x PBS, 3x 0.2% BSA, 3x PBS) coverslips were briefly air dried then mounted onto slides with 10µl Mowoil (Calbiochem) and allowed to dry overnight protected from the light. Mounted coverslips were viewed on a Leica microsystems TCS SP5 LAS AF confocal microscope using an Argon laser set at 488nm. Images were captured using supplied LAS AF software.

2.21 In Vivo Analysis

Experiment	Treatment time (Hours)	Particles	Treatment dose	Concentration
1	48	LMWCNT, SMWCNT, ufCB, DQ12, TiO_2, Long Amosite, Short Amosite	0.5ml/mouse (i.p.)	100µg/ml in 0.5ml
2	24	LMWCNT, LMWCNT extract, SMWCNT, SMWCNT extract, Long amosite, Long Amosite extract	0.5ml/mouse (i.p.)	100µg/ml in 0.5ml
3	48	LMWCNT, SMWCNT	0.5ml/mouse (i.p.)	200, 500, 750µg/ml in 0.5ml
4	164	LMWCNT, SMWCNT, ufCB, Short amosite, DQ12	0.5ml/mouse (i.p.)	200ug/ml in 0.5ml

Table 2.2. *In vivo* experiments performed upon C57BL/6 male mice. A table showing (from left to right) the experiments performed, with requisite exposure times (hours) , particles/treatments utilized, treatments volumes administered by injection to the peritoneal cavity (i.p.) and the particle concentrations delivered.

2.22 Peritoneal Lavage (PL)

Mice were killed initially by cervical dislocation and latterly by carbon dioxide exposure. The abdominal cavity was exposed to treatments and 2ml 0.9% saline lavage injected through the parietal peritoneum into the peritoneal cavity. The fluid filled cavity was gently massaged then the lavage drawn back and transferred into pre-chilled 15ml centrifuge tubes. This process was repeated three times for each animal with 5 - 6ml lavage fluid obtained per mouse, lavages were kept on ice. Peritoneal lavages were centrifuged at 1000rpm for 5 minutes and a 1ml fraction transferred into labelled eppendorf tubes for analysis of protein and LDH levels. Remaining supernatant was discarded and the cells re-suspended in 1 ml 0.9% saline (in later experiments this was buffered with 0.1% BSA) for cell counting.

2.23 Removal, fixation and histopathology of the diaphragm

Following peritoneal lavage the diaphragm was carefully removed and submerged in methacan fixative. Slices of the diaphragm were prepared and in embedded in paraffin from which sections were cut. Sections were stained with haematoxylin and eosin or serius Red and examined microscopically for the presence of granulomatous inflammation.

2.24 Total cell counts and cytospins

Cells were counted using the nucleostain system. Briefly, 10µl re-suspended lavage cells were diluted in 90µl 0.9% saline/0.1% BSA and treated with 100µl lysis buffer and then with 100µl stabilisation buffer. The lysed cell preparation was collected into a cell count cassette and loaded into the nucelostain counter for analysis. Using fresh cassettes this was repeated for each lavage sample. Based on total cell counts relevant volumes of each lavage were loaded onto cytospins and spun at 300rpm for 3 minutes onto clean glass slides. Slides were stained with haematoxylin and Eosin and mounted under glass coverslips with DPX for differential cell counting. Macrophages, Neutrophils and lymphocytes were identified by their characteristic shapes and counted. A minimum of 300 cells were counted per slide.

2.25 BSA total protein and LDH Cytotoxicity assays

BCA protein assays were performed as previously described from 1 ml fractions removed from peritoneal lavage fluid (PLF) supernatants. Cytotoxicity assays were performed as previously described using Roche LDH cytotoxicity kit; 100µl of the retained PLF supernatant (un-diluted) was loaded into a 96 flat bottomed plate and mixed with 100µl LDH assay solution then incubated for up to 30 minutes protected from light before being read on a microplate reader at 490nm. Cytotoxicity was assessed by comparative examination of absorption at 490nm for each sample.

2.26 Experiment 1: Intra-peritoneal injection of DPPC dispersed particles for 48 hours into C57BL/6 mice.

To assess the inflammatory affects of MWCNT and a panel of reference particles a cohort of 36 mice was split into nine groups of four animals. Animals were treated with 100μg/ml in 0.5ml DPPC/0.9% saline of MWCNT, ufCB, TiO_2, Long amosite and Short amosite asbestos by intra-peritoneal injection. Animals were killed after 48 hours following exposures and their peritoneal cavities lavaged. Inflammation was assessed from peritoneal lavage fluid (PLF) by total and differential cells counts and total protein assays; cytotoxicity was evaluated by LDH cytotoxicity assay (Roche).

2.27 Experiment 2: Intra-peritoneal injection of aqueous suspensions in saline of particles or aqueous particle extracts for 24 hours into C57BL/6 mice.

The capacity of particle/fibre surface associated materials soluble in aqueous solution to contribute to inflammation was assessed by preparing saline extracts of MWCNT and Long amosite asbestos. Fibres were suspended in 0.9% sterile saline at 400μg/ml, sonicated and kept on a roller over night. Suspensions were centrifuged and the supernatant 0.22μm sterile filtered as an extract stock solution, fibre pellets were suspended and washed by repeat centrifugation (1000g) and re-suspended in 4ml sterile saline. Upon the final re-suspension particles were made up to 400μg/ml then diluted to working concentrations of 100μg/ml; a fraction of each particle extract stock solution was diluted to the same extent. A group of 30 mice were split into 8 groups, particles and extract treatment groups contained 4 mice and an un-treated control group contained 2 mice. Mice were subjected to intra-peritoneal injections of 0.5ml of each treatment (controls were injected with saline alone) and sacrificed after 24 hours. Inflammation was assessed from peritoneal lavage fluid (PLF) by total and differential cells counts and total protein assays; cytotoxicity was evaluated by LDH cytotoxicity assay (Roche).

2.28 Experiment 3: Dose response of LMWCNT and SMWCNT injected I.P. into C57BL/6 mice for 48 hours.

Mice were exposed to increasing concentrations of LMWCNT and SMWCNT to discern differences in inflammatory potential between the two carbon nanotubes. A group of 21 animals were dived into 7 groups of 3 mice including a saline treated control group. Stock MWCNT suspensions were diluted to working concentrations and injected I.P. into mice at concentrations of 200, 500 and 750μg/ml in 0.5ml/mouse. After 48 hours animals were sacrificed and inflammation assessed from peritoneal lavage by total and differential cell counts, total protein concentration and LDH cytotoxicity.

2.29 Experiment 4: Examination of the diaphragms of C57BL/6 for evidence of granulomatous inflammation mice after seven day exposure to a particle panel including MWCNT.

A group of 12 mice were divided into 6 groups including 5 particle treatment groups and 1 untreated control group. Animals were exposed to LMWCNT, SMWCNT, SFA, DQ12 or TiO_2 to examine the capacity of each material to induce a granulomatous response on the peritoneal side of the diaphragm. Mice were exposed by I.P. injection to particles and fibres at a concentration of 100μg/ml in 0.5ml prepared in sterile 0.9% saline. After 7 days mice were sacrificed and their diaphragms were removed for processing (as previously described) and then microscopic examination.

Data Analysis

Data from all experiments was analysed by analysis of variance with the Tukey multiple comparison test. Analysis was carried utilising Graphpad Instat® 3.06 statistical software (32 bit for Windows).

Chapter 3

The *in vitro* free radical generating capacity and cytotoxicity of MWCNT

Chapter 3

In vitro cytotoxicity and free radical generating capacity of CNT and control particles

3.1 Introduction

In the paradigm of fibre toxicity there is a continuum of respirable industrial fibres including asbestos that vary in harmfulness based upon their dimensions (Hesterberg & Barrett 1984, Har et al 1994, Ye et al 1999, Riganti et al 2003, Zeidler-Erdely et al 2006) and ability to persist in the lungs (Donaldson & Lang Tran 2004). An increasing body of work hints at the inflammatory potential and cytotoxicity of both MWCNT and SWCNT *in vitro* (Monteiro-Riviere et al 2005, Murr et al 2005, Soto et al 2005, Kagan et al 2006, Tian et al 2006) and *in vivo* (Lam et al 2004, Muller et al 2005, Shvedova et al 2005, Grubek-Jaworska et al 2006). The harmful effects of CNTs may be a result of free radical production derived from residual metal catalyst, or from an inherent ability of CNTs or a combination of the two. The aims of the research in this chapter were to assess the toxicity of two different sizes of MWCNT and a range of reference particles in relation to their metal content, surface reactivity and free radical production. The cytotoxicity of carbon nanotubes and other environmental particles has been attributed in part to free radical production derived from their metal content or to the presence of a reactive surface. This was investigated by use of electron spin resonance (ESR) and DNA scission assays to quantify free radical production in an aqueous environment and haemolysis assays to assess the extent of surface reactivity of the particles under scrutiny.

3.2 Metal content analysis of MWCNT and Reference particles

Previous discoveries of the contribution of metals to environmental particle toxicity and the current uncertain role of metals in the reported toxicity of CNT has made characterisation of metal content of CNT samples used in this research vital. In addition to the metal content of CNT, that of a panel of reference particles was also quantified.

The percent residual cadmium (Cd), cobalt (Co), chromium (Cr), copper (Cu), iron (Fe), manganese (Mn), nickel (Ni), titanium (Ti), vanadium (V) and zinc (Zn) concentrations are shown in table 3.1. With the exception of both forms of titanium dioxide and ultrafine carbon black the principal metal impurity was found to be iron. Nano long (LMWCNT) and nano short MWCNT (SMWCNT) (Nanolab Inc, MA, USA) that had been acid purified still retained >1% (wt%) iron (1.16 and 1.76% respectively), both also contained negligible levels of copper (0.01%), nickel (0.01%) was also detected in SMWCNT samples. Although derived from LMWCNT, SWCNT were found to contain slightly greater residual iron levels than LMWCNT. Similarly there was a higher iron content of short (1.81%) compared to long fibre amosite (0.04%). Unlike long amosite, short amosite samples contained low levels of zinc (0.01%), titanium (0.02%) and manganese (0.14%). The mineral particle DQ12 was found to have the greatest metal content, the majority of which was iron (2.79%) with smaller amounts of manganese (0.25%), titanium (0.01%) and trace levels of the other metals. Japanese MWCNT contained around 3.4 and 5 times less residual iron (at 0.34%) than LMWCNT and SMWCNT respectively and only 0.01% cobalt. Only trace amounts (<0.01%) of all the metals tested for were found in ultrafine carbon black. Diesel exhaust particles were found to contain low levels

of iron (0.04%) and zinc (0.04%) and trace amounts of all other metals assayed for (<0.01%). Both anatase and rutile TiO_2 were found to contain small amounts of iron (0.01%) and zinc (0.02 and 0.04% respectively). Table 3.2 shows the amount of metal (wt %) that could be mobilised into solution. Despite a relatively high iron content compared to other samples only trace amounts of iron (<0.01%) could be solubilised from either LMWCNT or SMWCNT, similarly for all other samples with the exception of long and short amosite asbestos (0.09% and 0.06% respectively) less than 0.01% iron could be released into solution. Only trace levels (<0.01%) of the other metals were detected with the exception of Rutile TiO_2 where 0.29% Ti was liberated.

Metal Concentration (%)										
Sample	**Cd**	**Co**	**Cr**	**Cu**	**Fe**	**Mn**	**Ni**	**Ti**	**V**	**Zn**
Carbon black	<0.01	<0.01	<0.01	<0.01	0.01	<0.01	<0.01	<0.01	<0.01	<0.01
Nano long	<0.01	<0.01	<0.01	0.01	1.16	<0.01	<0.01	<0.01	<0.01	<0.01
Nano short	<0.01	<0.01	<0.01	0.01	1.76	<0.01	0.01	<0.01	<0.01	<0.01
Japanese MWCNT	<0.01	0.01	<0.01	<0.01	0.34	<0.01	<0.01	<0.01	<0.01	<0.01
Diesel exhaust particles	<0.01	<0.01	<0.01	<0.01	0.04	<0.01	<0.01	<0.01	<0.01	0.04
Long Amosite	<0.01	<0.01	<0.01	<0.01	0.04	<0.01	<0.01	<0.01	<0.01	<0.01
Short Amosite	<0.01	0.02	0.01	0.01	1.81	0.14	<0.01	0.02	<0.01	0.01
DQ12	<0.01	<0.01	<0.01	0.01	2.79	0.25	<0.01	0.01	<0.01	<0.01
Rutile TiO_2	<0.01	<0.01	<0.01	<0.01	0.01	<0.01	<0.01	1.88	<0.01	0.04
Anatase TiO_2	<0.01	<0.01	<0.01	<0.01	0.01	<0.01	<0.01	1.18	<0.01	0.02

Table 3.1. Metal content of a panel of MWCNT and reference particles.

Metal Concentration (%)										
Sample	**Cd**	**Co**	**Cr**	**Cu**	**Fe**	**Mn**	**Ni**	**Ti**	**V**	**Zn**
Carbon black	<0.01	<0.01	<0.01	<0.01	<0.01	<0.01	<0.01	<0.01	<0.01	<0.01
Long MWCNT	<0.01	<0.01	<0.01	<0.01	<0.01	<0.01	<0.01	<0.01	<0.01	<0.01
Short MWCNT	<0.01	<0.01	<0.01	<0.01	<0.01	<0.01	<0.01	<0.01	<0.01	<0.01
Japanese MWCNT	<0.01	<0.01	<0.01	<0.01	<0.01	<0.01	<0.01	<0.01	<0.01	<0.01
Diesel exhaust particles	<0.01	<0.01	<0.01	<0.01	<0.01	<0.01	<0.01	<0.01	<0.01	<0.01
Long Amosite	<0.01	<0.01	<0.01	<0.01	0.09	0.01	<0.01	<0.01	<0.01	<0.01
Short Amosite	<0.01	<0.01	<0.01	<0.01	0.06	<0.01	<0.01	<0.01	<0.01	<0.01
DQ12	<0.01	<0.01	<0.01	<0.01	<0.01	<0.01	<0.01	<0.01	<0.01	<0.01
Rutile TiO_2	<0.01	<0.01	<0.01	<0.01	<0.01	<0.01	<0.01	0.29	<0.01	<0.01
Anatase TiO_2	<0.01	<0.01	<0.01	<0.01	<0.01	<0.01	<0.01	<0.01	<0.01	<0.01

Table 3.2. Soluble metal content of a panel of MWCNT and reference particles.

3.3 MWCNT particle morphology

All of the CNT used during this research were hydrophobic and flocculated in aqueous solutions. To better understand the morphology of MWCNT in aqueous solution scanning electron microscopy (SEM) was employed. SEM micrographs of the LMWCNT and SMWCNT dispersed in water by sonication are shown in figure 3.1 A-F. These images clearly show that both types of MWCNT are tightly compacted into particulate matter despite ultrasonic treatment. Emanating from the surface of the compacted particles, ropes of LMWCNT can be observed (Figures 3.1A, B and C) whilst closer examination of the CNT aggregates reveals a matted surface composed of compacted LMWCNT ropes (figure 3.1C). The surface of the SMWCNT particles also consists of a tangled mass of ropes of nanotubes (Figures 3.1D, E, and F) with SMWCNT ropes projecting from their surface at four points (Figures 3.1E and F). These images clearly show that following limited ultrasound dispersion in aqueous solution, the MWCNT are substantially more particle than fibrous in nature. The visible MWCNT projections do not appear rigid straight ropes but present as more flexible hair like extensions. Figures 3.2 A-E show scanning electron micrographs of LMWCNT dispersed in methanol by ultrasound, Figures 3.2A and B reveal aggregated LMWCNT interspersed with both iron catalyst and catalyst support particles (indistinguishable from each other in these images), the nanotubes are individually dispersed but highly tangled. The tubes do not appear rigid and are of varying widths with variations in both tube inner and outer core diameters (figures 3.2C, D, and E), the outer and inner layers of some of the MWCNT appear discontinuous and may contain vacancies (holes) (figure 3.2C) whilst there appears to be a break in the side wall of a nanotube in figure 3.2E. The

end of an individual MWCNT is evident in figure 3.2D but appears faint and disrupted no other end caps are visible.

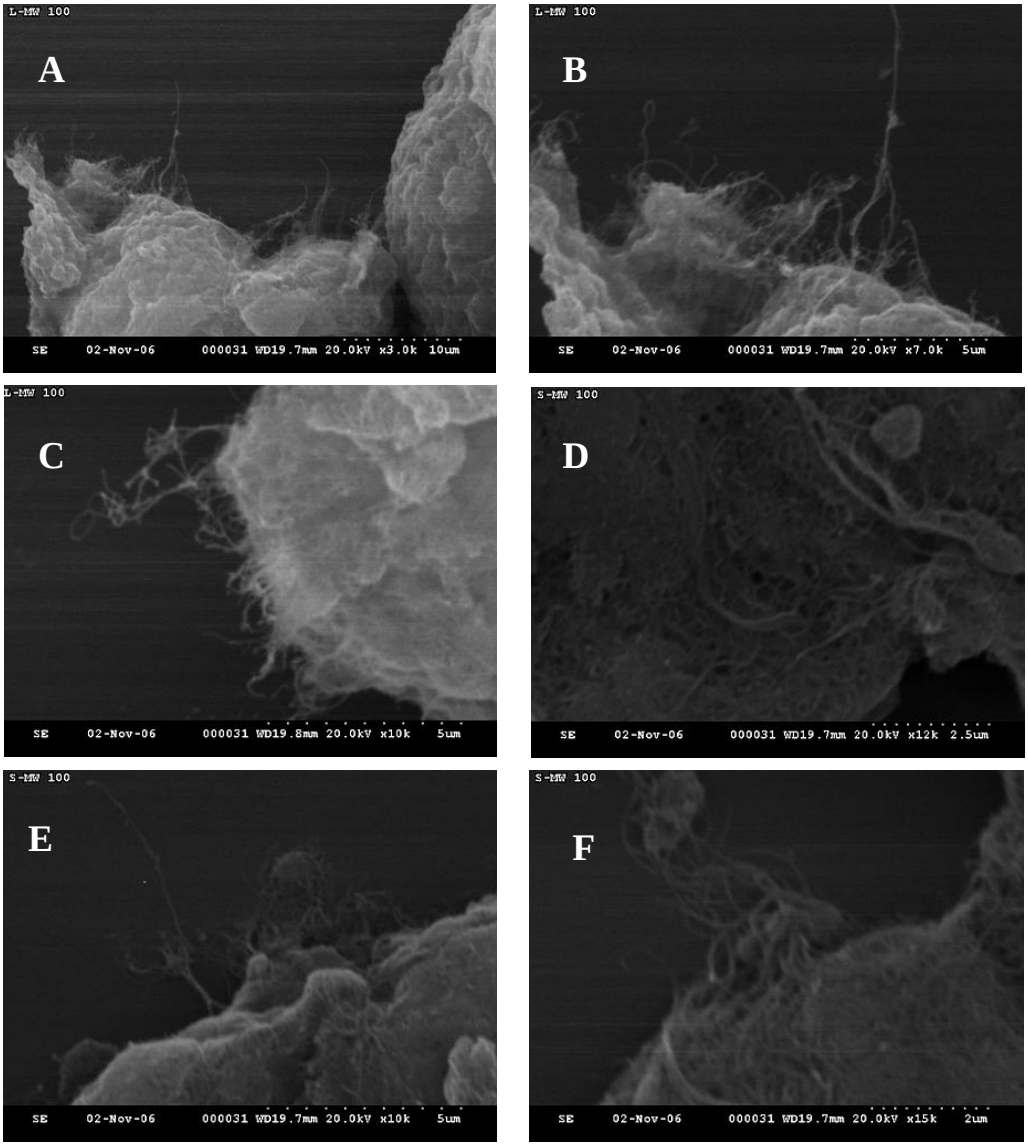

Figure 3.1 Scanning electron microscope micrographs of MWCNT. All images are of MWCNT dispersed in distilled deionised water at a concentration of 100µg/ml by short ultrasound treatment. A) LMWCNT (magnification x 3000), B) LMWCNT (magnification x 7000), C) LMWCNT (magnification X 10000), D) SMWCNT (magnification x12000), E) SMWCNT (magnification x 10000), F) SMWCNT (magnification x 15000).

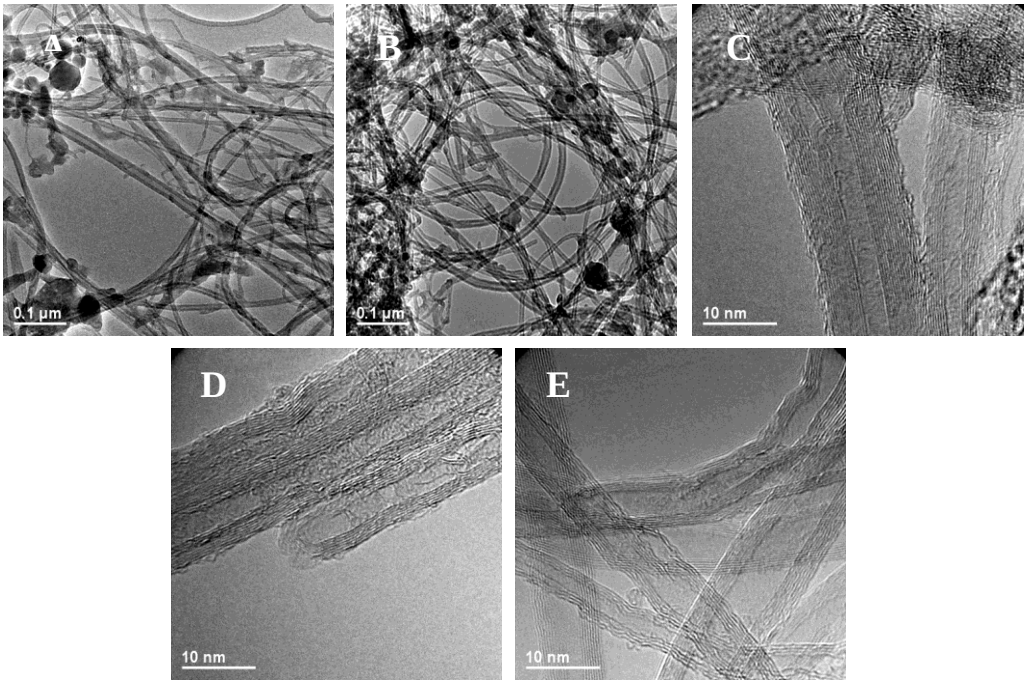

Figure 3.2 Scanning electron micrographs of Long MWCNT. All images are of LMWCNT dispersed in methanol with ultrasound treatment. Figures **A** and **B** show low resolution images of LMWCNT with residual particles visible. Figures **C**, **D**, and **E** are high resolution images of LMWCNT clearly showing the layer multiple walls of the nanotubes. Samples were prepared by Craig Poland, University of Edinburgh. All images are courtesy of Craig Poland (University of Edinburgh) and Steve Clark (Institute of occupational medicine, Edinburgh).

3.4 Acellular production of Reactive Oxygen Species (ROS) by MWCNT

The production of ROS has been implicated as a factor in the pathogenicity of particles and fibres (Lund et al 1994, Pan et al 2004) and this has often been attributed to the presence of transition metals undergoing Fenton chemistry or the surface reactivity of the material (Donaldson et al 1996, Stone et al 1998, Jimènez et al 2000, Dick et al 2003, Pan et al 2004). The ability of MWCNT to generate ROS due either to the presence of residual transition metals or inherent surface reactivity was investigated by plasmid DNA scission assay. This assay has been used to probe production free radicals (Halliwell & Okezie 1991, Pogozelski & Tullius 1998), in particular hydroxyl radicals, and to investigate the damage inflicted to DNA by particles and fibres (Kukielka & Cederbaum 1994, Lund et al 1994, Donaldson et al 1996).

Super-coiled plasmid DNA was incubated with either 100 or 500μg/ml of LMWCNT or SMWCNT in the presence or absence 1mM hydrogen peroxide. Hydrogen peroxide was included as an initiator for possible Fenton chemistry. From visual assessment of the agarose gels (Figure 3.3) in the absence of any kind of treatment most plasmid DNA remained in its super-coiled form whilst 1mM hydrogen peroxide appeared to increase the proportion of relaxed DNA. Incubating plasmid DNA with either 100 or 500μg/ml LMWCNT or SMWCNT in the absence of 1mM hydrogen peroxide appeared not to increase the conversion of super-coiled DNA to relaxed or linear forms of DNA. Incubation of plasmid DNA with either MWCNT did result in a decrease in the size and fluorescent intensity of the bands on the gel, the exception to this was the DNA band corresponding to relaxed DNA at 100μg/ml SMWCNT + 1mM hydrogen peroxide. At the 100μg/ml of LMWCNT or

SMWCNT in the presence of 1mM hydrogen peroxide there was slight conversion of super-coiled to linear DNA that was most apparent with SMWCNT.

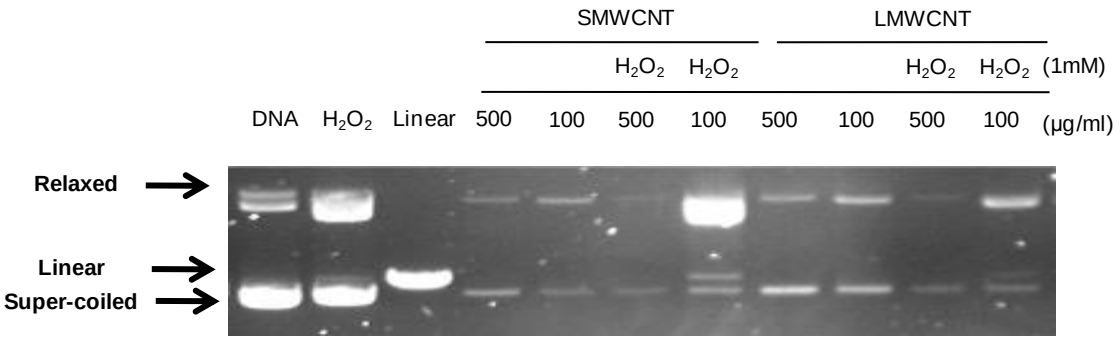

Figure 3.3 The effect of LMWCNT or SMWCNT on super-coiled DNA plasmid. LMWCNT or SMWCNT (100 or 500µg/ml) were incubated with φX174 RF1 plasmid DNA for 16 hours (over-night) at 37˚C. A linear control was prepared using the restriction enzyme PST-1. This figure is a representative plasmid DNA gel, treatments were repeated three times.

Electron spin resonance (ESR) was used as an additional method of detecting and quantifying free radical production from MWCNT and reference materials by spin trapping using the hydroxylamine TEMPONE H (1-hydroxyl-2, 2, 6, 6-tetramethyl-4-oxo-pipieridine). In this process the spin trap, TEMPONE-H (that detects peroxynitrile and superoxide radicals), combines with the radical (a diamagnetic molecule) to form a more stable nitroxide radical that can be detected (Dikalov et al 1997a, 1997b, Bartosz 2006).

The particles LMWCNT, SMWCNT, DQ12, TiO_2, Long fibre amosite (LFA) and short fibre amosite (SFA) (10μg/ml) were incubated with TEMPONE-H/EDTA in PBS for one hour at 37˚C during which time measurements of radical formation were taken every 15 minutes (Fig 3.4). A spin trap control was set up consisting of TEMPONE-H alone, the TEMPONE-H control progressively autooxidised in air resulting in accumulation of its nit oxide radical and an increasing ESR signal over time that was subtracted from readings taken from test materials. Both LMWCNT and SMWCNT (figure 3.4) caused a dramatic time dependent increase in formation of a radical at each time point. Reference materials DQ12, TiO2, and long amosite (LFA) (figure 3.4) failed to generate detectable levels of the radical over the course of the one hour assay resulting in lines touching the x-axis. Short amosite (SFA) (Figure 3.4) also time dependently produced free radicals that increased above those of DQ12, TiO_2 and LFA after 30 minutes. Free radical production from these materials did not reflect the metal content of respective particles particularly the difference in iron content between DQ12 and MWCNT. This suggests either differences in metal availability between MWCNT and particles' including DQ12 or that free radical production was independent of the

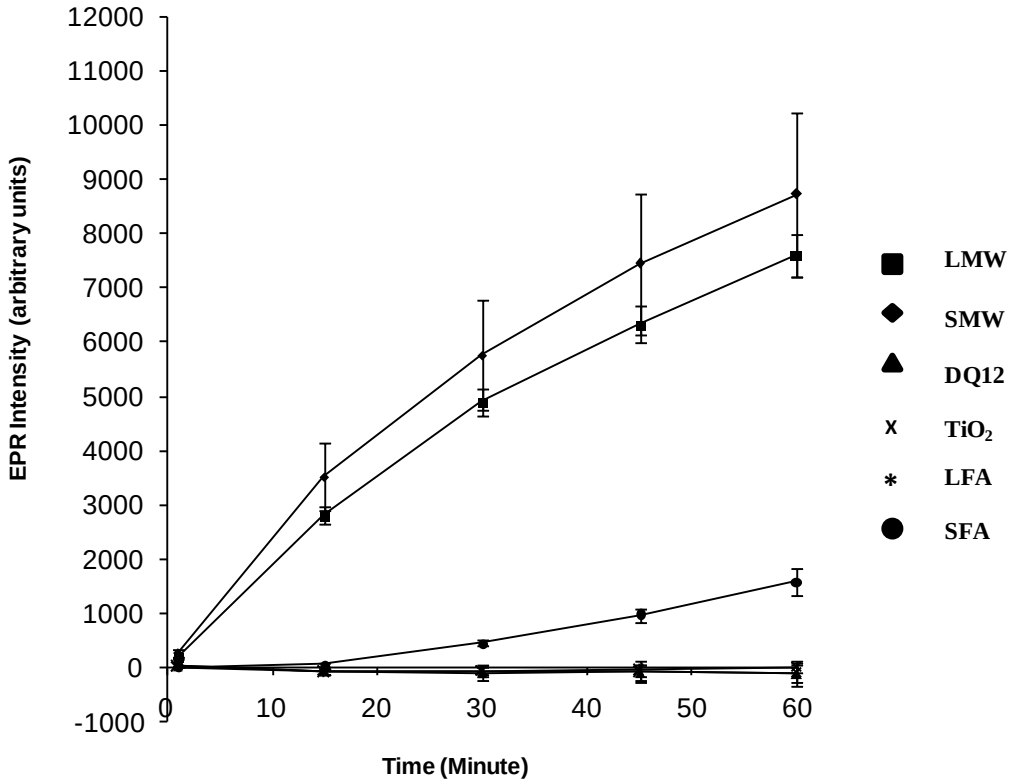

Figure 3.4. Free radical production by particles and fibres over one hour. Time course of comparative free radical production over one hour from particles and fibres including LMWCNT, SMWCNT, DQ12, TiO_2, LFA, and SFA, all particles were assayed at a concentration of 10μg/ml. LMWCNT and SMWCNT generated a large ESR output in comparison to all other test materials. DQ12, TiO_2 and LFA did not generate a species that could react with TEMPONE-H whilst SFA slowly began to generate a reactive species after 15 minutes. The graph represents the mean of four experiments, bars represent S.E.M.

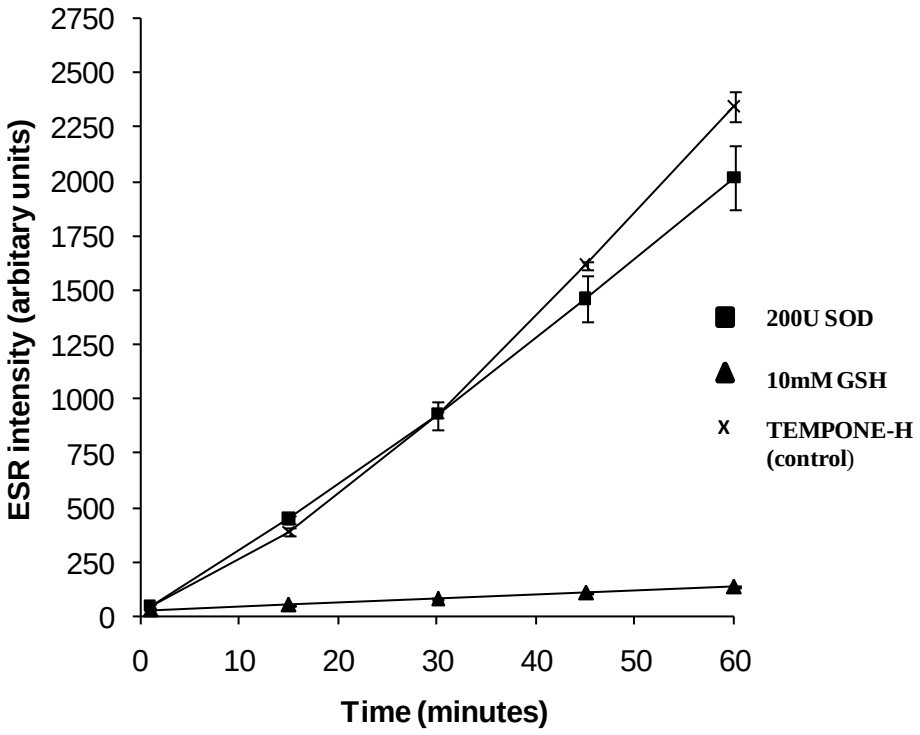

Figure 3.5. Effect of 10mM GSH or 200U SOD on the auto-oxidation of TEMPONE-H. The spin trap TEMPONE-H was incubated for one hour with either 10mM GSH or 200U SOD at 37°C, readings were taken every 15 minutes. Although the signal intensity for SOD decreased slightly towards the end of the assay in the presence of GSH the signal created by TEMPONE-H auto-oxidation was almost completely abolished. The graph represents the mean of three experiments. The bars represent the S.E.M.

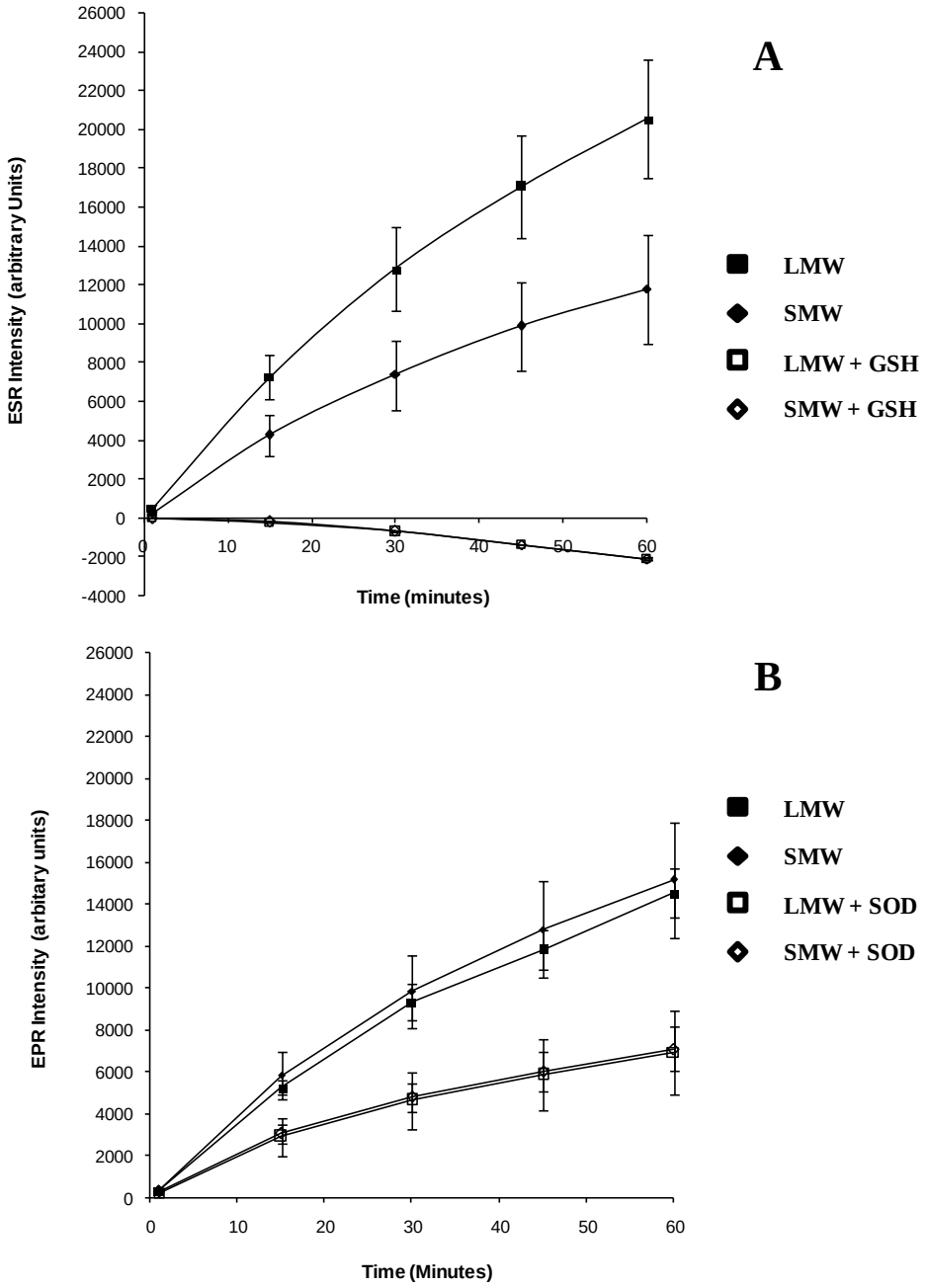

Figure 3.6. The effect of antioxidants on the ESR signal generated by LMWCNT and SMWCNT. LMWCNT and SMWCNT were incubated at 37°C for one hour with our without 10mM GSH (**A**) or 200U SOD (**B**) and readings were taken every 15 minutes. GSH completely abolished the signal generated by both MWCNT; this may have been partly due to reduction of the spin trap in addition to mopping up a reactive species generated by CNT. SOD also reduced the signal generated by MWCNT although not to the same extent as GSH. As SOD acts specifically against superoxide anions its reduction of the MWCNT signal suggests the CNT may be spontaneously producing superoxide anions. Graphs represent the mean of three experiments with bars representing the S.E.M.

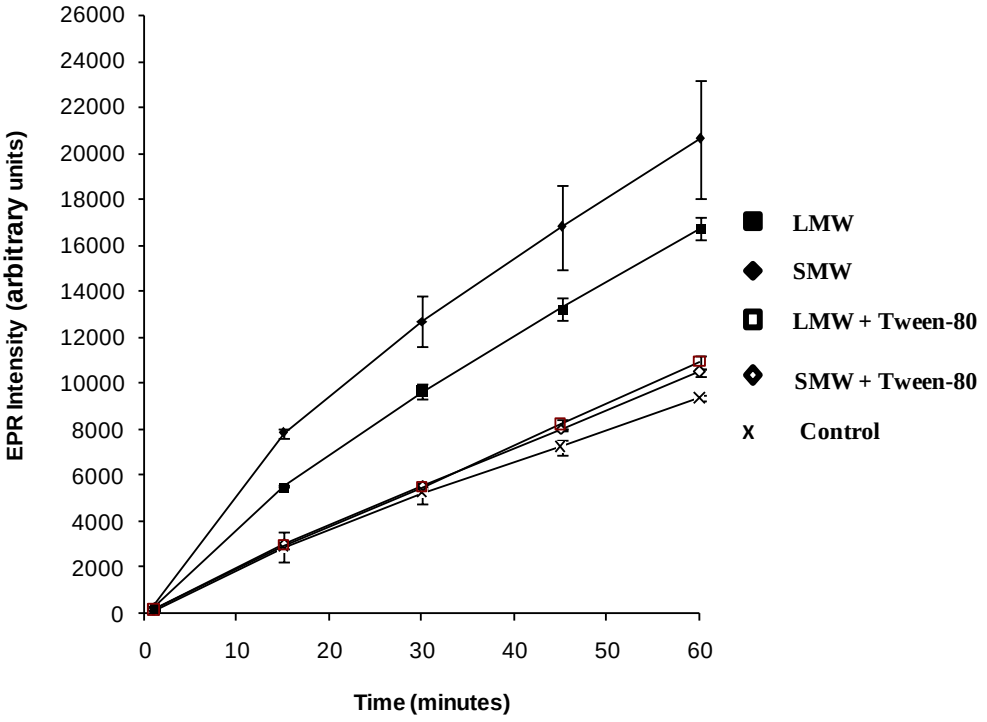

Figure 3.7. Effect of Tween-80 on the intensity of ESR signal generated by LMWCNT and SMWCNT. Both LMWCNT and SMWCNT were dispersed in 1% Tween-80 and incubated for one hour with TEMPONE-H; readings were taken every 15 minutes. In only PBS, both MWCNT generated a large ESR signal that was diminished upon their dispersion in a 1% v/v solution of the non-ionic surfactant Tween-80. The graphs represent the means of three experiments with bars representing the S.E.M.

metals present in the samples. A large difference in the rate of free radical formation between both MWCNT and SFA was also apparent; an obvious time lag between the start of the assay and production of the free radical by SFA existed that did not occur for either of the two MWCNT.

In order to confirm the ESR signal of MWCNT and short fibre amosite was due to a reactive species the assay was repeated in the presence of glutathione (GSH). Glutathione was included to mop up free radicals, as an antioxidant it is able to neutralise oxidising species including hydrogen peroxide, superoxide, and hydroxyl radicals (Yu et al 1994). Figure 3.5 shows the progressive auto-oxidation of TEMPONE-H to its nitroxide radical. This was diminished by GSH suggesting the antioxidant reduced nitroxyl radicals back to TEMPONE-H. In the absence of GSH both LMWCNT and SMWCNT increased ESR signal intensity above the control at all time points (figure 3.6A). Upon inclusion of LMWCNT and SMWCNT (figure 3.6A), GSH reduced the ESR signal below control levels by preventing free radical accumulation. From this it is possible to infer that MWCNT produce a level of free radicals that increases over time. In future assays a much lower concentrations of GSH might be sufficient to reduce the activity of MWCNT.

As TEMPONE-H detects superoxide and peroxynitrile radicals the enzyme superoxide dismutase (SOD) was included in the assay system in an attempt to identify the species. The enzyme SOD has been used previously to demonstrate that TEMPONE-H could be used for quantitative determination of superoxide radicals both in acellular and cellular environments (Dikalov et al 1997). Figure 3.6B shows that at a concentration of 200U SOD had little impact on the auto-oxidation of TEMPONE-H. In the presence of LMWCNT or SMWCNT SOD reduced

accumulation of free radicals by half (Fig 3.6B). These results suggest that MWCNT are spontaneously generating superoxide anions in aqueous solution. A higher concentration of the enzyme may have reduced the ESR signal closer to the x-axis.

Noticeable in all ESR studies is the variability in the maximum level of reactive species generated by MWCNT at 60 minutes. This was theorized to be as a result of variation in the level of MWCNT dispersion between assays. To investigate this MWCNT were dispersed in a 1% solution of Tween-80 (figure 3.7). Dispersed in Tween-80, the ESR output of both MWCNT was dramatically reduced. This Might indicate an antioxidant effect of the surfactant; alternatively Tween-80 may interfere in the ability of MWCNT to generate a reactive species or with detection of the reactive species.

3.5 Determination of the surface reactivity of LMWCNT and SMWCNT by human erythrocyte haemolysis assay

The pathogenicity of materials such as silica has been attributed to their capacity to damage cell membranes; the membrane of red blood cells has been used as a model for the interaction between a particle or fibre and a biological membrane (Summerton & Hoenig 1977). The haemolysis assay is a simple procedure for estimating and comparing toxicities between particles (Ottery & Gormley 1978). The particles LMWCNT, SMWCNT TiO2 and DQ12 were tested for their haemolytic capacity by incubation with human RBC's for 10 minutes. The particle DQ12 quartz (Figure 3.8A) was the only material to cause significant (***$p<0.001$) concentration dependent haemolysis at each of the doses, 2-4mg/ml, during an incubation time of 10 minutes, causing a maximum of 63.9% (±5.7%) haemolysis at the maximum concentration of 4mg/ml. The increase in haemolysis was found to be relatively linear up to 4mg/ml at which point it began to plateau. A concentration dependent increase in haemolysis caused by DQ12 was also observed by Ottery & Gormley (1977) although using lower concentrations and longer incubation times. The particles TiO_2 (Figure 3.8B), LMWCNT (Figure 3.8C), and SMWCNT (Figure 3.8D) also caused slight concentration dependent increases in the levels of haemolysis but these were all non significant with maximum levels of haemolysis not extending above 10%. It was observed that concentration for concentration LMWCNT caused a greater degree of haemolysis than the equivalent amount of SMWCNT, none of these differences were found to be significant however (data not shown).

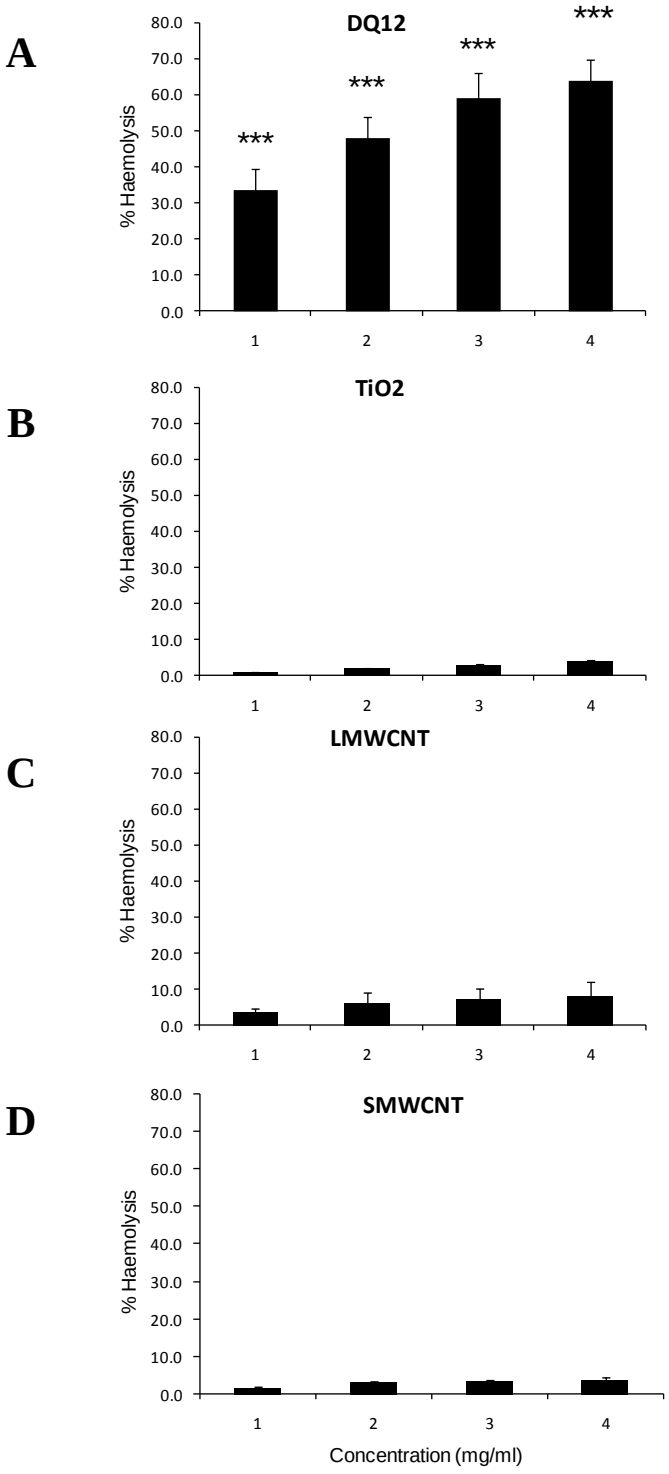

Figure 3.8. Effect of particles on the integrity of RBC membranes as measured by percent haemolysis. RBC were incubated for 10 minutes with 1, 2, 3, or 4mg/ml (A) DQ12, (B) TiO_2, (C) LMWCNT, (D) SMWCNT. Each graph represents the mean of three experiments in triplicate, bars represent S.E.M. ***$p<0.001$ compared to lowest experimental concentration.

3.6 Cytotoxicity of Carbon nanotubes, TiO_2 and DQ12 quartz

Haemolysis has been considered as an indicator of cytotoxicity (Ottery & Gormley 1978), data from the previous section would suggest DQ12 is the most toxic particle with TiO_2, LMWCNT and SMWCNT demonstrating limited, if any, affect. To establish cytotoxicity of LMWCNT, SMWCNT, DQ12 and TiO_2 release of the cytosolic enzyme Lactose dehydrogenase (LDH) from A549 cells into culture medium was quantified. The enzyme LDH is released from cells upon damage or rupture of their plasma membrane, the amount of enzyme activity detected in culture supernatant therefore correlates with the number of lysed or damaged cells. In this assay A549 cells were cultured after a period of serum starvation for 24 hours with particles ranging in concentration from 10.5-105.3μg/cm^2 (20-200μg/ml). As apparent from figure 3.9 only DQ12 and TiO_2 caused dose dependent increases in the cytotoxicity of A549 cells, concentrations of DQ12 of 21.1μg/cm^2 and above caused significant cell death after 24 hours ($p<0.001$) compared to untreated controls. Concentrations of TiO_2 above 31.6μg/cm^2 caused significant cell death after 24 hours exposure compared to control but there were no significant increases in cytotoxicity between increasing concentrations of the particle. Interestingly the cytotoxicity of TiO_2 indicated by LDH was not paralleled in the haemolysis assay. The increase in cytotoxicity of DQ12 occurred in two stages with a steep increase in cytotoxicity between 10.1-31.6μg/cm^2 and a shallower increase from 31.6-105.3μg/cm^2. The initial increase in DQ12 toxicity was one of 38% over a concentration range of 21.1μg/cm^2, compared to the second gentler increase in which a 37% increase in cytotoxicity occurred over a range of 73.7μg/cm^2. In comparison there was a much more linear increase in cytotoxicity of TiO_2 between 10.5-

105.3μg/cm^2 although this was shallower than either of those caused by DQ12 mirroring the lesser toxicity of this particle. Neither LMWCNT nor SMWCNT demonstrated any evidence of cytotoxicity according to LDH assay after 24 hours reflecting the result of the haemolysis assay described previously. A slight decrease in toxicity towards A549 cells upon MWCNT exposure (fig. 3.9) may be due to adsorption of LDH to the CNT however the closeness of the lines to the base line suggests that this may not be a real effect. Differences in length of the two MWCNT were not accompanied by differences in the extent of cytotoxicity as had been indicated by the haemolysis assay.

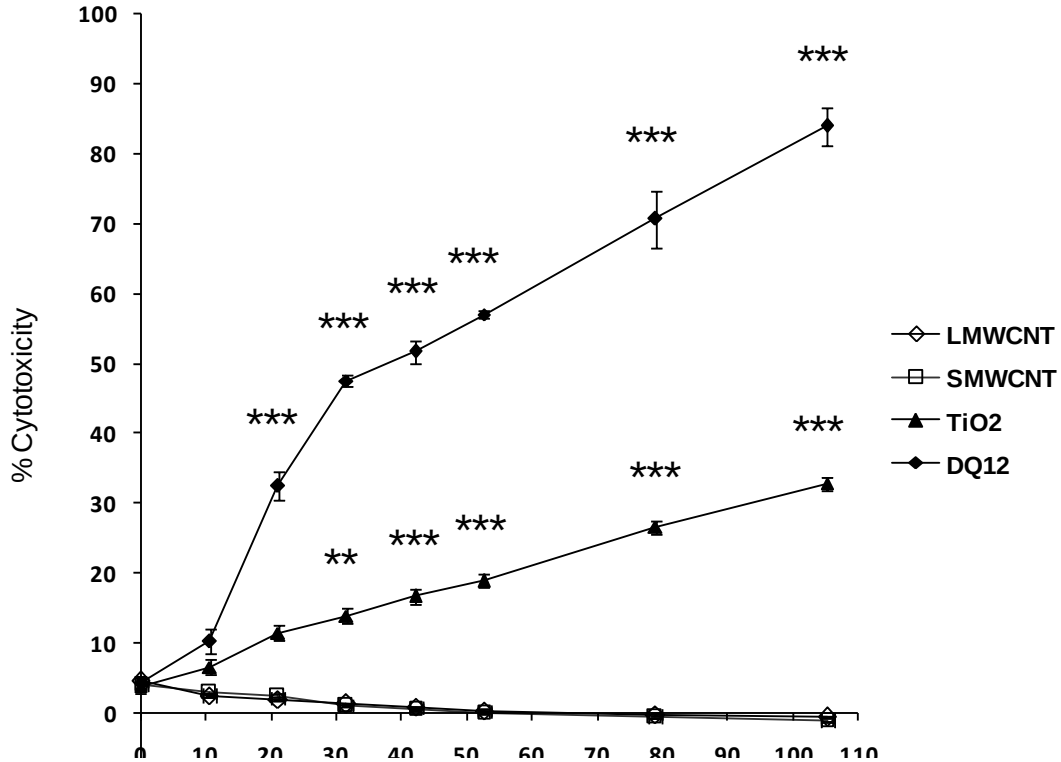

Figure 3.9. Release of LDH from A549 cells after 24 hours exposure to particles and MWCNT. LDH release is expressed as a percentage of the total LDH measured in cell lysate after 24 hours treatment with DQ12, TiO_2, LMWCNT and SMWNCT. The graph represents the mean of three experiments conducted in triplicate, bars represent S.E.M. *p<0.05, **p<0.01, ***p<0.001 compared to cells untreated with particles throughout the experiment.

3.7 Adsorption of LDH to carbon nanotubes

The possibility that the slight decrease in A549 toxicity exposed to an increasing concentration of MWCNT may have represented adsorption of LDH to MWCNT was investigated by LDH adsorption assays. Carbon nanotubes have been shown to have a high capacity for adsorption of some proteins including bovine serum albumin (Valenti et al 2007), fibrinogen (Song et al 2006), complement (Salvador-Morales et al 2006) and streptavidin (Bradley et al 2004). In the previous experiment both MWCNT caused decolouration of the serum free DMEM culture medium as result of adsorption of phenol red pH indicator an effect previously described by Casey et al 2007. Both Casey et al (2007) and Zhu et al (2006) have described how components of culture medium adsorb to SWCNT and MWCNT. The adsorptive capacity of MWCNT towards LDH was investigated by dispersion of increasing concentrations of LMWCNT or SMWCNT in PBS or 2% foetal calf serum (FCS) supplemented DMEM culture medium with cell derived LDH. The level of LDH remaining in solution was then measured after a prescribed period of time using the LDH detection system used for determination of cytotoxicity.

Dispersed only in PBS LMWCNT caused a significant concentration (***$p<0.001$) dependent increase in adsorption of cell derived LDH over the course of one hour (figure 3.12), this was completely attenuated in the presence of 2% FCS in cell culture medium although a small (non significant) concentration dependent increase in adsorption is still observable. The SMWCNT dispersed in PBS caused a similar significant (***$p<0.001$) concentration dependent increase in adsorption of LDH that was also almost totally attenuated by the presence of FCS. There was a divergence in the adsorptive capacity of the two MWCNT; from 100μg/ml

LMWCNT adsorbed significantly more LDH than the same concentration of SMWCNT. Based upon absorbance values of MWCNT in 2% DMEM closely matching those of LDH alone (control) (data not shown) the probability that residual MWCNT interfered in the LDH assay system itself was substantially decreased. These results suggest that in a cell culture medium not supplemented with FCS MWCNT would strongly adsorb extracellular LDH (possibly including the limited amount that would constitute a back ground level in a cell based assay). In this instance it is unlikely that LDH adsorption would explain the limited level of cytotoxicity determined biochemically for MWCNT by LDH assay. This is based on the lack of cytotoxicity of MWCNT at doses where adsorption would have a limited impact on percent cytotoxicity (10-40μg/cm^2) compared to particles such as DQ12 or TiO_2.

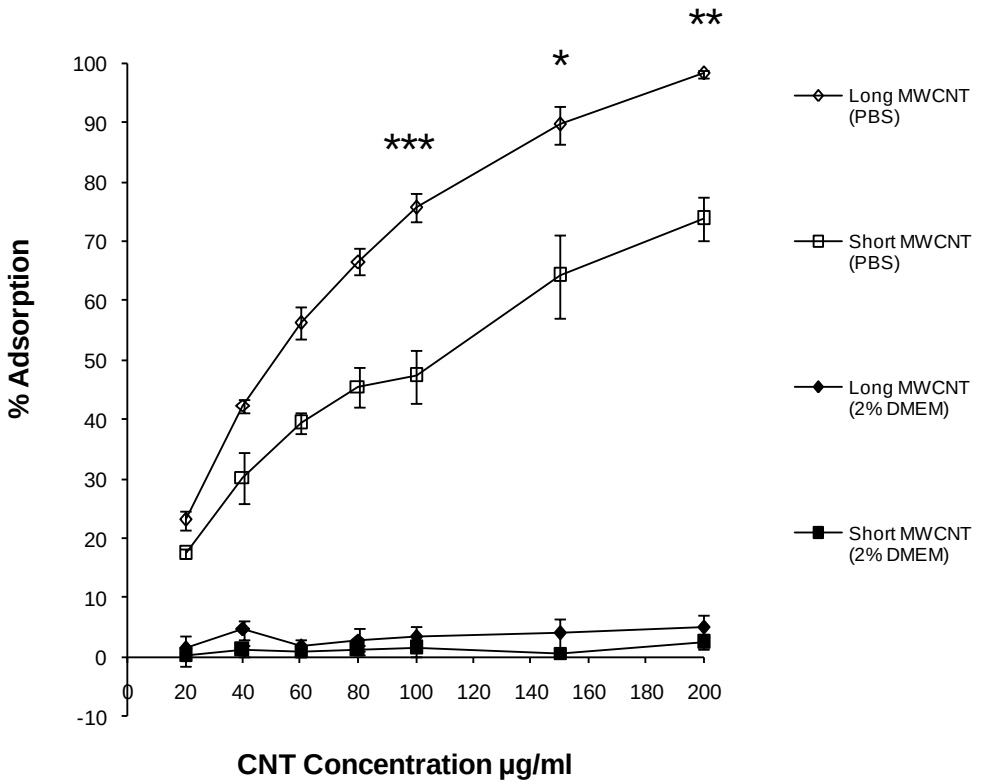

Figure 3.10. Extent of adsorption of LDH to MWCNT after one hour incubation at 37°C. MWCNT were dispersed in PBS or DMEM containing 2% FCS by ultrasonic treatment then incubated for one hour in LDH extracted from A549 cells. The level of LDH remaining was assessed as a percent of the negative control. The graph represents the mean of three experiments performed in triplicate, bars represent S.E.M. *$p<0.05$, **$p<0.01$, ***$p<0.001$ LMWCNT in PBS compared to SMWNCT PBS at equivalent concentrations. In the absence of serum all concentrations of both LMWCNT and SMWCNT adsorbed significantly (***$p<0.001$) more LDH than when dispersed in DMEM containing 2% serum.

Discussion

Metal content. The CNT purchased from Nanolab Inc. (MA, USA) for this study were grown on iron nanoparticles and were acid cleaned to a purity of >95%. From analysis of the metal content of LMWCNT and SMWCNT the level of residual iron was found to be 1.16% and 1.76% respectively. Inclusion of metal catalyst particles enables nucleation of carbon atoms for CNT growth to occur (Ding et al 2006, Amara et al 2008). At the start of their growth, carbon atoms form tight associations with metal nanoparticles that results at the end of synthesis with metal nanoparticles encapsulated within multi-layer graphitic shells or trapped in the tips of central cavities of CNT. This can protect catalyst particles from removal during purification (Zhang et al 2000, Thiên-Nga et al 2002, Jurkschat et al 2006, Li et al 2006). The iron content of LWCMT was found to be slightly less than SMWCNT; similarly the iron content of SFA was greater than LFA. The difference in iron content between MWCNT may simply be accounted for by a greater number of fibres per given mass of sample (of SMWCNT compared to LMWCNT) containing by chance slightly more iron. An alternative explanation may be that the additional acid treatment used to shorten LMWCNT to SMWCNT exposed fresh (additional) metal from with the CNT or graphitic capsules. Some of this may have been mobilised but without sufficient time for removal by the acid would have re-absorbed onto the SMWCNT (Lin et al 2008). DQ12 contained the greatest quantity of iron possibly complexed to its surface (Ghio et al 1992, Ghio et al 1994, Fubini et al 2000, Fubini & Hubbard 2003).

Very little iron could be mobilised into solution indicating a strong association between metal nanoparticle and CNT. This adds weight to the idea that residual iron

was encapsulated or trapped within the CNT (not exposed and surface bound) and inaccessible. This may indicate that *in vitro* in short term assays this iron is toxicologically irrelevant. Additional acid treatment, vigorous sonication and aging may increase availability (Mukhopadhyay et al 2002, Guo et al 2007). Liu et al (2008) suggested encapsulated nickel was stable for up to two months in simulated physiological oxidising conditions (2X phagolysosomal stimulant fluid, 2mM hydrogen peroxide, 2mM ascorbate and 0.2mM iron sulphate). The effect of longer times than this in oxidising conditions (*in vivo* relevant) needs to be established.

Electron microscopy. T.E.M. revealed MWCNT to be highly aggregated and compacted. Bundles of nanotubes were visible emanating from larger (tens of microns) particles, thus in aqueous solution MWCNT could be said to be more particulate than fibrous in nature. Aggregation is a result of extensive van der waals' forces (Bandyopadhyay et al 2002, Vaisman et al 2007). T.E.M. indicates that in aqueous solution, with limited sonication the designation of LMWCNT or SMWCNT was for designation only. S.E.M. of methanol dispersed tangled ropes revealed residual particles indicating purification was not wholly effective at removing impurities. Higher resolution S.E.M. of LMWCNT revealed discontinuities in side walls that could result from acid cleaning or ultra-sonication. These can represent regions of chemical reactivity due to the presence of dangling carbon bonds (Lu et al 1996, Monthioux et al 2001, Fenoglio et al 2008). Micrographs also revealed a mixture of curved and straight tubes; curvature can result from mechanical stress or structural defects (carbon rings other than hexagons) in the MWCNT side walls (Tsang et al 1993, Ebbesen & Takada 1994, Iijima et al 1996, Qian et al 2002).

Plasmid assays. Plasmid assays were conducted as an indirect measure of free radical production by MWCNT. Hydrogen peroxide alone did not cause linearization of DNA but with the inclusion of 100μg/ml MWCNT linearization occurred. This may suggest that MWCNT has some catalytic effect converting hydrogen peroxide to a more reactive species. Graphite can decompose and activate hydrogen peroxide to more reactive species (Lücking et al 1998) whilst graphitic carbon atoms at structural defects possess unpaired electrons that act as reductive centres and form ROS in solution (Miura & Morimoto 1988, Kung & Wang 1997, Vorob ‘ev-Desyatovskii et al 2006, Narayan 2007). This can also occur at the surface of some metal oxides where an electron is transferred (from the oxide) to molecular oxygen resulting in superoxide formation **(**Anpo et al 1999). Hydrogen peroxide (formed from spontaneous dismutation of superoxide) would react with superoxide to generate DNA cleaving hydroxyl radicals (Fridovich 1983). This could be a mechanism by which MWCNT may generate DNA damaging free radicals. Addition of hydrogen peroxide in the assay conducted with MWCNT may have fuelled a similar process or processes. Formation of hydrogen peroxide in close proximity to a transition metal catalyst could also result in Fenton chemistry and hydroxyl radical formation **(**Lesko et al 1980, Fridovich 1983, Halliwell & Cederbaum 1994, Peirre & Fontecave 1994, Koppenol 2001, Cooke et al 2003, Guo et al 2007). The likelihood of residual metal encapsulation with the lack of evidence of bio-available metal makes this latter mechanism to explain DNA cleavage unlikely however. The lack of an effect at higher MWCNT doses may have been due to poor dispersion and flocculation reducing the effective surface area of the MWCNT (a factor linked to increased particle reactivity) (Donaldson et al 1996,

Brown et al 2001, Höhr et al 2002). Noticeable on the gel image was the low fluorescent intensity and small sizes of most bands where DNA had been incubated with MWCNT. This could be due to adsorption of DNA to the CNT as has been demonstrated (Zhao and Johnson, Nakashima et al 2003, Zheng et al 2003, Singh et al 2005, Haggenmueller et al 2008). It is also possible that the interaction of DNA with MWCNT caused extensive condensation of plasmid DNA preventing ethidium bromide from intercalating with nucleic acids producing a correspondingly weak signal (Singh et al 2005).

E.S.R. LMWCNT and SMWCNT appeared to both spontaneously generate a reactive species. On the surface of activated carbons and carbon fibres and in solution in close proximity to their surfaces ROS (particularly superoxide ions) can be formed as a result of the contact of aqueous oxygen with radical type defects (Vorob ‘ev-Desyatovskii et al 2006). Defect sites exist on CNT (Yokomichi 2004) forming an active surface area (Vix-Guterl et al 2001) and this could explain ESR activity observed in this study. However the extent and number of defect sites and whether they are capable of activity in either LMWCNT or SMWCNT is unknown. After 45 minutes SFA was also observed to generate an ESR signal, similar activity was not observed for LFA. SFA was derived from grinding LFA; a process that Zalma et al (1987) observed increased its ESR signal using the spin trap DMPO. They also proposed an initial surface redox reaction that could generate superoxide (that TEMPONE-H is sensitive to) possibly explaining SFA’s observed ESR profile. Milling/grinding can alter the iron chemistry of fibres (Graham et al 1999) one apparent change is the increase in the proportion of ferrous to ferric iron in SFA compared to LFA. In its reduced (ferrous) form iron can reduce molecular oxygen to

superoxide (Valko et al 2005). A higher proportion of ferrous iron in SFA may therefore explain its ESR signal.

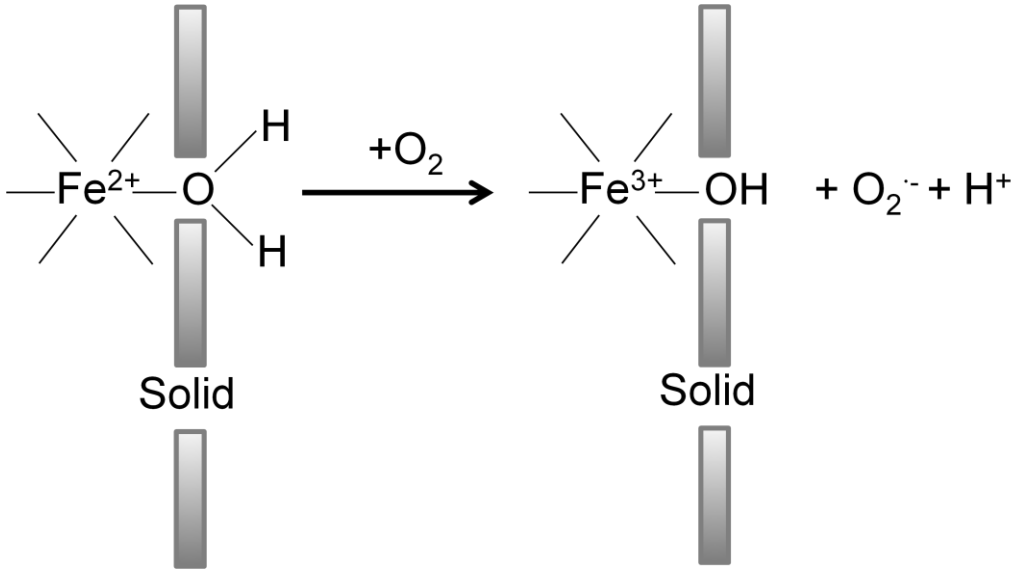

Figure 3.13 The reduction of oxygen to superoxide by transfer of electrons from donor sites on the surface of asbestos, in this example the active site is an OH_2 in low coordination with and linked to Fe^{2+} (Adapted from Zalma et al 1987).

Grinding and milling also increases a materials surface area and exposes fresh non-oxidised surfaces possibly also contributing to the difference in ESR profile between LFA and SFA. Importantly the substantial difference between the ESR profiles of SFA and MWCNT suggests the presence of iron in CNT was not responsible for its signal (as the iron content of SFA was greater than that of MWCNT).

Glutathione (GSH) significantly reduced the ESR signal generated by MWCNT, this indicates that MWCNT were in fact generating a reactive species (i.e. the result was not an artefact) although GSH also reduced the spin trap to an ESR silent form. In the presence of 200U superoxide dismutase (SOD) the ESR signal was also reduced to a lower level. This indicates the species generate by MWCNT may be the superoxide anion. A higher SOD concentration may have been required to produce a more marked effect, i.e. like GSH to reduce the ESR signal closer to the base line.

An alternative possibility is that SOD activity was reduced by its adsorption to MWCNT. CNT have been shown to adsorb proteins (Karajanagi et al 2003, Bradley et al 2004, Chen et al 2004, Asuri et al 2006, Bi et al 2006, Song et al 2006, Ito et al 2007, Valenti et al 2007) affecting their activity. However Bi et al (2006) demonstrated retention of SOD activity even upon adsorption to CNT suggesting adsorption to MWCNT may not diminish activity in this assay. SOD adsorption (if it occurs upon MWCNT) may concentrate the enzyme activity close to the source of free radical formation.

Tween-80 (a non ionic surfactant) was found to significantly reduce the ESR signal generated by MWCNT. In recent studies by Fenoglio et al (2006, 2008) MWCNT dispersed in SDS appeared to scavenge free radicals. SDS was ruled out as the reason for the reduction in radical activity however SDS has been found to scavenge hydroxyl radicals (Sostaric & Riesz, Mieisel et al 1977, El-Bagory et al 2007) as has Triton X-100 (Perkoski et al 2005). The relevance of this is that surfactants may interfere with the production or detection of free radicals generated during ESR possibly explaining the effect of Tween-80 in this assay and the scavenging capacity of CNT described by Fenoglio et al (2006, 2008).

Haemolysis. Neither LWMCNT nor SMWCNT caused significant haemolysis at the highest concentration of 5mg/ml; this was also true for TiO_2. In contrast DQ12 caused a significant dose dependant increase in haemolysis that reached 60% (of maximum) at 5mg/ml. This is line with previous studies (Summerton & Hoenig 1977, Ottery & Gormley 1978, Razzaboni & Bolsaitis 1990, Fubini 1998, Hadnagy et al 2003). The basis of quartz induced haemolysis is thought to be the silanol group (Pandurangi et al 1990, Fubini et al 1999, Hadnagy et al 2003) that hydrogen

bonds with and abstracts membrane components enabling potassium efflux and osmotic shock and cell lysis (Summerton et al 1977, Pandurangi et al 1990). Quartz's surface can also generate aqueous free radicals (due to surface bound radicals and/or surface bound iron) that may contribute to membrane damage (Fubini & Hubbard 2003). The inability of MWCNT to initiate haemolysis may be due to a failure to interact with erythrocytes as a result of their hydrophobic aggregate nature.

Cytotoxicity. MWCNT were not found to exert a cytotoxic effect upon A549 cells. There also appeared to be no relationship between their apparent capacity to generate free radicals (observed by ESR and to a more limited degree plasmid assay) and a cytotoxic effect. This was also true of haemolysis assays. This may indicate that aqueous free radicals have a limited impact upon toxicity generally and damage to cells is a result of a physical interaction between a particle/fibre and a cell or the intracellular generation of free radicals in close proximity to cell critical components. Also possible is that free radical production by MWCNT was not great enough to produce a cytotoxic effect that the species of radical produced was not reactive enough to have a significant detrimental effect (superoxide anions seem the most likely candidate) on the cells, or that constituents of the media buffered cells from free radical production. The aggregate nature, hydrophobicity and absorptive capacity of MWCNT likely also had a bearing on the lack of toxicity (and haemolyis) by limiting MWCNT exposure to cells and ensuring cultures were exposed to fine or course carbonaceous aggregates rather than nanosized fibres. That MWCNT exert a toxic effect towards cell in culture has been established in the human lung tumour cell lines H596, H446, Calu-1 and A549 by MTT assay (Magrez et al 2006, Lanone et al 2008), in a rat lung epithelial cell line by LDH and MTT

assay (Muller et al 2008), in the rat macrophage cell line NR8383 by MTT assay (Pulskamp et al 2007), in Murine alveolar macrophage cell lines RAW 264.7, RAW 267.9 and J774.1 by MTT assay, (Murr et al 2005, Soto et al 2005, Hirano et al 2008), in human macrophages by MTT assay (Schrand et al 2007), in fibroblasts by MTT assay, trypan blue exclusion assay, Hoechst nuclear stain and propidium iodide staining (Tian et al 2006, Ding et al 2007, Pensabene et al 2007), in human T-lymphocytes and the Jurkat T-lymphocyte cell line by Trypan blue exclusion (Bottini et al 2005) and human epidermal keratinocytes by neutral red assay (Monteiro-Riviere et al 2005). Although a number of papers have reported very no limited or no cytotoxicity observed during *in vitro* cell assays (Flahaut et al 2005, Chlopek et al 2006, Fenoglio et al 2006, Murugesan et al 2007, Pulskamp et al 2007, Usui et al 2008).

In contrast to MWCNT, TiO_2 and DQ12 exerted significant dose dependent increases in cytotoxicity. The toxicity of TiO_2 contrasts with its lack of haemolytic ability and ESR silence. A longer exposure time of cultured cells to titanium particles compared to erythrocytes may explain this difference although a substantially higher maximum dose used to haemolysis assays might be expected to compensate. Nano TiO_2 has been reported to generate hydroxyl radicals (Reeves et al 2008), that may have gone undetected in a TEMPONE-H based ESR assay. The cytotoxicity observed towards A549 cells in this study is supported by literature reports of TiO_2 toxicity towards human dermal fibroblasts, A549 cells and goldfish s-K1 cells (Sayes et al 2006, Reeves et al 2008). Toxicity has also been reported *in vivo* in mice and rats (Chen et al 2006, Warheit et al 2007). TiO_2 toxicity can be substantially increased by UV illumination (Sayes et al 2006, Reeves et al 2008) due

photo-generated hydroxyl radicals. Photo-excitation of TiO_2 creates electron-hole pairs energetic enough to oxidise or reduce surrounding molecules (Noda et al 1992, Chen et al 1997). Photo-generated electrons are trapped by titanium atoms:

$Ti^{4+} + e^{-} \rightarrow Ti_{3+}$

Superoxide anions can be formed by interfacial electron transfer from these reduced sites:

$Ti^{3+}{}_{surf} + O_2 \rightarrow Ti^{4+} \quad O_2^{-}$

Positive holes can be trapped on lattice oxide ions and at surface hydroxyl groups forming hydroxyl radicals:

$Ti^{4+} - O^{2-} + h^{+} \rightarrow Ti^{4+} - O^{-}$

$OH^{-} + h^{+} \rightarrow OH\cdot$

Other surface reactions may also occur resulting in the production of hydrogen peroxide:

$2OH\cdot \rightarrow H_2O_2$

(Murphy & Giamello 2002, Sayes et al 2006). Surface activity is concentrated at defect and edge and step edge sites and as particle size decreases the proportion of these atoms as a fraction of the total number in the nanoparticle increases (Quig-Gong et al 2006). Evidence has been put forward that TiO_2 nano-particles will generate hydroxyl radicals without photo-excitation (Reeves et al 2008). The toxicity demonstrated by TiO_2 in this study may therefore be attributable to hydroxyl radical generation.

Toxicity caused by DQ12 to A549 cells may result from several processes; (**1**) once in the presence of cells silica particles are believed to strongly adsorb membrane

components as a result of their silanol groups (Summerton &Hoenig 1977, Otterly & Gormley 1978, Singh et al 1983, Fubini 1998, Fubini et al 1999, Hadnagy et al 2003) and generate free radicals (Shi et al 1994, Schins et al 2002) as a result of the silanol dissociating in water (Merchant et al 1990, Fubini et al 1998) and surface transition metals that catalyse Fenton chemistry (the ability of silicates to catalyse oxidant generation *in vitro* has been found to be proportional to the amount of surface complexed Fe^{3+}) (Ghio et al 1992) by reacting with hydrogen peroxide generated at the minerals reactive surface (Razzaboni & Bolsaitis 1990). From metals analysis (Figure 3.1) it was found DQ12 quartz held the most iron of the listed materials. The adsorption of membrane components results in holes in the cell plasma membrane from which cytosolic constituents can leak out (Summerton & Hoenig 1977) whilst generation of free radicals from adsorbed silica may cause membrane damage or increase paracellular permeability by lipid peroxidation (Merchant et al 1990, Shi et al 1994). (**2**) Quartz particles may also gain entry into alveolar cells by binding to the cell membrane (Elias et al 2000). Kato et al (2003) demonstrated that alveolar type I and II cells could import lecithin coated beads by non phagocytic mechanisms whilst Geiser et al (2005) reported movement of ultrafine particles through cells. Hydrogen peroxide that either diffuses into the cell from its site of generation at the quartz particle or is generated within the cell could react with iron present on the surface of internalised quartz particles and by Fenton chemistry generate hydroxyl radicals. The production of both intracellular and extracellular free radicals and ROS results in oxidative stress and depletion of intracellular antioxidants such as reduced glutathione (Zhang et al 1999, Fenoglio et al 2003, Lin et al 2006). Quartz particles transported into the cells by phagocytic or endocytic mechanisms would be

incorporated in membranous vesicles (**3**) from which they may escape to the cytoplasm by Fenton mediated disruption of intracellular vesicle membranes (Pearsson 2005). Through the production of free radicals particles of DQ12 can cause damage to nucleic acids inflicting double strand breaks (Shi et al 1994, Saffiotti et al 1994). Double strand DNA breaks are attributed to the hydroxyl radical implying that for quartz to cause DNA strand scission it must be in close proximity to the nucleic acid (Halliwell & Aruoma 1991, Kukielka & Cederbaum 1994, Nunoshiba et al 1999, Fanizza et al 2006). It has been suggested that DNA binds to the surface of the quartz particle, indirect evidence for this comes from the observation that modification of the particles surface with aluminium lactate or PVNO attenuates DNA damage (Knaapen et al 2002). A physical interaction between quartz particles and DNA has been shown by Fourier transform infrared spectroscopy. Co-incubation of DNA and quartz in aqueous solution resulted in a change in the spectra of both suggesting the formation of a complex between the two probably as a result of hydrogen bonding between the phosphate sugar back bone and silanol groups on the quartz (Saffiotti et al 1994).

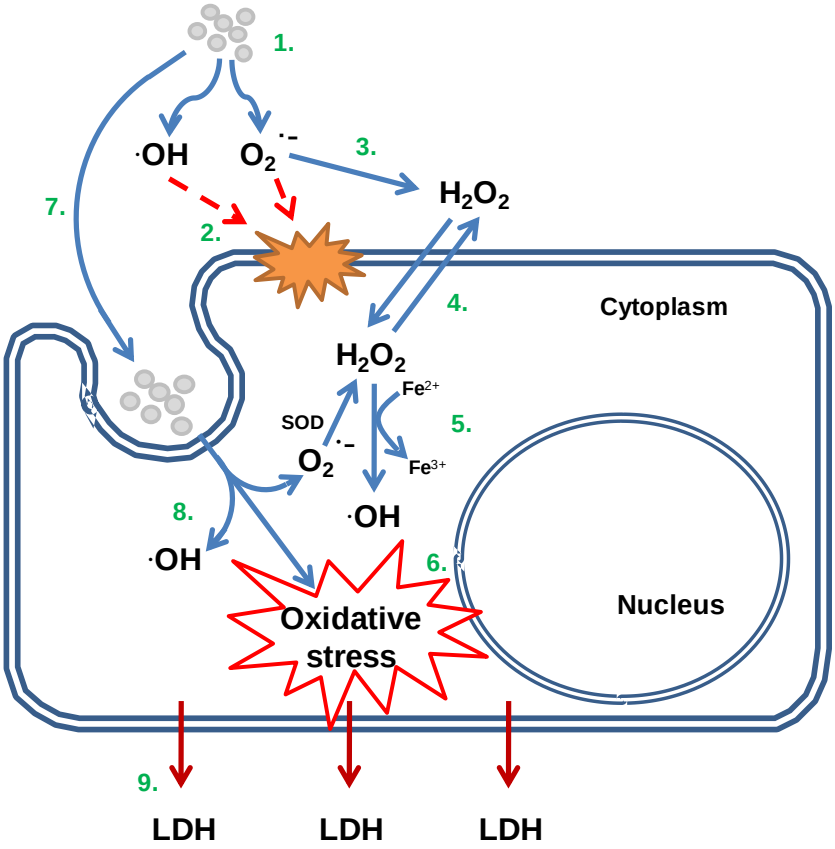

Figure 3.16 Possible mechanism of TiO_2 toxicity to cultured A549 cells. **1.** The surfaces of TiO_2 react with dissolved oxygen and water to generate hydroxyl and superoxide radicals (Noda et al 1992, Murphy et al 2002, Sayes et al 2006, Reeves et al 2008). **2.** Extracellular free radicals react with and damage the cell membrane (Halliwell & Gutteridge 1984, Betteridge 2000, Schafer et al 2000). **3.** Superoxide spontaneously dismutases to hydrogen peroxide **4.** crossing the plasma membrane into the cell, intracellularly superoxide is also subject to enzyme catalysed dismutation by superoxide dismutase (Halliwell & Gutteridge 1984, Zhu et al 1998, Bandyopadhyay et al 1999). **5.** Superoxide generated intracellularly can release iron from iron (Fe) storage proteins such as ferritin and from [4Fe-4S] containing clusters of dehydratases (Biemond et al 1986, Liocehv & Fridovich 1994). Fe^{2+} iron reduces hydrogen peroxide to the hydroxyl radical (Miller et al 1990, Pierre & Fontecave 1999). **6.** The hydroxyl radical in particular but also hydrogen peroxide depletes cellular antioxidants resulting in oxidative stress and damages cell apparatus and cell critical molecules (Farber 1994). **7.** TiO_2 nanoparticles may gain access to the cytoplasm through endocytic or non endocytic mechanisms; this would affect their localisation within the cell (Fletcher et al 1994, Davada & Labhasetwar 2002, Geiser et al 2005, Garcia-Garcia et al 2005). **8.** Silica particles have been shown to escape lysosomes into the cytoplasm through iron mediated rupture of their membranes; this has been attributed to intralysosomal Fenton type chemistry (Persson 2005). Generation of hydroxyl radicals by TiO_2 particles could also enable such an escape. In the cytoplasm the reactive surface of free particles would be able to continue generating reactive oxygen species. **9.** A combination of intracellular and extracellular damage reduces the integrity of the cell membrane allowing the escape of LDH.

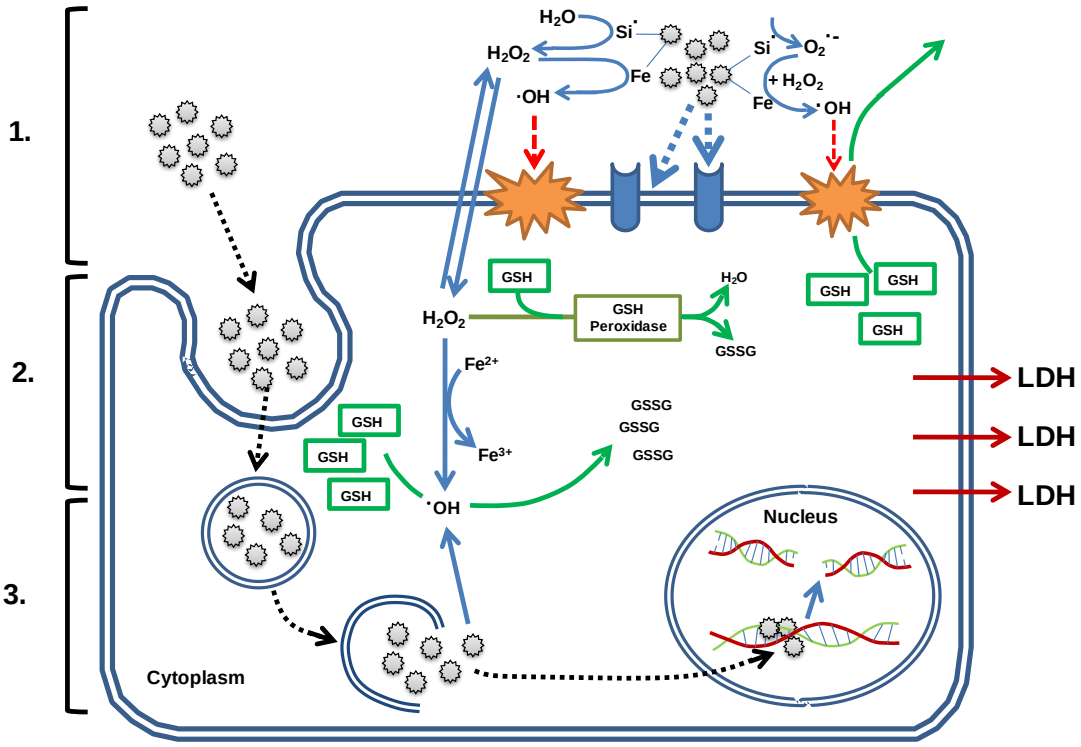

Figure 3.17 Potential mechanisms of silica toxicity to cells. A diagrammatic representation of the possible interaction of particles of DQ12 (Grey 12 point stars) with an A549 epithelial cell, **blue arrows:** Movement of free radicals/ROS, **double blue tram lines:** Plasma/vesicle/nuclear membrane, **broken blue arrows:** DQ12 interactions with plasma membrane or cell membrane proteins by hydrogen bonding, **blue ovoids:** Membrane bound proteins, **broken red arrows:** Damaging free radical interactions, **red explosion:** Free radical/ROS induced damage, **broken black arrows:** Movement of DQ12 particles, **green boxes:** Reduced (GSH)/oxidised glutathione (GSSG), **green arrows:** Movement/interaction of GSH with free radicals/ROS.

To summarise results from this section:

1. MWCNTs contain comparatively high levels of iron none of which could be mobilised.

2. In aqueous solution MWCNT form tight compact aggregates closer in resemblance to particles than fibres.

3. MWCNTs have a very limited capacity to cleave DNA and may adsorb DNA.

4. MWCNTs spontaneously generate a reactive species (as demonstrated by ESR) that could be diminished by GSH and more importantly by SOD. Diminution in ESR signal by SOD suggests MWCNT spontaneously generate superoxide anions.

6. MWCNT did not demonstrate any haemolytic potential even at extremely high concentrations (1-4mg/ml), in sharp contrast DQ12 was found to highly haemolytic.

7. In an aggregated state MWCNT demonstrated no cytotoxic potential to pulmonary type II epithelial cells. Both DQ12 and TiO_2 caused significant toxicity, in the case of TiO_2 this may be attributed to reactive edges generating free radicals and for DQ12 to silanol groups reacting with cell membranes and generating reactive species.

Chapter 4

The *in vitro* oxidative stressing and inflammatory potential of MWCNT

Chapter 4

The oxidative stressing and inflammatory potential *in vitro* of Multi-walled carbon nanotubes (MWCNT) and control particles towards the alveolar epithelial cell line A549.

4.1 Introduction

Oxidative stress is the imbalance between levels of free radicals/ROS and cellular and tissue anti-oxidant defences in favour of oxidation resulting in activation of anti-oxidant defences, inflammation or cellular injury (Nel et al 2006). For cells, this may result in activation of oxidative stress responsive pathways and potentially apoptosis and necrosis (Farber 1994, Chandra et al 2000, Kochevar et al 2000, Simon et al 2000). Such processes may result in inflammation, fibrosis, mutagenesis, carcinogenesis or tissue destruction (Wright et al 1994, Rahman et al 2006). To combat oxidative stress cells posses self sustained highly diverse but coordinated defences including glutathione (Sies 1993, Pal Yu 1994). Reduced glutathione (GSH) is a tri-peptide of γ-glutamyl-cysteine-glycine that is abundant in mammalian cells with intra-cellular concentrations ranging from 0.5-10mM. GSH reacts readily with free radicals and is a key epithelial cell anti-oxidant (Ray et al 1999). Oxidative stress can be expressed in terms of the ratio of reduced glutathione (GSH) to oxidised glutathione (GSSG) (Xia et al 2006). This ratio is frequently described in paradigms of particle toxicity (Xia et al 2006) including for silica, ufCB, and TiO_2 (Zhang et al 1999, Monteiller et al 2008). Decreases in GSH levels have been linked to activation of pro-inflammatory genes (and ultimately production of pro-inflammatory mediators) (Ginn-pease & Whisler 1996, Wilhelm et al 1997).

In response to oxidative stress epithelial cells may release inteleukin-8 (IL-8) (Martin et al 1997). This is a pro-inflammatory chemokine of the C-X family that is chemotactic and mediates neutrophil recruitment, it is produced through cooperative action of the transcription factors NF-κB and AP-1 (possibly also p38) (Baldwin et al 1990, Deforge et al 1993 Feghali and Wright 1997, Mukaida 2002, Kim et al 2005). It has been demonstrated to be produced in response to oxidative stress (Yamamoto et al 2003, Yang et al 2006, Boncoeur et al 2008) and has also been observed to be produced in response to ufCB exposure by a mechanism involving particle mediated oxidative stress (Stone et al 1998, Stone et al 2000, Jijon et al 2002, Li et al 2002, Gilmour et al 2003, Swain et al 2004, Kim et al 2005 Mroz et al 2007). To be effective and not destructive inflammation must be controlled and proportionate. This control is exercised partly through the cytokine tissue growth factor-β (TGF-β) (Sheppard et al 2004). Triggers for TGF-β production may include ROS and oxidative stress (Nath et al 1998, Bellocq et al 1999). This chapter explores the oxidative stressing capacity of MWCNT by examining the extent of depletion of glutathione in A549 cells following exposure. It was also predicted that exposure of epithelial cells may result in the induction of a pro-fibrotic response detectable by production of TGF-β.

4.2 The effect of long and short Multi-walled carbon nanotube exposure on intracellular GSH levels in alveolar epithelial cells.

Glutathione is an important cellular antioxidant a decline in the levels of which has been taken as an indicator of oxidative stress. The total GSH content of exposed cells was determined by spectroscopy based on its reduction of the sulphydryl reagent DTNB to its yellow product 2-nitro-5-thiobenzoic acid in the presence of NADPH. Assessment of A549 cell GSH content after exposure to MWCNT was conducted to determine if the free radical production detected by ESR resulted in oxidative stress. Treatment of A549 cells with LMWCNT and SMWCNT resulted in a dose dependent significant depletion of total GSH (fig 4.1). Treatment of cells with DQ12 resulted in a significant depletion of GSH ($p<0.001$) at the lowest tested concentration, with higher concentrations reducing GSH content to almost undetectable levels.

Total intracellular GSH concentration was analysed again after treatment with MWCNT dispersed in 2% FCS medium (fig 4.2). Serum was included as a natural dispersant to achieve a more stable finer dispersion of MWCNT, it was also considered possible that serum may act as buffer against the effects of reactive species generated by particles. All three materials caused significant dose dependent depletions of total GSH that were similar in scale, for both MWCNT GSH reductions became significant ($p<0.001$) at a concentration of 31.6μg/cm^2 and for positive control DQ12 at 10.5μg/cm^2. DQ12 caused the greatest GSH depletion at the lowest dose compared to the MWCNT, however the gradient of the reduction with increasing concentration was less than that observed for MWCNT resulting in the highest dose (52.6μg/cm^2) for all tested materials causing very similar levels of

GSH depletion. This observation might suggest that a protective capacity of serum exerted towards treated cells. Of the two MWCNT, SMWCNT was found to inflict a slightly greater reduction in total GSH levels at the highest dose than LMWCNT. This observation was also made for cells treated in serum free medium.

Cells were exposed to particles for 48 hours and their GSH content quantified (fig 4.2). It was apparent that extended culture of cells appeared to result in a decrease in their GSH content, this was apparent from the dramatic reduction in control cell GSH levels compared to previous assays. Cells exposed to the lowest concentration (10.5μg/cm^2) of MWCNT had a significantly higher total GSH levels than the control. The GSH content of cells exposed to 10.5μg/cm^2 DQ12 remained very similar to control levels. Exposure to increasing concentrations of LMWCNT and SMWCNT resulted in a concentration dependent decrease in total GSH levels. From 31.6μg/cm^2 LMWCNT significantly decreased total cellular GSH. The GSH content of DQ12 treated cells decreased between the lowest and highest concentrations but not concentration dependently and not significantly, in fact it was observed that the control levels of GSH after 48 hours were lower than those cells treated with 52.6μg/cm^2 of DQ12. Both MWCNT caused a greater depletion in GSH than DQ12 after 48 hours. The comparative lack of effect of DQ12 upon total GSH after 48 hours may represent a protective effect of the serum.

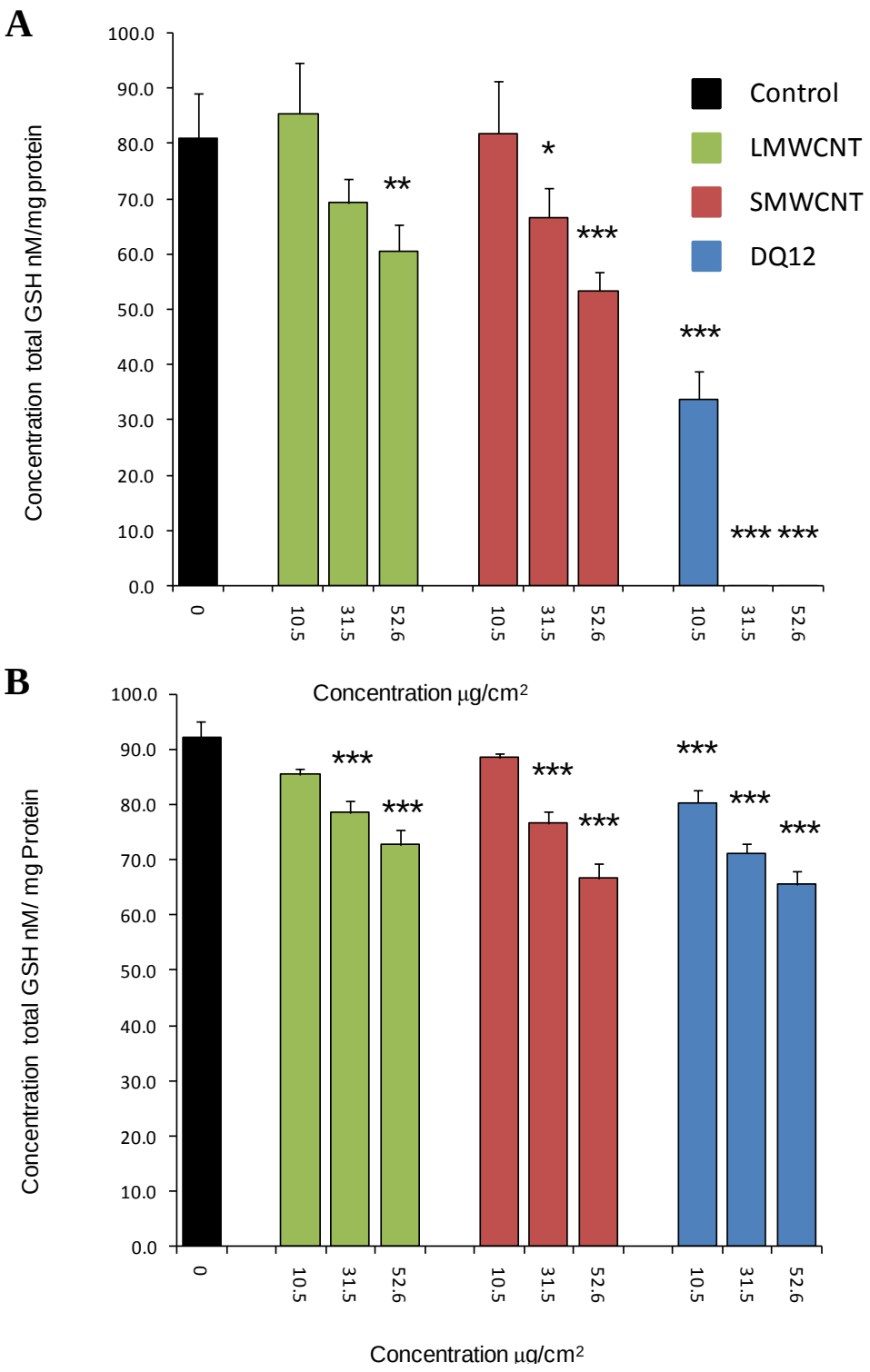

Figure 4.1. Effect of LMWCNT, SMWCNT and DQ12 on the total GSH content of A549 cells. (A) GSH content was assessed in cells serum starved for 24 hours then exposed to particles in serum free conditions for 24 hours. **(B)** GSH content was assessed in cells exposed to reduced serum (2%) conditions for 24 hours and then exposed to particles for 24 hours in 2% serum. Histograms represent the means of three experiments performed in triplicate, bars represent S.E.M. *p<0.05, **p<0.01, ***p<0.001.

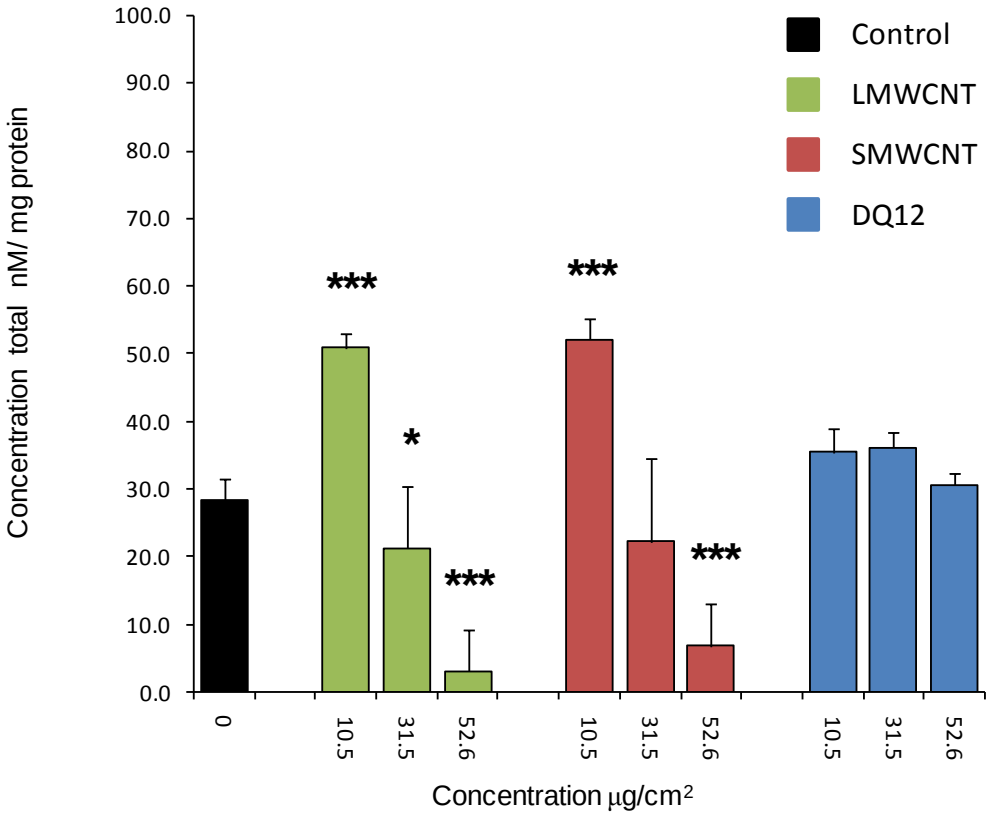

Figure 4.2. Effect of LMWCNT, SMWCNT and DQ12 on the total GSH of A549 cells. GSH content was assessed in cells cultured for 24 hours in 2% serum then exposed to particles for 48 hours in 2% serum. Histogram represents the means of three experiments performed in triplicate, bars represent S.E.M. *p<0.05, ***p<0.001.

4.3 Assessment of the capacity of MWCNT to adsorb GSH

The ability of MWCNT to adsorb glutathione was examined under serum free (in PBS) and reduced (2%) serum media conditions to assess the capacity for these materials to interfere in the assay or give a false impression of oxidative cellular depletion of GSH. MWCNT particles not incubated in serum containing medium overnight prior to incubation with a solution GSH demonstrated a concentration dependent ability to adsorb GSH that increased significantly with increasing concentration (fig 4.3A). This capacity was only slightly apparent for DQ12 that nominally adsorbed GSH in a concentration dependent manner. Following overnight incubation in DMEM supplemented with 2% FCS the capacity of either LMWCNT or SMWCNT to adsorb GSH was abolished (fig 4.3B). With increasing concentration of MWCNT the GSH concentration remained constant and stable as indicated by the plateau of the dose response lines. The lack of any apparent GSH adsorption by MWCNT demonstrated in figure 4.3B also suggests GSH was unable to competitively bind to the surface of nanotube particles and replace adsorbed FCS.

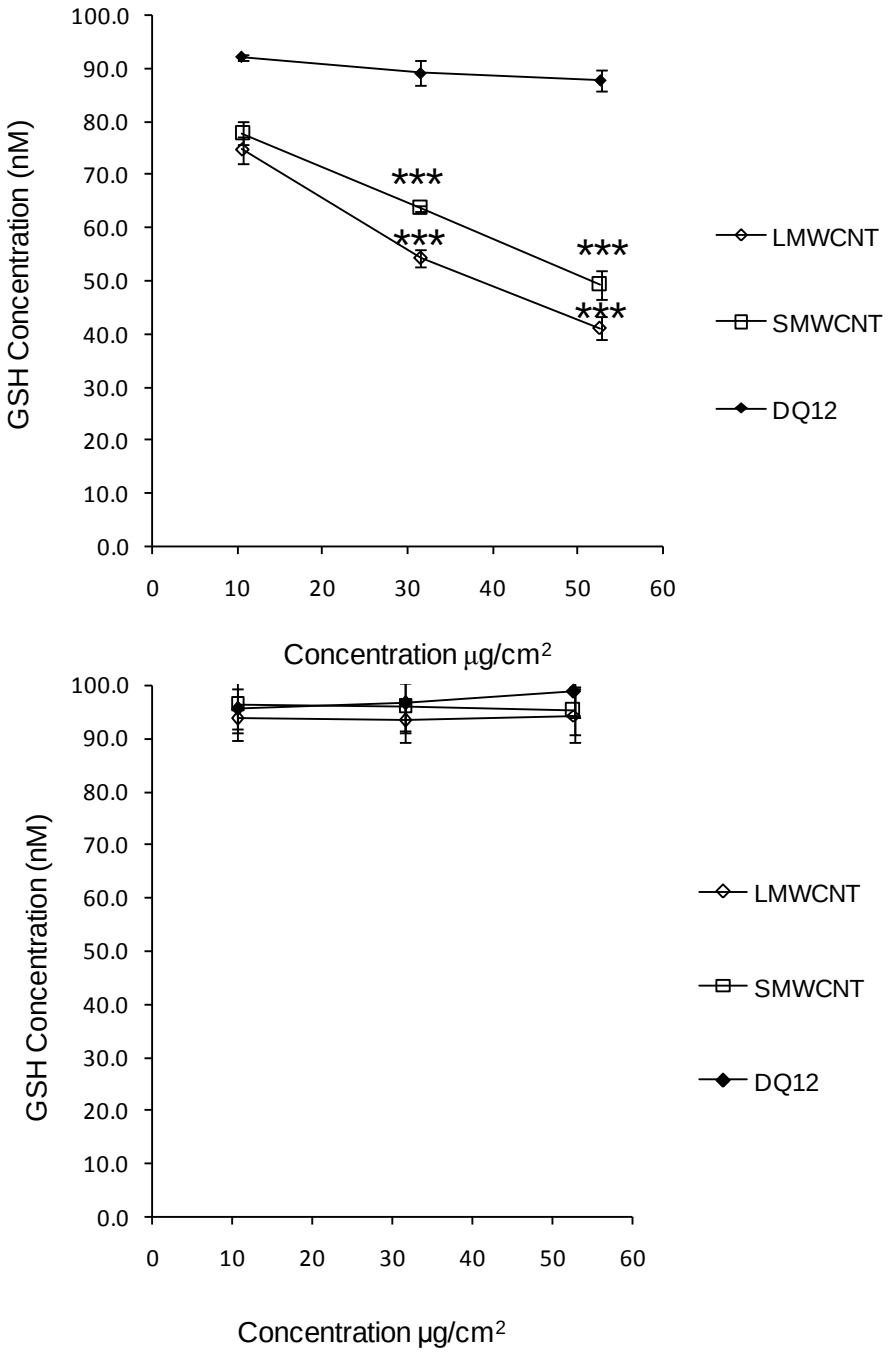

Figure 4.3. Adsorption of GSH to (A) MWCNT and DQ12 in PBS and (B) MWCNT and DQ12 in 2% DMEM. (A) Particles were prepared in PBS for one hour at RT with GSH. (**B)** Particles were sonicated and incubated over night in 2% DMEM prior to being spun down and supernatants re-suspended in GSH prepared in PBS, particles and GSH were incubated for one hour at RT. Graphs represent the means of three experiments performed in triplicate, bars represent S.E.M.***$p<0.001$.

4.4 Ability of MWCNT to induce pro-inflammatory effects in alveolar epithelial cells.

Based on their ability to generate free radicals and cause depletion of intra-cellular GSH, evidence of a resultant inflammatory response to this stress in epithelial cells was sought by measuring IL-8 production. Cells of the alveolar epithelial cell line A549 were exposed to LMWCNT, SMWCNT, DQ12 (positive control particle) or TNF-α (positive control for IL-8 production) for 6, 24 or 48 hours in serum free or 2% FCS DMEM and their IL-8 response assessed. After 24 hours treatment in serum free medium neither LMWCNT nor SMWCNT appeared to generate a detectable IL-8 response (fig 4.4). In fact background levels of IL-8 production were found to be significantly greater than those generated in response to MWCNT exposure ($p<0.001$, data not shown). In sharp contrast DQ12 caused a substantial dose dependent release of IL-8 that became significant (***$p<0.01$) at 31.5μg/cm^2. The complete lack of an IL-8 response to MWCNT even equivalent to background levels suggested adsorption of IL-8 to the test material. This notion is supported by published descriptions of the ability of CNT and carbon black to adsorb biological molecules including inflammatory mediators. To analyse this possibility a strategy of limited cellular exposure followed by a period of continued incubation in the absence of MWCNT was adopted. This was based on the idea that stress or injury inflicted during time limited exposures of MWCNT to cells might be responded to by prolonged production of IL-8 which, in the absence of MWCNT, might be detectable. Following six hours exposure to test materials A549 cells were washed and re-incubated in fresh serum free medium for 24 hours, IL-8 levels were then measured (figure 4.5). The pattern of IL-8 production was similar to that described

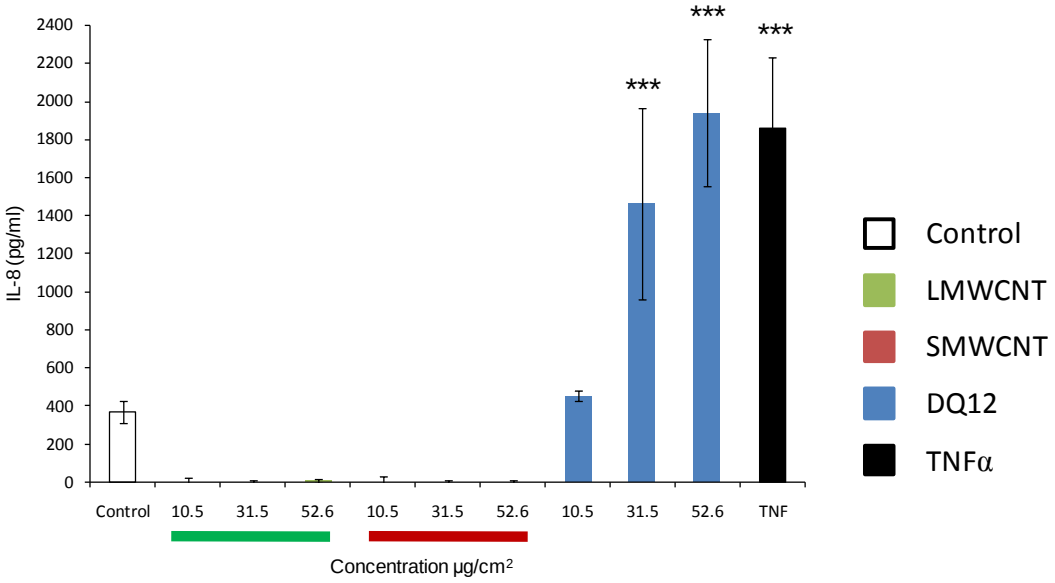

Figure 4.4. Effect upon IL-8 production by A549 cells of 24 hours exposure to LMWCNT, SMWCNT or DQ12. A549 cells were serum starved for 24 hours to test materials or TNFα. The histogram represents IL-8 levels in culture medium following this exposure period. Three independent experiments were conducted, bars represent S.E.M. ***p<0.001 compared to untreated control.

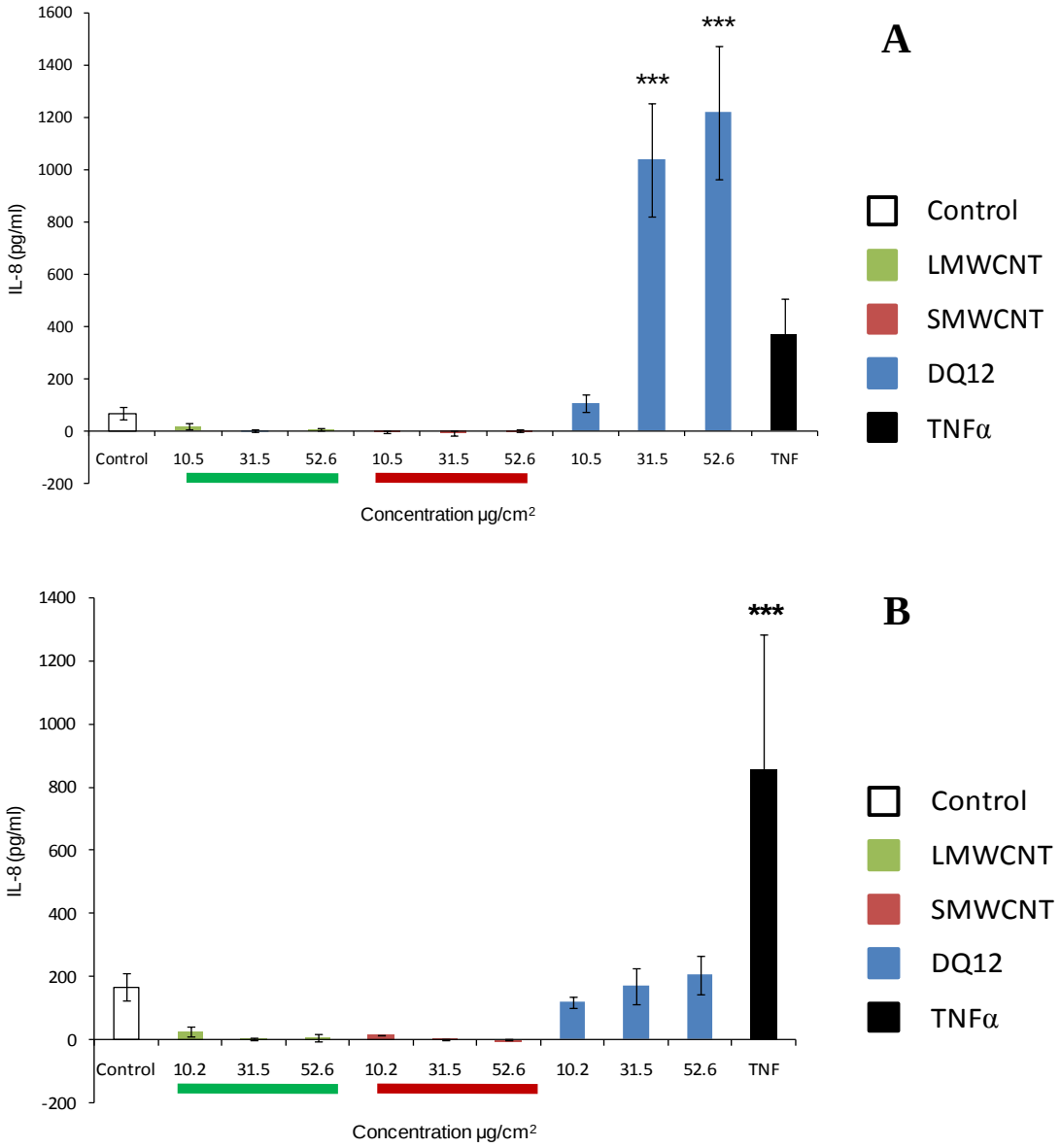

Figure 4.5. The effect upon IL-8 production by A549 cells of 6 or 24 hours particles exposure followed by 24 hours post exposure incubation in fresh medium. **(A)** Cells were serum starved then exposed for six hours to particles; particles were removed by washing and cells re-incubated in fresh medium for 24 hours. Il-8 released into culture medium was measured in fresh culture medium. **(B)** Cells were serum staved and treated with test materials for 24 hours, particles were removed by washing and cells culture for 24 hours in fresh medium. Il-8 levels were analysed in cell culture supernatant. Histograms represent means of three independent experiments, bars represent S.E.M. ***p<0.001 compared to untreated control.

in fig. 4.4, DQ12 caused a concentration dependent increase in IL-8 levels that became significant ($p < 0.001$) at 31.5μg/cm^2. The stepped concentration increase was not evident, a dramatic jump was observed between 10.5 and 31.5μg/cm^2 that began to plateau thereafter. Removal of a substantial fraction of the particles by washing reduced the IL-8 output by about half. Compared to fig. 4.4 a very small increase in IL-8 levels was apparent at a LMWCNT concentration of 10.5μg/cm^2 that disappeared with increasing concentration, this was not noticeable at any concentration of SMWCNT. The lack of IL-8 release even after washing the first treatment off could be due to continued adsorption of IL-8 by residual nanotubes tightly associated with the cell monolayer combined with a limited inflammatory ability that may not peak above control levels.

In response to the loss of the presence of TNF-α, the secretion of IL-8 was diminished. Whereas removal of a substantial fraction of DQ12 by washing still resulted in significant IL-8 production removal of most TNFα resulted a more immediate reduction in induced IL-8 production. This may represent a continued stress response to damage that takes time to repair as opposed to receptor mediated induction of IL-8 production that is quickly down scaled once the stimulus has been largely removed. The remaining level of IL-8 response may be a combination of the effect of residual TNFα (e.g. that bound to cells during washing) and a stress response to the washing and change of media itself.

This experiment was then repeated extending the exposure period prior to cell washing and re-incubation in fresh serum free medium up to 24 hours (Fig 4.5B). This was performed to determine if a prolonged exposure would produce a more

substantial IL-8 response that could be quantified. The overall pattern of results was similar to that described in fig. 4.5A; at 10.5μg/cm^2 LMWCNT and SMWCNT both demonstrated a level of IL-8 (unlike at six hours) production that was approximately 1/8th of the level of the untreated control. At higher MWCNT concentrations no IL-8 production was detected. The positive control DQ12 induced IL-8 production at all concentrations that increased in a concentration dependent manner but were not significantly greater than the control. The extent of the cytokines production at 10.5μg/cm^2 DQ12 was actually less than the negative control. The extent of IL-8 release from A549 cells in response to DQ12 was less at 24 hours than that detected at six hours indicating substantial cell death in the succeeding hours. The level of IL-8 release in response to TNF-α was increased significantly over that seen in fig 4.5A although with a substantial error bar.

It had previously been demonstrated by acellular assay that adsorption of FCS to CNT reduced the extent of adsorption of detectable bio-markers such as LDH and GSH to the surface of the nanotubes. In light of this it was thought that exposure of cells to particles in 2% serum containing medium may prevent adsorption of IL-8 to the surface of nanotubes by physical blockade by FCS. Particles were therefore prepared in 2% DMEM and cells treated for 24 or 48 hours, cell medium supernatant levels of IL-8 were analysed. After 24 hours (fig 4.6a) no evidence of induced IL-8 production from A549 cells in response to LMWCNT or SMWCNT exposure could be observed, DQ12 on the other hand caused a concentration- dependent increase in IL-8 production that was significantly ($p<0.001$) greater than control at the 31.6μg/cm^2. The primary cytokine TNFα induced a significant ($p<0.001$) level of IL-8 release after 24 hours. After 48 hours (fig 4.6b) an IL-8 response from A549

cells in response to treatment with LMWCNT was detected. This was observed to decrease with increasing concentration of LMWCNT indicating possible adsorption of the cytokine to the surface of the nanotube. Similarly, in response to the lowest concentration of SMWCNT (10.5μg/cm^2) a small increase in IL-8 production was noticeable but disappeared as MWCNT concentration increased. As for 24 hours exposure treatment with DQ12 caused a concentration dependent increase in IL-8 secretion that became significantly ($p<0.001$) greater than control at 31.5μg/cm^2. After 48 hours, treatment more than doubled the amount of IL-8 liberated from A549 cells in response to all concentrations of DQ12 indicating a possible time as well as concentration dependent effect. This result was repeated in the response of cells to TNF-α, exposure to this primary cytokine caused a significant ($p <0.001$) release of IL-8 substantially greater than that recorded at 24 hours.

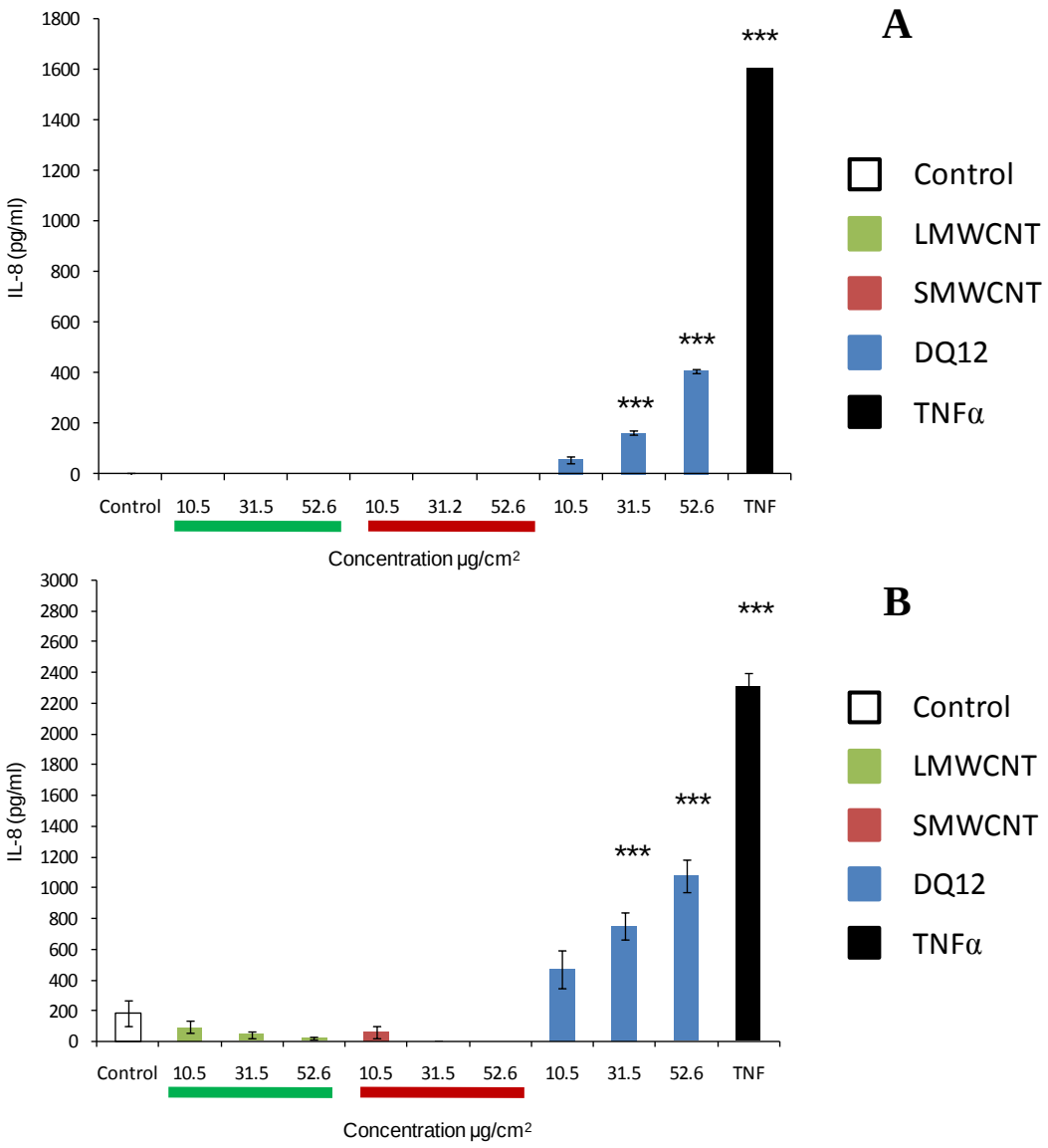

Figure 4.6. Effect of 24 or 48 hour treatment of A549 cells with MWCNT or DQ12 in 2% DMEM. (A) Cells were serum reduced before 24 hour treatment with test materials dispersed in 2% serum. Cell culture medium was removed and analysed for IL-8. **(B)** Cells were serum reduced prior to 48 hour exposure to test materials, cell culture medium was removed and IL-8 levels measured. Histograms represent means of three independent experiments, bars represent S.E.M. ***$p<0.001$ compared to untreated control.

4.5 The effect of MWCNT and DQ12 particles on IL-8 and TGF-β gene expression in alveolar epithelial cells

The IL-8 gene expression profiles of nanotube treated epithelial cells were examined. To determine the pro-inflammatory status of MWCNT reverse transcriptase PCR was used to examine changes in the steady state level of IL-8 gene expression of A549 cells. The gene expression profile of TGF-β was also examined, it had been suggested that *in vivo* CNT caused a very limited acute inflammatory response followed by a rapid and more severe fibrotic response characterised by increased levels of TGF-β (Shvedova et al 2005, 2007, 2008). Initially cells were exposed to the lowest MWCNT concentration tested during the IL-8 ELISA assays (10.5μg/cm^2) because their inflammatory potential was an unknown. Cells were also cultured with a variety of control particles including positive particle control DQ12, negative particle control TiO_2, and ufCB at 10.5μg/cm^2 and 10ng/ml the primary cytokine TNF-α (positive control) to serve as basis of comparison. Cells were treated for four and 24 hours with each of the particles types and TNF-α.

After four hours the only particle found to increase IL-8 expression above the level of the control was DQ12 (Fig 4.7), neither MWCNT induced an increase in IL-8 mRNA expression. Exposure of cells to TNF-α induced the greatest increase in IL-8 expression. To determine the influence of exposure time on IL-8 expression following MWCNT treatment the period of exposure was extended to 24 hours (Fig. 4.8). The particle DQ12 induced the greatest increase in IL-8 expression compared to the control. Smaller increases in expression were induced by both TiO_2, the cytokine TNF-α also induced a significant increase in IL-8 expression ($p < 0.01$). All other particles matched the un treated control in terms IL-8 mRNA production.

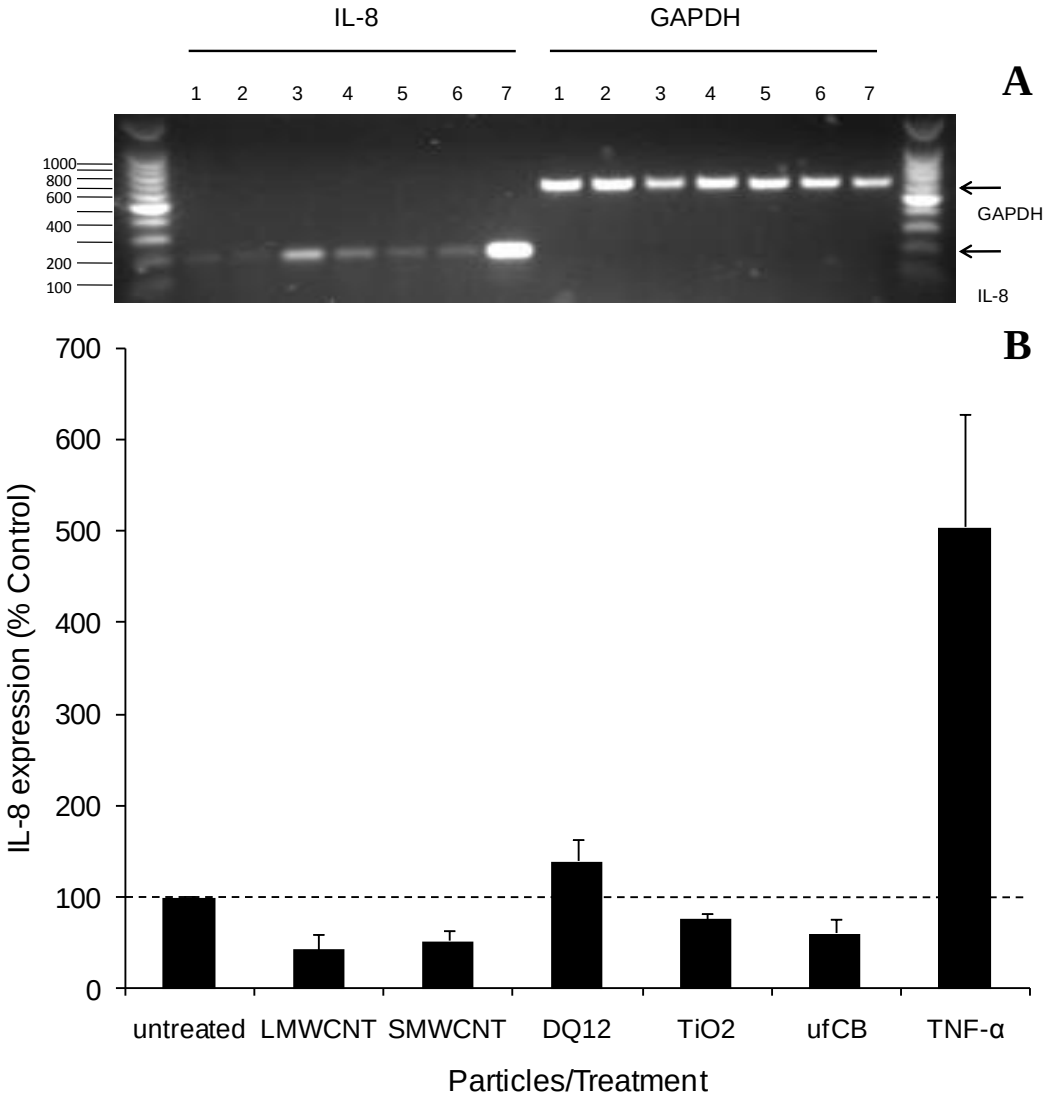

Figure 4.7. IL-8 gene expression profiles for A549 cells exposed for four hours to 10.5µg/cm^2 MWCNT and control particles. Cells were exposed for four hours to each particles in 0% DMEM, RNA was extracted and isolated and IL-8mRNA quantified by RT-PCR. **(A)** Representative PCR gel showing IL-8 and GAPDH bands; **(1)** LMWCNT **(2)** SMWCNT **(3)** DQ12 **(4)** TiO_2 **(5)** ufCB **(6)** untreated **(7)** TNFα. **(B)** Histogram of IL-8 gene expression as a percent of the untreated control (control level represented by dashed line). Histogram represents the mean of three experiments conducted on pooled triplicate samples. Il-8 expression was quantified from gels by densitometry and values expressed as a ratio of IL-8:GAPDH then as a percentage of the negative control. Bars represent S.E.M.

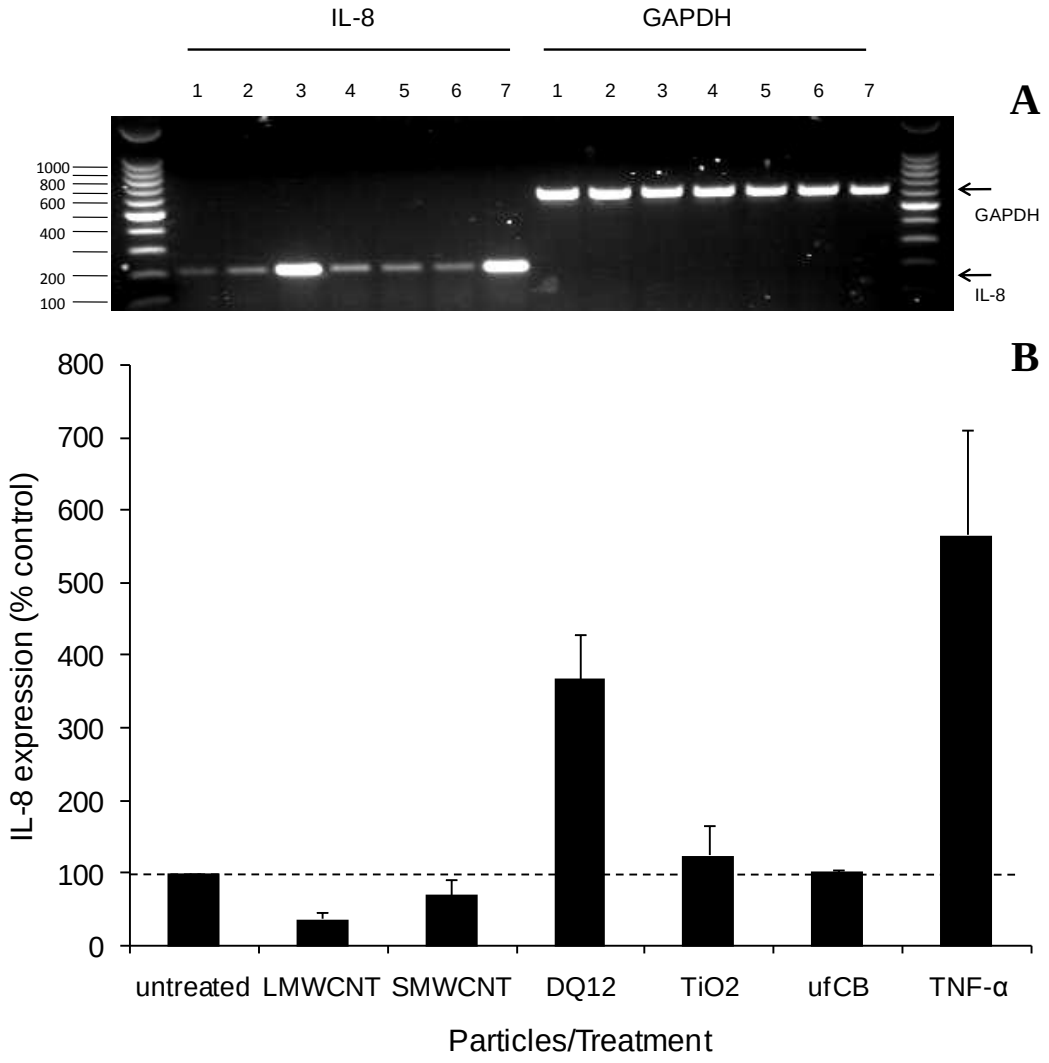

Figure 4.8. IL-8 gene expression profiles for A549 cells exposed for 24 hours to 10.5µg/cm^2 MWCNT and control particles. Cells were exposed for four hours to each particles in 0% DMEM, RNA was extracted and isolated and IL-8mRNA quantified by RT-PCR. **(A)** Representative PCR gel showing IL-8 and GAPDH bands; **(1)** LMWCNT **(2)** SMWCNT **(3)** DQ12 **(4)** TiO_2 **(5)** ufCB **(6)** untreated **(7)** TNFα. **(B)** Histogram of IL-8 gene expression as a percent of the untreated control (control level represented by dashed line). Histogram represents the mean of three experiments conducted on pooled triplicate samples. Il-8 expression was quantified from gels by densitometry and values expressed as a ratio of IL-8:GAPDH then as a percentage of the negative control. Bars represent S.E.M.

To explain a possible concentration dependent component to MWCNT induced IL-8 expression A549 treatment concentrations were increased from 10.5μg/cm^2 to 52.6μg/cm^2 for 24 hours (DQ12 concentration was maintained at 10.5μ/cm^2). An additional MWCNT was also included for comparison, designated Japanese multi-walled carbon nanotube (JMWCNT) after its manufacturing origin. After 24 exposures at 52.6μg/cm^2 (appendix VI) neither LMWCNT nor SMWCNT caused A549 cells to express IL-8 to a level greater than the untreated control. IL-8 expression was increased by JMWCNT to levels double background and those induced by LMWCNT and SMWCNT, IL-8 mRNA production was also slightly above that following ufCB exposure. As a result of treatment with TiO_2 IL-8 gene expression was increased fourfold above the level of the untreated control but also non-significantly. It was observed that only DQ12 substantially increased the expression of Il-8 cells after treatment.

A549 cells were cultured with LMWCNT, SMWCNT and the control particles TiO_2, DQ12, ufCB (at a concentration of 10.6μg/cm^2) as well as TNF-α (at 10ng/ml) for four (Fig. 4.9) and 24 hours (fig 4.10). The mRNA of treated cells was isolated and quantified by RT-PCR. After four hours (fig 4.9) all particle treatments appeared to reduce TGF-β expression to levels below that of the untreated control with the greatest decrease following LMWCNT exposure, other particles reduced TGF-β mRNA production in the order; DQ12 > SMWCNT > TiO_2 > ufCB. The level of TGF-β mRNA synthesis after TNF-α treatment closely matched that of the untreated control. After 24 hours (fig 4.10) TGF-β expression following particle exposure was still less than control levels although TNF-α caused a slight increase in expression of TGF-β.

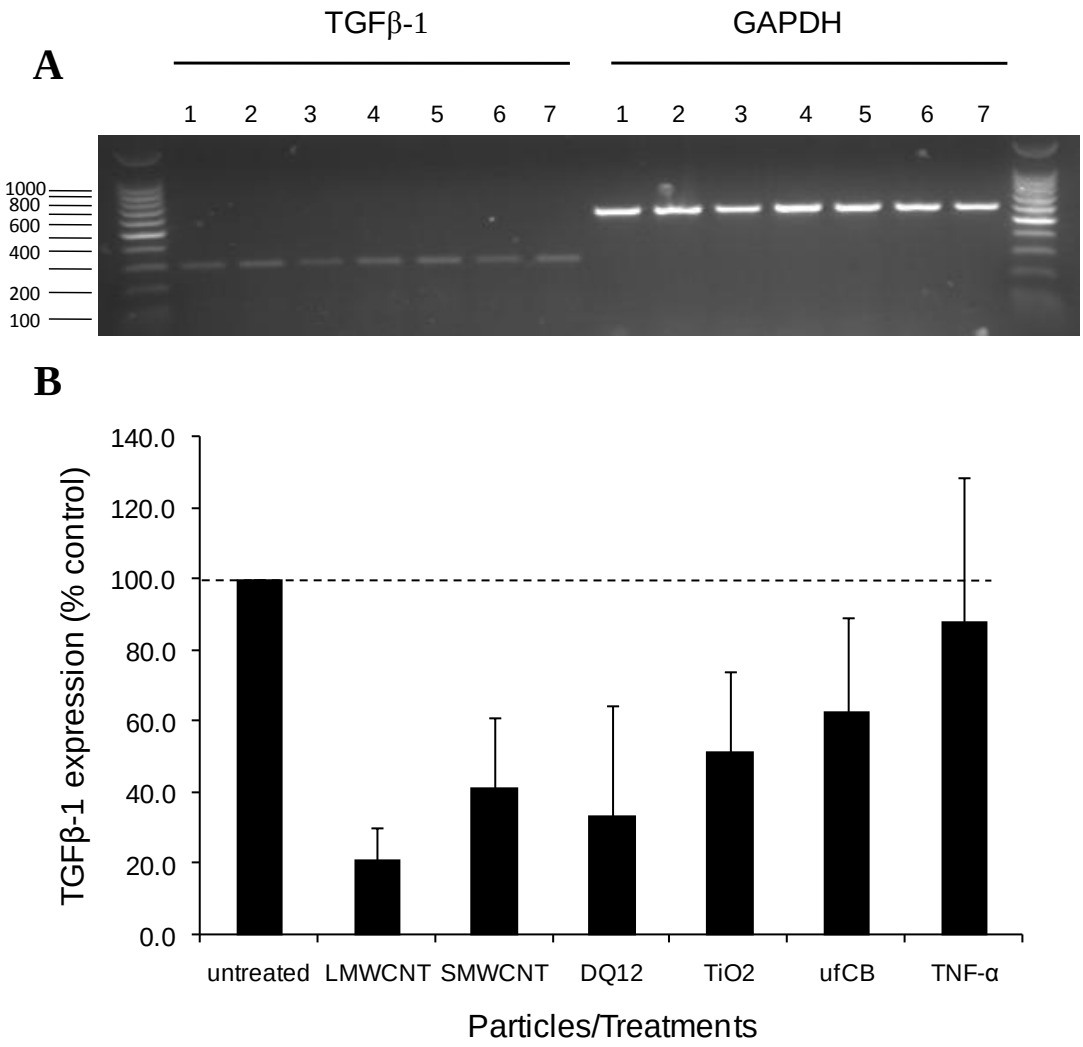

Figure 4.9. TGF-β gene expression profiles for A549 cells exposed for 4 hours to 10.5µg/cm^2 of MWCNT and control particles. Cells were exposed for four hours to each particle in 0% DMEM, RNA was extracted and isolated and TGF-β1 mRNA quantified by RT-PCR. **(A)** Representative PCR gel showing IL-8 and GAPDH bands; **(1)**Control (untreated) **(2)**LMWCNT **(3)** SMWCNT **(4)** DQ12 **(5)** TiO_2 **(6)** ufCB **(7)** TNFα. **(B)** Histogram of TGF-β gene expression expressed as a percent of the negative control. The histogram represents the mean of three experiments conducted on pooled triplicate samples. TGF-β expression was quantified from gels by densitometry and values expressed as a ratio of TGF-β:GAPDH and then as a percent of the negative control. Bars represent S.E.M.

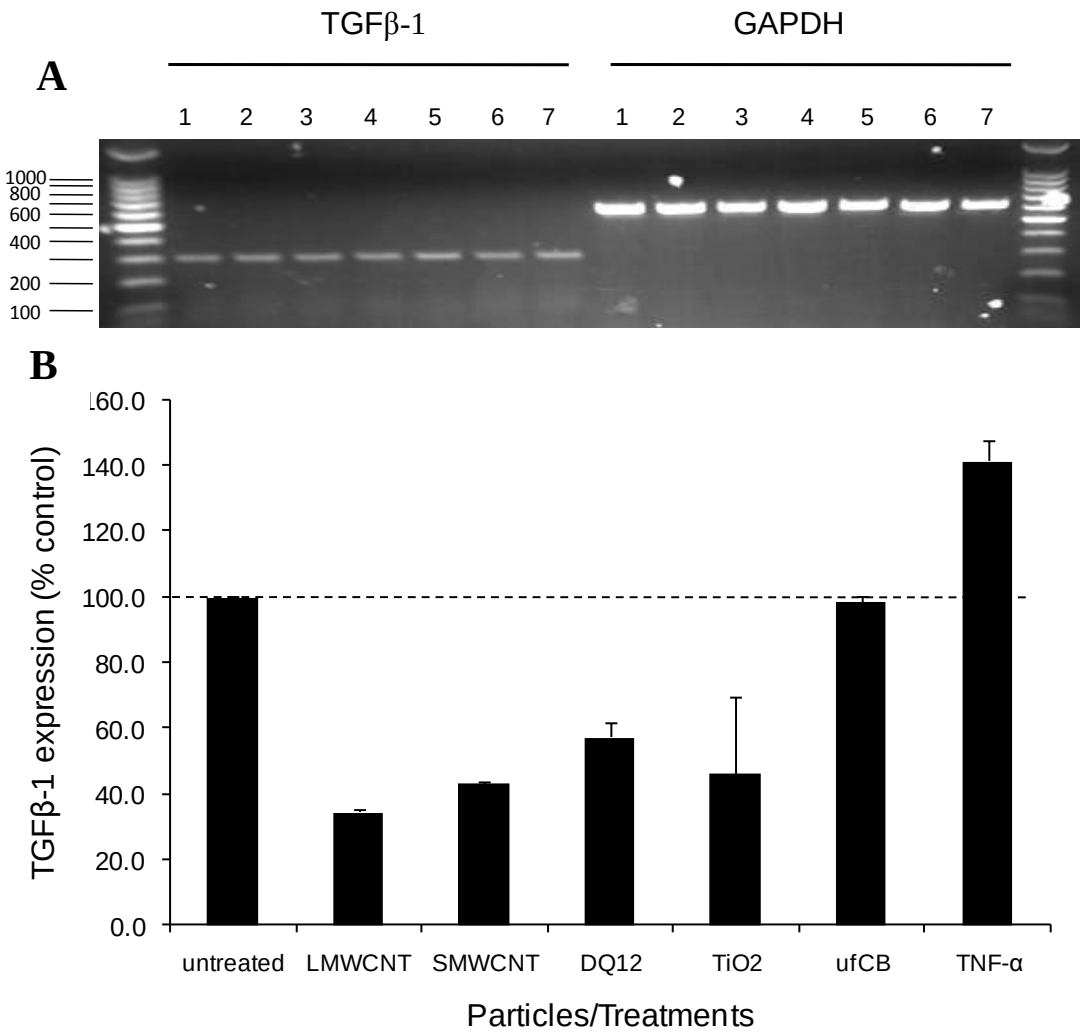

Figure 4.10. TGF-β gene expression profiles for A549 cells exposed for 24 hours to 10.5µg/cm^2 of MWCNT and control particles. Cells were exposed for four hours to each particle in 0% DMEM, RNA was extracted and isolated and TGF-β1 mRNA quantified by RT-PCR. **(A)** Representative PCR gel showing IL-8 and GAPDH bands; **(1)**Control (untreated) **(2)**LMWCNT **(3)** SMWCNT **(4)** DQ12 **(5)** TiO_2 **(6)** ufCB **(7)** TNFα. **(B)** Histogram of TGF-β gene expression expressed as a percent of the negative control. The histogram represents the mean of three experiments conducted on pooled triplicate samples. TGF-β expression was quantified from gels by densitometry and values expressed as a ratio of TGF-β:GAPDH and then as a percent of the negative control. Bars represent S.E.M.

4.6 Discussion

Work in this chapter was undertaken to examine a possible link between the free radical generating capacity of MWCNT and an ability to induce oxidative stress. Cellular levels of GSH have been established as markers for oxidative stress and determine susceptibility to ionising radiation and oxidants (Meister & Anderson 1983, Rahman 1998). GSH levels may also modulate pro-inflammatory cytokine production by exerting influence over signalling pathways and transcription factors (Deforge et al 1993, Wilhelm et al 1997, Gosset et al 1999, Rahman & MacNee 2000, Yamamoto et al 2003, Ji et al 2006). Central to oxidatively induced IL-8 synthesis in NF-κB (Desaki et al 2000), its activation can be indirectly mediated by oxidants (Anderson et al 1994, Janssen-Heininger et al 1999, Rahman et al 2002) and appears to be tied to the redox status of the cell, in particular the GSH:GSSG ratio (Gutter et al 1994, Ginn-Pease & Whisler 1996, Obin et al 1998, Manna et al 1999, Rahman & MacNee et al 2000).

Depletion of GSH. Exposure of serum starved cells for 24 hours to either LMWCNT or SMWCNT resulted in a significant concentration dependent depletion of total GSH at medium and highest doses. The extent of depletion was virtually identical perhaps suggesting the mechanism responsible was the same and unrelated to physical differences between samples. DQ12 significantly depleted total GSH at the lowest concentration and reduced GSH levels close to zero at high concentrations. The capacity of MWCNT to deplete GSH may be related to their ability to generate a reactive species as detected by ESR. As for ufCB, this ability appears to be independent of transition metals (Stone et al 1998, Brown et al 2000, Greenwell et al 2002, Wilson et al 2002, Gallagher et al 2003, Koike & Kobayashi et

al 2006, Yamawaki & Iwai 2006, Mroz et al 2007) and may be derived from reactive dangling bonds located at defect and edge sites (Kang & Wang 1997, Mannivannan et al 1999, Boehm 2002, Ungar et al 2002, Vorob'ev-Desyatovskii et al 2006, Cabrera-Sanfelix & Darling 2007) on carbon nanotubes from which electrons can be transferred (Ebbesen & Takada 1995, Kosaka et al 1995, Kang et al 1997, Mawhinney et al 2000, Vix-Guterlet al 2001, Banks et al 2004, Li et al 2005) to produce free radicals. The depletion of GSH in response to free radical production could occur as a result of lipid peroxidation in the plasma membrane (Pal Yu et al 1994) or as a result of flooding cells intracellular environment with an oxidising species (Farber et al 1994, Mulier et al 1998). Superoxide ions (one of the species possibly generated by MWCNT based on the limited radical specificity of the spin trap TEMPONE-H and the ability of SOD to reduce the MWCNT ESR signal) could compound this by liberating intracellular protein bound iron (Biemond et al 1986, Liochev & Fridovich 1994) providing iron for Fenton chemistry. This however would require that MWCNT exist free in the cells intracellular environment as superoxide anions would be incapable of crossing the plasma membrane.

DQ12 significantly depleted GSH. Its greater capacity to do so may be as a result of the mineral causing membrane damage and enabling efflux of GSH from the cell (Merchant et al 1990, Pandurangi et al 1990, Zhuo et al 1999). Haemolysis caused by DQ12 has been explained by a mechanism involving membrane damage that allows efflux of the contents of erythrocytes (Summerton et al 1977, Pandurangi et al 1990). MWCNT appeared unable to cause significant membrane damage (based on the results of haemolysis assays) possibly explaining their comparatively more limited effect on the GSH content of A549 cells. Reactive species generated

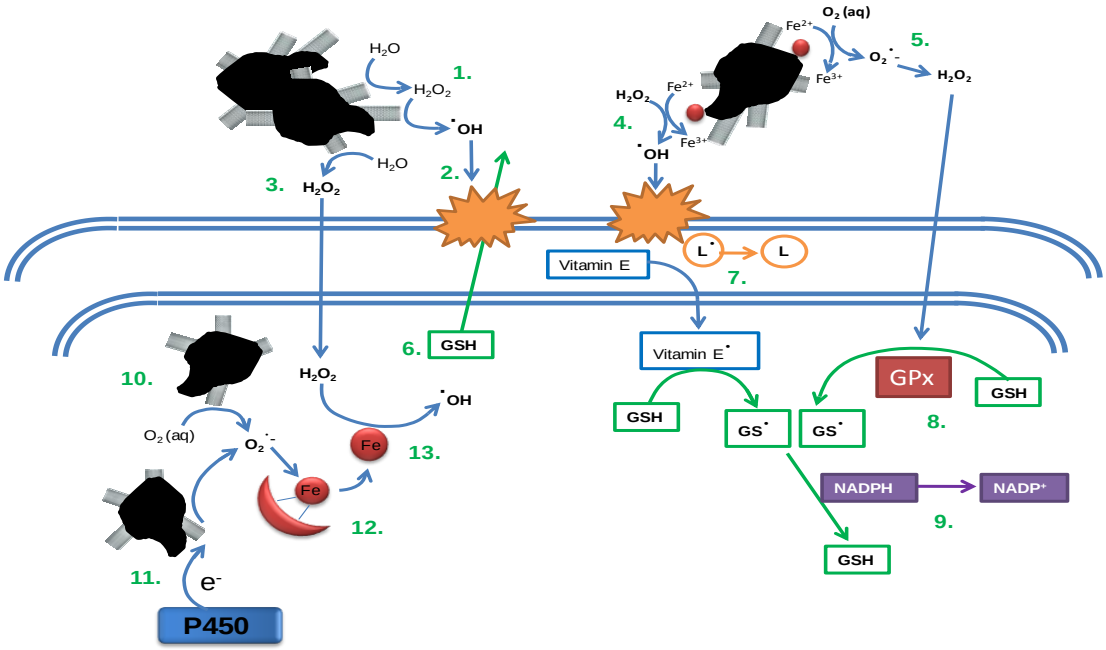

Figure 4.11. Diagrammatic representations of the hypothetical mechanisms of glutathione depletion following exposure to MWCNT. **(1)** Water reacts with reactive sites upon MWCNT aggregates to generate hydrogen peroxide that undergoes further oxidisation upon reactive sites to hydroxyl radicals. **(2)** Generated in close proximity to the plasma membrane hydroxyl radicals oxidise its lipid constituents. **(3)** Hydrogen peroxide derived from the reaction of water with reactive carbons diffuses through the plasma membrane into the cytosol. **(4)** Hydrogen peroxide reacts with accessible residual ion particles and produces hydroxyl radicals that attack the cell membrane. **(5)** Residual iron particles reduce aqueous oxygen to superoxide molecules that dismutase to hydrogen peroxide and permeate into the cell cytosol. **(6)** Changes in the permeability of the cell membrane as a result of oxidative damage allow an efflux of glutathione into the cell medium. **(7)** Lipid radicals ($L^{\cdot}$) generated by reaction with hydroxyl radicals are countered by vitamin E resulting in the production of a vitamin E radical and lipid molecules (L). Vitamin E radicals are returned to their reduced state by GSH resulting in the production of GSSG, at the cost of NADPH GSSG is re-reduced to GSH. **(8)** Hydrogen peroxide that gains access to the cytosol is countered by GPx utilising GSH. **(9)** Un-relenting expenditure of NADPH on the reduction of GSSG will result in its depletion ending with cellular reliance solely upon GSH and the thiols accelerated depletion. **(10)** Internalised MWCNT aggregates spontaneously produce superoxide radicals either as a result of the reaction of aqueous oxygen with reactive carbons or as a result of cytochrome P450 reduction of quinone groups on MWCNT **(11)**. **(12)** Superoxide generated from MWCNT reacts with Iron containing proteins liberating iron particles freely into the cytosol. **(13)** Free iron can react by Fenton chemistry with hydrogen peroxide to generate hydroxyl radicals and further add to an increasingly oxidised cellular environment.

aqueously (hydrogen peroxide, hydroxyl radicals, superoxide anions, singlet oxygen) from the reaction of surface silanol groups with water could also act as drain on GSH as a result of oxidative membrane damage (Pal Yu et al 1994) or by permeating the cell (e.g. hydrogen peroxide) and acting as a direct drain on GSH reserves (Farber 1994, Wright et al 1994, Mulier et al 1998, Zhuo et al 1999). DQ12 can also be ingested (Fanizza et al 2007) which potentially could result in free radicals generated intracellularly also depleting GSH. GSH can reduce ferric iron bound to the surface of particles to its reduced ferrous form, in this way GSH could speed up its own depletion by initiating Fenton chemistry (Fenoglio et al 2003, Fubini & Hubbard 2003).

Exposure of A549 cells to LWMCT, SMWCNT or DQ12 in 2% DMEM for 24 hours dose dependently and significantly decreased GSH. The overall GSH content of cells appeared higher (compared to cells serum starved and treated in 0% DMEM) possibly as a result of the presence of cysteine in the serum boosting cells intracellular cysteine pool and ultimately GSH content (Mulier et al 1998). The lack of cysteine in 0% DMEM could act as a limiting factor for GSH synthesis (Kang et al 1990, Attene-Ramos et al 2005). Particle driven depletion of GSH was consistently more substantial for cells treated in 0% DMEM than for cells treated in 2% DMEM. This may represent a combination of increased GSH synthesis or a coating (or buffering) effect of serum proteins shielding cells from the reactive surfaces or reactive species of or generated by DQ12 or the MWCNT.

Culture of cells for 48 hours in 2% DMEM halved basal GSH levels (control at 24 hours compared to control at 48 hours) with a similar effect for particle treated cells at the lowest concentration (24 vs. 48 hours). This decrease might be due to a

reduction in GSH synthesis by cells approaching or reaching confluence combined with an increase in ROS levels and the use of redox equivalents for other processes (such as ATP synthesis) that also occurs during the plateau phase of cell growth (Kang et al 1990, Ray et al 1999). The GSH content of A549 cells exposed to the lowest dose of MWCNT for 48 hours was significantly greater than control. A slower rate of proliferation due to the presence of low dose MWCNT may have meant GSH synthesis not being reduced to the same extent as control cells. Higher doses of MWCNT resulted in significant depletion of GSH suggesting either the effect of a continuous production of a MWCNT generated reactive species or a combined effect of a MWCNT generated reactive species depleting GSH reserves already diminished as a result of extended culture and growth phase. Comparatively, at 48 hours exposure DQ12 had no effect on GSH levels. If the under lying mechanism of DQ12 driven GSH depletion was efflux driven then this may represent blocking of this mechanism by serum coating of particles (Roach et al 2006). The cytotoxicity of quartz has been found to be reduced following coating of its surface (REF!!!).

Overall MWCNT have an apparent capacity to diminish GSH content of A549 cells that is diminished in the presence of serum. DQ12 also has a significant ability to deplete intracellular GSH but this capacity is substantially reduced in the presence of serum, more so than for MWCNT. This may represent different mechanisms by the different materials at causing GSH depletion e.g. an efflux driven mechanism requiring a physical interaction between particle and cells and blockaded by protein adsorption to the particles surface as opposed to a mechanism based on the generation of an aqueous reactive species.

GSH Adsorption. Both MWCNT demonstrated significant capacity to adsorb GSH that was abolished in the presence of serum. This indicates that in this instance GSH could not out compete the protein component of serum to bind to the surface of MWCNT. Very little adsorptive capacity was demonstrated by DQ12 for GSH.

IL-8 and TGFβ production. Neither LMWCNT nor SMWCNT induced a detectable IL-8 protein response after 24 hours exposure in 0% DMEM; in contrast DQ12 caused a significant dose dependent increase in IL-8 production. The complete lack of IL-8 response (not even to basal levels as demonstrated by the control) could have been due to adsorption of IL-8 protein to MWCNT for which CNT have a high and varied capacity (Karajanagi et al 2003, Bradley et al 2004, Chen et al 2004, Asuri et al 2006, Bi et al 2006, Song et al 2006, Ito et al 2007, Valenti et al 2007). Exposure followed by removal of treatments at six or 24 hours then continued culture in fresh media (interrupted exposure) produced a dose dependent IL-8 release from DQ12 (significant at 6 hours exposure) but no response from MWCNT treatments. Adsorption may have continued to have played a role even after washing due to the difficulty of fully removing CNT from the cell monolayer. Also as with other assays, cells were unlikely to be fully exposed to the full dose of MWCNT due to their hydrophobicity and the consequent tendency of a proportion of the dose to flocculate well above the cell layer.

The ability of quartz to generate free radicals at its surface (Fubini et al 2003, Albrecht et al 2005, Øvrevik et al 2005, Fanizza et al 2007, Singh et al 2007) has been found to have an inverse relationship with the GSH content of exposed cells (Zhuo et al 1999, Fenoglio et al 2003, Lin et al 2006). Given the association between oxidative stress and elevated IL-8 production (Deforge et al 1993, Rahman

et al 2003, Yamamoto et al 2003, Bonceoeur et al 2008) this might suggest DQ12 generated ROS induce oxidative stress that activates transcriptional events (Schins et al 2000, Øvrevik et al 2004, 2005, 2005a) culminating in IL-8 production. This tallies with the inverse correlation between the extent of DQ12 induced GSH depletion and IL-8 production (Figure 4.11). Depletion may not necessarily be due solely to ROS, as has been suggested earlier GSH efflux may be occurring also. The physical damage to the cell combined with the increasingly oxidising conditions (owing to loss of GSH) could also stimulate IL-8 release.

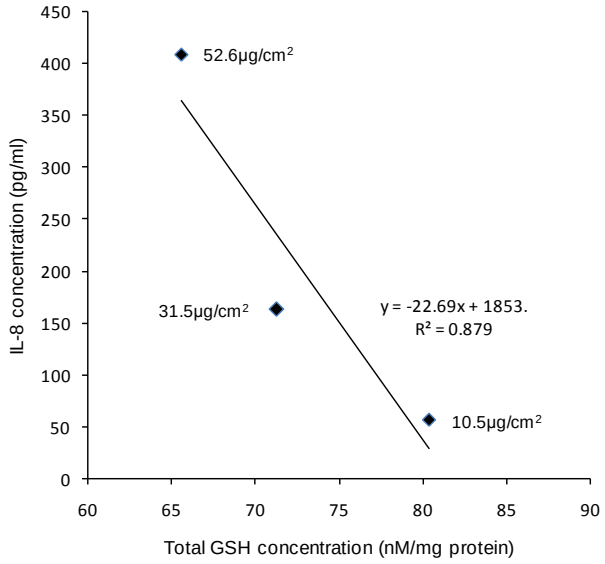

Figure 4.12. The correlation between GSH content (nM.mg protein) and IL-8 protein production (pg/ml) of A549 cells after 24 hours exposed to either DQ12 and LMWCNT in 2% FCS DMEM. (A) The graph shows an inverse correlation between cellular GSH content and IL-8 production in cells exposed to DQ12 in 2% FCS DMEM for 24 hours, at higher GSH contents the extent of IL-8 production is lower. As the GSH content of the cell decreases the output of IL-8 appears to be raised.

Following 24 hours interrupted exposure DQ12 induced IL-8 production was substantially decreased compared to that at six hours possibly as a result of a reduction in cell numbers.

Cells exposed to DQ12 in 2% DMEM for 24 hours dose dependently induced IL-8 secretion but to a level less than that seen for cells exposed in 0% serum. Again this may represent a protective effect of serum. After 48 hours exposure DQ12 significantly increased IL-8 production to an extent greater than that seen at any concentration following 24 hours exposure indicating a time and dose dependent effect.

Only DQ12 (10.6μg/cm^2) and TNFα up regulated IL-8 mRNA production in A549 cells after 4 hours, MWCNT, TiO_2 and ufCB had no effect. After extension of treatment time to 24 hours DQ12 increased IL-8 output fourfold indicative of a time dependent effect. MWCNT, $TiO_2$and ufCB were once again observed to have no effect. Increasing dose levels to 52.6μg/cm^2 for 24 hours resulted in a substantial level of IL-8 production from DQ12 exposed cells. IL-8 levels were elevated only slightly by MWCNT, $TiO_2$and ufCB. DQ12 has a reported capacity to induce pro-inflammatory signalling pathways resulting in IL-8 transcription (Desaki et al 2000, Schins et al 2000 Øvrevik et al 2004, 2005). Its limited effect after four hours may have the result of the relatively small dose and short treatment time, its lack of effect at anything but the highest dose might be a reflection of the aged nature of the quartz. Despite appearing to spontaneously generate a reactive species and deplete GSH levels (indicative of oxidative stress) of A549 cells this was not translated into IL-8 production. This may be partly due to the limited exposure of cells owing to the flocculated nature of the MWCNT, it may also represent a need for a threshold level of GSH depletion before a pro-inflammatory response such as IL-8 release in stimulated.

In vivo work has suggested CNT may induce a fibrotic response over a primary inflammatory response (Shvedova et al 2005, Mangum et al 2006, Li et al 2007). With the chance that MWCNT may have initiated a more fibrotic response *in vitro* from A549 cells the levels of TGFβ were measured in response to MWCNT exposure. TGFβ can be produced by alveolar epithelial cells (Bellocq et al 1999, Sheppard et al 2007, Stramer et al 2007) possibly in response to ROS or penetration of cells by mineral particles (Dai et al 1998). No particle was observed to induce TGFβ production, instead levels of this cytokine appeared to be reduce below the level of the control. This may have been due to under amplification of TGFβ products relative to the GAPDH housekeeping gene.

Summary. Both MWCNT were able to deplete GSH in A549 cells in a manner that was dependent on dose and duration of exposure. DQ12 also depleted GSH. Depletion of GSH was reduced in the presence of serum suggesting a protective effect for FCS. Neither MWCNT induced a pro-inflammatory response as measured by extent of IL-8 production, only DQ12 was able to induce a pro-inflammatory response from A549 cells. In aggregate flocculated form neither MWCNT appears to have an inflammatory potential despite a capacity to produce a reactive species (as quantified by ESR) and deplete total cellular GSH. MWCNT thus appear to be non toxic and non inflammatory.

Chapter 5

Activation of pro-inflammatory transcription factor nuclear factor kappa B (NF-κB) by MWCNT

Chapter 5

The effect of MWCNT upon activation of the transcription factor nuclear factor kappa B (NF-κB) in the alveolar epithelial cell line A549.

5.1 Introduction

NF-κB is a member of the Rel family, a group of proteins sharing sequence homology of over 300 amino acids that serve as transcription factors. They exist as homo or heterodimers each with slightly different binding preferences for a decameric sequence of DNA. The classically activated form of NF-κB is a construct of the proteins p65 (Rel A) and p50, other subunits such as p105, p100, c-rel and Rel B combine to form alternative forms of the transcription factor. In an un-stimulated cell NF-κB is held in the cytoplasm in an inactive form by the inhibitory protein Inhibitory-κB (IκB) that covers the transcription factors nuclear translocation signal preventing it from entering the nucleus. Stimulation of the cell results in the phosphorylation and detachment of IκB and phosphorylation of NF-κB and the addition of ubiquitin molecules to both. Freed of IκB, NF-κB moves to the nucleus and binds specific promoter regions of target genes resulting in their transcription and expression (Rahman & MacNee 1998). NF-κB is responsible for transcriptional regulation of a variety of genes (table 5.0) including IL-8 (Hoffman et al 2002, Jijon et al 2002) in response to a multitude of stimuli including oxidative stress and the products of oxidative stress (Anderson et al 1994, Ekstrand-Hammarström et al 2006) (although a central pathway involving ROS or oxidative stress has been questioned) (Bowie & O'Neill 2000). For example the ratio of GSSG to GSH has been found to be a factor in the activation of NF-κB and associated components (Galter et al 1994, Ginn-pease & Whisler 1996, Obin et al 1998,

Manna et al 1999, Rahman et al 2003) combined with the activity of histone deacetylases (Rahman et al 2002).

Genes regulated by NFκB						
Cytokines	Growth factors	Chemokines	Inflammatory mediators	Adhesion molecules	Immuno-receptors	Proto-oncogenes
TNF-α	Granulocyte macrophage colony stimulating factor (GMCSF)	IL-8	Inducible nitric oxide synthase (iNOS)	Intracellular adhesion molecule-1 (ICAM-1)	Interleukin-2 receptor (α-chain)	p53
IL-1β	Granulocyte colony stimulating factor (G-CSF)	Macrophage inflammatory protein 1 (MIP-1)	Inducible cyclo-oxygenase 2	Vascular cell adhesion molecule-1 (VCAM-1)	T-cell receptor (β-chain)	c-myc
IL-2	Macrophage colony stimulating factor	Macrophage chemotactic protein 1 (MCP-1)	5-lipoxygenase	E-selectin	Platelet activating factor receptor	ras
IL-3		Gro-α, β, γ	Cytosolic phospholipase A_2		CD11b	
IL-6		Eotaxin	C-reactive protein		CD48	
IL-12		RANTES	12-lipoxygenase			

Table 5.1 Categories of genes regulated by the transcription factor NF-κB. Adapted from Rahman & MacNee. 1998. Role of transcription factors in inflammatory lung diseases. *Thorax* 53: 601-612.

The inflammatory response of cells exposed to particulates has been linked to the activation of NF-κB through mechanisms that involve production of free radicals and/or reactive oxygen species and the induction of oxidative stress. Quartz has been demonstrated to activate NF-κB *in vitro* (Schins et al 2000, Hubbard et al 2002) through a free radical/oxidative stressed based mechanism (Chen et al 1998, Desaki et al 2000). Cellular exposure to fibres can result in the activation of NF-κB; this has been demonstrated upon macrophage ingestion of glass fibres in a manner related to fibre length and generation of ROS (Ye et al 1999). Also, in the synthesis and release of IL-6 by asbestos and H_20_2 in A549 and Bronchial epithelial cells mediated by NF-κB. This was diminished by treatment with antioxidants suggesting a role for free radicals (Simeonova et al 1997). Oxidative stress and generation of free radicals and ROS by carbon based particulates (Stone et al 1998, Dellinger et al 2001, Pan et al 2004, Xia et al 2006) have widely been incorporated as

part of the mechanisms leading to NF-κB activation (Takizwa et al 1999, Jimènez et al 2000, Shukla et al 2000, Mroz et al 2007). Its activation may be also insinuated following particulate exposure through the production and release of factors that require NF-κB transcriptional control such as IL-8 (Bayram et al 1998, Abe et al 2000, Monn & Becker 1999, Takano et al 2002, Gilmour et al 2003) although care should taken making this link (Kim et al 2005). Oxidative stress following keratinocyte exposure to SWCNT has been identified as the causative mechanism responsible for activation of NFκB (Manna et al 2005).

5.2 A study of the effect of MWCNT and control particles upon activation of the transcription factor nuclear factor kappa B (NF-κB) in the alveolar epithelial cell line A549

This investigation into possible toxicity of MWCNT has demonstrated an apparent ability to generate a free radical species and deplete the total glutathione of cultured epithelial cells. Based on the abundant literature links between these two events and the activation of the transcription factor NF-κB (oft associated with inflammatory outcomes), the capacity of LMWCNT and SMWCNT to activate NF-κB compared to a panel of control particles was investigated. Cells were exposed to two concentrations of MWCNT or particles (10.6 or 52.6μg/cm^2) for four hours. The proportion of NF-κB having migrated to the nucleus was investigated by immunocytochemistry and measured qualitatively by visual judgement of the extent of nuclear staining. This was aided by conversion of coloured images to black and white in which the density of black pixels correlated with areas of high p50 staining intensity.

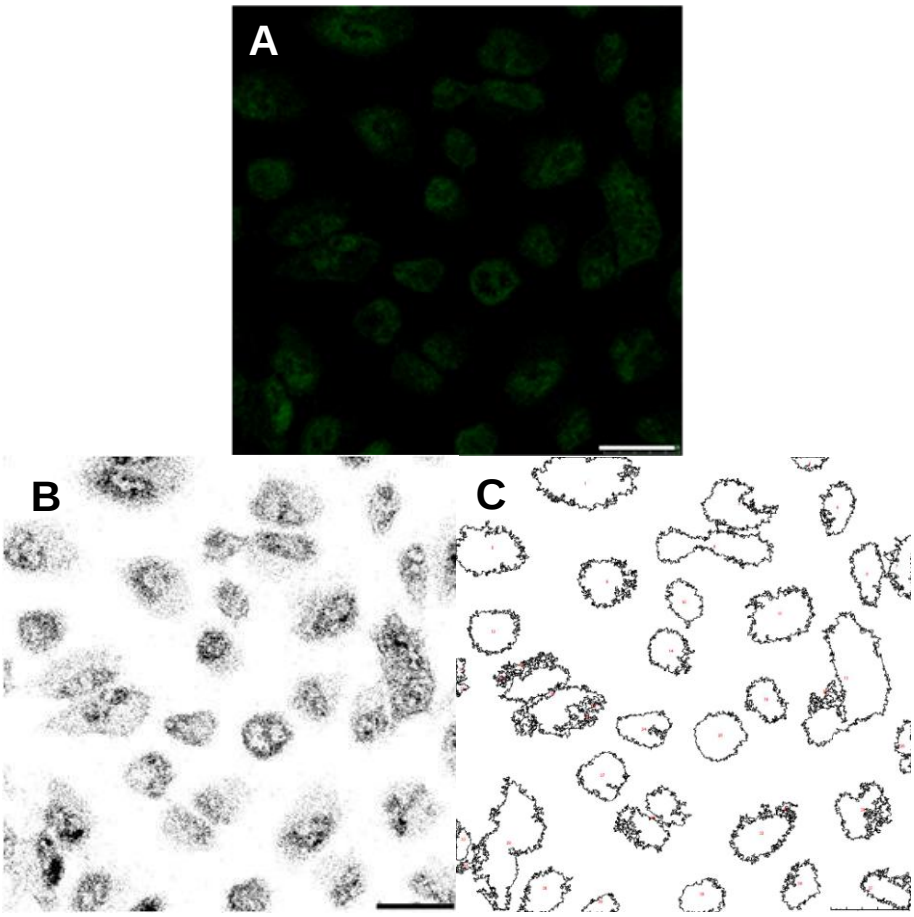

Figure 5.1 (A) Confocal image of untreated cells exposed to serum free conditions for four hours prior to staining. Darker stained green areas represent p50 sequestered in the cytoplasm whilst brighter green areas are p50 that has translocated into the nucleus. (**B) The local maxima of luminescence of confocal image (A)**, for this image luminescence was defined as the average of colours with dark areas representing brighter stained nuclei and lighter pixelated areas the cytoplasm. With no treatment little distinction in staining density could be made between nuclear and cytoplasmic regions suggesting little translocation of NF-κB into the nucleus (**C)** The numbered outlines of cells counted and measured by ImageJ. The scale bars represent 25μm.

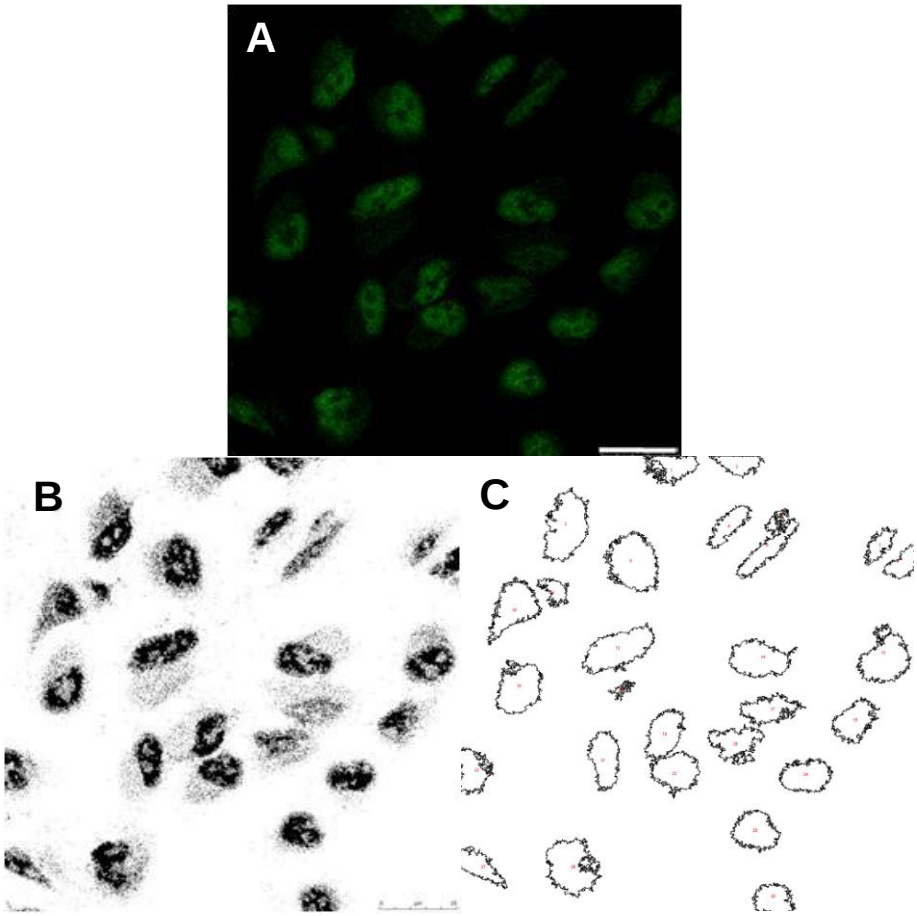

Figure 5.2 (A) Confocal image of TNFα treated cells in serum free conditions for four hours prior to staining. Darker stained green areas represent p50 sequestered in the cytoplasm whilst brighter green areas are p50 that has translocated into the nucleus. In this image compared to the untreated cells the majority of nuclei posses a bright green hue indicative of the TNFα stimulated translocation of NF-κB. The scale bar represents 25μm. (**B) The local maxima of luminescence of confocal image (A)**, for this image luminescence was defined as the average of colours with dark areas representing brighter stained nuclei and lighter pixelated areas the cytoplasm. In Comparison to the un-treated control most of the cells display clearly demarcated black nuclei indicating extensive luminescence and movement of the p50 unit of NF-κB into the nucleus, the scale bar represents 25μm. (**C)** The numbered outlines of cells counted and measured by ImageJ.

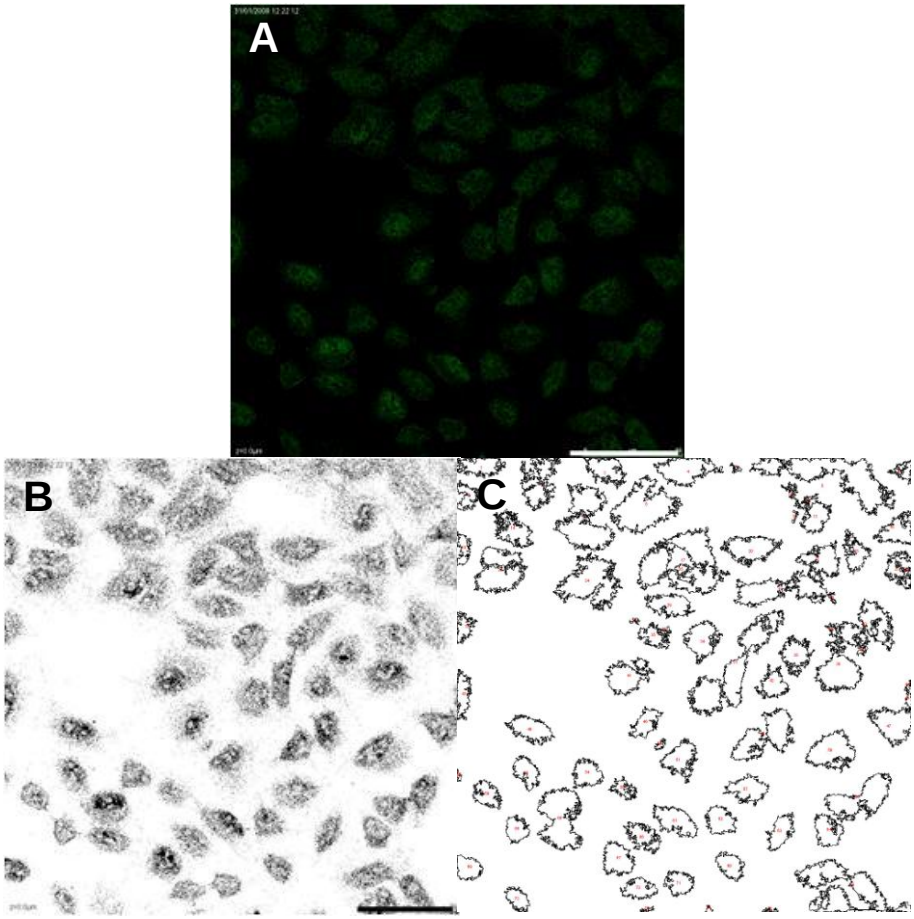

Figure 5.3 (A) Confocal image of cells treated with 10.5µg/cm^2 LMWCNT in serum free conditions for four hours prior to staining. Darker stained green areas represent p50 sequestered in the cytoplasm whilst brighter green areas are p50 that has translocated into the nucleus. LMWCNT (10µg/cm^2) failed to demonstrate extensive NF-κB translocation. The scale bar represents 50µm. (**B) The local maxima of luminescence of confocal image (A)**, most of the cells failed to show darkening of the nuclear region. Pixel distribution was uniform indicating a lack of accumulation of NFκB sub unit in the nucleus. The scale bar represents 50µm. (**C)** The numbered outlines of cells counted and measured by ImageJ.

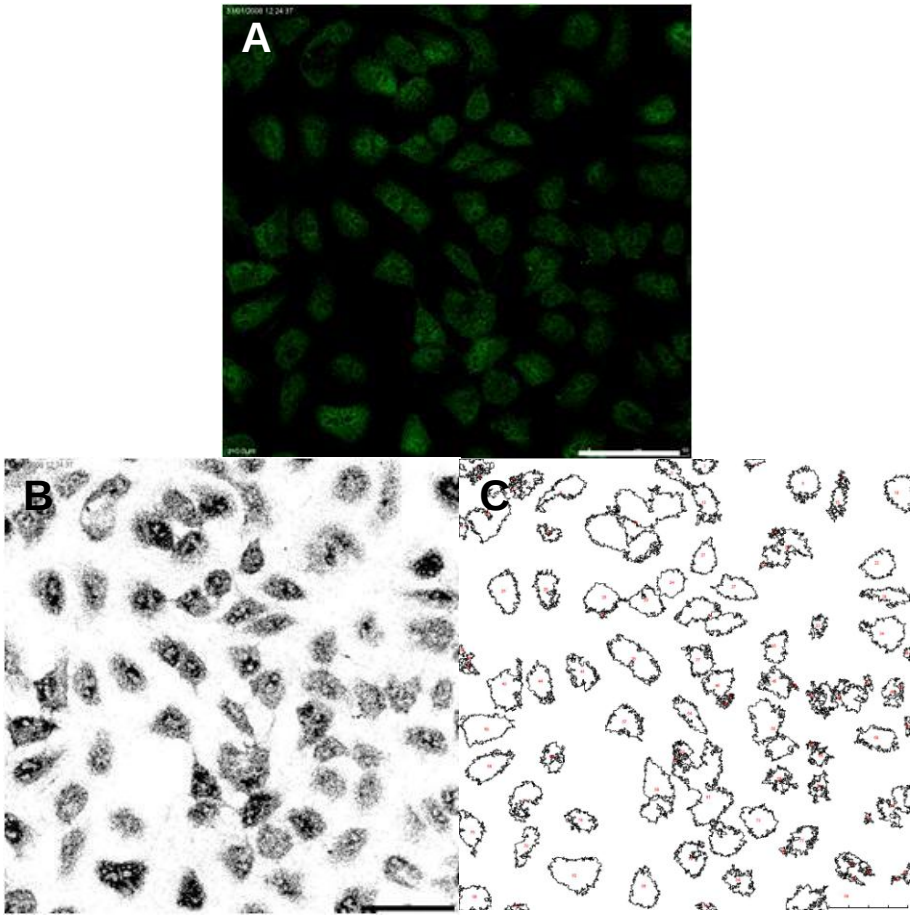

Figure 5.4 (A) Confocal image of cells treated with 52.6µg/cm^2 LMWCNT in serum free conditions for four hours prior to staining. Darker stained green areas represent p50 sequestered in the cytoplasm whilst brighter green areas are p50 that has translocated into the nucleus. A higher concentration of LMWCNT (52.6µg/cm^2) caused more extensive movement of NF-κB into the nucleus in this individual assay. The scale bar represents 50µm. (**B)** The local maxima of luminescence more clearly shows a greater number of cells with a greater density of pixels localised to the cell nucleus indicating movement of NFκB. As this effect was amplified at 52.6 as opposed to 10.5µg/cm^2 it is suggestive of a concentration dependent effect, the scale bar represents 50µm. (**C)** The numbered outlines of cells counted and measured by ImageJ.

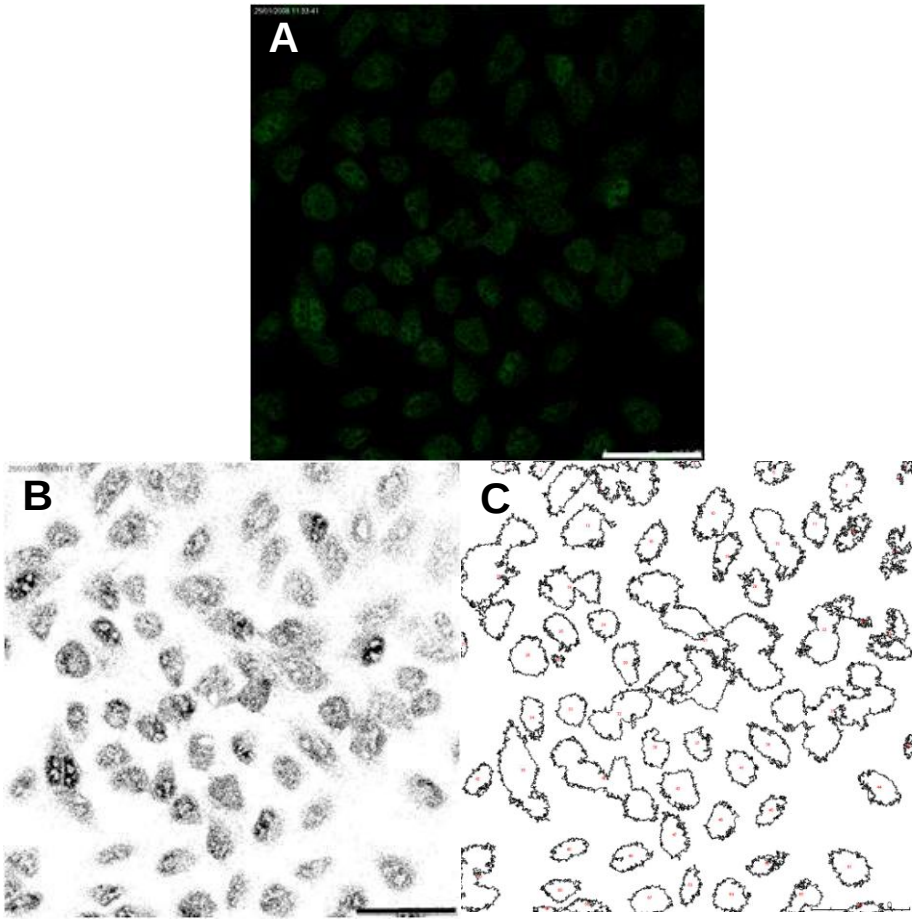

Figure 5.5 (A) Confocal image of cells treated with 10.5µg/cm^2 SMWCNT in serum free conditions for four hours prior to staining. Darker stained green areas represent p50 sequestered in the cytoplasm whilst brighter green areas are p50 that has translocated into the nucleus. A concentration of 10.5µg/cm^2 SMWCNT caused only slight movement of NFκB into the nucleus in this assay. The scale bar represents 50µm. (**B)** The local maxima of luminescence showed few cells with heavily stained nuclei, the majority of cells demonstrated uniform pixel density and thus limited NF-κB translocation. The scale bar represents 50µm. (**C)** The numbered outlines of cells counted and measured by ImageJ.

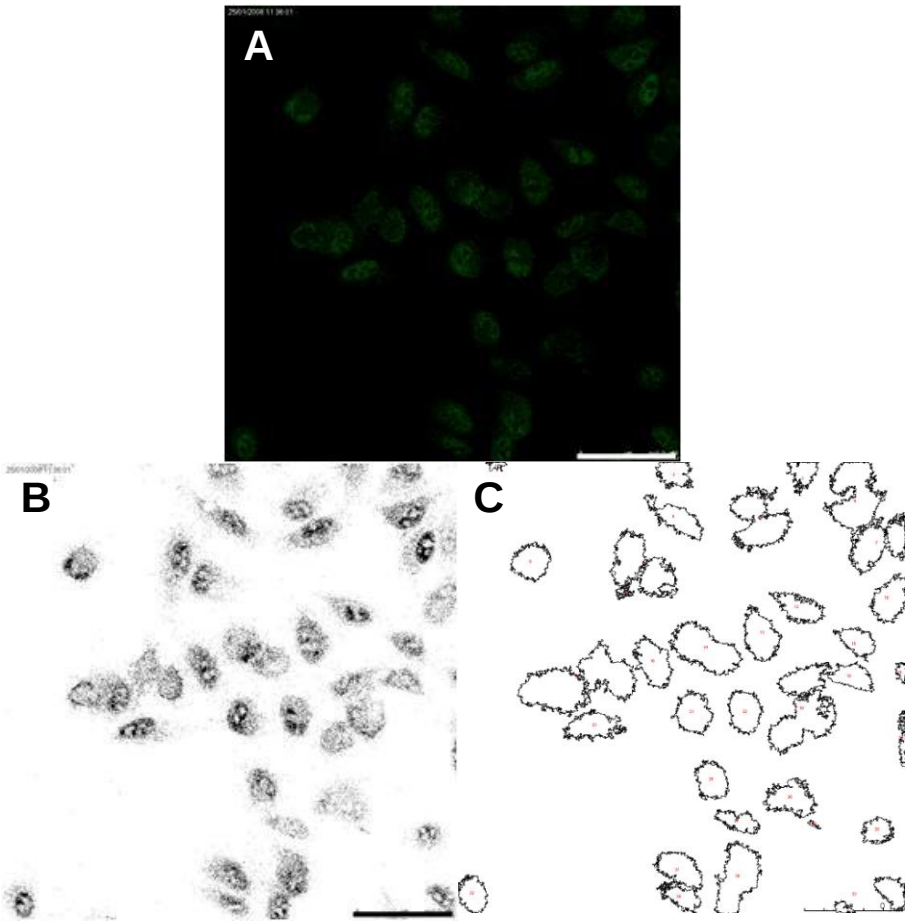

Figure 5.6 (A). Confocal image of cells treated with 52.6µg/cm^2 SMWCNT in serum free conditions for four hours prior to staining. Darker stained green areas represent p50 sequestered in the cytoplasm whilst brighter green areas are p50 that has translocated into the nucleus. A concentration of 52.6µg/cm^{2}SMWCNT failed to cause an obvious extensive increase in the level of nuclear staining. The scale bar represents 50µm. **(B).** The local maxima of luminescence showed no obvious increase in nuclear staining density and thus little movement of NF-κB into the nucleus. The scale bar represents 50µm. **(C).** The numbered outlines of cells counted and measured by ImageJ.

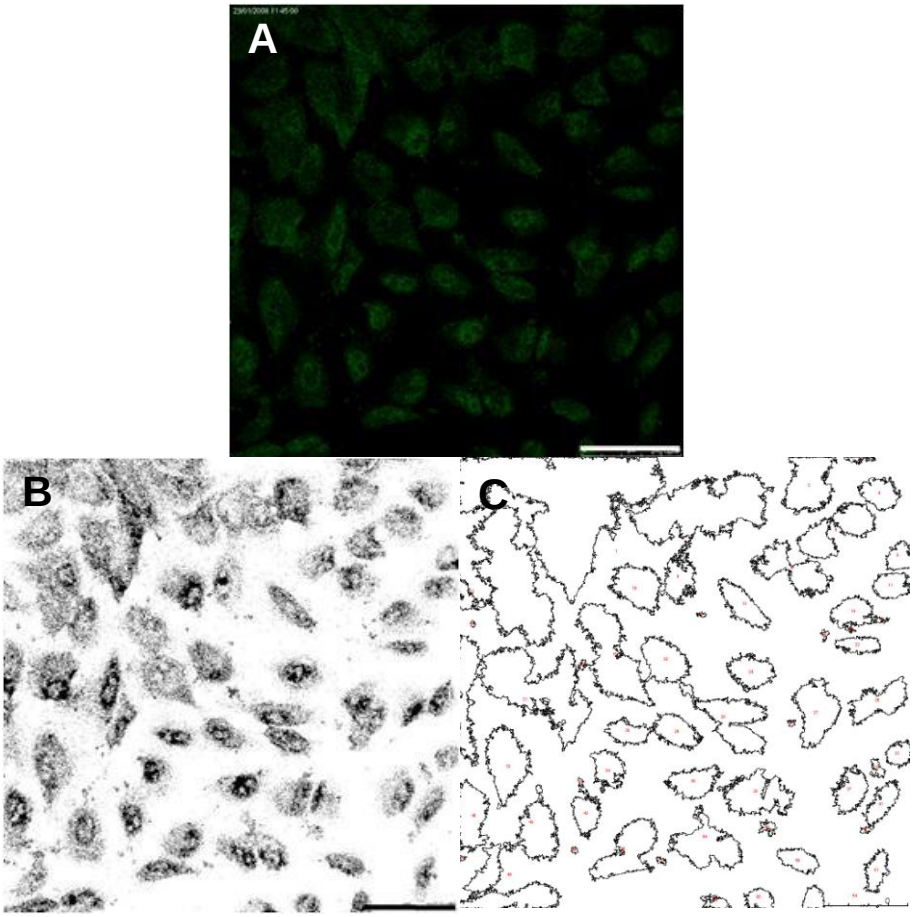

Figure 5.7 (A). Confocal image of cells treated with 10.5µg/cm^2 TiO_2 in serum free conditions for four hours prior to staining. Darker stained green areas represent p50 sequestered in the cytoplasm whilst brighter green areas are p50 that has translocated into the nucleus. A concentration of 10.5µg/cm^2 TiO_2 caused some movement of NFκB into the nucleus in this assay. The scale bar represents 50µm. **(B).** The local maxima of luminescence demonstrated few cells with densely stained nuclei. In comparison to other images there appeared to be a greater scattering of pixels between cells (outside of and between regions of high pixel densities corresponding to cells). This may represent interference of residual TiO_2 particles with confocal imaging. The scale bar represents 50µm. **(C).** The numbered outlines of cells counted and measured by ImageJ.

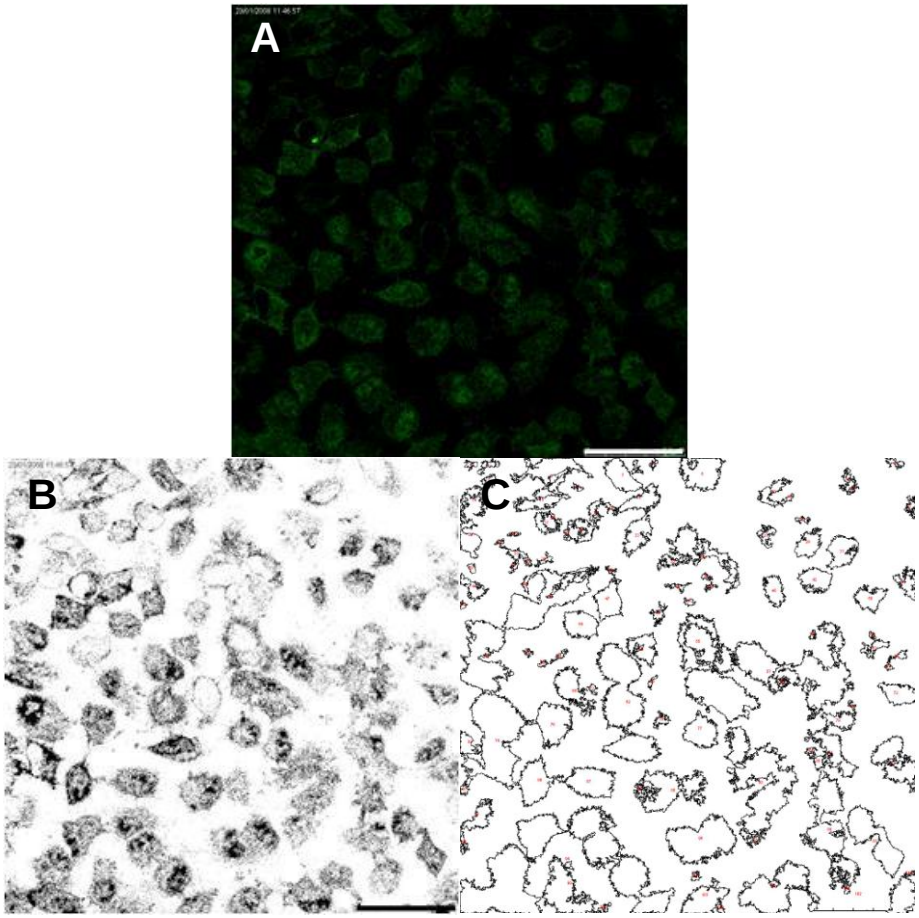

Figure 5.8 (A) Confocal image of cells treated with 52.6µg/cm^2 TiO_2 in serum free conditions for four hours prior to staining. Darker stained green areas represent p50 sequestered in the cytoplasm whilst brighter green areas are p50 that has translocated into the nucleus. A concentration of 52.6µg/cm^2 TiO_2 failed to increase the level of nuclear staining compared to 10.5µg/cm^2. The scale bar represents 50µm. **(B)** The local maxima of luminescence showed no obvious increase in cells with heavily stained nuclei. As with the lower concentration of TiO_2 there appeared some interference from residual nanoparticles. The scale bar represents 50µm. **(C)** The numbered outlines of cells counted and measured by ImageJ.

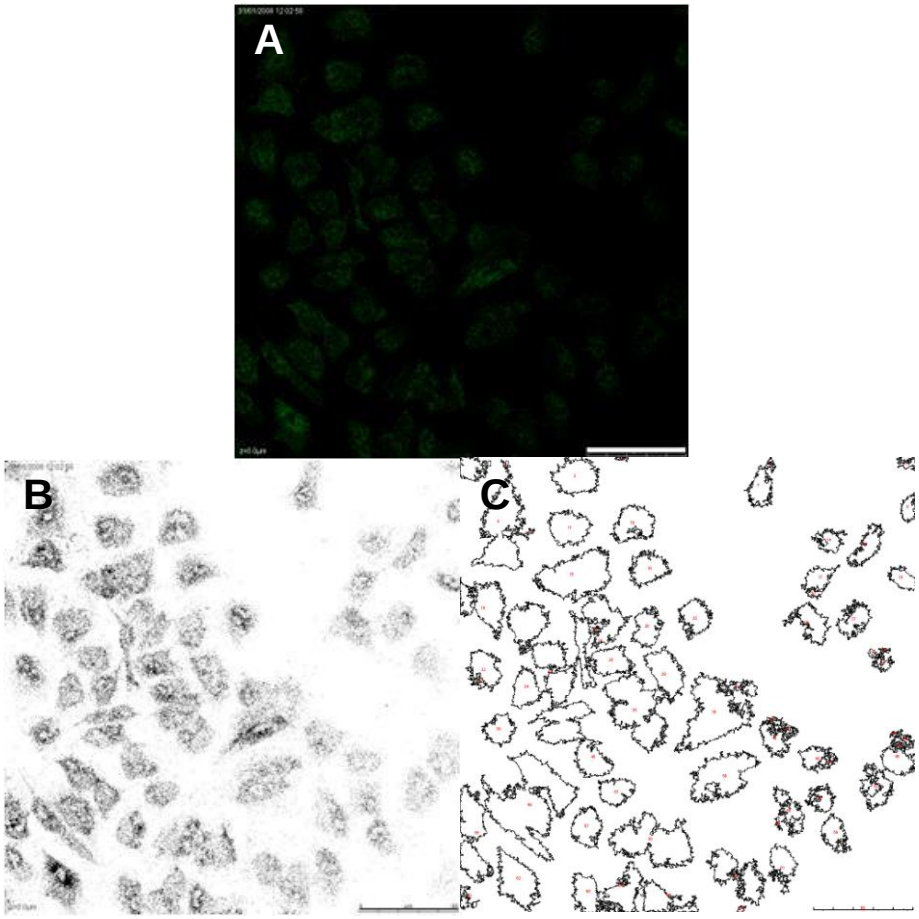

Figure 5.9 (A) Confocal image of cells treated with 10.5µg/cm^2 DQ12 in serum free conditions for four hours prior to staining. Darker stained green areas represent p50 sequestered in the cytoplasm whilst brighter green areas are p50 that has translocated into the nucleus. A concentration of 10.5µg/cm^2 DQ12 caused no movement of NF-κB into the nucleus. The scale bar represents 50µm. (**B)** The local maxima of luminescence indicated uniform pixel density with no concentration in the nuclear region suggesting little to no translocation of p50. The scale bar represents 50µm. (**C)** The numbered outlines of cells counted and measured by ImageJ.

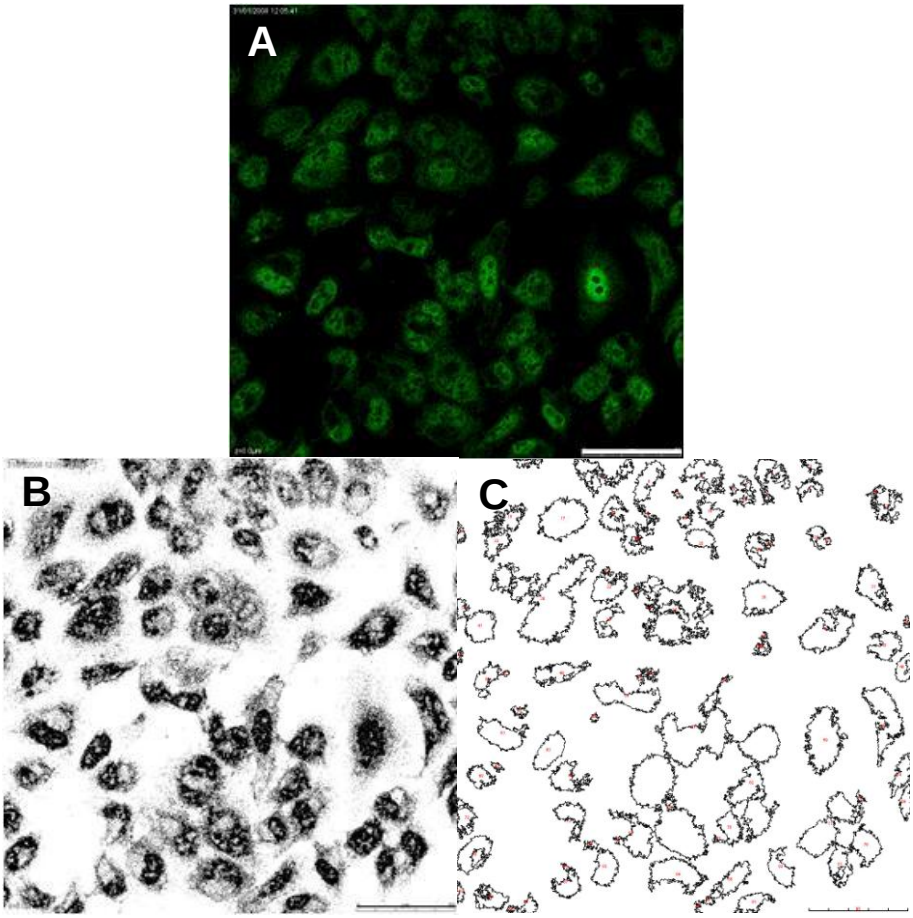

Figure 5.10 (A) Confocal image of cells treated with 52.6µg/cm^2 DQ12 in serum free conditions for four hours prior to staining. Darker stained green areas represent p50 sequestered in the cytoplasm whilst brighter green areas are p50 that has translocated into the nucleus. A concentration of 52.6µg/cm^2 DQ12 caused extensive nuclear staining compared to 10.5µg/cm^2 and the negative control. The scale bar represents 50µm. **(B)** Following exposure to a higher concentration of DQ12 a dramatic increase in the pixel density of nuclei became apparent matching the heavy staining seen in 5.10A and indicating extensive movement of p50 into the nucleus. The scale bar represents 50µm. **(C)** The numbered outlines of cells counted and measured by ImageJ.

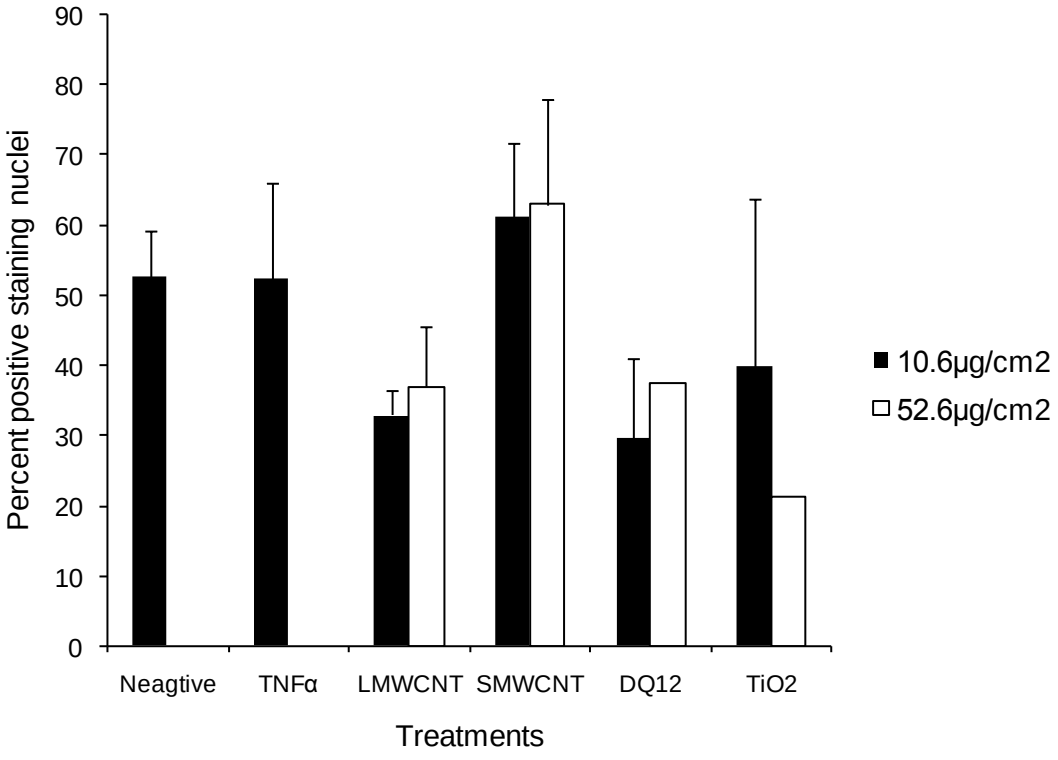

Figure 5.11 The extent of NF-κB p50 translocation from the cytoplasm to the nucleus of A549 cells after four hours particle treatment with either 10.5 or 52.6µg/cm^2. Cells were grown on coverslips and treated for four hours with each particle prior to being exposed to antibodies recognising the p50 subunit of NF-κB. The extent of p50 translocation was visualised by immunofluorescence using confocal microscopy. Assessment of particle induced nuclear translocation was made by counting positive p50 nuclei staining cells and expressing these as a percentage of the total cells. Solid black bars represent the negative control, cells treated with 10ng/ml TNFα and cells treated with 10.5µg/cm^2 particle. White bars represent cells treated with 52.5µg/cm^2 particles. This chart is representative of three experiments performed in duplicate.

Figures 5.1 – 5.10 represent individual assays, the aggregate result of three assays revealed no significant induction of nuclear translocation of p50 by any particle at any concentration into the nucleus of A549 cells (Fig. 5.11). Fig 5.11 reveals a high back ground level of p50 translocation (52.2 ± 6.4%) and comparatively little effect of TNFα (52.3 ± 13.5%), the only particle to induce greater p50 translocation than TNFα and the negative control was SMWCNT (61.3 ± 10.3 and 62.9 ± 7.9% at 10.5 and 52.5μg/cm^2 respectively). All other particles; LMWCNT (32.8 ± 3.6% and 36.9 ± 4.7% at 10.5 and 52.6μg/cm^2 respectively), DQ12 (29.4 ± 11.5% and 37.5 ± 8.7% at 10.5 and 52.6μg/cm^2 respectively) and TiO_2 (39.8 ± 23 9% and 21.3 ± 15.2% at 10.5 and 52.6μg/cm^2) failed to cause p50 translocation to the nucleus to an extent similar or greater than the negative control.

5.3 Discussion

Exposure of lung cells to a wide assortment of different particles including carbon and combustion derived particles, mineral particles and metal particles is associated with the generation of oxidative stress and inflammation by activation of the redox sensitive transcription factor NF-κB (Stone et al 1998, Arimoto et al 1999, Chen et al 1998, Takizawa et al 1999, Abe et al 2000, Brown et al 2000, Elias et al 2000 Shulka et al 2000, Greenwell et al 2002, Hubbard et al 2002 Takano et al 2002, Gilmour et al 2003, Albrecht et al 2004, Dybdahl et al 2004, Pan et al 2004, Felix et al 2005, Kim et al 2005, McNeilly et al 2005, Lin et al 2006, Mroz et al 2007).

Carbon nanotubes have been purported to generate ROS and /or oxidative stress (Manna et al 2005, Kagan et al 2006, Pulskamp et al 2007a, b, Sharma et al 2007, Yan et al 2007). Adverse effects have also been linked to the physical interactions of these materials with cells (Cui et al 2005, Monteiro-Riviere et al 2005, Tian et al 2006, Pensabene et al 2007, Hirano et al 2008). A general capability of CNT (in their own right) to generate ROS is not established; a couple of groups have reported ROS scavenging activity for nanotubes (Watts et al 2003, Fenoglio et al 2006, Muller et al 2008) and the possible contribution of residual (largely transition) metals can't be ignored (Kagan et al 2006, Pulskamp et al 2007, Muller et al 2008). The presence of transition metals is important not only due to their established ability to produce free radicals (Ghio et al 1992, Stohs & Bagchi 1995, Urbański & Beresewicz 2000, Fenoglio et al 2003, Felix et al 2005, Valko et al 2005) but also due their ability to activate NF-κB through both ROS dependent and independent mechanisms. Many metals posses a duel activation/inhibition capability for NF-κB depending on their concentration (Chen & Shi et al 2002). For this reason metal availability should be an important consideration in the study of the effect of CNT on the activation status of transcription factors such as NF-κB.

In this study individual assay results indicated particle driven NF-κB activation, a dose dependent effect of LMWCNT and DQ12 was observed, however this was not substantiated consistently over three repeats. The relatively muted effect of particles and TNFα upon NF-κB translocation reflects a greater than expected levels of positive staining nuclei amongst negative control cells. This is partly a function of the variation in the number of countable nuclei between treatments and likely technical issues with the assay such as variations of fluorescent signal intensity between assays and loss of signal due to bleaching of the fluoro-probe during the image capturing process. A more effective method may be to quantify the amount of NF-κB in the nucleus after various treatments (relative to an untreated control) rather than looking at the cell as a whole, assay techniques such as by EMSA technique or NF-κB ELISA should therefore be used in addition to or in place of confocal imaging..

In a large body of published literature quartz generated free radicals mediate oxidative stress that is associated with NF-κB activation (Ghio et al 1992, Xu et al 1999, Desaki et al 2000, Deshpande et al 2002, Fenoglio et al 2003, Fubini et al 2003, Rahman et al 2003, Albrecht et al 2005, Fanviza et al 2007, Boncoeur et al 2008). Quartz has been hypothesised to modulate NF-κB activity directly as a result of the action of ROS on components of the transcription factors activation chain (Flohè et al 1997, Chen & Shi et al 2002), through activation of possible histone acetylation regulatory MAPK pathways that enhance NF-κB activation (Gilmour et al 2003, Øvrevik et al 2006), through proteins such as APE/Ref-1 (Albrecht et al 2005) and/or by changing the cells internal redox environment through the depletion of intracellular antioxidants such as GSH. Changes in the redox state of GSH can regulate the activity of proteins with redox sensitive thiols (Kang et al 1990) that may include a protein/s affecting the phosphorylation status of IκB (and therefore the activation status of NFκB) (Flohè et al 1997). Previous results indicated a correlation between depletion of GSH and increased production of the NF-κB regulated cytokine, IL-8 (Xu et al 1999, Desaki et al 2000, Rahman et al 2003, Øvrevik et al 2004, Boncoeur et al 2008) (although NF-κB may not have the monopoly on control of production of this cytokine

[Singh et al 2007]). This indirectly lends credence to results indicating NF-κB nuclear translocation did occur following DQ12 exposure. Unfortunately no conclusions can be drawn about the effect of MWCNT upon the position of NF-κB, previous assays assessing levels of IL-8 mRNA expression, IL-8 protein production and GSH depletion failed to indicate any differences between MWCNT that may explain or should be reflected in NFκB translocation. No dramatic differences in the residual metal content of either sample were also apparent to offer explanation.

Probably as a result of technical issues, assays to study the effect of MWCNT on the occurrence of NF-κB translocation failed to return consistent results. Positive controls, both particle (DQ12) and non particle (TNFα), did not appear to stimulate NF-κB activation and translocation that previous published works suggested could be expected. This was compounded by higher levels of translocation demonstrated in untreated cells (or rather higher levels of fluorescent signal). As a result of this it cannot be concluded that aggregated MWCNT either caused translocation or failed to cause translocation of NF-κB following exposure to A549 cells.

Chapter 6

The inflammatory effects of MWCNT *in vivo*

Chapter 6

The inflammatory potential of LMWCNT and SMWCNT *in vivo.*

6.1 Introduction

Cell free assays (ESR) demonstrated a free radical generating capacity for MWCNT although of insufficient quantity, or not of the necessary species to directly cleave DNA. *In vitro* models (to investigate the molecular mechanisms of potential inflammatory responses induced by MWCNT) failed to reveal clear signs of acute toxicity or inflammatory responses to MWCNT. Neither was there any *in vitro* markers indicating a rapidly developing fibrotic response to nanotubes that some animal studies have suggested occurs in the absence of chronic inflammation.

The peritoneal cavity of C57BL/6 mice was chosen as the site of exposure of MWCNT to study their inflammatory and fibrogenic potential *in vivo*. Intraperitoneal (IP) injections represent an alternative to inhalation studies as inflammation and fibrosis (and mesotheliomas) can be produced in this region in addition to the lungs (Donaldson et al 1982). The peritoneal cavity, despite questions of relevance of this mode of exposure to human beings, has been a site of interest for carcinogenicity screening of fibres and as a site that can model all the responses of pleura exposed to fibres – inflammation, fibrosis and mesothelioma. The inflammatory response in the peritoneal cavity has also been found to be acutely responsive to fibres and much less so towards particles (Donaldson 1996). The apparent selectivity of the peritoneal cavity to fibres posed the question of how a

theoretically (or ideally) fibrous material with an aggregate morphology more akin to a particle would interact with serosal cells and the type and intensity of response that would be elicited.

To date exposure of animals (principally mice and rats) to CNT have focused largely on pulmonary instillation with granulomatous inflammation being a common (but not universal) outcome of exposure. The formation of granulomas is usually in response to persistent pathogens, pathogen products or inert poorly soluble foreign materials. They are characterised by monocytic derived cells directed at walling off and eliminating foreign bodies (Williams & Williams 1983, Diaz et al 2000). Both host factors and the nature of the foreign material determine the course of a granulomatous reaction (Williams & Williams 1983). The cause of CNT induced pulmonary granulomas is not clear but has been attributed to the presence of insoluble aggregates in the lungs (Muller et al 2005, Shvedova et al 2005, Grubek-Jaworka et al 2006, Li et al 2007) sometimes contained in macrophages (Mangum et al 2006, Chou et al 2008) as a foreign body response. Studies have also reported effects distant from localised aggregates including thickening of interstitium (Mangum et al 2006) and alveolar walls (Li et al 2007) possibly related to:

a) Better distribution

b) Some factor produced by granulomas that has its own effect on alveolar walls and interstitium.

This chapter focuses upon the effect of MWCNT injected directly into the peritoneal cavity of C57BL/6 mice by measurement of LDH leakage and protein levels, the extent of inflammatory cell infiltration and by histological examination.

6.2 STUDY 1 – Assessment of the effect of instillation of DPPC dispersed MWCNT, Asbestos and a panel of control particles into the peritoneal cavity of C57BL/6 mice.

Stock suspensions (concentration 200μg/ml) of TiO_2, DQ12, ufCB, short fibre amosite (SFA), long fibre amosite (LFA), long fibre amosite (saline dispersed- LFA SAL), long multi-walled carbon nanotubes (LMWCNT) and short multi-walled carbon nanotubes (SMWCNT) were prepared in sterile physiological saline and sonicated. Immediately prior to injection samples were diluted to working concentrations (100μg/ml) in a sterile solution of DPPC and sonicated again. Male C57BL/6 mice were divided into treatment groups of four animals, each treatment group was injected I.P. with 0.5ml working concentration of each particle/fibre or 0.5ml DPPC solution alone (negative control). After 48 hours exposure mice were sacrificed and their peritoneal cavities lavaged three times with 2ml saline, lavages (peritoneal lavage fluid or PLF) were pooled into chilled 15ml falcon tubes and cell death assessed by measurement of LDH and the extent of inflammation assessed by cell counts and protein levels.

After 48 hours only LFA and LFA (Sal) induced a large increase in the number of cells infiltrating the peritoneal cavity compared to the negative control ($22.3 \pm 2.6 \times 10^6$ and $17.2 \pm 6.7 \times 10^6$ respectively compared to control $0.11 \pm 0.03 \times 10^6$) (Fig. 6.1A). The total inflammatory cell infiltration induced by SFA and SMWCNT was $8.3 \pm 3.8 \times 10^6$ and $8.0 \pm 2.1 \times 10^6$ respectively, for LMWCNT total cell numbers were found to be just over half that of SMWCNT at $4.6 \pm 2.0 \times 10^6$. The effect of the particles TiO_2, DQ12 and ufCB upon the total cell numbers was found to be no

different from the negative control at $3.0 \pm 0.3 \times 10^6$, $1.5 \pm 0.4 \times 10^6$ and $2.4 \pm 0.7 \times 10^6$ respectively compared to that induced by saline/DPPC at $2.6 \pm 0.7 \times 10^6$. Median levels (figure 6.1B) of cell influx induced by TiO_2, DQ12, LMWCNT and ufCB were found to be very similar to the low levels induced by the negative control DPPC. The control (DPPC), TiO_2, DQ12 and ufCB demonstrated very little spread in data; greater variability was seen for LMWCNT with a skew towards the low end of cell influx. Overall LMWCNT demonstrated no real capacity above that of the control to induce substantial cell influx following instillation. The median level of cell influx induced by SMWCNT and SFA were also of a similar level, about four times greater than the DPPC control. LFA and LFA (Sal) induced the greatest effect that was in fact very similar based on the closeness of their median values. There was greater variability in infiltrating cell numbers induced by LFA (sal) compared to LFA.

Acute inflammation is characterised by an influx of neutrophils (neutrophilia), and so the total neutrophils were determined from differential counts (Fig. 6.2A). The neutrophil influx induced by MWCNT was not substantially greater than the negative control. Neutrophil infiltration induced by TiO_2, DQ12, ufCB or SFA was equal to or only slightly greater than the control. Only LFA and LFA (Sal) increased the neutrophil influx into the peritoneal cavity substantially ($7.8 \pm 0.83 \times 10^6$ and $4.25 \pm 1.77 \times 10^6$ cells respectively). Analysis of median levels of neutrophil influx (figure 6.2B) induced by DPPC (control), TiO_2, DQ12, SFA, LMWCNT and ufCB were almost identical underlying their lack of effect. Neutrophil infiltration was greatest for LFA>LFA (sal)>>SMWCNT. Median levels of neutrophil influx induced by LFA and LFA(sal) was about half the number of the induced macrophage

influx, for SMWCNT, median neutrophil levels were about a quarter of the median macrophage levels indicative of a comparatively much lower inflammatory potential To further quantify the effect of each particle or fibre indices of inflammation and cell damage were assessed in PLF including protein levels (a measure of cell and capillary permeability and damage) and total LDH levels (a measure of damage to cell membranes). Analysis of total protein levels (figure 6.3A) reveals three levels of response. The greatest level of response was induced by LFA (DPPC dispersed) that caused a significant accumulation of protein in the peritoneal cavity (***$p<0.001$). The secondary level of response was caused by LFA (Sal) and SMWCNT that also significantly ($p<0.001$) increased protein levels. There was also a significant difference between LMWCNT and SMWCNT ($p<0.001$) The third and lowest level of response was caused by SFA, LMWCNT, TiO_2, DQ12 and ufCB that had no effect upon protein levels in the peritoneum. A relatively consistent pattern of results was evident between total cell counts, neutrophil counts, and protein whilst the LDH pattern (figure 6.3B) did not quite follow the trend of the others and there were no significant differences. This suggests a common mechanism underlying neutrophil influx, protein leakage and to a lesser degree particle induced cytotoxicity. Also apparent was the long fibre specific effect as evidenced by the greater influx of neutrophils and greater protein and LDH leakage induced by LFA and LFA (Sal) compared to particulate materials and shortened LFA (SFA). This trend was upset to an extent by SMWCNT that matched LFA (Sal) in its ability to cause protein and LDH leakage into the peritoneal cavity although not in its ability to cause neutrophil influx. Also apparent was an augmentation of the inflammatory potential and toxicity of LFA dispersed in DPPC/saline compared to LFA in saline

alone. The link between inflammatory cell influx and protein leakage into the peritoneal cavity was strengthened by plotting the two data sets against each other resulting in a positive correlation with an R^2value of 0.788(Fig. 6.4), thus the high degree of cell influx prompted by LFA was also associated with a high degree or protein leakage whereas the limited cell infiltration caused by TiO_2 or DQ12 was associated with a lack of protein leakage into the peritoneal cavity.

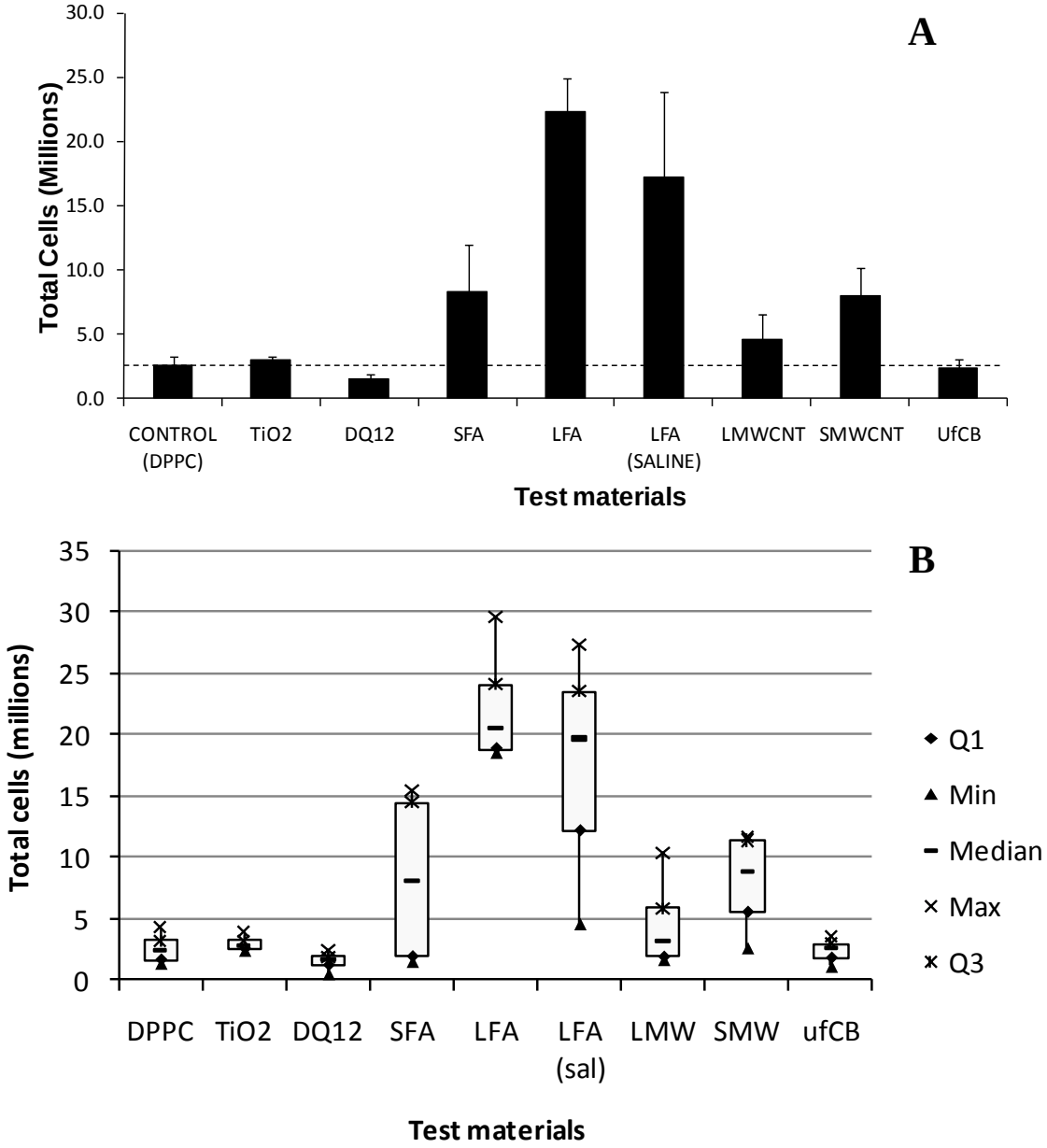

Figure 6.1. Total number of neutrophils in PLF 48 hours after instillation of MWCNT, asbestos fibres and a panel of control particles. Mice were i.p. instilled with either saline/DPPC, TiO_2, DQ12, ufCB, LMWCNT, SMWCNT, SFA and LFA dispersed in DPPC/saline or LFA dispersed in saline alone (LFA [Sal]). Particles were instilled at a concentration of 100µg/ml in 0.5ml. Each treatment group contained four animals exposed for 48 hours to particles prior to sacrifice and peritoneal lavage. **(A)** Histogram of the mean number of total cell infiltrating the peritoneal cavity 48 hours after particle influx. Dashed line represents the mean level of cell influx induced by the DPPC control. Bars represent the S.E.M. **(B)** Box and whisker plot of the total cell influx into the peritoneal cavity 48 hours after particle instillation. This plot demonstrates the spread (variability) of the data within each treatment group and compares the distribution of data between groups.

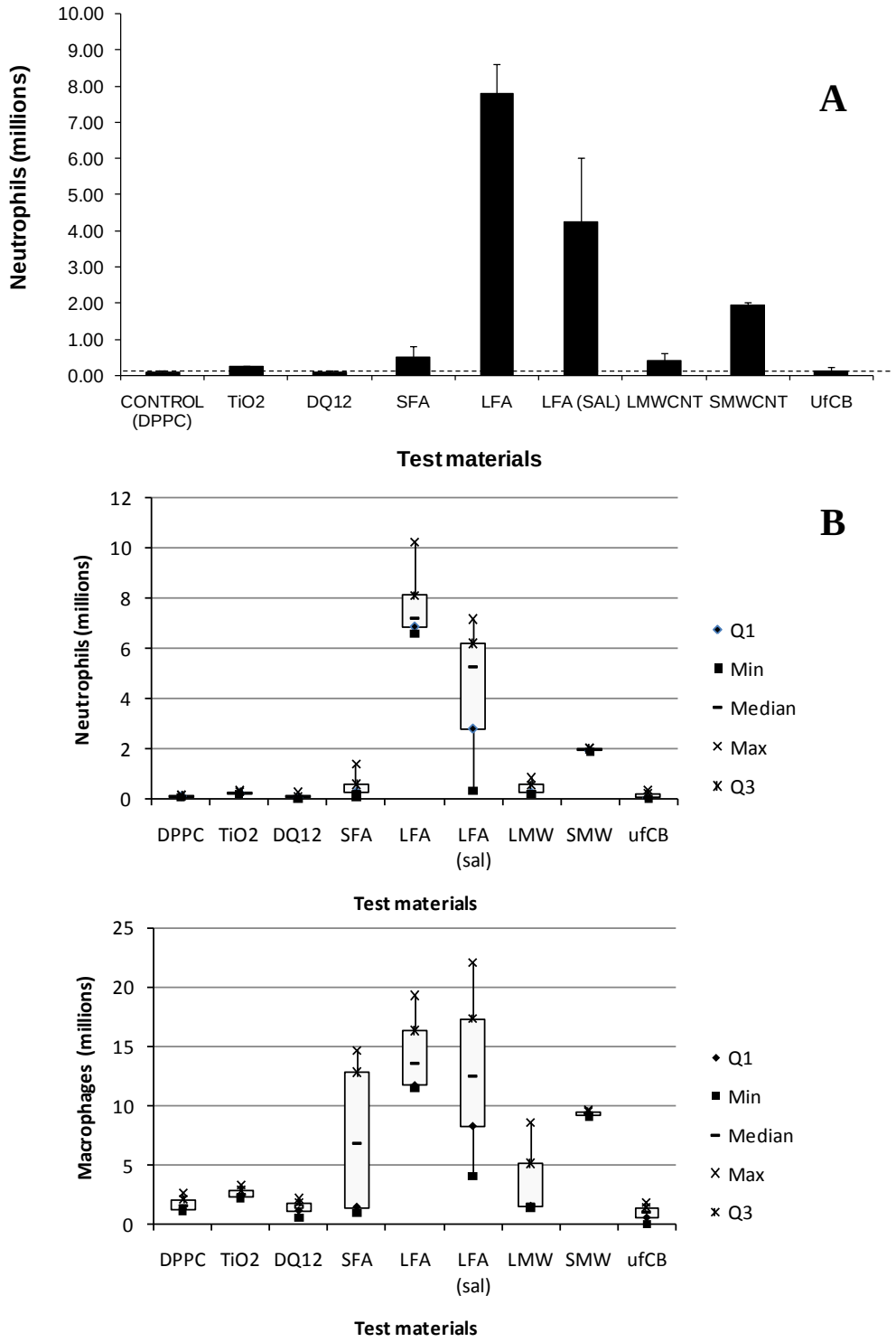

Figure 6.2. Number of neutrophils in PLF 48 hours after instillation of MWCNT, asbestos fibres or control particles (100µg/ml in 0.5ml). (A) Histogram of the mean number of neutrophils infiltrating the peritoneal cavity 48 hours following treatment. Neutrophil and macrophage counts were performed form cytospins prepared from lavages from each animal in a treatment group (four animals per treatment group) and then averaged across the treatment group. **(B)** Box and whisker plot of neutrophil counts for each treatment group **(C)** Box and whisker plot of infiltrating macrophage numbers for each treatment group.

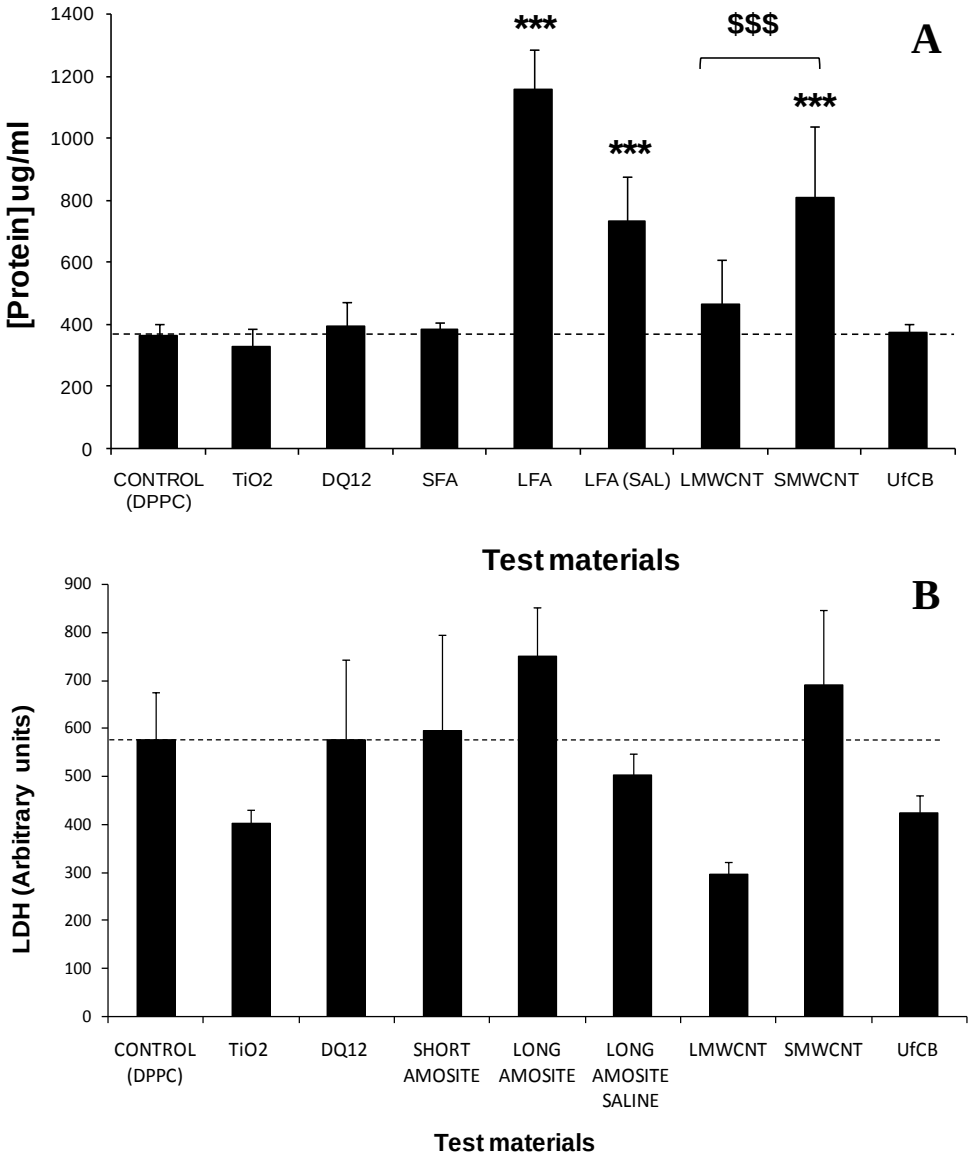

Figure 6.3. (A) Total protein levels in PLF after 48 hours following instillation of particles and fibres (100µg/ml in 0.5ml). Significant ($p<0.001$) increases in protein levels were caused by LFA, LFA (sal) and SMWCNT. There was also a significant ($p<0.001$) difference in the level of protein found in PLF between LMWCNT and SMWCNT treated mice \$\$\$$p<0.001$) and between LFA and LFA (sal) $p<0.001$. The histogram represents the mean results from four animals per treatment group with protein levels for each animal analysed in triplicate. The dashed line represents the mean level of protein in PLF from control treatments as a minimum level of effect. Bars represent S.E.M. ***$p<0.001$ compared to DPPC control. **(B) Total LDH levels measured in PLF after 48 hours following instillation of 100µg/ml in 0.5ml particles and fibres.** LDH levels were measured in PLF from each animal of a treatment group in triplicate; the histogram represents the mean LDH levels of each treatment group. The dashed line represents the level of LDH caused by control treatments as a measure of the minimum level of effect. Bars represent S.E.M.

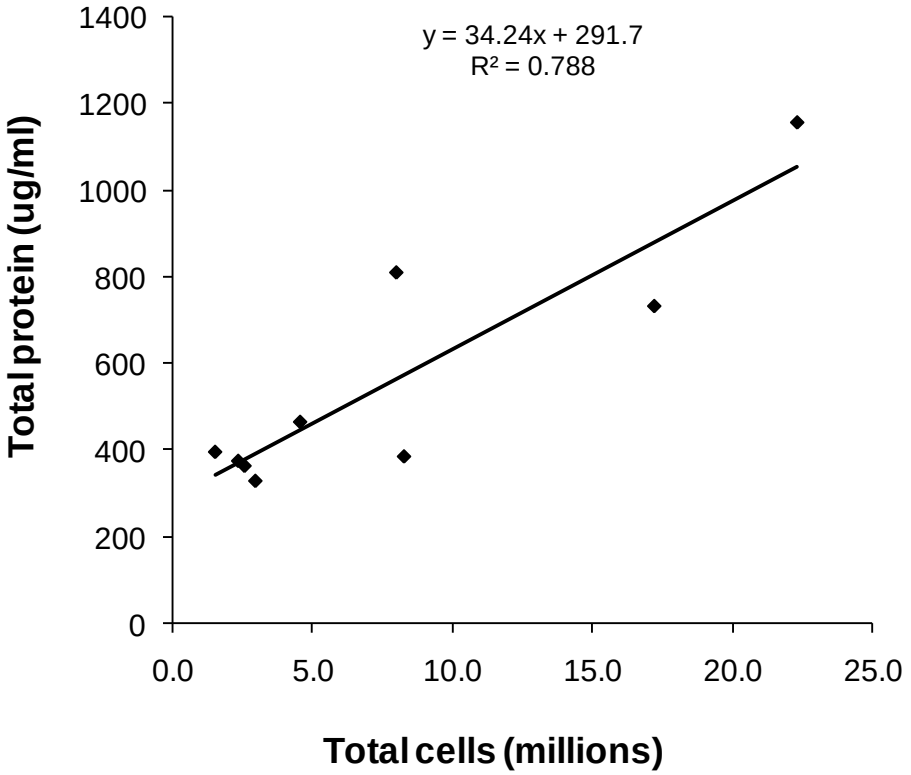

Figure 6.4. The correlation between the extent of total inflammatory cell influx and the level of protein leakage into the peritoneal cavity of mice. Mean data of four animals for total cells was plotted against mean total protein levels in PLF for each particle following 48 hours treatment. The extent of total inflammatory cell influx into the peritoneal cavity induced by each treatment was found to be positively associated with the extent of protein leakage with an R^2 value of 0.788.

6.3 STUDY 2 – Markers of injury in peritoneal lavage fluid from mice following 24 hour instillation of MWCNT, long and short amosite asbestos and soluble extracts derived from test materials.

In the assessment of the toxicity of a variety of particles it has become clear that there is a quantifiable contribution of soluble factors. For example organic components adsorbed to the carbonaceous nuclei of diesel exhaust particles (Yanagisawa et al 2003) and the extractable metal fractions from environmental particulate matter (PM) (Dye et al 1999) or welding fumes (McNeilly et al 2005). The importance of extractable particle components to particle toxicity was effectively demonstrated when it was shown that washing nano-sized welding fume particles eliminated their inflammatory potential as a result of the loss of a transition metal fraction (McNeilly et al 2005).

In the previous section it was shown that SMWCNT showed a trend towards greater levels of inflammation than LMWCNT. Previous data confirm that for fibres length can be a critical parameter in the materials toxicity and long fibres are more damaging than short fibres (Donaldson et al 1989, Hesterberg & Barrett 1984, Ohyama et al 2001, Riganti et al 2003, Castranova et al 2006). The state of the MWCNT assessed in these studies was more akin to particles (similar in size and nature to each other) than fibres thus a toxicological distinction between the two based on length was not likely (and based upon previous results, contrary to published works since the short had more activity than the long).

It has been suggested that LMWCNT and SMWCNT might differ in terms of availability of metals forming part of, or adsorbed to these structures. Jurkschat et al

(2007) found that even after vigorous acid washing single walled carbon nanotubes contained significant quantities of iron. Although largely encapsulated either by graphitic shells or within the CNT structure a proportion of residual iron is fluid-accessible (Guo et al 2007). One possibility therefore is that shortening of CNT by extensive refluxing could make trapped residual iron more accessible.

Suspensions of 0.4mg/ml LMWCNT, SMWCNT, LFA and SFA were prepared in sterile 0.9% physiological saline, sonicated and kept on a roller overnight. Leachate was separated from particles by centrifugation and the test materials (solid fraction) washed by repeated cycles of centrifugation and re-suspension in sterile saline. The solid test fraction was diluted to a working concentration of 100μg/ml and leachates equivalently diluted. Thirty mice (C57BL/6) were divided into six test groups of four, a single control group of four saline treated animals with a single untreated control group of two animals. Suspensions of particles (0.5ml) were injected I.P. and the mice treated for 24 hours before being sacrificed and the peritoneal cavity lavaged three times with 2ml saline. Lavages were spun down at 1000rpm and 1.5ml supernatant collected for quantification of protein and LDH levels. Cell pellets were re-suspended for cytospins and total cell counts.

After 24 hours exposure only LFA substantially increased the total number of infiltrating inflammatory cells in the peritoneal cavity ($12.05 \pm 1.97 \times 10^6$) compared to the negative control ($4.12 \pm 0.47 \times 10^6$) (Fig. 6.5A). Neither LMWCNT ($2.59 \pm 0.40 \times 10^{6)}$ nor SMWCNT ($3.62 \pm 0.69 \times 10^6$) increased the numbers of inflammatory cells found in the peritoneal cavity above control levels. Aqueous extracts made from each of the three materials did not increase the total number of inflammatory cells above those counted in untreated animals. Median total cell

influx (fig. 6.5B) for LMWCNT (2.8 x 10^6), SMWCNT (3.5 x 10^6) and their extracts (LMWe and SMWe) were on a par with or less than negative control levels (4.0 x 10^6). Median levels of cell influx induced by LFA fibre (13.05 x 10^6) were substantially greater than the negative control with median levels induced by LFA extract (LFAe) (3.6 x 10^6) almost identical to negative control levels. This further confirms that the extracts had no inflammatory effect.

Quantification of the number of neutrophils (Fig. 6.6A) revealed LFA (3.1 ± 1.7 x 10^6) induced a dramatic increase in numbers infiltrating the peritoneal cavity. The effect of LMWCNT (0.2 ± 0.04 x 10^6) and SMWCNT (0.4 x 10^6) was not found to be greater than induced by injection of saline alone (0.5 ± 0.28 x 10^6). Of the extracts, those derived from LFA caused a slightly increased peritoneal neutrophil level compared to MWCNT and controls, that induced by MWCNT was no greater than the effect of injection of saline alone. Analysis of median levels of neutrophil and macrophages (fig. 6.6B) revealed no inflammatory potential for the extracts with very little spread in the data and the medians never more than the negative control.

Instillation LMWCNT and SMWCNT (0.92 ± 0.18, 0.55 ± 0.05 and 0.68 ± 0.11mg/ml respectively) increased total protein levels in PLF (Fig. 6.7A) above those found in untreated (0.45 ± 0.01mg/ml) and saline (0.49 ± 0.02mg/ml) controls although not significantly. LFA was found to cause significant protein leakage into the peritoneal cavity ($p<0.001$) paralleling its effect on the level of cell infiltration. Of the extracts only that derived from LFA (0.58 ± 0.04mg/ml) increased protein levels above controls but this effect was non-significant. Analysis of LDH levels (Fig. 6.7B) produced no clear particle/fibre specific or extract specific effect or increase that was significantly greater than untreated or saline controls. Of the solid

materials the greatest release of LDH was caused by SMWCNT (681.7 ± 437.9) (a result similar to that seen in study 1 comparing SMWCNT to LFA [saline]) followed by LMWCNT (409.1 ± 83). None of the extracts increased LDH levels significantly above those achieved as a result of instillation of saline alone.

These results suggested that the inflammatory effect of LFA and the limited effects of LMWCNT and SMWCNT were centred on the presence of the solid material in the peritoneal cavity rather than as a result of easily extractable/soluble elements (certainly over a 24 hour time period). The materials LFA, LMWCNT and SMWCNT could consistently be ranked (LFA>SMWCNT>LMWCNT) in terms of their ability to increase the levels of inflammatory cells and protein in the peritoneal cavity. The extent of LDH release however did not conform to this pattern. In comparison to the inflammatory effect LFA exerted over 48 hours that seen in this study over 24 hours was considerably less suggestive of a time dependent effect. The slightly greater toxicity and inflammatory potential of SMWCNT over LMWCNT observed in the mean data was carried over into this study but to a much more limited degree. This could suggest a time dependent effect however given the variability of the total inflammatory cell influx (fig 6.1B) and the degree of overlap between smallest and largest outliers for LMWCNT and SMWCNT this may suggest that this is not a real difference in toxicity between the two materials.

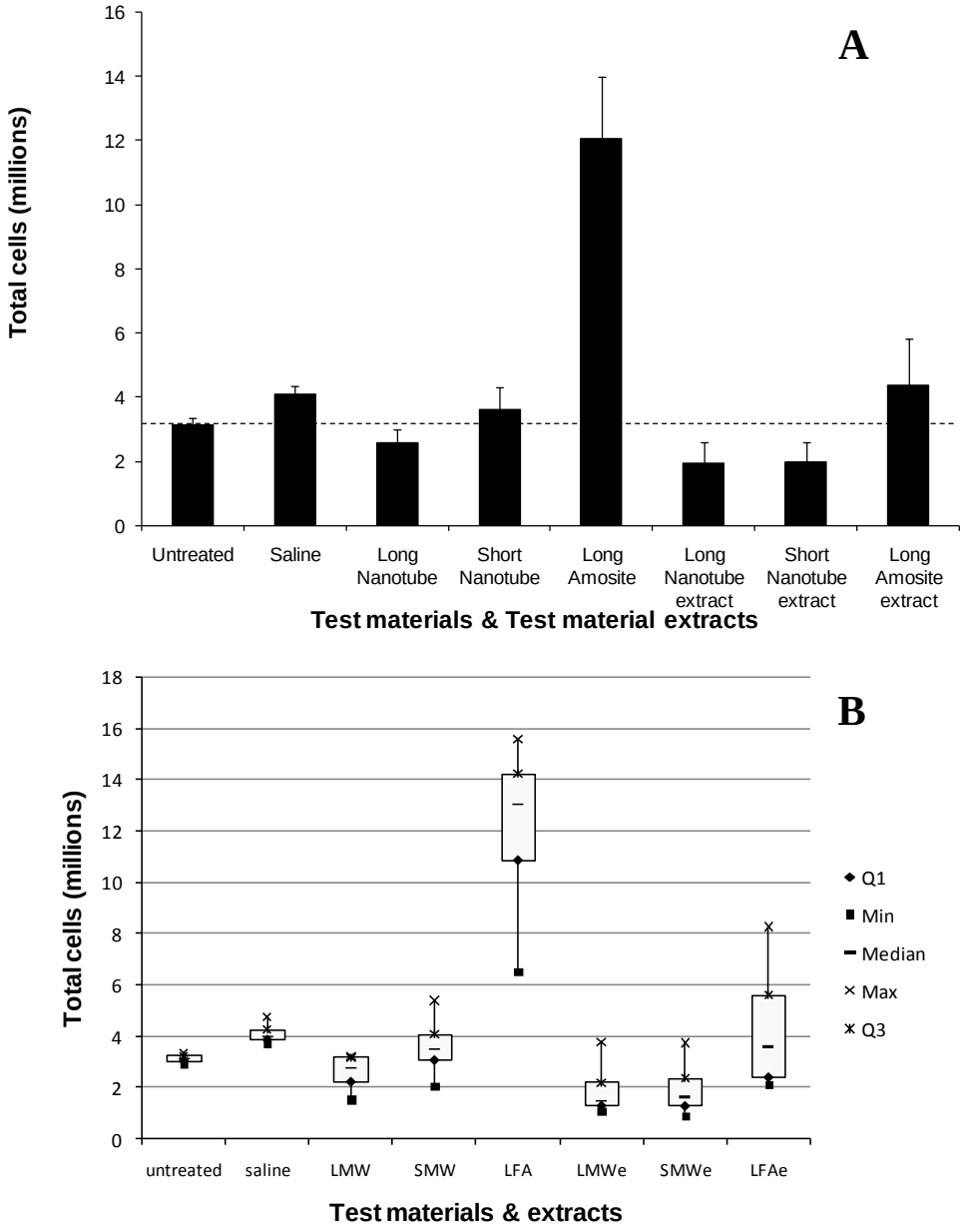

Figure 6.5. (A) Total cells in PLF following 24 hours exposure to 100µg/ml in 0.5ml of LMWCNT, SMWCNT or LFA or aqueous extracts of particles. Following 24 hours exposure to particles or their aqueous extracts mice were sacrificed and peritoneal cavities lavaged. Control animals consisted of mice left un-treated for the duration of the experiment or i.p. injected with 0.9% physiological saline alone. Treatment groups contained four animals. Histogram represents the mean total number of cells from peritoneal lavages from four animals. Untreated control group consisted of two animals. Bars represent S.E.M. **(B)** A box and whisker plot of total cell data for particle and extract treated mice. Although mean levels of LFA extract appear to suggest an effect slightly greater than control this is not borne out by similarities in median values. LMWe = LMWCNT extract, SMWe = SMWCNT extract, LFAe = LFA extract.

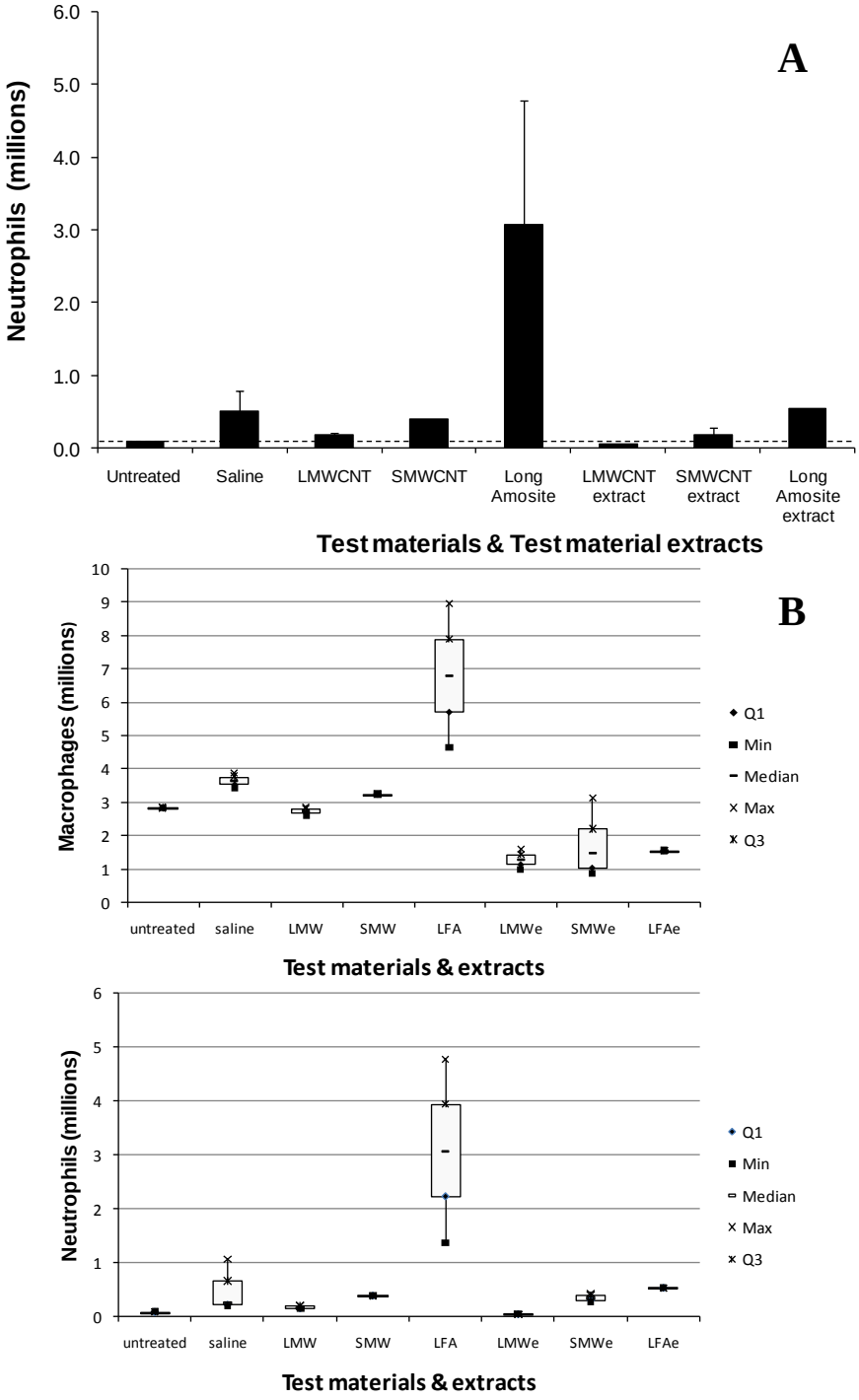

Figure 6.6. The number of neutrophils in PLF following 24 hours exposure to LMWCNT, SMWCNT, LFA and their aqueous extracts (LMWe, SMWe, and LFAe). (A) Neutrophils counts were performed on cytospins prepared form lavages from each animal of each treatment group, numbers were averaged across treatment groups. The histogram represents the mean number of neutrophils counted for each treatment in groups containing four animals. Bars represent S.E.M. **(B)** Box and whisker diagrams for neutrophil and macrophage counts for each treatment group comparing the spread of data and medians between groups.

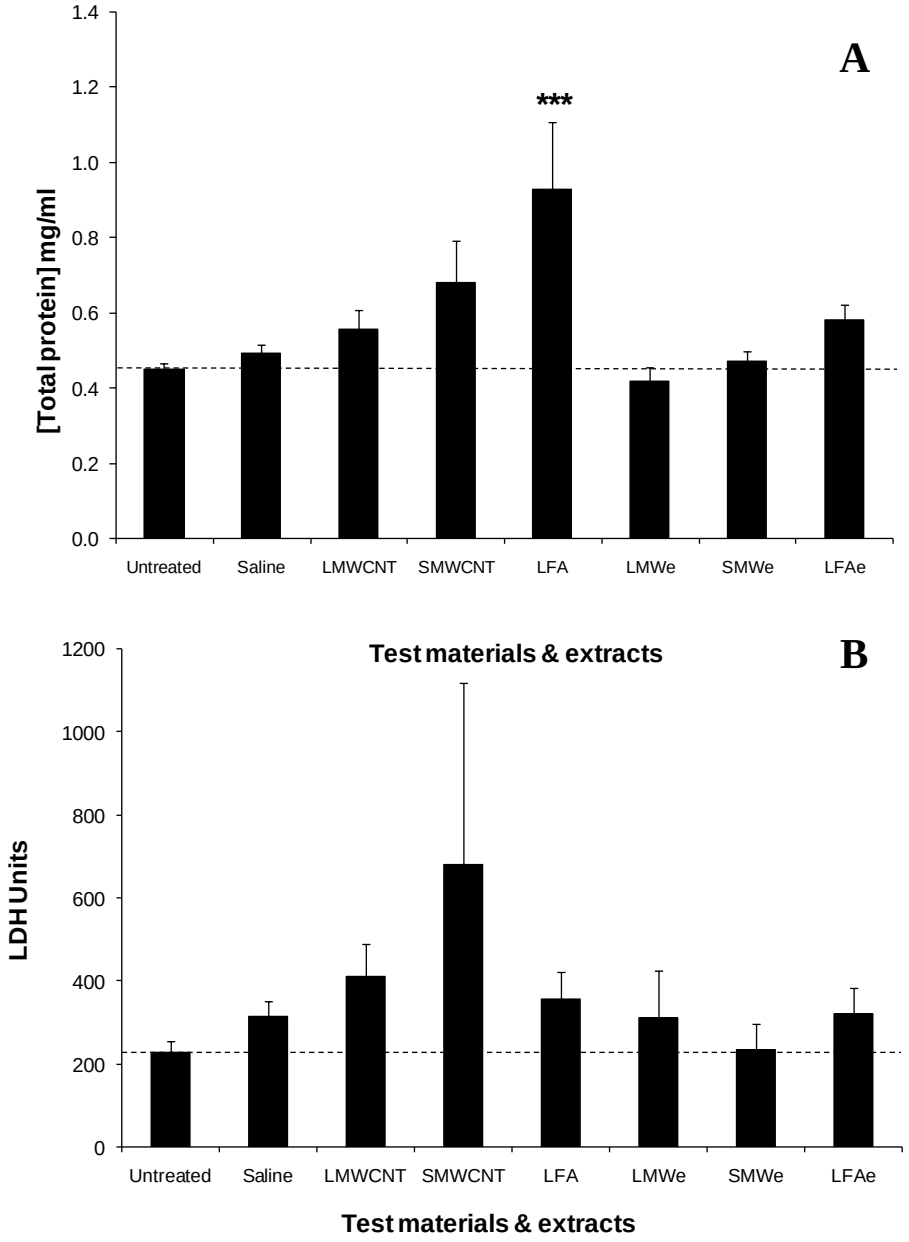

Figure 6.7. (A) Total protein levels in PLF following 24 hours exposure to particles and fibres and their aqueous extracts. Total protein levels in PLF were measured, the histogram represents the mean results of four animals per treatment group with protein levels of each animals analysed in triplicate. Only protein leakage induced by LFA installation was found to differ significantly from both controls (***$p<0.001$) after 24 hours. Bars represent S.E.M. **(B) Total LDH levels in PLF following 24 hours exposure to particles, fibres and their aqueous extracts.** LDH levels of each PLF sample were analysed in triplicate, the histogram represents the mean level of LDH in PLF for each treatment group (four animals per group). Dashed line represents the level of LDH measured in the untreated mice. Bars represent S.E.M.

6.4 STUDY 3 – An investigation into the capacity of MWCNT to induce a dose dependent inflammatory effect in the peritoneal cavity of C57BL/6 mice after 48 hours exposure.

To explore the possibility of a difference in the inflammatory capacity of LMWCNT and SMWCNT the peritoneal cavities of C57BL/6 mice were instilled with increasing concentrations of both MWCNT for 48 hours. Suspensions of 200, 500 and 750μg/ml LMWCNT and SMWCNT were prepared in sterile 0.9% physiological saline and sonicated to disaggregate. A total of 24 mice were divided into seven treatment groups of three animals, two groups were set aside as control groups, one untreated and one instilled (I.P. injection) with saline alone. The remaining six groups of three animals received by I.P. injection 200, 500 or 750μg/ml of LMWCNT or SMWCNT in 0.5ml saline and treated for 48 hours. After treatment mice were sacrificed and the peritoneal cavity lavaged three times with 2ml saline. Peritoneal lavage fluid was spun down and 1.5ml supernatant was set aside for biochemical analysis, the cell pellet was re-suspended in 1ml 0.9% physiological saline and used for total cell counts and preparation of cytospins.

After 48 hours instillation of MWCNT induced an influx of cells into the peritoneal cavity that was more than twice as great as the saline only control (Fig. 6.8A). A slight concentration dependent effect was observed for LMWCNT resulting in total cell counts of $14.1 \pm 4.2 \times 10^6$, $15.2 \pm 3.0 \times 10^6$ and $15.5 \pm 1.45 \times 10^6$ for 200, 500 and 750μg/ml respectively. The magnitude of the increase in total cell numbers did not appear to be proportional to level of the concentration increase however. No concentration dependent increase in total cell numbers was observed for SMWCNT,

the level of increase at each concentration was less than that induced by LMWCNT ($11.8 \pm 2.8 \times 10^6$, $12.6 \pm 1.5 \times 10^6$ and $12.4 \pm 3.5 \times 10^6$ induced by 200, 500 and 750μg/ml respectively). Compared to the previous study carried out over 48 hours (study 1) the inflammatory effect of LMWCNT (in terms of total cell numbers) was greater than of SMWCNT in a reversal of the previous results. The median levels of total inflammatory cell numbers infiltrating the peritoneal cavity are also greater than the negative controls (fig. 6.8B) however there is no evidence of a dose related effect and the spread of the data shows a great deal of overlap between increasing dose groups. Also apparent is the variation between animals of the same treatment group in the numbers of infiltrating cells. This may result from flocculation of MWCNT affecting to some extent the size of the dose delivered to each animal. The increase in cell numbers in response to instillation of MWCNT appears to be a non specific effect. Borne out in both mean and median data is the greater influx of inflammatory cells induced by LMWCNT compared to SMWCNT.

Increasing the concentration of instilled MWCNT did not increase numbers of neutrophils in the peritoneal cavity (fig. 6.9A) in a concentration dependent capacity although all treatments increased the number of neutrophils above that of the negative control ($0.5 \pm 0.2 \times 10^6$). The greatest increase was caused by SMWCNT at a concentration of 500μg/ml (5.6×10^6). The lack of a concentration dependent increase in neutrophil numbers combined with the lack of a parallel between total cell numbers and neutrophil numbers (either within a treatment group or between LMWCNT and SMWCNT) indicates these materials have little inflammatory potential *in vivo* and the effect of their instillation in the peritoneal cavity upon inflammatory state was a non-specific response to the presence of a non soluble mass

of material. Analysis of box plots for macrophage and neutrophil influxes (fig. 6.9B) in response to increasing concentrations for MWCNT reveals the pattern of macrophage numbers matches that described for total cells. Neutrophil influx data is highly variable both within and between groups and shows no dose dependence. Although median neutrophil levels following both LMWCNT and SMWCNT instillation are greater than controls the lack of a dose dependent effect and variability in the spread of the data between groups suggests this is not related to increasing inflammatory potential with increasing dose of MWCNT.

Examination of total protein levels (Fig.6.10A) revealed all concentrations of LMWCNT and SMWCNT increased levels above that of the saline control (not significantly). For LMWCNT treatments protein concentration did not increase in parallel with nanotube concentration with protein levels being less at 750μg/ml (0.73mg/ml ± 0.26) than at 500μg/ml (0.85μg/ml ± 0.10), for SMWCNT there was a concentration dependent increase in protein levels. Upon assessment of PLF LDH levels it was determined that increasing MWCNT concentration did not consistently increase LDH release; all treatments increased the level of LDH in PLF above that of the saline control but none significantly. For LMWCNT the greatest measurement of LDH was taken at 750μg/ml (1380.6 ± 405.9) whilst SMWCNT induced the greatest release at 500μg/ml (1214 ± 331.9).

Across all of the assessed markers of inflammation and toxicity neither LMWCNT nor SMWCNT consistently produced an upward or downward trend, although all markers were increased above those of the negative control. Instillation of nanotubes into the peritoneal cavity results in an inflammatory outcome although

this appears to be non-specific and does not appear to be due to a particular aspect of the material (a toxicity factor).

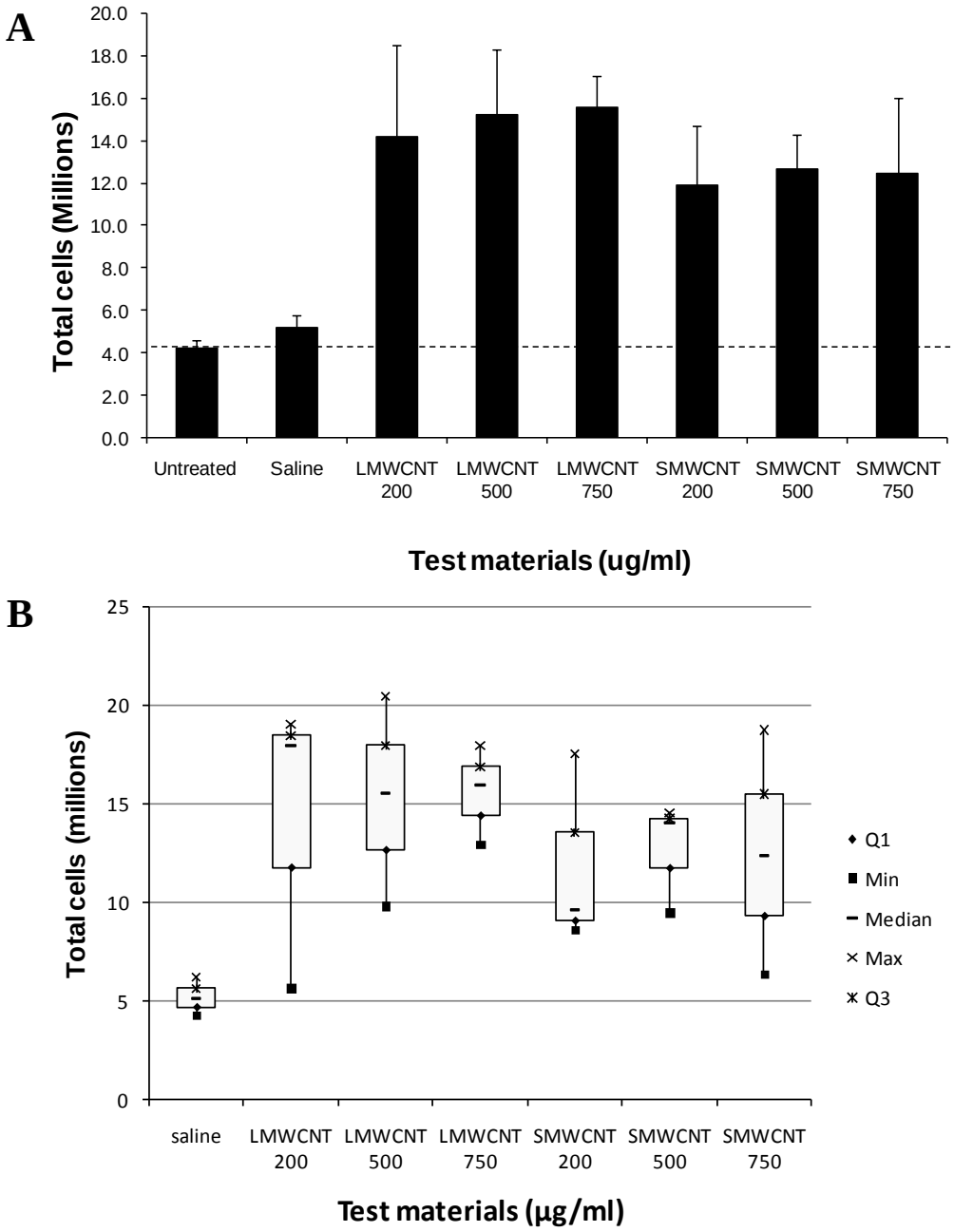

Figure 6.8. (A) The total cell numbers in PLF following 48 hours exposure to increasing doses of LMWCNT and SMWCNT. Mice wee i.p. instilled with saline or 200, 500, or 750µg/ml LMWCNT or SMWCNT dispersed in saline. The histogram represents the mean number of cells counted for each treatment group, treatments groups consisted each of three animals. Bars represent S.E.M. **(B)** Box and whisker plot of the total cell count data. Although no dose dependent effect was apparent the median levels of cell influx induced by LMWCNT were consistently greater than that induced by SMWCNT mirroring the pattern of result observed in mean data.

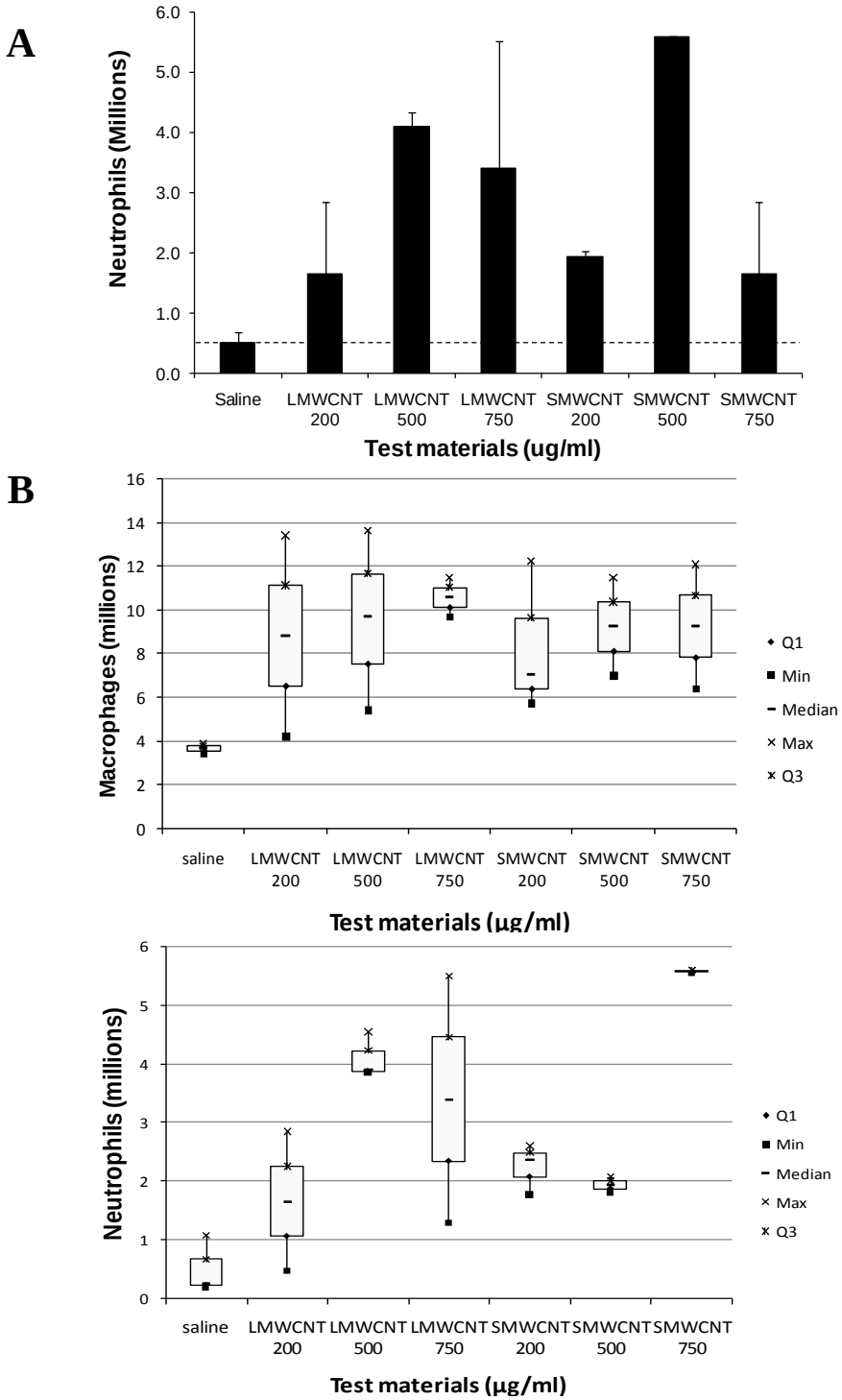

Figure 6.9. (A) The total neutrophil numbers in PLF following 48 hours exposure to increasing doses of LMWCNT and SMWCNT. Neutrophil counts were taken from cytospins prepared from each animal of each treatment group. The histogram represents the mean number of neutrophils per treatment group of three animals. No dose dependent pattern to the data was observed. **(B)** Box and whisker plots for macrophage and neutrophil numbers obtained from cytospins. Median macrophage numbers and spread of the data indicates no difference in influx induced by either LMWCNT or SMWCNT at any dose. Plot for neutrophil numbers indicates no relation between MWCNT or dose in terms of neutrophil response as indicated by median results and data spread.

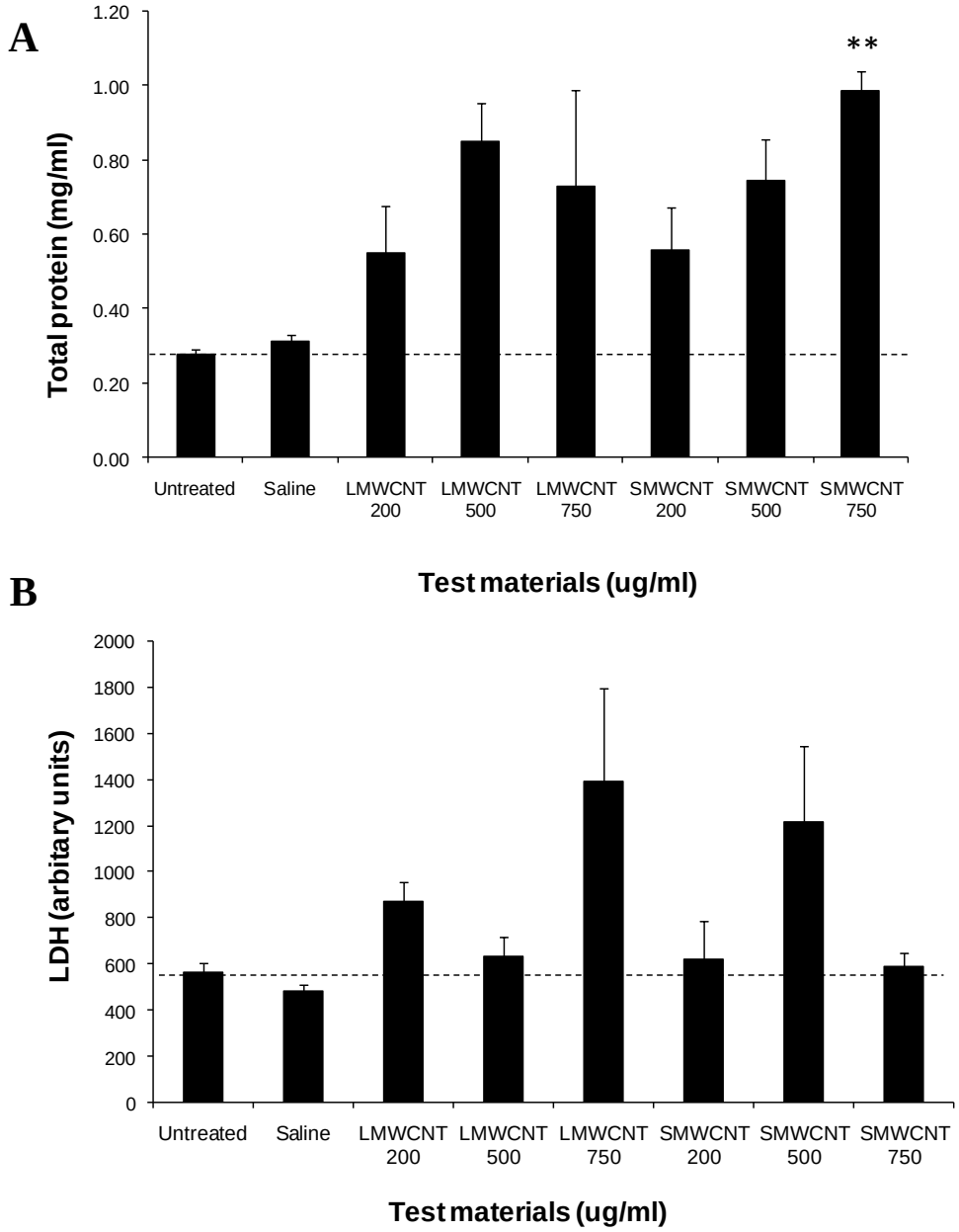

Figure 6.10. (A) Total protein levels in PLF following 48 hours exposure to increasing doses of LMWCNT and SMWCNT. PLF form each animal was analysed for protein levels in triplicate, the histogram represents the mean level of protein measured in PLF from each treatment group of three animals. Only the highest dose of SMWCNT (750µg/ml) was found to cause a significant level of protein leakage into the peritoneal cavity (**p>0.01). Bars represent S.E.M. **(B) Total LDH levels measured in PLF following 48 hours treatment with increasing doses of LMWCNT or SMWCNT.** PLF samples were analysed in triplicate for LDH, the histogram represents the mean level of LDH measured in each treatment group of three animals. Bars represent S.E.M.

6.5 STUDY 4 – A study of the cellular effects of LMWCNT and SMWCNT on the peritoneal surface of the diaphragms of C57BL/6 mice after seven days exposure.

Groups of two C57BL/6 mice were exposed by peritoneal injection to 100µg/ml of LMWCNT, SMWCNT, DQ12, SFA or ufCB delivered in 0.5ml sterile saline with exposures lasting seven days. Animals were then sacrificed and their diaphragms removed and placed in methacan fixative for histological processing. Microscopic analysis of H & E stained sections of diaphragms revealed no inflammatory change to their exposed peritoneal surfaces following SFA (Fig. 6.20), DQ12 (Fig. 6.19) or ufCB (Fig. 6.18) exposure. Examination of PSE stained sections revealed no evidence of a fibrotic response. In mice exposed to DQ12, SFA or ufCB no particles were seen at microscopy. In contrast in mice exposed to either LMWCNT (Fig. 6.14 & 6.15) or SMWCNT (fig. 6.16 & 6.17) residual particles could be observed tightly corralled in multi-cellular structures forming part of or sitting just above the mesothelial lining of the diaphragm. It should be noted that the mesothelial cell layer has become detached from the underlying musculature along most of the lengths of the diaphragms during processing. In both cases these lesions formed above and were localised to a small area of the central tendinious window of the diaphragm. Close examination of these structures revealed the presence in high numbers of macrophages and multi-nucleated giant cells surrounding large (much greater than cell size) aggregates of particles. A comparison of the nature of the aggregates formed by LMWCNT and SMWCNT and trapped within the structures

reveals that SMWCNT formed much more compact and tight bundles whilst LMWCNT formed looser bundles although still very much particulate in nature. This conformed to observations made about the particles *in vitro* and to the nature of the MWCNT when dry.

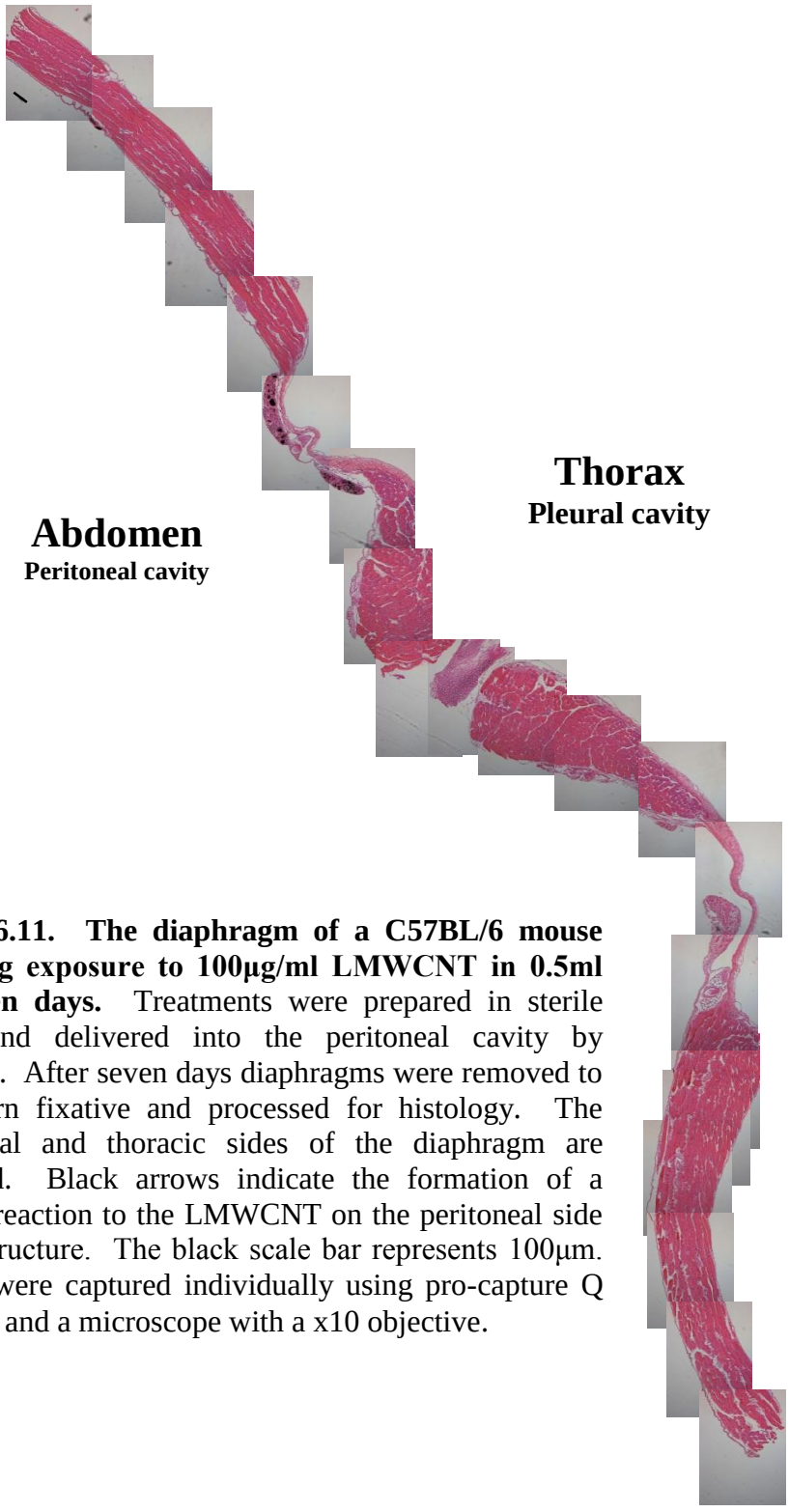

Figure 6.11. The diaphragm of a C57BL/6 mouse following exposure to 100µg/ml LMWCNT in 0.5ml for seven days. Treatments were prepared in sterile saline and delivered into the peritoneal cavity by injection. After seven days diaphragms were removed to methacarn fixative and processed for histology. The abdominal and thoracic sides of the diaphragm are indicated. Black arrows indicate the formation of a cellular reaction to the LMWCNT on the peritoneal side of the structure. The black scale bar represents 100µm. Images were captured individually using pro-capture Q software and a microscope with a x10 objective.

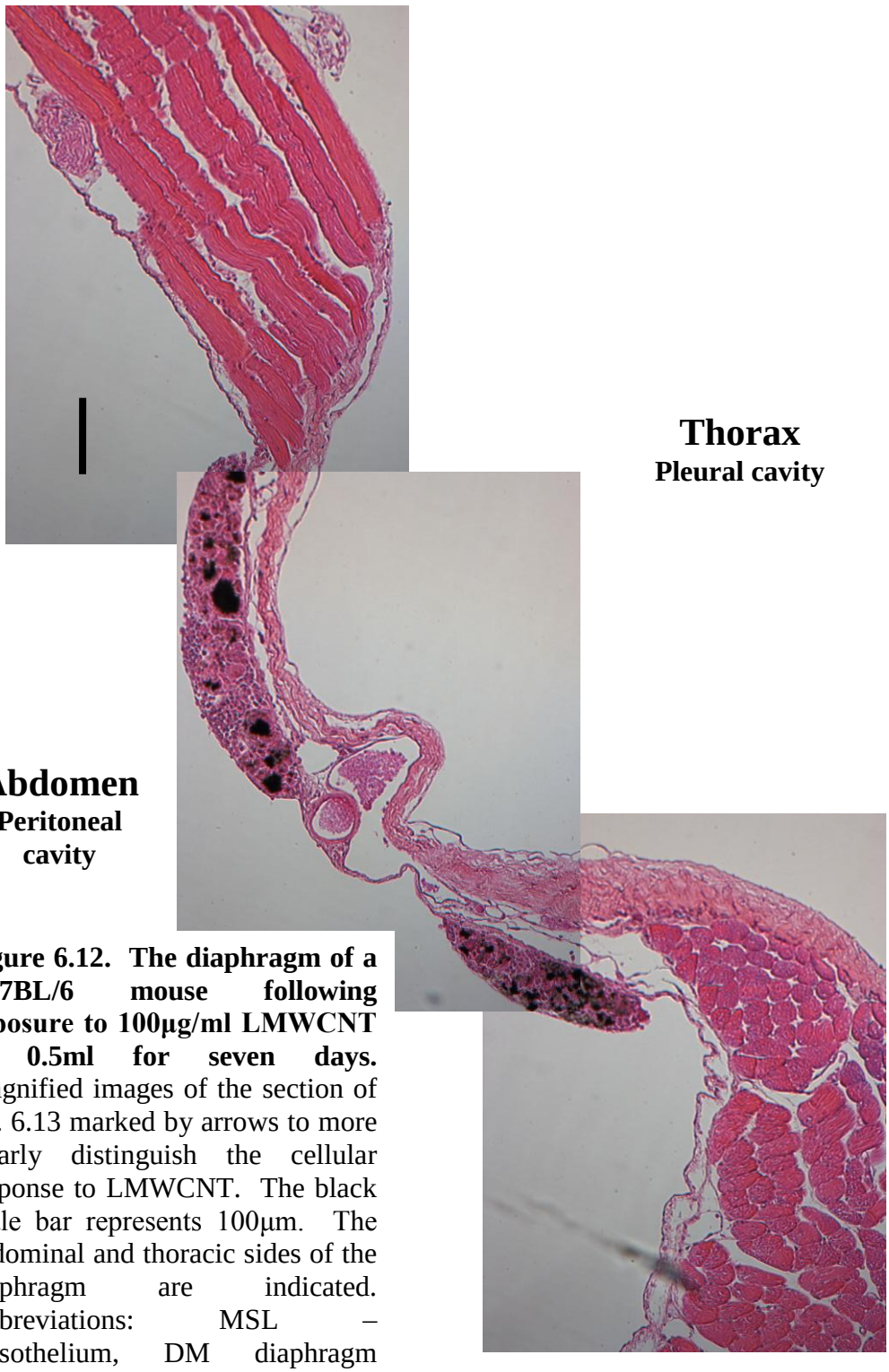

Figure 6.12. The diaphragm of a C57BL/6 mouse following exposure to 100µg/ml LMWCNT in 0.5ml for seven days. Magnified images of the section of fig. 6.13 marked by arrows to more clearly distinguish the cellular response to LMWCNT. The black scale bar represents 100µm. The abdominal and thoracic sides of the diaphragm are indicated. Abbreviations: MSL – mesothelium, DM diaphragm muscle.

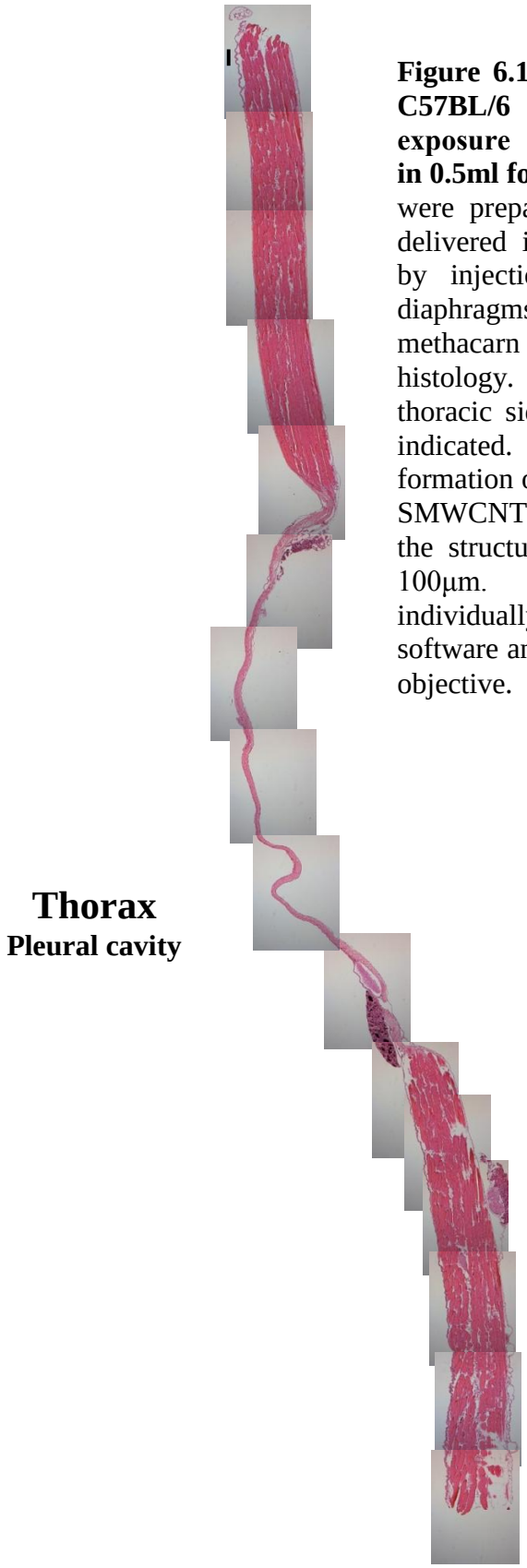

Figure 6.13. The diaphragm of a C57BL/6 mouse following exposure to 100µg/ml SMWCNT in 0.5ml for seven days. Treatments were prepared in sterile saline and delivered into the peritoneal cavity by injection. After seven days diaphragms were removed to methacarn fixative and processed for histology. The abdominal and thoracic sides of the diaphragm are indicated. Black arrows indicate the formation of a cellular reaction to the SMWCNT on the peritoneal side of the structure. Scale bar represents 100µm. Images were captured individually using pro-capture Q software and a microscope set to x10 objective.

Figure 6.14. The diaphragm of a C57BL/6 mouse following exposure to 100µg/ml SMWCNT in 0.5ml for seven days. Magnified images of the section of fig. 6.15 marked by arrows to more clearly distinguish the cellular response to SMWCNT. The black scale bar represents 100µm. The abdominal and thoracic sides of the diaphragm are indicated. Abbreviations: MSL – mesothelium, DM – diaphragm muscle.

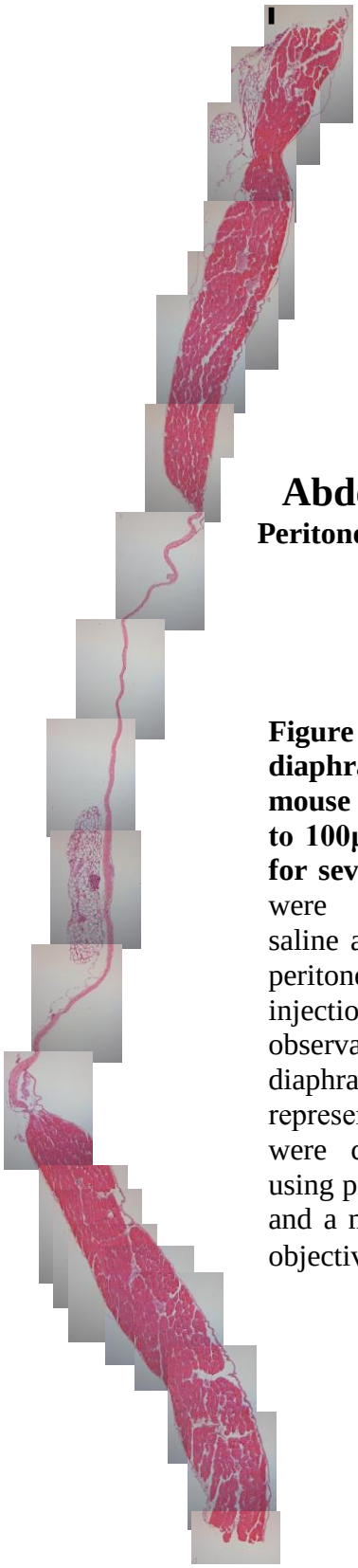

Figure 6.15. The diaphragm of a C57BL/6 mouse following exposure to 100µg/ml ufCB in 0.5ml for seven days. Treatments were prepared in sterile saline and delivered into the peritoneal cavity by injection. ufCB caused no observable reaction on the diaphragm. Scale bar represents 100µm. Images were captured individually using pro-capture Q software and a microscope set to x10 objective.

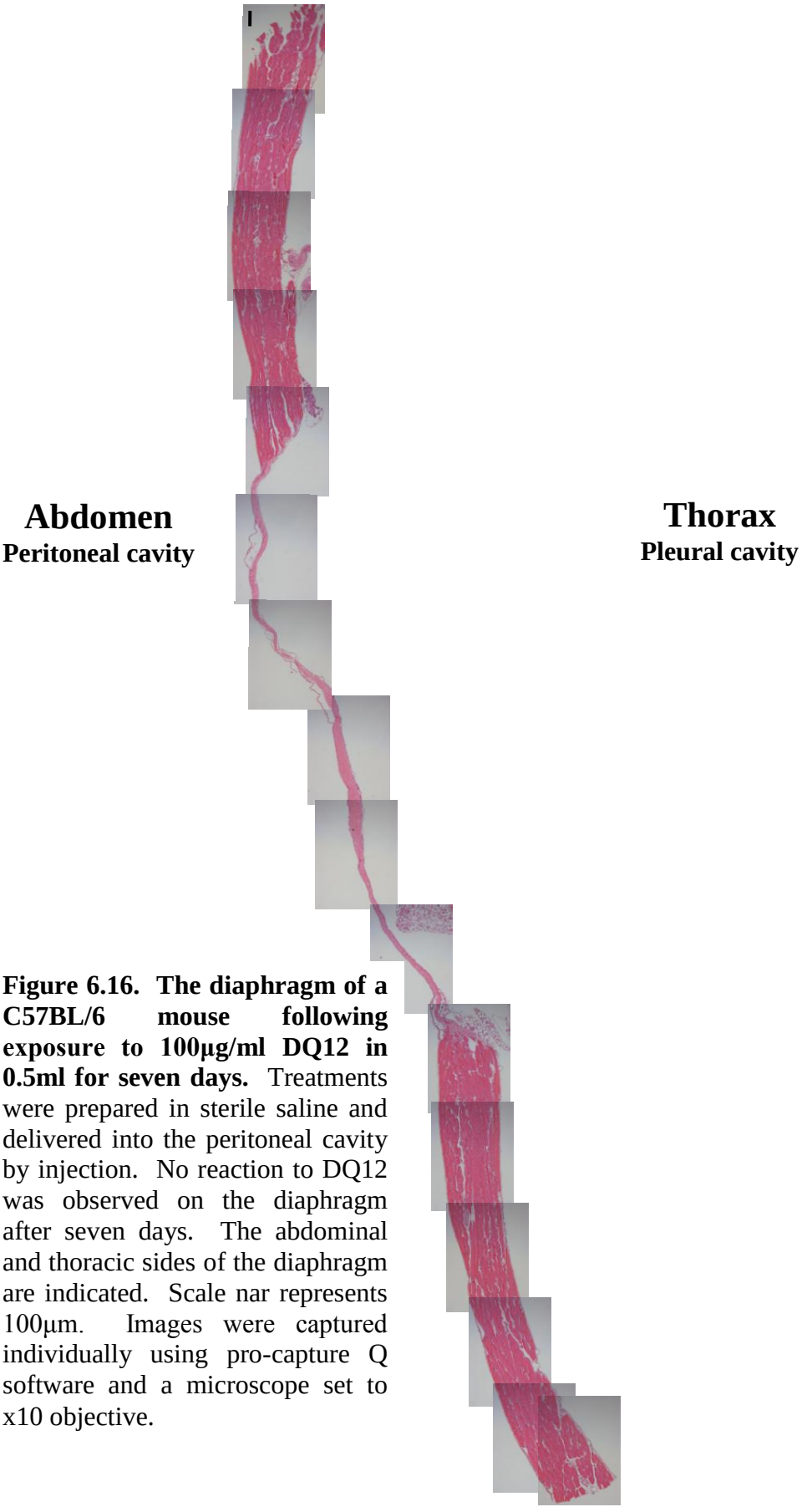

Figure 6.16. The diaphragm of a C57BL/6 mouse following exposure to 100µg/ml DQ12 in 0.5ml for seven days. Treatments were prepared in sterile saline and delivered into the peritoneal cavity by injection. No reaction to DQ12 was observed on the diaphragm after seven days. The abdominal and thoracic sides of the diaphragm are indicated. Scale nar represents 100µm. Images were captured individually using pro-capture Q software and a microscope set to x10 objective.

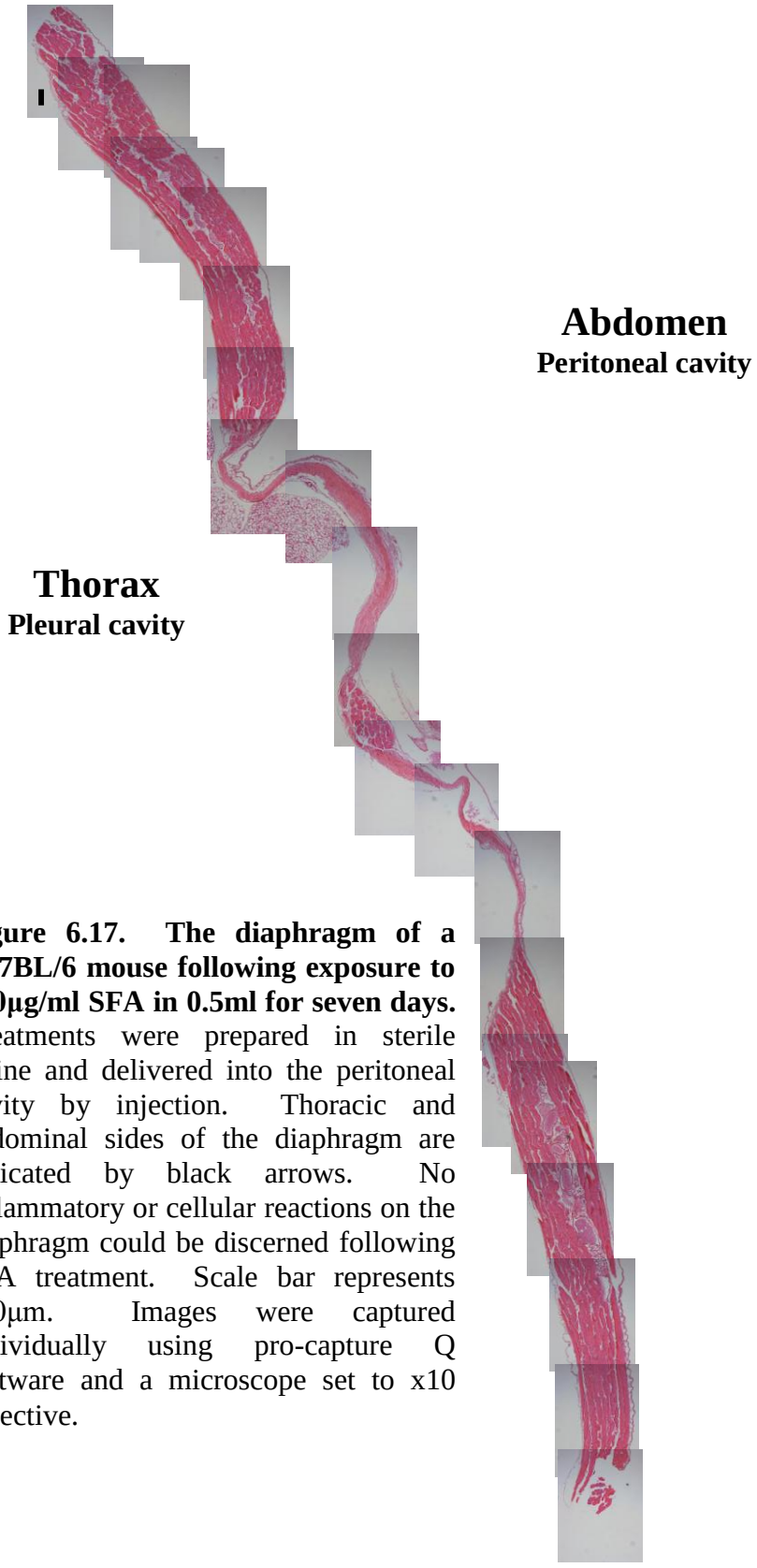

Figure 6.17. The diaphragm of a C57BL/6 mouse following exposure to 100µg/ml SFA in 0.5ml for seven days. Treatments were prepared in sterile saline and delivered into the peritoneal cavity by injection. Thoracic and abdominal sides of the diaphragm are indicated by black arrows. No inflammatory or cellular reactions on the diaphragm could be discerned following SFA treatment. Scale bar represents 100µm. Images were captured individually using pro-capture Q software and a microscope set to x10 objective.

6.6 Discussion

The purpose of the studies carried out in this chapter was to determine the effect of instilling MWCNT into the peritoneal cavity of mice. The peritoneal cavity is a region that responds specifically to fibres in terms of the magnitude of the inflammatory response generated compared to particles. MWCNT are fibrous but unless thoroughly dispersed present as particles, the question lying behind the animal work presented here was whether a fibrous material whose aggregate morphology was particulate would cause inflammation or fibrosis. Also assessed was the capacity of MWCNT to induce granulomas.

LFA dispersed in saline/DPPC or saline induced greater influx of inflammatory cells than shortened versions of the same material or other particles. This is in keeping with the hypothesis that fibre length is a key determinant of toxicity (Dodson et al 2003) and parallels published works (Hesterberg & Barrett 1984, Donaldson et al 1989, Ye et al 1999, Ohyama et al 2001, Riganti et al 2003, Zeidler-Erdely et al 2006). The reasons for length to be a facet of fibre toxicity are not settled but includes the generation of free radicals upon interaction of long fibres with cells (Zalma et al 1987, Prandi et al 2001, Ueki et al 2001, Riganti et al 2003), frustrated phagocytosis (Ye et al 1999, Zeidler-Erdely et al 2006), the orientation of phagocytising cells with respect to the target (speculated to control the strength of the respiratory burst (Ohyama et al 2001)) or disruption of cellular redox metabolism in particular the pentose-phosphate pathway (Riganti et al 2003).

The presence of DPPC may have enhanced the inflammatory potential of LFA. This is borne out by the significant difference in protein levels between LFA and LFA (Sal) but not by cell data. Both median total cell data for LFA and LFA (Sal) and

median neutrophil levels for LFA and LFA (Sal) were of similar levels. DPPC may have a slight inflammatory potential of its own revealed by the sensitivity of the peritoneal cavity to insult. Alternatively better dispersion of LFA in the presence of DPPC may enhance its ability to cause inflammation.

The peritoneal cavity has been demonstrated to be particularly sensitive to long fibres (Donaldson et al 1989). SMWCNT caused a greater inflammatory response than LMWCNT (measured by the influx of inflammatory cells and protein). This is unlikely related to differences in physical dimensions of the MWCNT but could be attributable to differences in features such as specific surface area, chemical composition, solubility, trace metal content, trace organic content, surface charge (at physiological pH) and surface reactivity (Dodson et al 2003). SMWCNT were generated from LMWCNT by extensive acid treatment a process that can introduce groups onto their surfaces (including radicals) (Ohotrub et al 2004) that may affect solubility and surface charge. However the difference between MWCNT may simply have been a numbers of particles effect, for the same mass there should have been a greater number of SMWCNT than LMWCNT. This notion is backed up the by the fact this trend was not repeated in studies 2 or 3.

Despite all three being composed of carbon both LMWCNT and SMWCNT induced greater influxes of cells (including neutrophils) than ufCB (although not significant). This conforms to some published work *in vitro* (Murr et al 2005, Tian et al 2006) that may be explained by particular surface activity possessed by CNT and not by ufCB (Fenoglio et al 2008a, b). An alternative explanation is the difference may result from a difference in the way DPPC interacts with ufCB compared to CNT. Certain carbon blacks have been reported to adsorb substantial quantities of DPPC

(Wallace et al 2007) that perhaps attenuated surface activity as with quartz (Schimmeleeng et al 1992, Gao et al 2001).

Saline derived extracts of MWCNT and LFA produced no significant increases in total cell numbers, neutrophils or protein levels in the peritoneal cavity. This suggests that little or no metal was mobilised from MWCNT of LFA. Iron release from amosite at pH7 has been found fairly slow and occurs only from the surface, mobilisation more easily occurs at acidic pH, by chelators or a strong oxidative process (Prandi et al 2001) possibly explaining the limited effect of a saline only based extract. Lund & Aust (1992) determined that in the absence of ascorbate and citrate or a chelator, amosite and crocidolite failed to cause detectable levels of DNA single strand breaks. Biological conditions can chemically modify some asbestos fibres (Spurny 1983) however for others like amosite and crocidolite more stringent treatments (Lund & Aust 1992, Gold et al 1997, Dai et al 2001) than agitation in saline are required to extract levels of iron that could cause pathogenesis.

Increasing concentrations of MWCNT did not induce a dose dependent of influx of cells into the peritoneal cavity however all concentrations of MWCNT more than doubled total cell numbers compared to the control. No dose response was observed in peritoneal neutrophil numbers although all treatments produced an increase greater than controls. All treatments increased protein content of lavage fluid but this was not dose responsive. This suggests the inflammatory changes were a generalised response to the presence of a non toxic non degradable foreign body introduced at high concentration into the peritoneal cavity similar to that described by Donaldson et al (1988) upon instillation of TiO_2 into mice peritoneal cavities. This contrasts with long fibre shaped CNT which are highly inflammogenic and

fibrogenic in the peritoneal cavity (Poland et al 2008). This highlights the necessity of testing CNT in the right model. Whilst the peritoneal cavity is highly responsive to fibres it is much less so far particles and so for assessing the particle type effects of CNT the lung may represent a better target.

After seven days exposure LMWCNT and SMWCNT both induced small localised granulomas on the mesothelial cell layer overlying the tendinious windows of the diaphragms. These lesions were restricted to MWCNT with no injurious effects induced by SFA, DQ12 or ufCB. Granuloma formation has been widely reported as a consequence of pro-longed exposure to both MWCNT and SWCNT (Lam et al 2004, Muller et al 2005, Shvedova et al 2005, Yokoyama et al 2005, Grubek-Jaworska et al 2006, Koyama et al 2006, Li et al 2007, Chou et al 2008). Granulomas represent a form of chronic inflammation that fall morphologically into two categories – epithelioid or foreign body types – based on the presence or absence of epithelioid cells or an injurious body. Granulomas are aggregates of macrophages, epithelioid and giant cells that form a demarcated focal lesion whose formation is linked to defending the body against persistent irritants. The damaging agent is walled off and sequestered by macrophages keeping it contained. The materials resistance to degradation is important in determining whether granuloma formation occurs, typically poorly soluble, persistent, un-digestible materials cause granulomas (Williams et al 1983). Aggregation, poor solubility and an inability to be cleared by cells has been linked to CNT induced granulomas (Muller e al 2005, Shvedova et al 2005, Grubek-Jaworska et al 2006, Li et al 2007). In this study only MWCNT induced a granulomatous response, ufCB the other carbonaceous particle, did not produce a similar reaction in keeping with published work (Lam et al 2004).

The likely explanation for this is that although ufCB is insoluble it did not form large numbers of aggregates greater than cell size. In both cases MWCNT produced granulomas localised to the tendinious area of the diaphragm. The position of the lesions on the diaphragm is highly significant both with respect to a clearance function for the diaphragm and with regard to the relation of aggregate size to clearance of MWCNT. The peritoneum is an active tissue with filtering abilities carried out through a lymphatic drainage system located in the diaphragm (Fig. 6.21). The mesothelial lining of the diaphragm on the peritoneal side overlies a system of lymphatic lacunae with openings to the peritoneum through stomata. This provides a direct link between the peritoneal cavity and the lymphatic system providing a pathway for adsorption from the peritoneal cavity (Abu-Hijleh et al 1995). Stomata connect to an under lying plexus of flattened lymphatics running parallel to the diaphragm (Abu-Hijleh et al 1995, Shinohara et al 1997). Under exposure to MWCNT it is possible smaller aggregates contacting the mesothelium were cleared either by phagocytosis or through the lacunae. Large aggregates trapped against the mesothelial layer and unable to be phagocytised or cleared through the diaphragmatic sieve could have then triggered a foreign body granulomatous response. Fibrosis can be a complication of granulomatous inflammation responsible for tissue damage even after a persistent and damaging material is removed (Williams et al 1983). Upon instillation of CNT into animals where a granulomatous response has been observed an associated fibrotic response has also been reported. No evidence of fibrosis was observed upon examination of the MWCNT exposed mouse diaphragms in this study. This may be a consequence

of the shorter exposure time compared to some works (up to 90 days in some instances) and the relatively limited nature of the granulomatous response.

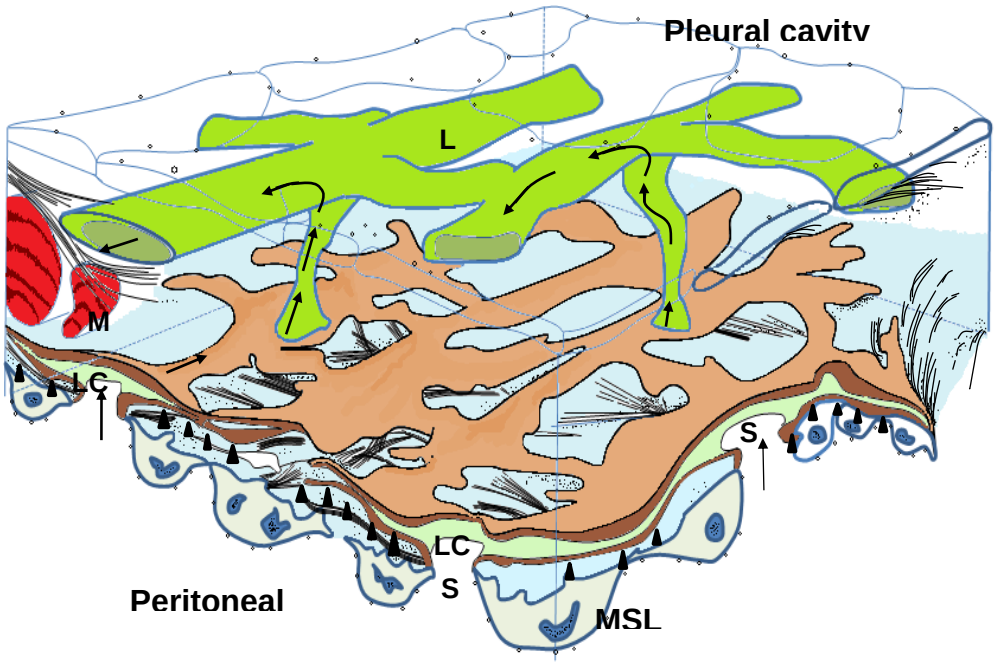

Figure 6.21. 3D representation of the lymphatic sieve of the mouse diaphragm. The flow of lymph through the system is indicated by black arrows, the sub-peritoneal lymphatic vessels (indicated by black arrow heads and coloured light brown) are flattened in appearance with each lumen forming narrow channels in ultrathin sections. In some places the lymphatic lumens increase in size and form lacunae (LC). The sieve is open on to the peritoneal side through stomata (S). Fluid flows from the peritoneal cavity through the stomata into the lacunae and through the network of sub-peritoneal lymphatics into the pleural lymphatic system (L, coloured green). Abbreviations: L – lymphatics, LC – lacunae, M – muscle fibres, MSL – mesothelial cells, S - Stomata. Adapted from Shinohara 1997.

Chapter 7

Summary and future work

Chapter 7

Summary and future work

The work undertaken in this thesis set out to determine the extent of toxicity and inflammatory potential of two commercially available MWCNT samples in comparison with known pathogenic particles and fibres. Work was carried out *in vitro* and *in vivo* and the activation/production of markers associated with initiation of inflammation in pulmonary epithelial cells and the peritoneal cavity of C57BL/6 mice was analysed.

Carbon nanotubes are crystalline graphene sheets rolled into seamless cylinders (Kim & Sigmund 2005) commonly depicted as fibrous (i.e. possessing high aspect ratio) but with a tendency to form tightly aggregated bundles or ropes. S.E.M. of MWCNT dispersed in water revealed tightly aggregated micron sized particles. MWCNT were synthesized using metal catalysts, a proportion of which remain even after extensive purification and may contribute to their toxicity. ICP/AES (section 3.2) revealed iron to be the principal residual metal within MWCNT although forming less than 2% MWCNT by weight and could not be extracted into solution. Use of citrate or ascorbate buffers (Gold et al 1997), desferrioxamine (Jimènez et al 2000) or aqueous acid (Pan et al 2004) extraction techniques should be attempted with the quantity or remaining metal and water-soluble metals quantified by ICP/AES in any future work.

Free radical production has been associated with detrimental cellular effects of CNT (Mann et al 2004). Work carried out here using electron spin resonance (ESR) with a peroxynitrile/superoxide anion sensitive spin trap TEMPONE-H revealed free radical generating capacity (section 3.4) although this did not translate into a clear

capacity to cleave plasmid DNA. The MWCNT generated ESR signal was diminished by GSH and SOD indicative that the CNT were generating a reactive species although the effect of possible antioxidant adsorption to MWCNT needs to be considered. Due to the nature of the spin trap the species responsible for the ESR signal could not be positively identified. Nitrozolium blue could be used to confirm superoxide anion production; other spin traps (e.g. DMPO (Clouter et al 2001)) should also be used to examine the range of free radicals that may be generated. ESR analysis of fully metal-extracted CNT should be undertaken to determine the possible influence of residual metals upon ERS signals. The origin of the reactive species generated could not be confirmed, in other carbonaceous materials reactivity has been attributed to defect sites (Lücking et al 1998, Vix-Guterl et al 2001, Narayan et al 2004, Vorob'ev-Desytovskii et al 2006). One way of examining the contribution of these sites would analysis of CNT with different levels of defects (measurable by Raman spectroscopy). Levels of defects could be engineered out of samples by differential thermal annealing followed by ESR analysis. The non-ionic surfactant Tween-80 was also found to diminish the ESR signal by un-known mechanisms. Authors such as Fenoglio et al (2006) have reported antioxidant effects for CNT dispersed in SDS so future work should be undertaken to fully characterise the effects of surfactants (and proteins) on the ESR profile of CNT. Possible intracellular free radical production induced by MWCNT using ROS sensitive fluorescent probe DCFH-DA should also be considered. The toxicity of CNT as Fenoglio et al (2005) suggests may be due to features other than their ability to generate free radicals however. For example protein adsorption to CNT may lead to toxicity as a result of the chaotic nature of binding that leads to conformational

changes and the formation of protein derived breakdown products (Tang and Eaton 1993).

MWCNT did not exhibit any haemolytic or cytotoxic activity (sections 3.5 and 3.6). Numerous other works have also found only limited toxicity of CNT materials (Murr et al 2005, Soto et al 2005, Pulskamp et al 2007, Yehia et al 2007). In any future work longer exposure periods for MWCNT towards cells should be investigated since only 24 hours was used here. As a result of CNT potential to interfere in colourimetric assays a battery of different assays should be carried out to search out a reliable assay. Monitoring cell proliferation for deviation above or below the normal rate upon exposure to CNT could also be performed. The mechanisms of particle and fibre toxicity are frequently attributed (at least in part) to their ability to generate ROS and free radicals. Although LMWCNT and SMWCNT depleted GSH in a concentration-dependent manner in A549 cells the mechanism responsible was not established (section 4.2). Mechanisms such as efflux need to be investigated as does the capacity of MWCNT to generate intracellular ROS (i.e. by DCFH-DA). Use of the metal sensitive probe calcein (Stäubli et al 1998) could also be used to investigate the possibility of Fenton chemistry generated from metal ions liberated from endogenous proteins by superoxide anions produced by MWCNT. Future work should also focus upon measuring changes in the ratio of GSH: GSSG as well as total intra-cellular GSH in response to MWCNT exposure.

MWCNT did not generate a pro-inflammatory or a pro-fibrotic response *in vitro*. In any future work a pro-fibrotic response should be looked for from a fibroblast cell line cell exposed to MWCNT. Immunocytochemical analysis of the effect of MWCNT and a panel of other particles upon NF-κB failed to provide a clear and

consistent indication of the level of its translocation (section 5.2). In future work immunocytochemical analysis of NF-κB translocation should be repeated in conjunction with alternative techniques such as electro-mobility shift assays (Gilmour et al 2002, Mroz et al 2007) or NF-κB ELISA.

The inflammatory potential of MWCNT, TiO_2, DQ12, LFA, and SFA was examined in C57BL/6 mouse peritoneal cavity. LFA was found to induce greater peritoneal inflammation than SFA (section 6.2) supporting the hypothesis that length is key determinant of fibre pathogenicity and of the sensitivity of the peritoneal cavity to long fibres, the basis of this sensitivity appears to the extreme sensitivity of the mesothelium to long fibres and so this assay system has special relevance for mesothelioma hazard. MWCNT did not consistently cause significant peritoneal inflammation. Despite its detrimental effects *in vitro* DQ12 failed to cause any inflammation in the peritoneal cavity in keeping with the selective sensitivity of the region to long fibres. After seven days within the peritoneal cavity both MWCNT caused small granulomatous reactions. This fits with *in vitro* work by Murr et al (2005) and Soto et al (2005) comparing the toxicities of a panel of particles including MWCNT and SWCNT that observed nanotube toxicity was solely as an adverse reaction to the presence of particulates not attributable to a specific toxicity factor or factors. Failure or inability of lymphatic clearance to deal with hydrophobic highly aggregated carbon nanotubes may be a contributory factor to the development of granulomatous inflammation.

In summary MWCNT where found not to be acutely toxic or to display inflammatory potential *in vitro* or *in vivo*. However prolonged *in vivo* exposure

resulted in the formation of Granulomatous inflammation as a result of their aggregation and consequent inability to be cleared.

Chapter 8

References

Abe S, Takizawa H, Sugawara I, Kudoh S. (2000). Diesel exhaust (DE) - induced cytokine expression in human bronchial epithelial cells in vitro. *Am. J. Respir. Cell Mol. Biol.* 22: 296-303.

Abu-Hijleh MF, Habbal OA, Moqattash ST. (1995). The role of the diaphragm in lymphatic adsorption from the peritoneal cavity. *J. Anat.* 186: 453-467.

Adler V, Yin Z, Tew KD, Ronai Z. (1999). Role of redox potential and reactive oxygen species in stress signalling. *Oncogene* 18: 6104-6111.

Ajayan PM. (1999). Nanotubes from carbon. *Chem. Rev.* 99: 1787-1800.

Ajayan PM, Zhou OZ. (2001). Applications of carbon nanotubes. *Topics Appl. Phys.* 80: 391-425.

Albrecht C, Schins RPF, Höhr D, Becker A, Shi T, Knaapen AM, Borm PJA. (2004). Inflammatory time coarse after quartz instillation - Role of tumour necrosis factor α and particle surface. *Am. J. Respir. Cell Mol. Biol.* Vol. 31: 292-301.

Albrecht C, Schins RPF, Hohr D, Becker A, Shi T, Knaapen AM, Borm PJA. (2004). Inflammatory time course after quartz instillation. *Am. J. Cell Mol. Biol*. 31: 292-301.

Albrecht C, Knaapen AM, Becker A, Hohr D, Haberzettl P, Van Schooten FJ, Borm PJA, Schins RPF. (2005). The crucial role of particle surface reactivity in respirable quartz induced reactive oxygen/nitrogen formation and APE/ Ref 1 induction in the rat lung.

Amara H, Bichara C, Ducastelle F. (2008). Understanding the nucleation mechanisms of carbon nanotubes in catalytic chemical vapour deposition. *Phys. Rev. Lett.* 100: 1-4.

Anderson MT, Staal FJT, Gitler C, Herzenberg LA, Herzenberg LA. (1994). Separation of oxidised initiated and redox regulated steps in NFκB signal transduction pathways. *PNAS* Vol. 91: 11527-11531.

Andrews R, Jacques D, Qian D, Dickey EC. (2001). Purification and structural annealing of multiwalled carbon nanotubes at graphitization temperatures. *Carbon* 39: 1681-1687.

Anpo M, Che M, Fubini B, Garrone E, Giamello E, Paganini MA. (1999). Generation of superoxide at oxide surfaces. *Topics in catalysis* 8: 189-198.

Archer VE, Dixon WC. (1979). Carcinogenicity of fibres and films: A theory. *Medical hypotheses* 5: 1257-1262.

Arimoto T, Yoshikawa T, Takano H, Kohno M. (1999). Generation of reactive oxygen species and 8-hydroxy-2-deoxyguanosine formation from diesel exhaust particle components in L1210 cells. *Jpn J. Pharmacol*. 80: 49-54.

Asuri P, Kaeajanagi SS, Yang H, Yim TJ, Kane RS, Dordick JS. (2006). Increasing protein stability through control of the nanoscale environment. *Langmuir* 22: 5833-5836.

Atamas SP. (2002). Complex cytokine regulation of tissue fibrosis. *Life sciences* 72: 631-643.

Atamas SP, White B. (2003). Cytokine regulation of pulmonary fibrosis in scleroderma. *Cytokine and Growth factor reviews* 14: 537-550.

Attene-Ramos MS, Kitiphongspatlana K, Ishii-schrade K, Gaskim HR. (2005). Temporal changes of multiple redox couples from proliferation to growth arrest in IEC-6 intestinal epithelial cells. *AJP Cell Physiol* 289: 1220-1228.

Aust AE, Ball JC, Hu AA, Lightly JS, KR, Staccia AM, Veranth JM, Young W. (2002). Particle characteristics responsible for effects on human lung epithelial cells. *Health effects institute, research report* 110: 1-74.

Avouris P. (2004). Carbon nanotube electronics and opto electronics. *MRS Bulletin*: 403-410.

Balakrishna S, Lomnicki S, McAvery KM, Cole RB, Dellinger B, Cormier SA. (2009). Environmentally persistent free radicals amplify ultrafine particle mediated cellular oxidative stress and cytotoxicity. *Part. Fibre Toxicol.* 6: 11.

Balasubramanian K, Burghard M and Burhard M. (2005). Chemically functionalised Carbon nanotubes. *Small*.1, 2:180-192.

Baldys A, Aust AE. (2005). Role of Iron in activation of epidermal growth factor receptor after asbestos treatment of human and pleural target cells. *Am. J. Respir. Cell. Mol. Biol.* Vol. 32: 436-442.

Baldwin ET, Weber IT, Charles RS, Xuan JC, Apella E, Yamada M, Matsushima K, Edwards BFP, Clore GM, Gronenborn AM, Wlodower A. (1991). Crystal structure of interleukin-8: symbiosis of NMR and crystallography. *PNAS* Vol. 88: 502-506.

Bandyopadhyay U, Das D, Banerjee RK. (1999). Reactive oxygen species: oxidative damage and pathogenesis. *Current Science* Vol. 77, No. 10: 658-666.

Bandyopadhyay R, Nativ-Roth E, Regrav O, Yeroshalmi Rozen R. (2002). Stabilization of industrial carbon nanotubes in aqueous solution. *Nanoletters* Vol. 2, No. 1: 25-28.

Banerjee S, Hemraj-Benny T and Weng SS. (2005). Covalent surface chemistry of Carbon nanotubes. *Advanced Materials* 17: 17-29.

Banks CE, Moore RR, Davies TJ, Compton RG. (2004). Investigation of modified basal plane pyrolytic graphite electrodes: definitive evidence for electrocatalytic properties at the ends of carbon nanotubes. *Chem. Commun.* 1804-1805.

Banks CE, Davies TJ, Wildgoose GG, Compton RG. (2004). Electrocatalysis at graphite and carbon nanotube modified electrodes: edge plane sites and tube ends are reactive sites. *Chem. Commun*.

Barlow PG, Clouter-Baker A, Donaldson K, MacCallum J, Stone V. (2005). Carbon black nanoparticles induce type II epithelial cells to release chemotaxins for alveolar macrophages. *Part. Fibre Toxicol*. 2: 11.

Bartosz G. (2006). Use of spectroscopic probes for detection of reactive oxygen species. *Clinica chemica Acta* 368: 53-76.

Barcellos-Hoff MH, Dix TA. (1996). Redox mediated activation of latent transforming growth factor β1. *Molecular endocrinology* 10: 1077-1083.

Bayram H, Devalia JL, Sapsford RJ, Ohtoshi T, Miyabara Y, Sagai M, Davies RJ. (1998). The effect of diesel exhaust particles on cell function and release of inflammatory mediators from human bronchial epithelial cells in vitro. *Am. J. Respir. Cell Mol. Biol.* 18: 441-448.

Bellomo G, Jewell SA, Thor H, Orrenius S. (1982). Regulation of intracellular calcium compartmentalization: Studies with isolated hepatocytes and t-butyl hydroperoxide. *PNAS USA* Vol. 79: 6842-6846.

Bellozq A, Zoulay E, Maizillo S, Flahault A, Fourqueray B, Philippe C, Cadranel J, Baud L. (1999). Reactive Oxygen and Nitrogen species intermediates increase transforming growth factor β1 release from Human epithelial alveolar cells through two different mechanisms. *Am. J. Respir. Cell Mol. Biol.* 21: 128-136.

Bellmann B, Muhle H. (1994). Investigation of the biodurability of wollastonite and xonothite. *Environ. Health Perspect*. Vol. 102, Supp. 5: 191-195.

Bertino P, Marconi A, Palumbo L, Bruni BM, Barbone D, Dogan AU, Tassi GF, Porta C, Mutti L, Gaudino G. (2007). Eronite and Asbestos cause transformation of human mesothelial cells. *Int. J. Cancer* 121: 12-20.

Betteridge DJ. (2000). What is oxidative stress. *Metabolism*, Vol. 49, No. 2, suppl. 1: 3-8.

Bi YH, Huang ZL, Zhao YD. (2006). The interface behaviour and biocatalytic activity of superoxide dismutase at carbon nanotube. *Biosensors & Bioelectronics* 21: 1350-1354.

Bianco A, Hoebeke J, Godefroy S, Chaloin O, Pantarotto D, Briand JP, Muller S, Prato M, Particles CD. (2005). Cationic carbon nanotubes bind CpG oligodeoxynucleotides and enhance their immuno stimulatory properties. *J. Am. Chem. Soc.* 127: 58-59.

Biemond P, Swaak AJG, Beindorf CM, Koster JF. (1986). Superoxide-dependent and independent mechanisms of Iron mobilization from ferritin by xanthine oxidase. *Biochem. J.* 239: 169-173.

Biemond P, Swaak AJG, Eijk HG, Koster JF. (1987). Superoxide dependent Iron release from ferritin in inflammatory diseases. *Free rad. Biol. And Med.* Vol. 4: 185-198.

Binkova B, Cerna M, Pastorkava A, Jelinek R, Benes I, Novak J, Sram RJ. (2003). Biological activities of organic compounds adsorbed onto ambient air particles: comparison between the cities of Telpice and Prague during the summer and winter seasons 2000-2001. *Mutat. Res.* 525: 43-59.

Bissonette E, Rola-Pleszezyriski M. (1989). Pulmonary inflammation and fibrosis in a murine model of asbestosis and silicosis. *Inflammation*, Vol. 13, No. 3: 329-339.

Boehm HP. (2002). Surface oxides on carbon and their analysis: a critical assessment. *Carbon* 40: 145-149.

Boland S, Baeza Squiban A, Fournier T, Houcine O, Gendeon MC, Chevrier M, Jouvenot G, Coste A, Aubier M, Marano F. (1999). Diesel exhaust particles are taken up by human airway epithelial cells in vitro and alter cytokine production.

Boncoeur E, Saint Ceiq V, Borwin E, Roque T, Henrion-Caude A, Gruenert DC, Clement A, Jacquot J, Tabary O. (2008). Oxidative stress induces extracellular signal related kinase 1/2 mitogen activated protein kinase in cystic fibrosis lung epithelial cells: potential mechanisms for excessive IL-8 exposure. *Int. J. Biochem. Cell Biol*. 40: 432-446.

Bonif M, Meuwis MA, Close P, Benoit V, Heyninisick K, Chapelle JP, Bours V, Merville MP, Piette J, Beyaet R, Charoit A. (2006). TNFα and IKKβ mediated TANF/ I-TRAF phosphorylation: implications for interaction with NEMO/ IKKγ and NFκB activation. *Biochem J*: 394-603.

Bowie AG, Moynagh PN, O'Niell AJ. (1997). Tumour necrosis factor but not interleukin-1 in the human endothelial line ECV304. *J. Bio. Chem*, Vol. 272, No. 41: 25941-25950.

Bowie A, O'Niell LAJ. (2000). Oxidative stress and nuclear factor κB activation. *Biochem. pharmacol* Vol. 59: 13-23.

Bottini M, Bruckner S, Nika K, Bottini N, Bellucci S, Magrini A, Beryamaschi A, Mustelin T. (2005). Multi walled carbon nanotubes induce T-Lymphocyte apoptosis. *Toxicol Lett.*

Boylan AM, Sanan DA, Sheppard D, Broaddus VC. (1995). Vitronectin enhances internalization of crocidolite asbestos by Rabbit pleural mesothelial cells via the integrins avbB5. *J. Clin. Invest*. 96: 1987-2001.

Bradley JR. (2008). TNF-mediated inflammatory disease. J. *Pathol*. 214: 149-160.

Bridges JP, Davis HW, Bamodarasamy M, Kuroki Y, Howles G, Huri DY, McCormack FX. (2000). Pulmonary surfactant protein A and D are potent endogenous inhibitors of lipid peroxidation and oxidative cellular injury. *J. Bio. Chem* Vol. 275, No.

Brown DM, Beswick PH, Donaldson K. (1999). Induction of nuclear translocation of NFkB in epithelial cells by respirable mineral fibres. *J. pathol* 189: 8458-8462.

Brown DM, Stone V, Findlay P, MacNee W, Donaldson K. (2000). Increased inflammation and intracellular calcium influx caused by ultra fine carbon black is independent of transition metals or other soluble components. *Occup. Environ. Med* 57: 685-691.

Brown DM, Wilson MR, MacNee W, Stone V, Donaldson K. (2001). Size dependant proinflammatory effects of ultrafine polystyrene particles: Role for surface area and oxidative stress in the enhanced activity of ultrafines. *Toxicol. appl. Pharmacol*. 17

Brown SC, Kamal M, Masreen N, Baumurativ A, Sharma P, Antony VB, Moudgil B. (2007). Influence of shape, adhesion and stimulated lung mechanics on amorphous silica nanoparticles toxicity. *Advd powder Technol*. Vol 18, No. 1: 69-79.

Brown DM, Donaldson K, Borm PJA, Schins RP, Dehnhardt M, Gilmour P, Jimenez LA, Stone V. (2004). Calcium and ROS mediated activation of transcription factors TNFa cytokines gene expression in macrophages exposed to ultrafine particles. *Am. J. Physiol.* 286:

Buzea C, Pacheco Blandino II, Robbie K. (2007). Nanomaterials and nanoparticles: sources and toxicity. *Bio-interphases* Vol. 2, Iss. 4: MR14-172.

Cabrera-Sanfelix P, Darling GR. (2007). Dissociative adsorption of water at defects in graphite. *J. Phys. Chem*. 111: 18258-18263.

Cairo G, Tacchini L, Recalcoli S, Azziimonti B, Minotti G, Bernelli-Zazzera A. Effect of reactive oxygen species on iron regulatory protein activity. Annals New York Academy of sciences: 179-186.

Cannon GJ, Swanson JA. (1992). The macrophage capacity for phagocytosis. *J. Cell Sci.* 101: 907-913.

Casey A, Davoren M, Herzog E, Lyng FM, Byrne HJ, Chambers G. (2007). Probing the interaction of single walled carbon nanotubes within cell culture medium as a precursor to toxicity testing. *Carbon* 45: 34-40.

Cederwall T, Lynch I, Lindman S, Beggard T, Thulin E, Nilson H, Dawson KA, Linse S. (2007). Understanding the nanoparticle-protein corona using methods to quantify exchange rates and affinities for nanoparticles. *PNAS*. Vol. 104, No. 7: 2050

Chandra J, Samali A, Orrenius S. (2000). Triggering and modulation of apoptosis by oxidative stress. *Free Rad. Biol. Med*. Vol. 29, No. 3/4: 323-333.

Chang CC, Chiu HF, Wu YS, Li YC, Tsai ML, Shen CK, Yang CY. (2005). The induction of vascular endothelial growth factor by ultrafine carbon black contributes to the increase of alveolar capillary permeability. *Environ. Health Perspec*. 113: 454-460.

Chatterjee PK, Cuzzocera S, Thiemermann C. (1999). Inhibitors of poly(ADP-ribose) synthetase protect rat proximal tubular cells against oxidant stress. *Kidney international* 56: 973-984.

Cheng LX, Rajh T, Wang Z, Thurnauer MC. (1997). XAFS studies of surface structures of TiO_2 nanoparticles and photocatalytic reduction of metal ions. *J. Phys. Chem*. 101: 10688-10697.

Chen F, Lu Y, Demers LM, Rojanasakul Y, Vallyathan V, Castranova V. (1998). Role of hydroxyl radicals in silica induced NF Kappa B activation in macrophages. *Annls. clin. lab. sci.* Vol. 28, Iss. 1: 1-13.

Chen G, Goeddel DV. (2002). TNFR1 signalling: A beautiful pathway. *Science* Vol. 296: 1634-1635.

Chen F, Shi Z. (2002). Signalling from toxic metals and beyond: Not just a matter of reactive oxygen species. *Environ. Health Perspect*. 110 (Suppl. 5): 807-811.

Chen K, Vita JA, Berk BC, Keany JF. (2001). C-Jun N-terminal kinase activation by hydrogen peroxide in endothelial cells involves ser-dependent epidermal growth factor receptor transactivation. *J. Biol. Chem.* Vol. 276, No. 19: 16045-16050.

Chen YW, Hwang KC, Yen CC, Lai YL. (2004). Fullerene derivatives protect against oxidative stress in RAW 264.7 cells and ischemia reperfused lungs. *Am.J. Physiol. Regul. Integr. Comp. Physiol*. 287: 21-26.

Cherukuri P, Gannon CJ, Leeuw TK, Schmidt HK, Smalley RE, Curley SA, Weisman RB. (2006). Mammalian pharmacokinetics of carbon nanotubes using intrinsic near infrared fluorescence. *PNAS* Vol. 103, No. 50: 18882-18886.

Chlopeck J, Czajkowska B, Szaraniec B, Frackowiak E, Szostak K, Beguin F. (2006). In vitro studies of carbon nanotube biocompatibility. *Carbon* 44: 1106-1111.

Cho S, Urata Y, Lida T, Goto S, Yamaguchi M, Sumikawa K, Kondo T. (1998). Glutathione down regulates the phosphorylation of IκB: Auto loop regulation of NFκB mediated expression of NFκB subunits by TNFα in mouse vascular endothelial cells. Biochemical and *Biophys. res. commun*. 250: 104-108.

Chou CC, Hsiao HY, Hong QS, Chen CH, Peng YW, Chen HW, Yang PC. (2008). Single walled carbon nanotubes can induce pulmonary injury in mouse model. *Nano Lett.* Vol. 8, No. 2: 437-445.

Clouter A, Brown D, Hohr D, Borm P, Donaldson K. (2001). Inflammatory effects of respirable quartz collected in workplaces versus standard DQ12 particle surface correlates. *Toxicol Sci.* 63:90-98.

Ciencewicki J, Trivedi S, Kleeberger SR. (2008). Oxidants and the pathogenesis of lung diseases. J. *Allergy Clin. Immunol*. 122: 456-470.

Collins PG, Avouris P. (2000). Nanotubes for electronics. *Scientific American* 62-69.

Cooke MS, Evans ED, Dizdaroglu M, Lunec J. (2003) Oxidative DNA damage: mechanisms, mutation and disease. *FASEB J* 17: 1195-214.

Cross CE, Van der Vliet A, O'Niell CA, Louie S, Halliwell B. (1994). Oxidants, Antioxidants and respiratory tract lining fluids. *Environ. Health Prspect*. Vol. 102, (Supplement 10, Oxygen radicals and lung injury): 185-191.

Crystal RG, Randell SH, Engelhardt JF, Voynow J, Sunday ME. (2008). Airway epithelial cells – Current concepts and challenges. *Proc. Am. Thorac. Soc.* Vol. 5:772-777.

Cui D, Tian F, Ozkan CS, Wang M, Gao H. (2005). Effect of single wall carbon nanotubes on human HEK293 cells. *Toxicol. lett* 155: 73-85.

Dai J, Gilks B, Price K, Churg A. (1998). Mineral dusts directly induce epithelial and intestinal fibrogenic mediators and matrix components in the airway wall. *Am. J. Crit. Care Med*. 158: 1907-1913.

Dai J, Churg A. (2001). Relationship of fibre surface iron and active oxygen species to expression of pro-collagen, PDGF-A, TGF-β, in tracheal explants exposed to amosite asbestos. *Am. J. Cell Mol. Biol*. Vol. 24: 427-435.

Davoren M, Herzog E, Casey A, Cottineau B, Chambers G, Byrne HJ, Lyng FM. (2007). In vitro toxicity evaluation of single walled carbon nanotubes on human A549 cells. *Toxicol. In vitro* 21: 438-448.

Davis JMG. (1994). The role of clearance and dissolution in determining the durability or biopersistence of mineral fibres. Environ. *Environ. Health Perspect.* 102 (suppl. 5): 113-117.

Deforge LE, Preston AM, Takeuchi E, Kenney J, Boxer LA, Remick DG. (1993). Regulation of interleukin-8 gene expression by oxidant stress. *J. Biol Chem.* Vol. 286, No. 34: 25566-25576

Dellinger B, Pryer WA, Cueto R, Squadrito GL, Hedge V, Deutsch WA. (2001). Role of free radicals in the toxicity of airborne fine particulate matter. *Chem. Res. Toxicol.* 14: 1371-1377.

Deshpande NN, Sorescu D, Seshiah P, Ushio Fukai M, Akers M, Yin Q, Griendling KK. (2002). Mechanism of hydrogen peroxide induced cell cycle arrest vascular smooth muscle. *Antiox. Redox. Signal.* 4: 845-854.

Devin A, Cook A, Lin Y, Rodriguez Y, Kelliher M, Liu Z. (2000). The distinct roles of TRAF2 and RIP in IKK activation by TNFR-1: TRAF2 recruits IKK to TNFR1 while RIP mediates IKK activation. *Immunology* Vol. 12: 419-429.

Desaki M, Takizawa H, Kasama T, Kobayashi K, Morita Y, Yamamoto K. (2000). Nuclear factor kappa B activation in silica induced interleukin 8 production by human bronchial epithelial cells. *Cytokine* Vol. 12, No. 8: 1257-1260.

Devin A, Lin Y, Yamooka S, Li z, Karin M, Liu Z. (2001). The α and β subunits of IκB Kinase mediate TRAF2 dependent IKK recruitment to tumour necrosis factor receptor 1 in response to TNF. *Molec. cell. Biol.* Vol. 21, No. 12: 3986-3994.

Diaz A, Willis AC, Sin RB. (2000). Expression of the proteinase specialised in bone resorption, cathepsin K, in granulomatous inflammation. *Molecular medicine* 6: 648-659.

Dick CAJ, Brown DM, Donaldson K, Stone V. (2003). The role of free radicals in the toxic and inflammatory effects of four different ultrafine particles. *Inhal. Toxicol.* 15: 39-52

Ding M, Ding Z, Chen F, Pack D, Ma W, Ye J, Shi X, Castranova V, Vallyathan V. (1999). Asbestos induces activator protein 1 transactivation in transgenic mice. *Cancer Research* 59: 1884-1889.

Ding F, Rosèn A, Campbell EFB, Falk LKL, Bolten K. (2006). Graphitic encapsulation of catalyst particles in carbon nanotube production. *J. Phys. Chem*. B 110: 7666-7670.

Ding F, Larsson P, Larsson JA, Ahuja R, Duan H, Rosen A, Bolton K. (2007). The importance of strong carbon-metal adhesion for catalytic nucleation of single walled carbon nanotubes. *Nanoletters*, Vol. 0, No. 0: A-F.

Dodson RF, Atkinson MAL, Levin JL. (2003). Asbestos fibre length as related to potential pathogenicity: A critical review. *Am J. Ind. Med*. 44: 291-297.

Donà M, Dell Aica I, Calabrese F, Benelli R, Morini M, Albini A, Gabina s. (2003). Neutrophil restraint by green tea: inhibition, associated angiogenesis and pulmonary fibrosis. *J. Immunol.* 170: 4335-4341.

Donaldson K, Davis JMG, James K. (1982). Characteristics of peritoneal macrophages by asbestos injection. *Environ Res.* 29: 414-424.

Donaldson K, Browm GM, Brown DM, Bolton RE, Davis JMG. (1989). Inflammatory generating potential of long and short fibre amosite asbestos samples. *Br J. Ind. Med*. 46: 271-276

Donaldson K, Miller BG, Sara E, Slight J, Brown RC. (1993). Asbestos fibre length dependent detachment injury to alveolar epithelial cells in vitro: role for finbronectin binding receptor. *Int. J. Exp. Pathol.* 74: 243-250.

Donaldson K. (1996). Short term animal studies for detecting inflammation, fibrosis, and pre-neoplastic changes induced by fibres. *IARC scientific publications*, mechanisms of fibres carcinogenesis, No. 140: 97-106.

Donaldson K, Borm PJA. (1998). The quartz hazard: a variable entity. *Ann. Occup. Hyg.* Vol. 42, No. 5: 287-294.

Donaldson K, Stone V. (2003). Current hypothesis on the mechanisms of toxicity of ultrafine particles. *Ann 1rst super Samita* 39: 405-410.

Donaldson K, Lang Tran C. (2004). An introduction to the short term toxicology of respirable industrial fibres. *Mutation research* 553: 5-9.

Dopp E, Saedler J, Stopper H, Weiss DG, Schiffmann D. (1995). Mitotic disturbances and micronucleus induction in Syrian hamster embryo fibroblast cells caused by asbestos fibres. *Environ Health Perpect.* 103: 268-271.

Dorger M, Allmeling AM, Kiefmann R, Schropp A, Krombach F. (2002). Dual role of inducible nitric oxide synthase in acute asbestos induced lung injury. *Free Rad. Biol. Med.* Vol. 33, No 4: 491-501.

Driscoll KE, Carter JM, Howard BW, Hassenbien D, Janssen YMW, Mossman BT. (1998). Crocidolite activates NFκB and MIP-2 gene expression in rat alveolar epithelial cells. Role of mitochondrial derived oxidants. *Environ. Health perspec.* 106 (suppl. 5): 1171-1174.

Dye JA, Adler KB, Richards JH, Dreher KL. (1999). Role of soluble metals in oil fly ash induced airway epithelial injury and cytokine gene expression. *Am J. Physiol*. 277: 498-510.
Fridovich I. (1983). Superoxide radical: an endogenous toxicant. *Annu Rev Pharmacol Toxicol*. 23: 239-257.

Ebbesen TW and Takada T. (1995). Topological and SP^3 defects in nanotubes. *Carbon* 33, 7: 973-978.

El-Bagory. (2007). Protective effect of scavengers and surfactants on gamma irradiated cortisone acetate solutions. *J. Drug Delivery Sci. Technol.* Vol. 17, No. 6: 437-442.

Elias Z, Poirot O, Daniere MC, Terzetti F, Marande AM, Dzurigaj S, Pezeat H, Fenoglio I. (2000). Cytotoxic and transforming effects of silica particles with different surface properties in Syrian hamster embryo cells. *Toxicol. in vitro* 14: 409-422.

Enesa K, Ito K, Luong LA, Thorbjornsen I, Phua C, To Y, Dean J, Haskard DO, Boyle J, Adcock I, Evans PC. (2008) Hydrogen peroxide prolongs nuclear localisation of NF-κB in activated cells by suppressing negative regulatory mechanisms. *J. Biol. Chem.* 283, No. 27: 18582-18590.

Fanvizza C, Ursini CL, Paba E, Ciervo A, Francesco A, Maiello R, De Seimone P, Cavallo D. (2007). Cytotoxic and DNA damage in human lung epithelial cells exposed to respirabe alpha quartz. *Toxicol. in vitro* 21: 586-594.

Farber JL. (1994). Mechanisms of cell injury by activated oxygen species. *Environ. Health. Perspect.* 102 (Suppl. 10): 17-24.

Fehrenbach H. (2001). Alveolar epithelial type II cell: defender of the alveolus revisited. *Respir. Res.* 2: 33-46.

Felix K, Manna SK, Wise K, Barr J, Ramesh GT. (2005). Low levels of Arsenite activates nuclear factor κB and activator protein-1 in immortalized mesencephalic cells. *J. Biochem. Toxicol.* Vol. 19: 67-77

Feghali CA, Wright TM. (1997). Cytokines in acute phase inflammation. *Frontiers in bioscience* 2: 12-26.

Fenoglio I, Martra G, Coluccia S, Fubini B. (2000). Possible role of ascorbic acid in the oxidative damage induced by inhaled crystalline silica particles. *Chem. Res. Toxicol* 13: 971-975

Fenoglio I, Fonsato S, Fubini B. (2003). Reaction of cysteine and glutathione (GSH) at the freshly fractured surface: A possible role in silica related diseases? *Free Rad. Biol. Med.* Vol. 35, No. 7: 752-762.

Fenoglio I, Tomatis M, Lison D, Muller J, Fonseca A, Nogy JB, Fubini B. (2006). Reactivity of carbon nanotubes: free radical generation or scavenging activity. *Free Rad. Biol. Med.* 40: 1227-1233.

Fenoglio I, Grico G, Tomatis M, Muller J, Raymundo-Pinero E, Benguis F, Fonsecca A, Nagy JB, Lison D, Fubini B. (2008). Structural defects play a major role in acute lung toxicity of multiwalled carbon nanotubes: Physico-chemical aspects. *Chem. Res. Toxicol.*

Flahaut E, Durrieu MC, Zemy-Zolghadri M, Bareille R, Baquey CH. (2006). Investigation of the cytotoxicity of CCVD carbon nanotubes towards human umbilical vein endothelial cells. *Carbon* 44: 1093-1099.

Fletcher GG, Rossetto FE, Turnball JD, Nieboer E. (1994). Toxicology, uptake and mutagenicity of particulate and soluble Nickel compounds. *Environ. Health Perspect.* Vol. 102, Suppl 3: Molecular mechanisms of metal toxicity and carcinogenicity.: 69-79.

Flohè L, Brigelius-Flohè R, Saliou C, Traber MG, Packer L. (1997). Redox regulation of NF-kappa B activation. *Free Rad. Biol. Med.* Vol. 22, No. 6: 1115-1126.

Fridovich I, Freeman B. (1986). Antioxidant defences in the lung. *Ann. Rev. Physiol.* 48: 693-702.

Fridovich I. (1993). Superoxide radical: An endogenous toxicant. *Ann. Rev. Pharmacol. Toxicol.* 23: 239-257.

Frodovich I. (1995). Superoxide and superoxide dismutases. *Annu. Rev. Biochem.* 64: 97-112.

Fubini B. (1997). Surface reactivity in the pathogenic response to particulates. *Environ. Health Perspect.* 105; 5.

Fubini B. (1998). Surface chemistry and quartz hazard. *Ann. Occup. Hyg.* Vol. 42, No. 8: 521-530.

Fubini B, Zanetti A, Altilia S, Tiozzo R, Lison D, Saffiotti V. (1999). Relationship between surface properties and cellular responses to crystalline silica: Studies with heat treated Cristobalite. *Chem. Res. Toxicol.* 12: 737-745.

Fubini b, Hubbard A. (2003). Reactive oxygen species and reactive nitrogen species in lung injury and diseases. *Free Rad. Biol. Med.* Vol. 34, No. 12: 1507-1516.

Gallager J, Sams R, Gelein R, Inmon J, Elder A, Oberdorster G, Prahad AK. (2003). Formation of 8-oxo-7,8-dihydro-2-deoxyguanosine in rat lung DNA following sub chronic inhalation of carbon black. *Toxicol. Appl. Pharmacol.* 190: 224-231.

Galter D, Mihm S, Droge W. (1994). Distinct effects of glutathione disulphide on the nuclear transcription factor kB and activator protein 1. *Eur. J. Biochem*. 221: 639-648.

Garcia-Garcia E, Andrieux K, Gil S, Kim HR, De Doon T, Desmaele D, d'Angelo J, Taran F, Geogin D, Couveur P. 2005. A methodology to study intracellular distribution of nanoparticles in brain and endothelial cell. Int. J. Pharmaceutics.

Garcon G, Gosset P, Garry S, Marez T, Hannothiaux MH, Shirali P. (2001). Pulmonary induction of pro-inflammatory mediators following the rat exposure to benzo(a)pyrene coated onto Fe_2O_3 particles. *Toxicol. Lett.* 121: 107-117.

Garza KM, Soto KF, Murr LE. (2008). Cytotoxicity and reactive oxygen species generation from aggregated carbon and carbonaceous nanoparticle materials. *Int. J. Nanomed*. 3: 83-94.

Gauldie J, Bonniaud P, Sime P, Ask K, Kolb M. (2007). TGF-β, smad-3 and the process of progressive fibrosis. *Biochemical society transactions*. Vol. 35, part 4: 661-664.

Gehr P, Schurch S. Surface forces displace particles deposited in airways towards the epithelium. *News in physiological sciences* Vol. 7: 1-5.

Gehr P, Geiser M, Hof VI, Schurch S. Surfactant ultrafine particle interactions: What we can learn from PM10. *Phil. Trans. R. Soc. Lond.* A 358: 2707-2718.

Gehr P, Geiser M, Hof VI, Schurch S, Waber V, Baumann M. (1993). Surfactant and inhaled particle in the conducting airways: Structural, stereological and biophysical aspects. *Microscopy research and techniques* 26: 423-436.

Geiser M, Matter M, Maye I, Hof V, Gehr P, Schurch S. (2003). Influence of airspace geometry and surfactant on the retention of manmade vitreous fibres (MMVF 10a). *Environ. Health Perspect.* 111: 895-901.

Geiser M, Rothen-Rutishauser B, Kapp N, Schurch S, Krayling W, Schulz H, Semmler M, Hof VI, Heyder J, Gehr P. (2005). Ultrafine particles cross cellular membranes by non phagocytic mechanisms in lungs and in cultured cells. *Environ. Health Perspect.* 113: 1555-1560.

Ghio AJ, Kennedy TP, Whorton R, Crumbliss AL, Hatch GE, Hoidal JR. (1992). Role of surface complexed iron in oxidant generation and lung inflammation induced by silicates. *Am. J. Physiol (lung cell. Mol. Physiol.)* 263: L511-L518

Ghio AJ, Fracica PJ, Young SL, Plantadosi CA. (1993). Synthetic lung surfactant scavenges oxidants and protects against hyperoxic lung injury. *J. Appl. Physiol.* 77: 1217-1223.

Ghio AJ, Jaskot RH, Hatch GE. (1994). Lung injury after silica instillation is associated with an accumulation of iron in rats. *AJP: (lung cell. Mol. Physiol.)* 267, 7: L686-L692.

Gilmour PS, Rahman I, Donaldson K, MacNee W. (2003). Histone acetylation regulates epithelial IL-8 release mediated by oxidative stress from environmental particles. *AJP: Lung cell Mol. Physiol.* 284: L533-L540.

Gloire G, Legrand-poles, Piette J. (2006). NFkB activation by reactive oxygen species: Fifteen years later. *Biochemical pharmacology* 72: 1493-1505.

Gold J, Amandusson H, Krozer A, Kasemo B, Ericsson T, Zanetti G, Fubini B. (1997). Chemical characterisation and reactivity of iron chelator treated amphibole asbestos. *Environ. Health Perspect.* 105 (Suppl. 5): 1021-1030.

Goldkorn, Balaban N, Shannon M, Ceha V, Matsukuma K, Gilchrist D, Wang H, Chan C. (1998). H2O2 acts on cellular membranes to generate ceramide signaling and initiate apoptosis in tracheobronchial epithelial cells. *J. Cell Sci.* 111: 3209-3220.

Gosset P, Wallaert B, Tonnel AB, Founeau C. (1999). Thiol regulation of the production of TNFα, IL-6 and IL-8 by human alveolar macrophages. *Eur. J. Respir*. J. 14: 98-105.

Graham A, Higinbotham J, Allan D, Donaldson K, Beswick PH. (1999). Chemical differences between long and short amosite asbestos: differences in oxidation state and coordination sites of iron detected by infrared spectroscopy. *Occup. Environ. Med*. 56: 606-611.

Greenwell LL, Moreno T, Richards RJ. (2003). Pulmonary antioxidants exert differential protective effects against carbon and individual particulate matter. *J. Biosci.* 28: 101-107.

Grubek-Jaworska H, Nejman P, Czuminska K, Przybylowski T, Huczko A, Lange H, Bystrejewski M, Baranowski P, Chazan R. (2006). Preliminary results on the pathogenic effects of intratracheal exposure to one dimensional nanocarbons. *Carbon* 44: 1057-1063.

Guthrie GD. (1997). Mineral properties and their contribution to particle toxicology. *Environ. Health Perspect*. 105: 5

Guo L, Morris DG, Liu X, Vaslet C, Hurt RH, Kane AB. (2007). Iron bioavailability and redox activity in diverse nanotube samples. *Chem. Mater.* 19: 3472-3478.

Haddad JJ. (2002). Antioxidant and pro-oxidant mechanisms in the regulation of redox-sensitive transcription factors. *Cellular signalling* 14: 879-897.

Haddard JJ. (2004). Oxygen sensing and oxidant/redox related pathways. *Biochem. Biophys. Res. Commun*. 316: 969-977.

Hadnagy W, Marsetz B, Idel H. (2003). Haemolytic activity of crystalline silica - separated erythrocytes versus whole blood. *Int. J. Environ. Health* 206: 103-107.

Haggenmuller R, Rahatekar SS, Fagan JA, Chun J, Becker ML, Nauk RR, Krauss T, Carlson L, Kadla JF, Trulove PC Fox DF, Delong HC, Fang Z, Kelly SO, Gilman JW. (2008). Comparison of the quality of aqueous dispersions of single walled carbon nanotubes using surfactants and bio molecules. *Langmuir* 24: 5070-5078.

Halliwell B, Gutteridge JM. 1984. Oxygen toxicity, oxygen radicals, transition metals and disease. *Biochem J*. 219: 1-14.

Halliwell B, Aruoma OI. (1991). DNA damage by oxygen derived species: its mechanism and measurement in mammalian systems. *FEBS* Vol. 281, No. 1,2: 9-19.

Harmsen AG, Muggenbury BA, Snipes BM, Bice DE. (1985). The role of macrophages in particle translocation from lungs to lymph nodes. *Science* 230: 1277-1281.

Hart GA, Coste A, Aubier M, Marano F. (1994). In vitro cytotoxicity of asbestos and manmade fibres: roles of length, diameter and composition. *Carcinogenesis* Vol. 15, No. 5: 971-977.

Hardy JA, Aust AE. (1995). Iron in asbestos chemistry and carcinogenicity. *Chem Rev*. 95: 97-118.

Hayakawa M, Muashita H, Sakamoto I, Kitagawa M, Tanaka H, Yasuda H, Karin M, Kitugawa K. (2003). Evidence that reactive oxygen species do not mediate NFkB activation. *EMBO J*. Vol. 22, No. 13: 3356-3366.

Hayden MS, Ghosh S. (2004). Signalling to NFkB. *Genes and development* 19: 2195-2224.

Heppleston AG. (1984). Pulmonary toxicity of silica, coal and asbestos. *Environ. Health Perspect.* Vol. 55: 111-127.

Herzog EL, Brody AR, Colby TV, Mason R, Williams MC. (2008). Known's and unknown's of the alveolus. *Proc. Am. Thorac. Soc.* Vol. 5: 778-782.

Hesterberg TW, Barret JC. (1984). Dependence of asbestos and mineral dust induced transformation of mammalian cells in culture on fibre dimensions. *Cancer research* 44: 2170-2180.

Hill CA, Wallace WE, Keane MJ, Mike PS. (1995). The enzymic removal of a surfactant coating from quartz and kaolin by PD288D1 cells. *Cell biol. Toxicol.* 11: 119-128.

Hirano S, Kanno S, Fuziyama A. (2008). Multi walled carbon nanotubes injure the plasma membrane of macrophages. *Toxicol. Appl. Pharmacol.*

Hirota K, Murata M, Sachi Y, Nakamura H, Takeuchi J, Kenjro M, Yodoi J. (1999). Distinct role of thioredoxin in the cytoplasm and the nucleus. *J. Biol Chem.* Vol. 274, 4: 27801-27897.

Hirsch A. (2002). Functionalisation of single walled carbon nanotubes. *Angewandte chemie International Ed. 41, Iss. 11*: 1853-1859.

Hoffmann E, Dittrich-Breiholz O, Holtman H, Kracht M. (2002). Multiple control of interleukin-8 gene expression. *J. Leukocyte Biol.* 72: 847-855.

Hoffman A; Baltimore D. (2006). Circuitry of nuclear factor kB signalling. *Immunological reviews* Vol. 20: 171-186.

Höhr D, Steinfartz Y, Schins RPF, Knaapen AM, Martra G, Fubini B, Borm PJA. (2002). The surface area rather than the surface coating determines the acute inflammatory response after instillation of fine and ultrafine TiO_2 in the rat. *Int. J. Hyg* 205: 239-244.

Holtmann H, Winzen R, Hollund P, Eickemeier S, Hofmann E, Wallach D, Malinin NL, Cooper JA, Resch K, Kracht M. (1999). Induction of interleukin-8 synthesis integrates effects on transcription and mRNA degradation from at least three different cytokine or stress activated signal transduction pathways. *Mol. Cell. Biol.* Vol. 19, No. 10: 6742-6753.

Huang W, Lin Y, Taylor S, Gaillard J, Rao AM, Sun YP. (2002). Sonication assisted functionalization and solubilisation of carbon nanotubes. *Nanoletters* Vol. 2, No. 3: 231-234.

Hubbard AK, Timblin CR, Shulkla A, Rineon M, Mossman BT. (2002). Activation of NFkB dependent gene expression by silica in lungs of luciferase reporter mice. *AJP: Lung Cell Mol. Physiol.* 282: L968-L975.

Huczko A. (2002). Synthesis of aligned carbon nanotubes. *Appl. Phys.* A 74:617-638.

Huczko A, Lange H, Bystrzejewski M, Baranowski P, Ando Y, Zhao X. (2006). Formation of SWCNT in arc plasma: Effect of graphitisation of Fe-doped anode and optical emission studies. *J. Nanosci. Nanotechnol*. 6: 1319-1324.

Hume LA, Rimstiat JB. (1992). The bioavailability of chrysotile asbestos. *American mineralogist* 77: 1125-1128.

Hurst SM, Wilkinson TS, Mcloughlin RM, Jones SA, Horiuchi J, Yamamoto N, Rose-John S, Fuller GM, Topley N, Jones SA. (2001). IL-6 and its soluble receptor orchestrate a temporal switch in the pattern of leukocyte recruitment seen during acute inflammation. *Immunity* Vol. 14,: 705-714.

Iijima S, Brabec C, Maiti A, Berholc J. (1996). Structural flexibility of carbon nanotubes. *J. Chem. Phys.* 104: 2089-2092.

Islam MF, Rojas E, Bergey DM, Johnson AT, Yodh AG. (2003). High fraction surfactant solubilization of single wall carbon nanotubes in water. *Nanoletters,* Vol. 3, No. 10: 1379-1382.

Ito Y, Venkatesan N, Hirako N, Sugioko N, Takada K. (2007). Effect of fibre length of carbon nanotubes on the adsorption of erythroprotein from small rat intestine. *Int. J. pharmaceutics.*

Jacob RA. (1995). The integrated antioxidant system. *Nutrition research*, Vol. 15, No. 5: 755-766.

Jacobsen NR, Saber L, Douglas GR, Wallin H. (2007). Increased mutant frequency by carbon black, but not quartz in the lacZ and CII transgenes of Muta ^{TM} mouse lung epithelial cells. *Environmental and molecular mutagenesis*, 48: 451-461.

Janssen YMW, Barchowsky A, Treadwell M, Driscoll KE, Mossman BT. (1995). Asbestos induces nuclear factor kB (NFkB) DNA binding activity and NFkB dependent gene expression in tracheal epithelial cells. *PNAS* Vol. 92: 8458-8462.

Janssen-Heininger YMW, Macara I, Mossman BT. (1999). Cooperatively between oxidants and tumour necrosis factor in the activation of nuclear kappa factor (NF) κB. Requirement of Ras/ Mitogen activated protein kinases in the activation of NFκB by oxidants. *Am. J. respir cell mol. Biol.* 20: 942-952.

Jefferson DA. (2000). The surface activity of ultrafine particles. *Phil. Trans R. Soc. Lond*. A 358: 2683-2692.

Ji L, Gomez-Cabrera MC, Vina J. (2006). Exercise and hormesis activation of cellular antioxidant signalling pathway. *Ann NY Acad. Sci.* 1067: 425-435.

Jia G, Wang H, Yan L, Wang X, Pei R, Yan T, Zhao Y, Guo X. (2005). Cytotoxicity of carbon nanomaterials: Single-wall nanotube, multi-wall nanotube, and fullerene. *Environ. Sci. Technol.* 39: 1378-1383.

Jiang L, Gao L, Sun J. (2003). Production of aqueous colloidal dispersions of carbon nanotubes. Journal of colloid interface *Science* 260: 83-94.

JiJon HB, Panenka WJ, Madsen KL, Parsons HG. (2002). MAP kinases contribute to IL-8 secretion by intestinal cells via post transcriptional mechanisms. *AJP: cell Physiol.* 283: C31-C41.

Jim Kim S, Denhez F, Kim KY Hott JT, Sporn MB, Roberto AB. (1989). Activation of the second promoter of the transforming growth factor β1 gene by transforming growth factor β1 and phorbal ester occurs through the same target sequences. *J. Biol. Chem.* Vol. 264, No. 32: 19373-19378.

Jimenez LA, Zanella C, Fung H, Janssen YMW, Vacek P, Charland C, Goldberg J, Mossman BT. (1997). Role of extracellular signal related protein kinases in apoptosis by asbestos and H_2O_2. *AJP 273 (Lung Cell Mol. Physiol 17)*: L1029-1035.

Jimenez LJ, Brown DA, Rahman I, Antoniceli F, Duffin R, Drost EM, Hay RT, MacNee W. (2000). Activation of NFkB occurs via an iron mediated mechanism in the absence of IkB degradation. *Toxicol. Appl. Pharmacol.* 166; 101-110.

Johnson KJ, Fantone JC, Kaplan J, Ward PA. 1981. In vivo damage of rat lungs by oxygen metabolites. *J. Clin. Invest.* 67: 983-993.

Jurkschat K, Ji X, Crosseley A, Compton RG, Banks CE. (2007). Super washing does not leave single walled nanotubes iron free. *Analyst* 132: 123-132.

Ka Ming Chan F, Chun HJ, Zheng L, Siegel RM, Bui KL, Lenardo MJ. (2000). A Domain in the TNF receptors that mediates ligand independent receptor assembly and signalling. *Science* Vol. 288: 2351-2354.

Kagan VE, Tyutina YY, Tywin VA, Kondova NV, Poptpvich AI, Osipov AN, Kisin ER, Schwegler-Berry D, Mercer R, Castranova V, Shvedova AA. (2006). Direct and indirect effects of single walled carbon nanotubes on Raw 265.7 cells: Role of Iron. *Toxicol. Lett.*

Kamata H, Shibukawa Y, Oka SI, Hirata H. (2000). Epidermal growth factor receptor is modulated by redox through multiple mechanisms. Effects of reductants and H_2O_2. *Eur. J. Biochem.* 267: 1933-1944.

Kamp DW, Dunn MM, Sbalchiero JS, Knap AM, Weitzman SA. (1994). Contrasting effects of alveolar macrophages and neutrophils on asbestos induced pulmonary epithelial injury. *AJP: Lung Cell. Mol. Physiol.* 266: L84-L91.

Kamp DW, Weitzman SA. (1999). The molecular basis of asbestos induced lung injury. *Thorax* 54: 638-652.

Kamp DW, Panduri V, Weitzman SA, Chandel N. (2002). Asbestos induced alveolar epithelial cell apoptosis: role of mitochondrial dysfunction caused by iron derived free radicals. *Mol. Cell Biochem*. 234-235: 153-160.

Kane RS, Stroock AD. (2007). Protein-nanomaterial interactions. American chemical society and American institute of chemical engineers; A-D.

Kang YJ, Enger MS. (1990). Glutathione content and growth in A549 human lung carcinoma cells. *Exp. cell Res.* 187: 177-179.

Kang ZC and Wang ZL. (1997). Chemical activities of graphitic carbon spheres. Journal of molecular catalysis A: Chemical 118: 215-222.

Kaplanski G, Marin V, Montero-Julian F, Mantovani A, Farnarier C. (2003). IL-6: a regulator of the transition from neutrophil to monocyte recruitment during inflammation. *Trends in immunology* Vol. 24, No. 1: 25-29.

Karajanagi SS, Vertegal AA, Kane RS, Dordick JS. (2004). Structure and function of enzymes adsorbed onto single walled carbon nanotubes. *Langmuir* 20: 11594-11599.

Kim SN, Lao Z, Papdimitrahopoulous F. (2005). Diameter and metallicity dependant Redox influences on the separation of single walled carbon nanotubes. *Nanoletters* Vol. 3, No. 2: 2500-2504.

Kim H, Sigmund W. (2004). Effect of a graphitic structure on the stability of FCC Iron. *J. Crystal Growth.* 267: 738-744.

Kim H, Sigmund W. (2005). Iron particles in carbon nanotubes. *Carbon* 43: 1743-1748.

Kim YM, Reed W, Lenz AG, Jaspers I, Silbaforis R, Nick HS, Samet JM. (2005). Ultrafine carbon particles induce interleukin-8 gene transcription and p38 MAPK activation in normal human bronchial epithelial cells. *AJP-Lung* 288: 432-441.

Kinnuala VL, Raivio KO, Linnainnvaci K, Ekman A, Klockars M. (1995). Neutrophil and asbestos fibre induced cytotoxicity in cultured human mesothelial and bronchial epithelial cells. *Free Rad. Bio. Med*., Vol. 18, No. 3: 391-399.

Kinnula VL, Fattmann CL, Tan RJ, Oury TD. (2005). Oxidative stress in pulmonary fibrosis - A possible role for redox modulatory therapy. *Am. J. Respir. Crit. Care Med.* Vol. 172.

Klatt P, Moluna E, De Lacota MG, Padilla CA, Martinez-Galisteo E, Barcena JA, Lamas S. (1999). Redox regulation of c-Jun DNA binding by reversible s-glutathiolation. *FASEB J*. 13: 1481-1490.

Knaapen AM, Albrecht C, Becker A, Hohr D, Wirizer A Hanen GR, Borm PJA, Schins RPF. (2002). DNA damage in lung epithelial cells isolated from rats exposed to quartz: Role for surface reactivity and neutrophil inflammation. *Carcinogenesis* Vol. 23, No. 7: 1111

Kochevar IE, Lynch MC, Zhuang S, Lambert CR. (2000). Singlet oxygen but not oxidising radicals induces apoptosis in HL-60 cells. *Photochemistry and photobiology* 72: 548-553.

Koike E, Kobayashi T. (2006). Chemical and biological oxidative effects of carbon black nanoparticles. *Chemosphere* 65: 946-951.

Kopáni M, Celec P, Danisovic L, Michalka P, Biro C. (2006). Oxidative stress and electron spin resonance. *Clinica Chimica Acta* 364: 61-66.

Koppenol WH. (2001). The Haber-Weiss cycle - 70 years later. *Redox Report* Vol. 6, No. 4: 229-234.

Kosaka M, Ebbesen TW, Hiura H, Tanigaki K. (1995). Annealing effect on carbon nanotubes. An ESR study. *Chem. Phys. Lett.* 233: 47-51.

Koyama S, Haniu H, Osaka K, Koyama H, Kuroiwa N, Endo M, Kim YA, Hayashi T. (2006). Medical application of carbon nanotube filled nanocomposites: the microcatheter. *Small* 2: 1406-1411.

Kukielka E, Cederbaum AI. (1994). DNA strand cleavage as a sensitive assay for the production of hydroxyl radicals by microsomes: Role of cytochrome P450 2E1 in the increased activity after ethanol treatment. *Biochem J.* 392: 773-779.

Lam CW, James JT, McCluskey R, Hunter RL. (2003). Pulmonary toxicity of single wall carbon nanotubes in mice 7 and 90 days after intratracheal instillation. *Toxicol. Sci.* 77: 126-134.

Langer AM, Nolan RP. (1994). Chrysotile: Its occurrence and properties as variable controlling biological effects. *Ann. Occup. Hyg*. Vol. 38, No. 4: 427-451.

Langenbeck EG, Bergofzsky EH, Halpern JG, Foster AM. (1990). Submicron sized particle clearance from alveoli: routes and kinetics. *J. Appl. Physiol* 69: 1302-1308.

Laskin DL, Pendino KJ. (1995). Macrophages and inflammatory mediators in tissue injury. *Annu. Rev. Pharmacol. Toxicol.* 35: 655-677.

Le Bouffant L, Daniel H, Henin JP, Martin JC, Normund C, Tichoux NG, Trolevel F. (1987). Experimental study on the long term effects of inhaled MMVF on the lungs of rats. *Ann. Occup. Hyg.* Vol. 31, No. 4B: 765-790.

Lee KP, Trchimowioz HJ, Reinhardt CF. (1985). Transmigration of titanium dioxide particles in rats after inhalation exposure. *Exp. Mol. Pathol.* 42: 331-343.

Lee EG, Boone DL, Chai S, Libby S, Chien M, Lodolce JP, Ma. A. (2000). Failure to regulate TNF induced NFκB B and cell death responses in A20 deficient mice. *Science* Vol. 289: 2350-2354.

Lehnert BE. (1992). Pulmonary and thoracic macrophage sub-populations and clearance of particles from the lung. *Environ Health Perspec.* Vol. 97: 17-46.

Lennart Persson H. (2005). Iron dependent lysosomal destabilisation initiates silica induced apoptosis in murine macrophages. *Toxicol Lett.* 159: 124-133.

Lesko SA, Lorentzen RJ, Tso POP. (1980). Role of superoxide in deoxyribose acid strand scission. *Biochemistry* 19: 3023-3028.

Lesur O, Veldhivzen RAW, Whitsett JA, Hull WM, Possmayer F, Cantin A, Begin R. (1993). Surfactant associated protein (SPA-SPB) are increased proportionally to alveolar phospholipids in sheep silicosis. *Lung* 171: 67-74.

Lesser M, Chany JC, Galicki NI, Edelman J, Cardoio C. (1989). Cathepsin B and D activity in alveolar macrophages from rats with pulmonary granulomatous inflammation or acute lung injury. *Agents and actions* Vol. 28: 264-271.

Li J, Kartha S, Lasvovskaia S, Tan A, Bhat RK, Manaligod M, Page K, Brasier AR Hershenson MB. (2002). Regulation of human airway epithelial IL-8 expression by MAP kinases. *AJP: Lung cell Mol. Physiol.* 283: L690-L699.

Li J, Li W, Xu J, Cai X, Lui R, Li Y, Zhao Q, Li Q. (2007). Comparative study of pathological lesions induced by multiwall carbon nanotubes in the lungs of mice by intra-tracheal instillation and inhalation. *Environ. Toxicol* 22: 415-421.

Li N, Karim M. (1999). Is NFkB the sensor of oxidative stress. *FASEB J.* 13:1137-1143.

Li Z, Hulderman T, Salmen R, Chapman R, Leonard SS, Young SH, Shvedova A, Luster MI, Simeonova PP. 2007. Cardiovascular effects of pulmonary exposure to single wall carbon nanotubes. Environmental health perspect. 115, No. 3: 377-382.

Li X, Yuan G, Brown A, Westwood A, Brydson R, Rand B. (2006). The removal of encapsulated catalyst particles from carbon nanotubes using molten salts. *Carbon* 44: 1699-1705.

Light WG, Wei ET. (1977). Surface charge and asbestos toxicity. *Nature* Vol. 265: 5-37.

Lin T, Bajpai V, Ji T, Dai L. (2003). Chemistry of carbon nanotubes. *Aust. J. Chem*. 56: 635-651.

Lin T, Zhang WD, Huang J, He C. (2005). A DFT study of the Animation of Fullerenes and carbon nanotubes; reactivity and curvature. *J Phys. Chem B* 109: 13755-13760.

Lindermann SW, Yost CC, Denis MM, Mcintyre TM, Weyrich AS, Zimmerman GA. (2004). Neutrophils alter the inflammatory milieu by signal dependent translation of constitutive messenger RNAs. *PNAS USA* 101: 7076-7081.

Lippmann M, Yeates DB, Albert RE. (1980). Deposition, retention and clearance of inhaled particles. *Brit. J. Ind. Med.* 37: 337-362.

Liochev SI, Fridovich I. (1993). The role of superoxide in the production of hydroxyl radicals: in vitro and in vivo. *Free Rad. Biol. Med.* Vol. 16: 29-33.

Liu W, Ernst JD, Broaddus VC. (2000). Phagocytosis of crocidolite asbestos induces oxidative stress DNA damage and apoptosis in mesothelial cells. *Am. J. Respir. Cell Mol. Biol.* Vol. 23: 371-378.

Lu KL, Lago RM, Chen YK, Green MLH, Harris PFF, Tsang SC. (1996). Mechanical damage of carbon nanotubes by ultrasound.

Lucking F, Koser H, Jank M, Ritter A. (1998). Iron powder, graphite and activated carbon as catalysts for the oxidation of 4-Chlorophenol with hydrogen peroxide in aqueous solution. *Wat. Res.* Vol. 32, No. 9: 2607-2614.

Lund LG, Aust AE. (1992). Iron mobilisation from crocidolite dependent formation of DNA single strand breaks in ΦX174 RF1 DNA. *Carcinogenesis* Vol. 13, No. 4: 637-642.

Lund LG, Williams MG, Dodson RF, Aust AE. (1994). Iron associated with asbestos bodies is responsible for formation of single strand breaks in ΦX174 RFI DNA. *Occ. Environ. Med.* 51: 200-204.

Luster MI, Simeonova PP. (1998). Asbestos induced inflammatory cytokines in the lung epithelial cells - Role of reactive oxygen species. *The J. Immunol.* 159: 3921-3928.

Magrez A, Kasas S, Salico V, Pasquier N, Seo JW, Celio M, Catsicas S, Schwaller B, Forro L. (2006). Cellular toxicity of carbon based nanomaterials. *Nanoletters* Vol. 6, No. 6: 1121-1125.

Mangum JB, Turpin EA, Antao -Menezes A, Cesta MF, Bermudez E, Bonner JC. (2006). Single walled carbon nanotube (SWCNT) induced interstitial fibrosis in the lungs of rats associated with increased levels of PDGF mRNA and the formation of unique intercellular carbon structures that bridge alveolar macrophages in situ. *Part Fibre Toxicol.* 3: 15.

Manivannan A, Chirila M, Giles NC, Seehra MS. (1999). Microstructure dangling bonds and impurities in activated carbons. *Carbon* 37: 1741-1747.

Manna SK, Tien Kuo M, Aggarwal BB. (1999). Over expression of y-glutamylcysteine synthase suppresses tumour necrosis factor induced apoptosis and activation of nuclear factor kappa B and activator protein 1. *Oncogene* 18: 4371-4382.

Manna SK, Sarker S, Barr J, Wise K, Barrera EV, Jelelowo O, Rice-Ficht AC, Ramesh GT. (2005). Single walled carbon nanotubes induces oxidative stress and activates nuclear transcription factor κB in human keratinocytes. *Nanolett.* Vol. 5, No. 9: 1676-1684.

Marin V, Julian-Montero EA, Gris S, Boulay V, Bongrand P, Farnarier C, Kaplanski G. (2001). The IL-6 soluble IL-6Rα Autocrine loop of endothelial activation as a intermediate between acute and chronic inflammation: an experimental model involving thrombosis. *The J. Immunol.* 167: 3435-3442.

Martin LD, Rochelle LG, Fischer BM, Krunkosky TM, Adler KM. (1997). Airway epithelium as an effector of inflammation: Molecular regulation of secondary mediators. *Eur. Respir J.* 10: 2139-2146.

Martindale JL, Holebrook NJ. (2002). Cellular responses to oxidative stress: Signalling for suicide and survival. *J.cell. Physiol.* 192: 1-15.

Maxim LD, Hadley JG, Potter RM, Niebo R. (2006). The role of fibre durability/biopersistence of silica based synthetic vitreous fibres and their influence on toxicology. *Regul Toxicol Pharmacol* 46: 42-62.

Maynard AD, Knempel ED. (2005). Airborne nanostructure particles and occupational health. *Journal of Nanoparticle research* 7: 587-614.

Mawwhinney DB, Naumenko V, Kuznetsova A, Yates JT, Liu J, Smalley RE. (2000). Surface defect density on single walled carbon nanotubes. *Chem. Phys. Lett.* 324:213-216

McEuen PL, Fuhrer MS, Park H. (2002). Single walled carbon nanotube electronics. *IEEE Transactions of Nanotechnology* Vol. 1, No. 1: 78-85.

McNeilly JD, Jimènez LA, Clay MF, MacNee W, Howe A, Heal MR, Beverland IJ, Donaldson K. (2005). Soluble transition metals on welding fumes cause inflammation via activation of NFκB and AP-1. *Toxicol Lett.* 158: 152-157.

Meisel D, Matheson MS, Ralzini J. (1978). Photolytic and radiolytic studies of $Ru(bpy)_3^{2+}$ in micellar solution. *J. Am. Chem. Soc.* 100; 1: 117-122.

Meistel A, Anderson ME. (1983). Glutathione. *Ann. Rev. Biochem.* 52: 711-760.

Merchant RK, Peterson MW, Hunnighake GW. (1990). Silica directly increases permeability of alveolar epithelial cells. *J. Appl. Physiol.* 68: 1354-1359.

Meszaros AJ, Reichner JS, Albina JE. (2000). Macrophage induced neutrophil apoptosis. *J. Immunol.* 165: 435-441.

Micheau O, Tschopp J. (2003). Induction of TNF receptor 1 mediated apoptosis via two sequential signaling complexes. *Cell* 114: 181-190.

Miller DM, Buettner GR, Aust SD. (1990). Transition metals as catalysts of auto oxidation reactions. *Free Rad. Biol. Med.* Vol. 8: 95-108.

Mijata Y, Maniura Y, Kataura H. (2006). Selective oxidation of semi-conducting single wall carbon nanotubes by hydrogen peroxide. *J. Phys. Chem.* B 110: 25-29.

Mĭsĭk V, Riesz P (1996). Nitric oxide formation by ultrasound in aqueous solutions. *J. Phys. Chem.* 100: 17986-17994.

Miura K, Morimoto T. (1998). Adsorption sites for water on graphite 4: chemisorption of water on graphite at room temperature. *Langmuir* 4: 1283-1288.

Modur V, Li Y, Zimmerman GA, Prescott SM, McIntyre TM. (1997). Retrograde inflammatory signalling from neutrophils to endothelial cells by soluble interleukin-6 receptor Alpha. *J. Clin. Invest.* 100: 2752-2756.

Mon C, Becker S. (1999). Cytotoxicity and induction of pro-inflammatory cytokines from Human monocytes exposed to fine ($PM_{2.5}$) and coarse particles ($PM_{10-2.5}$) in outdoor and indoor air. *Toxicol. Appl. Pharmacol.* 155: 245-252.

Monteiro-Riviere NA, Inman AO, Wang YY, Nemanich RJ. (2005). Surfactant effects on carbon nanotube interactions with human keratinocytes. *Nanomed. Nanotech. Biol. Med.* 1: 293-299.

Monteiro-Riviere NA, Nemanich , Inman AO, Wang YY, Riviere JE. (2005). Multi-walled carbon nanotubes interactions with human epidermal keratinocytes. *Toxicol. Lett.* 155: 377-384.

Monthioux M, Smith, BW, Burteaux B, Claye A, Fischer JE, Luzzi DE. (2001). Sensitivity of single walled carbon nanotubes to chemical processing: an electron microscopy investigation. *Carbon* 39: 1251-1272.

Monteiller C, Tran L, MacNee W, Faux S, Jones A, Miller B, Donaldson K. (2008). The pro-inflammatory effects of low toxicity low solubility particles , nanoparticles and fine particles on epithelial cells in vito : the role of surface area. *Occup. Environ. Med*. 64: 609-615.

Moore M, Thor H, Moore G, Nelson S, Moldeus P, Orrenius S. (1985). The toxicity of acetaminophen and N-acetyl-P-benzoquinone Imine in isolated hepatocytes is associated with that depletion and increased cytosolic $Ca2^{+}$. *J. Biol. Chem.*

Morgan A, Holmes A, Talbot RJ. (1977). The haemolytic activity of some fibrous amphiboles and its relation to their specific surface areas. *Ann. Occup. Hyg.* Vol. 20: 39-48.

Morgan A, Holmes A, Davison W. (1982). Clearance of sized glass fibres from the rat lung and their solubility in vivo. *Ann. Occup. Hyg.* Vol. 25, No. 3: 317-331.

Mossman BT, Churg A. (1998). Mechanisms in the pathogenesis of asbestos and silica. *Am. J. Respir. Crit. Care. Med.* Vol. 157: 1666-1680.

Mroz RM, Schins RPF, Li H, Drost EM, MacNee W, Donaldson K. (2007). Nanoparticle carbon black driven DNA damage induces growth arrest and AP-1 and NFκB DNA binding in lung epithelial cell line. *J. Physiol & Pharmacol.* 58, Suppl. 5: 461-470.

Muhle H, Bellman B, Potf F. (1994). Comparative investigation of the biodurability of mineral fibres in the rat lung. *Environ. Health. Perspect.* Vol. 102: 163-168.

Muhle H, Bellmann B. (1995). Bio persistence of manmade vitreous fibres. *Annals of occupational hygiene*. Vol. 39, No. 5: 655-660.

Mukaida N. (2003). Pathophysiological roles of interleukin-8/CXCL8 in pulmonary disease. *Am. J. Lung Cell Mol. Physiol*. 284:L566-577

Mukhopadhyay K, Durivedi CD, Mather GN. (2002). Conversion of carbon nanotubes to carbon nanofibres by sonication. *Carbon* 40: 1369-1383.

Mulier B, Rahman I, Wathorn T, Donaldson K, MacNee W, Jeffery PK. (1998). Hydrogen peroxide induced epithelial injury: the protective role of intracellular non protein thiols. *Eur. Respir. J*. 11: 384-391.

Muller JO, Su DS, Jentoft RE, Wild U, Schlogl R. (2006). Diesel engine exhaust emission: oxidative behaviour and microstructure of black smoke soot particulate. *Environ. Sci. Technol*. 40: 1231-1236.

Muller J, Decordier I, Hoet P, Lombaert N, Thomassen L, Huaux F, Lison D, Kirsch-Volders M. (2008). Clastogenic and Aneugenic effects of multi wall carbon nanotubes. *Carcinogenesis.*

Muller J, Huaux F, Fonseca A, Nagy JB, Moreau N, Delos M, Raymundo-Pinero E, Beguin F, Kirsh-volders M, Fenoglio I, Fubini B, Lison D. (2008). Structural defects play a major role in the acute lung toxicity of multi-walled carbon nanotubes: Toxicology aspects. *Chem. Res. Toxicol*

Murphy DM, Giamello E. (2002). EPR of paramagnetic centres on solid surfaces electron paramagnetic resonance. *Royal society of chemistry*, Vol. 18: 183-221.

Murr LE, Garza KM, Soto KF, Carrasco A, Powell TG, Ramirez DA, Guerrero PA, Lopez DA, Venzor J. (2005). Cytotoxicity assessment of some carbon nanotubes and related carbon nanoparticle aggregates and the implications for anthropogenic carbon nanotube aggregates in the environment. *Int. J Environ. Res*. 2: 31-42.

Murray DK, Harrison JC, Wallace WE. (2005). A ^{13}C CP/MAS and ^{31}P NMR study of the interactions of dipalmitoylphosphatidylcholine with respirable silica and kaolin. *J. Colloid & interface Sci.* 268: 166-170.

Nakashima N, Okuzono S, Murakami H, Nakai T, Yoshikaura K. (2003). DNA dissolves single walled carbon nanotubes in water. *Chemistry letters,* Vo. 32, No. 5: 456-457.

Nash T, Allison AC, Harrington JS. (1966). Physiochemical properties of silica in relation to its toxicity. *Nature* 210: 259-261.

Nath KA, Grande J, Croatt A, Haugen J, Kim Y, Rosenberg ME. (1998). Redox regulation of renal DNA synthesis, transforming growth factor β1 and collagen gene expression. *Kidney international* Vol. 53: 367-381.

Nathan C. (2002). Points of control in inflammation. *Nature,* Vol. 420: 846-852.

Narayan RJ. (2004). Sterilising properties of carbon nanotube composites. *Mat. Res. Soc. Symp. Proc.* Vol. 785: 2.1-2.6.

Nel A, Xia T, Madler L, Li N. (2006). Toxic potential of materials at the nanolevel. *Science* 311, No. 5761: 622-627.

Nimmagadda D, Cherala G, Ghatta S. (2006). Chemical modification of SWCNT alters in vitro cell SWCNT interactions. *J. Biomed. Mater. Res. A* 76: 614-625.

Niyogi S, Hamon HA, Hu H, Zhao B, Bhourmik P, Sen R, Hadon RC. (2002). Chemistry of single walled carbon nanotubes. *Acc. Chem. Res.* 35: 1105-1113.

Noda H, Oikawa K, Kamada H. (1992). ESR study of active oxygen radicals from photo excited semiconductors using the spin trapping technique. *Bull. Chem. Soc. Jpn.* 65: 2505-2509.

Nunoshiba T, Obata F, Boss AC, Oikawa S, Mori T, Kawanisha S, Yamamoto K. (1999). Role of Iron and superoxide for generation of hydroxyl radical, oxidative DNA lesions and mutagenesis in *Escherichia coli. J. Biol. Chem.*, Vol. 274, No. 49: 34832-34837.

Oberdorster D. (2000). Toxicology of ultrafine particles: In vivo studies. *Phil. Trans. R. Soc. Lond*. A 358: 2719-2740.

Obin M, Shang F, Gong X, Handleman G, Blumberg J, Taylor A. (1998). Redox regulation of ubiquitin containing enzymes: Mechanistic in sites using the thiol specific oxidant diamide. *FASEB J*. 12: 561-569.

O'Connell MJ, Eibergen EE, Doorn SK. (2005). Chiral selectivity in the charge transfer bleaching of single walled carbon nanotube spectra. *Nature Materials* Vol. 4: 412-419.

O'Grady N, Preas HL, Pugin J, Fiuza C, Tropea M, Reda D, Banks S, Suffredini AF. (2001). Local inflammatory responses following bronchial endotoxin instillation in humans. *Am J. Crit. Care Med.* 163: 1591-1598.

Ohyama M, Otake T, Morinaga K. (2001). Effect of size of man-made and natural fibres on chemiluminscent response in human monocyte derived macrophages. *Environ. Health Perspect.* Vol. 109, No. 10: 1033-1338.

Okotrub V, Bulusheva LG, Gusel'nikov AV. (2004). Effect of purification on the electron structure filed emission characteristics of a carbonaceous material containing single walled carbon nanotubes.

Otero Arian C, Barcelo F, Fenoglio I, Fubini B, Xamena FX, Tomatis M. (2001). Free radical activity of natural and heat treated amphibole asbestos. *Journal of inorganic biochemistry* 83: 211-216.

Ottery J, Gormley JP. (1978). Some factors affecting the haemolytic activity of silicate materials. *Ann. Occup. Hyg*. Vol. 21: 131-139.

Ovrevik J, Lag M, Schwarze P, Refsnes M. (2004). P38 and src-ERK 1/2 pathways regulate crystalline silica induced chemokine release in pulmonary epithelial cells. *Toxicol. Sci.* 81: 480-490.

Ovrerik J, Refsnes M, Namok E, Becher R, Sandnes D, Schwaze PE, Lag M. (2005). Mechanisms of silica induced IL-8 release from IL-8 A549 cells: Initial kinase activation does not require EGFR activation of particle uptake. *Toxicol.* 227: 105-116.

Øvrevik J, Refsnes M, Namork E, Becher R, Sandnes D, Schiarze PE, Låg M. (2006). Mechanisms of silica induced IL-8 release from A549 cells: Initial kinase activation does not require EGFR activation or particle uptake. Toxicol. 227: 105-116.

Pal Yu B. (1994). Cellular defences against damage from reactive oxygen species. *Physiol. Rev.* Vol. 74, No. 1: 139-162.

Pan CG, Schmitz DA, Cho AK, Frones J, Fukuto JM. (2004). Inherent Redox properties of diesel exhaust particles: catalysis of the generation of ROS by biological reductants. *Toxicol. Sci.* 81, 225-232.

Pandurangi RS, Seehra MS, Razzaboni BL, Bolsitis P. (1990). Surface and bulk infrared modes of crystalline and amorphous silica particles: A study of the relation of surface structure to cytotoxicity of respirabe silica. *Environ. Health Perspect.* Vol. 86:327-336.

Panduri V, Weitzman SA, Chandel N, Kamp DW. (2003). The mitochondria-regulated death pathway mediates asbestos induced alveolar epithelial cell apoptosis. *Am. J. Respir. Cell. Mol. Biol.* Vol. 28: 241-248.

Pantarotto D, Briand JP, Prato M, Bianco A. (2004). Translocation of bioactive peptides across cell membranes by carbon nanotubes. *Chem. Commun*: 16-17.

Parceles JL, Burghard M. (2004). Dispersions of individual carbon nanotubes of high length. *Langmuir* 20: 5149-5152.

Pearsson HL. (2005). Iron dependant lysosomal destabilisation initiates silica induced apoptosis in murine macrophages. *Toxicol. Lett.* 159:124-133.

Pensabene V, Vittorio O, Raffia V Menciassi A, Dario P. (2007). investigation of CNTs interaction with fibroblast cells. *Proceedings 29th Ann. Int. Con. IEEE EMBS*: 6620-6623.

Perez Gil J. (2002). Molecular interactions in pulmonary surfactant films. *Biol. Neonate* 81 (Suppl 1): 6-15.

Perkowski J, Mayer J, Kos L. (2005). Reactions of no ionic surfactants Triton X-n type, with OH radicals. A review. *Fibres and textiles in eastern Europe*, Vol. 13, No. 2: 81-85.

Pierre JL, Fontecave M. (1999). Iron activated species in biology: The basic chemistry. *Biomaterials* 12: 195-199.

Pogozelski WK, Tullus TD. (1998). Oxidative strand scission of nucleic acids: Routes initiated by hydrogen abstraction from the sugar moiety. *Chem Rev.* 98: 1089-1107.

Poland CA, Kinloch I, Maynard A, Wallace WA, Seaton A, Stone V, Brown S, MacNee W, Donaldson K. (2008). Carbon nanotubes introduced into the peritoneal cavity of mice show asbestos like pathogenicity in a pilot study. *Nat Nanotechnol.* 3: 423-428

Prandi L, Bodourdo S, Penazzi N, Fubini B (2001). Redox state and mobility of iron at the asbestos surface: a voltametric approach. *J. Mater. Chem* 11: 1495-1501.

Pulskamp K, Diabates S, Krug HF. (2007). Carbon nanotubes show no signs of acute toxicity but induce reactive oxygen species is dependent on contaminants. *Toxicol. Lett.* 168: 58-74.

Pulskamp K, Wörle-Knirsh JM, Hennrich F, Kern K, Krug HF. (2007). Human lung epithelial cells show biphasic oxidative burst after single walled carbon nanotube contact. *Carbon* 45: 2241-2249.

Putman E, Van Golde LMG, Haagsman HP. (1997). Toxic oxidant species and their impact on the pulmonary surfactant system. *Lung* 175:75-103.

Qian D, Wagner GJ, Liu WK, Yu MF, Ruoff RS. (2002). Mechanics of carbon nanotubes. *Appl. Chem. Res*. 35: 1026-1034.

Quig-Gong X, Selloni A, Batzill M, Diebold U. (2006). Steps on anatase TiO_2 (101). *Nature materials* Vol. 5: 665-670.

Quinlan TR, BeruBe KA, Hacker MP, Taatjes DJ, Timblin CR, Goldberg J, Kimberley O, O'shaughnessy P, Hemenway D, Torino J, Jimenez LA, Mossman BT. (1998). Mechanisms of asbestos induced nitric oxide production by rat alveolar macrophages in inhalation and in vitro models. *Free Rad. Biol. Med.* Vol. 24, No. 5: 778-788.

Rahman I, MacNee W. (1998). Role of transcription factors in inflammatory lung diseases. *Thorax* 53: 601-612.

Rahman I, Smith CAD, Antoncielli F, MacNee W. (1998). Characterisation of γ-glutamylcysteine synthetase heavy subunit promoter: a critical role for AP-1. *FEBS letters* 427: 129-133.

Rahman I, MacNee W. (2000). Oxidative stress and regulation of glutathione in lung inflammation. *Eur. Respir J*. 16: 534-554.

Rahman I, Gilmour PS, Jimènez AL, MacNee W. (2002). Oxidative stress and TNFα induced histone acetylation and NFκB/AP-1 activation in alveolar epithelial cells: potential mechanisms in gene transcription in lung inflammation. *Mol. Cell Biochem*. 234/235: 239-248.

Rahman I, Gilmour PS, Jimènez AL, Biswas SK, Antonicelli F, Aruoma OI. (2003). Ergothioneine inhibits oxidative stress, TNFα induced NFκB activation and interleukin 8 release in alveolar epithelial cells. *Biochem. & Biophys. Res Commun* 302: 860-864.

Rahman I, Biswas SK, Kode A. (2006). Oxidant and antioxidant balance in the airways and airway diseases. *Eur. J. Pharmacol*. 533: 222-239.

Raja PMV, Connalley J, Ganesan GP, Ci L, Ajayan PM, Nalamasuo O, Thompson DM. (2007). Impact of carbon nanotube exposure, dosage and aggregation on smooth muscle cells. *Toxicol. Lett.* 169: 51-63.

Romano M, Sironi M, Toniatti C, Polentarutti N, Frucella P, Ghezzi P, Faggioni R, Luini W, van Hinsbergh V, Sozzani S, Bussolino F, Ciliberto G, Mantovani A. (1997). Role of IL-6 and its soluble receptor in induction of chemokines and leukocyte recruitment. *Immunity* 6: 315-325.

Raush LJ, Bisinger EC, Sharma A. (2004). Carbon black should not be classified as a human carcinogen based on rodent bioassay data. *Regulatory toxicology and pharmacology* 40: 28-41.

Ray S, Misso NLA, Lenzo JC, Robinson C, Thompson PJ. (1999). Gamma glutamylcysteine Synthase activity in human lung epithelial A549 cells. *Free Rad. Biol. Med.* Vol. 27, No. 11/12: 1346-1356.

Razzaboni BL, Bolsaitis P. (1990). Evidence of an oxidative mechanism for the haemolytic activity of silica particles. *Environ. health perspect*. Vol. 87: 337-341.

Reddy KV, Kumar TC, Prasad M, Reddanna P. (1998). Pulmonary lipid peroxidation and antioxidant defence s during exhaustive physical exercise: The role of vitamin E and Selenium . *Nutrition* Vol. 14, No. 5: 448-451.

Reeves JF, Davies SJ, Dodd NJF, Jha AN. (2008). Hydroxyl radicals are associated with titanium dioxide induced cytotoxicity and oxidative DNA damage in fish cells. *Mutation research (fundamental & molecular mechanisms of mutagenesis)* 640: 113-122.

Rejman J, Oberle V, Zuhorn IS, Hoekstra D. (2004). Size dependant internalisation of particles via the pathways of clathrin and caveolae mediated endocytosis. *Biochem. J.* 377: 39-51.

Renwick LC, Brown D, Clouter A, Donaldson K. (2004). Increased inflammation and altered macrophage response caused by two ultrafine particle types. *Occup Environ Med* 61: 442-447.

Riganti C, Aldieri E, Bergandi L, Tomatis M, Fenoglio I, Costamagna C, Fubini B, Bosia A, Ghigo D. (2003). Long and short fibre amosite asbestos alters at a different extent the redox metabolism in human lung epithelial cells. *Toxicol. Appl. Pharmacol.* 193: 106-115.

Roach P, Farrar D, Perry CC. (2006). Surface tailoring for controlled protein adsorption: Effect of topography at the nanometre scale and chemistry. *J. Am.Chem. Soc*. 128: 3939-3945.

Rohn S, Kroh LW. (2005). Electron spin resonance - A spectroscopic method for determining antioxidant activity. *Mol. Nutr. Food Res.* 49: 898-907.

Rothen-Rutishauser B, Kiama SG, Gehr P. (2005). A three dimensional cellular model of the human respiratory tract to study the interaction with particles. *Am. J. Respir. Cell Mol. Biol.* Vol. 32: 281-289.

Saffiotti V, Daniel LN, Mao Y, Shi X, Olufemi Williams A, Kaighn ME. (1994). Mechanisms of carcinogenesis by crystalline silica in relation to oxygen radicals. *Environ. Health Perspect.* (Suppl. 10), 102: 159-164.

Saitoh M, Nishitoh H, Fuji M, Takeda K, Tobiume K, Sauwada K, Kawabala M, Miyazono K, Ichijo H. (1998). Mammalian thioredoxin is a direct inhibitor of apoptosis signal regulating kinase 1. *EMBO Journal* Vol. 17, No. 9: 2596-2606.

Salvador-Morales, Flahaut E, Sum E, Sloan J, Green MLH, Dimm RB. (2006). Complement activation and protein adsorption by carbon nanotubes. *Mol. Immunol.* 43: 193-201.

Sakaida I, Thomas A, Farber JL. (1991). Increases in cytosolic calcium ion concentration can be dissociated from the killing of cultured hepatocytes by tert-butyl hydroperoxide. *J. Biol. Chem.* Vol. 266, No. 2: 717-722.

Sandblom RE, Johnson KJ, Killen PD, Sage H, Hudson LD, Striker GE. (1983). Alveolar injury by oxygen metabolites alters the composition of extracellular matrix. *Chest* 83 (Suppl 5): 42S-43S.

Sarada A, Himadri P, Chitaranjan M, Geetali P, Shi Ram M, Ilavazhagan G. (2008). Role of oxidative stress and NF-κB in hypoxia induced pulmonary Edema. *Exp. Biol. Med.* 233: 1088-1098.

Sato Y, Yokoyama A, Shibata K, Akimoto Y, Ogino S, Nodasaka Y, Kohgo T, Tamura K, Akasaka T, Uo M, Motomiya K, Jeyadevan B, Ishiguro M, Hataeyama R, Watari F, Tohji K. (2005). Influence of length on cytotoxicity of multiwalled carbon nanotubes against human acute monocytic leukemia cell line THP-1 in vitro and subcutaneous tissue of rats in vivo. *Mol. BioSyst.* 1: 176-182.

Sayes CM, Liang F, Hudson JL, Mendez J, Guo W, Beach JM, Moore VC, Doyle CD, West JL, Billups WE, Ausman K, Colvin V. (2006). Fictionalisation density dependence of single wall carbon nanotubes cytotoxicity in vitro. *Toxicol. Lett.* 161: 135-142.

Sayes CM, Waki R, Kurian PA, Liu Y, West JL, Auman KD, Warheit DB, Colvin VL. (2006). Correlating nanoscales titania structure with toxicity: A cytotoxicity and inflammatory response study with human dermal fibroblasts and human lung epithelial cells. *Toxicol. sci.* 92: 174-185.

Sayes CM, Waki R, Kurian PA, Liu Y, West JL, Ausman KD, Warheit DB, Colvin VL. (2006). Correlating nanoscale titania structure with toxicity: A cytotoxicity and inflammatory response study with human dermal fibroblasts and human lung epithelial cells. *Toxicol. Sci.* 92: 174-185.

Schiedercit C. (2006). IkB Kinase complexes: Gateways to NFκB activation and transcription. *Oncogene* 25: 6685-6705.

Schimmelpteng J, Drosselmeyer E, Hofheinz V, Seidel A. (1992). Exposure geometry on the effects of quartz and asbestos on alveolar macrophages. *Environ. Health Perspect*. Vol. 97: 225-231.

Schins RPF, McAlinden A, MacNee W, Jimenez LA, Ross RA, Guy K, Faux SP, Donaldson K. (2000). Persistent depletion of I kappa B alpha and interleukin-8 expression in human pulmonary epithelial cells exposed to quartz particles. *Toxicol. Appl. Pharmacol*. 167:

Schins RPF, Duffin R, Hohr D, Knaapen AM, Shi T, Wieshaupt C, Stone V, Donaldon K, Borm PJA. (2002). Surface modification of quartz inhibits toxicity, particle uptake and oxidative DNA damage in human lung epithelial cells. *Chem. Res. Toxicol.* 15: 39-52.

Schefer DW, Brown JM, Anderson DP, Zhao J, Chokalingham K, Tomlin D, Ilavsky J. (2003). Structure and dispersion of single wall carbon nanotubes. *App. Cryst*. 36: 553-557.

Scholze H, Conradt H. (1987). An in vitro study of the chemical durability of silicaceous fibres. *Ann. Occ. Hyg.* Vol 31, No. 48: 683-692.

Schraufstatter IU, Daniel BH, Hyslop PA, Spragg RG, Cochrane CG. (1986). Oxidant injury of cells. *J. Clin Invest.* 77: 1312-1320.

Schurch S, Geiser M, Lee MM, Gehr P. (1999). Particles at the airways interfaces of the lung. *Colloids and surfaces B* 15: 339-353.

Schrand AM, Dai L, Schlager JJ, Hussain SM, Osauza E. (2007). Differential biocompatibility of carbon nanotubes and nano diamonds. *Diamond and related materials* 16: 2118-2123.

Sesko A, Cabot M, Mossman B. (1990). Hydrolysis of inositol phospholipids proceeds cellular proliferation in asbestos related tracheobronchial epithelial cells. *PNAS*. Vol. 87: 7385-7389.

Sharma CS, Sarker S, Peryiyakaruppas A, Barr J, Wise K, Thomas R, Wilson BL, Ramesh GT. (2007). Single walled carbon nanotubes induced oxidative stress in rat lung epithelial cells. *J. Nanosci. Nanotech.* 7: 2466-2472.

Sheppard D. (2006). Transforming growth factor β - A critical modulator of pulmonary and airway inflammation and fibrosis. *Proc. Am. Thorac. Soc.* Vol. 3: 413-417.

Sherman LM. (2008). Carbon nanotubes, lots of potential if the price is right. Plastics technology. *www.ptonline.com/articles/article*

Shi kam NW, Dai H. (2005). Carbon nanotubes as intracellular protein transporters: Generality and biological functionality. J. *Am. Chem. Soc*. 127: 6021-6026.

Shi X, Mao Y, Lambert DN, Saffiotti U, Dalal NS, Vallyathan V. (1994). Silica radical induced DNA damage and lipid peroxidation. *Environ. Health Perspect.* 102, Suppl. 10: 149-154.

Shi X, Sitharaman B, Pham QP, Spicer PP, Hudson JL, Wilson LJ, Tour JM, Raphael RM, Mikos AG. (2007). In vitro cytotoxicity of single wall carbon nanotubes/biodegradable polymer nanocomposites. *Mater. Res*.

Shinohara H. (1997). Lymphatic system of the mouse diaphragm: Morphology and function of the lymphatic system. *Anat. Rec.* 249: 6-15.

Shololenko I, Venediktova N, Bochkareva A, Wilson GL, Alexeyev MF. (2009) Oxidative stress induces degradation of mitochondrial DNA. *Nucleic acids Res*. 37, No. 8: 2539-2548.

Shvedova AA, Kisin ER, Mercer R, Murray AR, Johnson VJ, Potapovich AI, Tyurina YY, Gorelik O, Arepalli S, Schwegler-Berry D, Hubbs AF, Antonini J, Evans DE, Ku BK, Ramsey D, Maynard A, Kagan VE, Castranova V, Barron P. (2005). Unusual inflammatory and fibrogenic pulmonary responses to single walled carbon nanotubes in Mice. *AJP: Lung* 289: L698-L708.

Shvedova AA, Kisin ER, Murray AR, Gordik O, Arepalli S, Castranova V, Young SH, Gao F, Tyurina YY, Oury TD, Kagan VE. (2007). Vitamin E deficiency enhances pulmonary inflammatory response and oxidative stress induced by single walled carbon nanotubes in C57BL/6 mice. *Toxicol. Appl. pharmacol.* 221: 339-348.

Shvedova AA, Kisin ER, Murray AR, Kommineni C, Castranova V, Fadeel B, Kagan VE. (2008). Increased accumulation of neutrophils and decreased fibrosis in the lung of NADPH oxidase deficient C57BL/6 mice exposed to carbon nanotubes. T*oxicol. Appl. Pharmacol*

Shulka A, Timblin C, BeruBe K, Gordon T, McKinney W, Driscoll K, Vacek P, Mossman BT. (2000). Inhaled particulate matter causes expression of nuclear factor (NF) - κB - related genes and oxidant dependent NFκB activation in vitro. *Am. J. Respir. Cell Mol. Biol*. Vol. 23: 182-187.

Sies H. (1993). Strategies of antioxidant defence. *Eur. J. Biochem*. 215: 213-219.

Sies H. (1997). Oxidative stress: oxidants and antioxidants.. *Experimental physiology* 82: 291-295.

Simenova PP, Torriumi W, Kommineni C, Munson AE, Rom WN, Luster MI. (1997). Molecular regulation of IL-6 activation by asbestos in lung epithelial cells: Role of reactive oxygen species. *J. Immunol.* 159: 3921-3928.

Simon HU, Haj-yehia A, Levi-Schaffer F. (2000). Role of reactive oxygen species (ROS) in apoptosis induction. *Apoptosis* 5: 415-418.

Simon H. (2003). Neutrophil apoptosis pathways and their modifications in inflammation. *Immunological reviews*, Vol. 193: 101-103.

Singh SV, Visuanathan PN, Rahman Q. (1990). Interaction between erythrocytes plasma membrane and silicate dusts. *Environ. Health. Perspect*. Vol. 51: 55-60.

Singh R, Pantarotto D, McCarthy D, Chaloin O, Hoebeke J, Parotids CD, Briand JP, Prato M, Bianco A, Kostarelos K. (2005). Binding and condensation of plasmid DNA onto functionalised carbon nanotubes: Towards the construction of nanotube based gene delivery vectors. *J. Am. Chem. Soc.* 127: 4388-4396.

Song L, Meng J, Zhong J, Liu L, Dou X, Liu D, Zhao X, Liuo S, Zhang Z, Xiang Y, Xu H, Zhou W, Wu Z, Xie S. (2006). Human fibrinogen adsorption onto single walled carbon nanotube films. *Colloids and surfaces B: Bio-interfaces* 49: 66-70.

Sorokin SP, Brian JD. (1975). Pathways of clearance in mouse lungs exposed to iron oxide aerosols. *Anatomical Record.* 181 Iss. 3: 581-625.

Sostaric JZ, Riesz P. Sonochemistry and sonodynamic therapy: spin trapping and ESR studies. Virtual Free radical school, society for free radical biology and medicine; *sonochemistry*: 1-27.

Soto KF, Carrasco A, Powell TG, Geirza KM, Murr LE. (2005). Comparative in vitro cytotoxicity assessment of some manufactured nano particulate materials characterised by transmission electron microscopy. *J. Nanoparticle Res.* 7: 145-160.

Spech RW, Winiowski P, Kachel DL, Wright JR, Martin WJ. (2000). Surfactant protein A prevents silica mediated toxicity to rat alveolar macrophages. *AJP: Lung cell Mol. Physiol.* 278: L713-L718.

Spurny KR. (1983). Measurement and analysis of chemically changed mineral fibres after experiments in vitro and in vivo. *Environ Health Perspect*. 51: 343-355.

Stark PE, Hock JB, Farber JL. (1986). Calcium dependent and calcium independent mechanisms of irreversible cell injury is cultured hepatocytes. *J. Biol. Chem.* Vol. 261, No. 7: 3006-3012.

Stäubli A, Boclsterli UA. (1998). The labile Iron pool in hepatocytes: pro-oxidant induced increase in free iron proceeds oxidative cell injury. *AJP: Gastrointest Liver Pathol.* 274: 1031-1037.

Stearns RC, Paulauskis JD, Godlski JJ, (2001). Endocytosis of ultrafine particles by A549 cells. *Am J. Respir. Cell Mol. Biol.* Vol. 24: 108-115.

Storz P, Doppler H, Toker A. (2004). Activation loop phosphorylation control protein kinase D dependent activation of nuclear factor kappa B. *Mol. Pharmacol.* 66: 870-879.
Storz P, Toker A. (2003). NF-KappaB signalling an alternate pathway for oxidative stress response. *Cell Cycle* 2: 9-10.

Stramer BM, Mori R, Martin P. (2007). The inflammation-fibrosis link? A jeyll and hyde role for blood cells during wound repair. *J. Invest Dermatol*. 127: 1009-1017.

Strano MS, Moore VC, Miller MK, Allen MJ, Haroz EH, Kittrell C, Hauge RH, Smalley RE. (2003). The role of surfactant adsorption during ultrasonication in dispersion of single walled carbon nanotubes. *J. Nanosci. Nanotechnol.* 3: 81-86.

Srivastava D, Brenner DW, Schall JD, Ausmann KD, Yu M, Ruoff RS. (1999). Prediction of enhanced chemical reactivity at regions of local conformational strain on carbon nanotubes: Kinky Chemistry. *J. Phys. Chem B* 103: 4430-4337.

Stohs SJ, Bagchi D. (1994). Oxidative mechanisms in the toxicity of metal ions. *Free Rad. Biol. Med*. Vol. 18, No. 2: 321-336

Stone V, Shaw J, Brown DM, MacNee W, Faux SP, Donaldson K. (1998). The role of oxidative stress in the prolonged inhibitory effect of ultrafine carbon black on epithelial cell function. *Toxicol. in vitro*, 12: 649-659.

Stone V, Tuinman M, Vamvakopoulos JE, Shaw J, Brown D, Petteron S, Faux SP, Borm P, MacNee W, Michaelangeli F, Donaldson K. (2000). Increased calcium influx in a monocytic cell line on exposure to ultrafine carbon black. *Eur. Respir. J.* 15: 297-303.

Stramer BM, Martin P. (2007). The inflammation fibrosis link? A Jekyll and Hyde role for blood cells during wound repair. *J. Investigative Dermatology* 127: 1009-1017.

Strieter RM. (2008). What differentiates normal lung repair and fibrosis. *Proc. Am. Thorac. Soc.* Vol. 5: 305-310.

Stuart BO. (1976). Deposition of inhaled particles. *Environ. Health Perspect.* Vol. 55: 369-390.

Summerton, Hoenig S, Butler C, Chavapil M. (1977). The mechanism of haemolysis by silica and its bearing on silicosis. *Experimental and molecular pathology* 26: 113-128.

Swain WA, O'Byrne K, Faux SP. (2004). Activation of p38 MAP kinase by asbestos in rat mesothelial cells is mediated by oxidative stress. *AJP: Lung cell Mol. Physiol.* 286: L859-L865.

Szabo C, Zingarelli B, O'Conner M, Salzman A. (1990) DNA strand breakage, activation of poly(ADP-ribose) synthetase, and cellular energy depletion are involved in the cytotoxicity in macrophages and smooth muscle cells exposed to peroxynitrite. *PNAS Biochemistry* 93: 1753-1758.

Szarka RJ, Wang N, Gordon L, Nation PN, Smith R. (1997). A murine model of pulmonary damage induced by lipopolysaccharide via intranasal instillation. *J. Immunol. Methods* 202: 49-57.

Takano H, Yanagisawa R, Ichinose T, Sadakane, Yoshikawa T, Morita M. (2004). Diesel exhaust particles enhance lung injury related to bacterial endotoxin through expression of pro-inflammatory cytokines, chemokines and intracellular adhesion molecule-1. *Am. J. Respir. Crit. Care Med.* Vol. 165: 1529-1335.

Takizawa H, Ohtoshi T, Kawasaki S, Kohyama T, Desaki M, Kasama T, Kobayashi K, Nakahara K, Yamaoto K, Matsushima K, Kodoh S. (1999). Diesel exhaust particles induce NFκB activation in humans Bronchial epithelial cells in vitro: importance in cytokine transcription. *J. Immunol.* 162: 4705-4711.

Terrones M, Terrones H. (2003). The carbon nanocosmos: novel materials for the twenty first century. *Philos. Transact. A Math Phys Eng. Sci*. 361: 2789-2806.

Thayer AM. (2007). Carbon nanotubes by the metric ton. *Chemical and engineering news*, Vol. 85, No. 46: 29-35.

Thiên-Nga L, Hernadi K, Ljubović E, Garaj S, Forró L. (2002). Mechanical purification of single walled carbon nanotube bundles from catalytic particles. *Nanoletters* Vol. 2, No. 12: 1349-1352.

Thompson AB, Robbins RA, Romberger DJ, Sisson JH, Spurson JR, Teschler H, Rennard SI. (1995). Immunological functions of the pulmonary epithelium. *Eur. Respir. J.* 8: 127-149.

Tian F, Cui D, Schwarz, Estrada GG, Kobayashi H. (2006). Cytotoxicity of single wall carbon nanotubes on human fibroblasts. *Toxicol. In vitro*.

Toews GB. (2001). Cytokines and the lung. *Eur. Respir. J.* 18, Suppl. 34: 3s-17s.

Tonks A, Morris RHK, Price AJ, Thomas AW, Jones KP, Jackson SK. (2001). Dipalmitoylphosphatidylcholine modulates inflammatory functions of monocytic cells independently of mitogen activated protein kinases. *Clin. Exp. Immunol.* 124: 86-94.

Topinka J, Loli P, Georadis P, Dusinska M, Hurbankova M, Kovacikova Z, Volkovova K, Kazimirova, Marancokova M, Tatrai E, Oesterle D, Wolff T, Kyrtopopoulos SA. (2004). Mutagenesis by asbestos in the lung of Lambda-Lac transgenic rats. *Mutation research* 553: 67-78.

Tosis D, Tagmatarchis N, Geagahilas V, Prato M. (2003). Soluble carbon nanotubes. *Chem Eur. J.* 9: 4000-4008.

Tosis D, Tagmatarchis N, Bianco A, Prato M. (2006). Chemistry of carbon nanotubes. *Chem. Rev.* 106:1105-1136.

Tours GB. (2001). Cytokines and the lung. *Eur. Respir. J.* 18, Suppl. 34: 3s-17s.

Tsang SC, Harris PJF, Green MLH. (1993). Thinning and opening of carbon nanotubes by oxidation using carbon dioxide. *Nature* 362: 520-522.

Tsuda A, Stringer BK, Mijailovich SM, Rogers RA, Hamada K, Gray ML. (1999). Alveolar cell stretching in the presence of fibrous particles induced Interleukin 8 responses. *J. Respir. Cell. Mol. Bio.* 21: 455-462.

Ungar T, Gubicza J, Ribarik G, Pantea C, Zerda Waldek T. (2002). Micro structure of carbon blacks determined by X-ray diffraction profile analysis. *Carbon* 40: 929-937.

Upadhyay D, Kamp DW. (2003). Asbestos induced pulmonary toxicity: Role of DNA damage and apoptosis. *Exp. Biol. Med.* 228: 650-659

Urbanski NK, Beresewicz A. (2000). Generation of hydroxyl radical initiated by interaction of Fe2+ and Cu+ with di-oxygen; comparison with Fenton chemistry. *Acta biochemica polonica* Vol. 47: 951-962.

Usai Y, Aoki K, Narita N, Nakanura I, Nakamura K, Ishigaki N, Yamazaki H, Horiuchi H, Kato H, Taruta S, Ahm Kim Y, Endo M, Sato N. (2008). Carbon nanotubes with high bone - tissue compatibility and bone formation acceleration effects. *Small* 4, No. 2: 240-246.

Vaisman L, Wagner HD, Marom G. (2007). The role of surfactant in dispersion of carbon nanotubes. Advances in colloid interface science.

Valenti LE, Fiorito PA, Gariva CD, Giacomelli CE.(2007). The adsorption-desorption process of bovine serum albumin on carbon nanotubes. *J. Colloid and Interface science* 307: 349-356.

Valko M, Morris H, Cronin MTD. (2005). Metals. Toxicity and oxidative stress. *Current medicinal chemistry* 12: 1161-1208.

Van der Schans CP. (2007) Bronchial mucus transport. *Respir. Care* 52: 1150-1156.

Verrecchia F, Mauviel A. (2007). Transforming growth factor β and fibrosis. *World J. Gastroenterol.* 13: 3056-3062.

Vincent JH, Jones AD, Johnston AM, McMillin C, Bolton RE, Courie H. (1987). Accumulation of inhaled mineral dust in the lung and associated lymph nodes: implications for exposure and dose in occupational lung disease. *Ann. Occup. Hyg.* Vol. 31, No. 3: 375-39

Vix-Guterl C, Dentzer J, Ehrburger P, Mètènier K, Bonnamy S, Beguin F. (2001). Surface properties and micro-texture of catalytic multiwalled carbon nanotubes. *Carbon* 39: 287-324.

Vorob e'v-Desyatovski NV, Ibraginova RI, Gordeev DK, Nikolaev BP. (2006). Chemical processes on active carbon surface: A new example of nitrogen fixation. *Russian Journal of General chemistry* Vol. 76, No. 6: 946-954.

Wallace WE, Keane MJ, Murry DK, Chisholm WP, Maynard AD, Ong TM. (2007). Phospholipid lung surfactant and nanoparticle surface toxicity: Lessons from diesel soots and silicate dusts. *J. Nanoparticle research* 9: 23-38.

Wallace EJ, Sansom MSP. (2007). Carbon nanotube/detergent interactions via coarse grained molecular dynamics. *Nanoletters* Vol. 7, No. 7: 1923-1928.

Warheit DB, Webb TR, Colvin VL, Reed KL, Sayes CM. (2007). Pulmonary bioassay studies with nanoscale and fine quartz particles in rats: toxicity is not dependent upon particle size but on surface characteristics. *Toxicol Sci.* 95: 270-280.

Watt PCP, Fearson PK, Hsu WK, Billingham NC, Kroto HW, Walton DRM. (2003). Carbon nanotubes as polymer antioxidants . *J. Mat. Chem.* 13: 491-495.

Weihel ER. (2009). What makes a good lung. *Swiss Med. Wkly.* 139: 27-28.

Wellmann j, Weiland SK, Neiteler G, Klein G, Straif K. (2006). Cancer mortality in German carbon black workers 1976-1998. *Occup. Environ Med*. 63: 513-521.

Wenweleers W, Vlasov II, Goovaerts E, Obraztsova ED, Lobach AS, Bouwen A. (2004). Efficient isolation and solubilisation of pristine single walled nanotubes in bile salt Micelles. Adv. Funct. Mater. 14, No. 11: 1105-1112.

Wick P, Manser P, Limbach LK, Dettlaf-Weglikowska U, Krumeich F, Roth S, Stark WJ, Bruinink A. (2007). The degree and kind of agglomeration affect carbon nanotube toxicity. *Toxicol. Lett.* 168: 121-131.

Wilson MR, Lightbody JH, Donaldson K, Sales J, Stones V. (2002). Interactions between ultrafine particles and transition metals in vivo and in vitro. *Toxicol. Appl. Pharmacol.* 184: 172-179.

Wilhelm D, Bender K, Knebel A, Angel P. (1997). The level of intracellular glutathione is a key regulator for the induction of stress activated signal transduction pathways including Jun-N terminal protein kinases and p38 kinase signalling by alkylating agents. *Mol. Cell. Biol*, Vol. 17, No. 8: 4792-4800.

Williams GT, Williams WJ. (1983). Granulomatous inflammation - a review. J. *Clin. Pathol.* 36: 723-733.

Win KY, Feng S. (2005). Effects of particle size and surface coating on cellular uptake of polymeric nanoparticles for oral delivery of anti-cancer drugs. *Biomaterials* 26: 2713-2722.

Witzmann FA, Monteirs-Riviere NA. (2006). Multiwalled carbon nanotube exposure alters protein expression in human keratinocytes. *Nanomed. Nanotech. Biol. Med.* 2: 158-168.

Wright JR. (1997). Immunomodulatory functions of surfactant. *Phys. Rev.* Vol. 77, No. 4: 931-954.

Wu J, Liu W, Koenig K, Idell S, Broaddus VC. (2000). Vibronectin adsorption to chrysotile asbestos increases fibre phagocytosis and toxicity for mesothelial cells. *Am J. Lung Cell Mol. Physiol.* 279: L916-923.

Wynn TA. (2008). Cellular and molecular mechanisms of fibrosis. *J. Pathol.* 214: 199-210.

Xia T, Kovochich M, Brant J, Hotze M, Sempf J, Oberley T, Sioutas C, Yeh JI, Wiesner MR, Nel AE. (2006). Comparison of the abilities of ambient and manufactured nanoparticles to induce cellular toxicity according to an oxidative paradigm. *Nanoletters* Vol. 6, No. 8: 1794-1807.

Yan L, Zhongzheng L, Kai W, Xu Y. (2007). The latent toxic effects of carbon nanotubes serving as bio-medicine. *IEEE*: 342-345.

Yamawaki H, Iwai N. (2006). Mechanisms underlying nanosized Air-pollution mediated progress of atherosclerosis carbon black causes cytotoxic injury and inhibits cell growth in vascular endothelial cells. *Circ J*. 70: 129-140.

Yang K, Arealroli JJ, Abraham E. (2003). Early attractions in neutrophil activation are associated with outcome in acute lung injury. *Am. J. Crit. Care Med.* Vol. 167: 1567-1574.

Yates LL, Gorecki DC. The nuclear factor kappa B (NFkB): From a versatile transcription factor to a ubiquitous therapeutic target. *Acta Biochimica Polonica* Vol 53, No. 4: 651-662

Ye J, Shi X, Jones X, Rojanasakul Y, Cheng N, Schwegler-Berry D, Baron P, Deye GJ, Castranova V. (1999). Critical role of glass fibre length in TNFa production and transcription factor activation in macrophages. *AJP: Lung cell. Mol. Physiol.* 276:

Yeh HC, Phalen RF, Raabe OG. (1976). Factors influencing the deposition of inhaled particles. *Environ Health Perspect.* 15: 147-156.

Yehia HN, Draper RK, Mikorgak C, Walker EK, Baja P, Musselman IH, Daigreport MC, Dieckmann GR, Pantano P. (2007). Single walled carbon nanotube interactions with HeLa cells. *Journal of nanobiotechnology* 5: 8.

Yokomichi H, (2004). Changes in electron spin resonance of carbon nanotubes by thermal annealing. *Vacuum* 74: 677-681.

Yokoyama A, Sato Y, Nodasaka Y, Yamamoto S, Kauasaki T, Shindoh M, Kohgo Y, Akasako T, Uo M, Watari F, Tohjii K. (2005). Biological behaviour of hat stacked carbon nanofibres in the subcutaneous tissue in rats. *Nanoletters* Vol. 5, No. 1: 157-161.

Yu BP. (1994). Cellular defences against damage from reactive oxygen species. *Physiological reviews* Vol. 74, No. 1: 139-155.

Yu CP, Ding YJ, Zhang L, Oberdorster G, Mast RW, Maxim V, Utell MJ. (1996). A clearance model of refactory ceramic fibres (RCF) in the rat lung including fibre dissolution and breakage. *Journal of aerosol science* Vol. 27, No. 1: 151-159.

Yuan C, Zhao D, Liu A, Ni J. (1995). A NMR study of the interaction of silica with dipalmitoylphosphatidylcholine liposomes. *Journal of colloid interface science* 172: 536-538.

Zalma R, Bonneau L, Guignard J, Pezerat H, Jaurand MC. (1987). Formation of oxy radicals by reduction arising from surface activity of asbestos. *Can. J. Chem.* 65: 2238-2241.

Zauner W, Farrow NA, Haines AMR. (2000). In Vitro uptake of polystyrene microsphere: effect of particle size, cell line and cell density. *Journal of colloid release* 71: 39-51.

Zanella CL, Timblin CR, Cummins A, Jung M, Goldberg J, Raabe R, Tritton TR, Mossman BT. (1999). Asbestos induced phophorylation of epidermal growth factor receptor is linked to c-fos and apoptosis. *AJP: Lung cell Mol. Physiol.* 21, 271: L684-L693

Zeidler-Erdely PC, Calhoun WJ, Ameredes BT, Clark MP, Deye GJ, Baron P, Jones W, Blake T, Castranova V. (2006). In vitro cytotoxicity of Manville code 100 glass fibres: Effect of fibre length on human alveolar macrophages. *Part. Fibre. Toxicol*, 3: 5.

Zhang Y, Shi Z, Gu Z, Iijima S. (2000). Structure modification of single walled carbon nanotubes. *Carbon* 38: 2055-2059.

Zhang J, Zou H, Qing Q, Yang Y, Li Q, Liu Z, Guo X and Du Z. (2003). Effect of chemical oxidation on the structure of single walled carbon nanotube spectra. *J. Phys. Chem. B.* 107: 3712-3718.

Zhang Y, Chen F. (2004). Reactive oxygen species (ROS). Trouble makers between Nuclear factor κB (NFκB) and C-Jun NH terminal kinase (JNK). *Cancer research* 64: 1902-1905.

Zhang Z, Berg A, Levanon H, Fessenden, Meissel D. (2003). On the interactions of free radicals with Gold nanoparticles. *J. Am. Chem. Soc.* 125: 7959-7963.

Zheng M, Diner BA. (2004). Solution Redox chemistry of carbon nanotubes. *Am. Chem. Soc.* 126: 15490-15494.

Zheng M, Jagota A, Semke ED, Diner BA, Mclean RS, Lustig SR, Richardson RE, Tassi NG. (2003). DNA assisted dispersion and separation of carbon nanotubes. *Nature materials*, Vol. 2: 338-342.

Zhou MJ, Petty HR. (1993). Superoxide mediated lysis of erythrocytes: The role of colloid osmotic forces. *J. Cellular physiology* 157: 555-561.

Zhu S, Manuel M, Tanaka S, Choe N, Kagan E, Mataton S. (1998). Contribution of reactive oxygen and reactive nitrogen species to particulate induced lung injury. *Environ. Health Perspect*., Vol. 106, Suppl. 5: 1157-1163.

Zhu Y, Ran T, Li Y, Guo J, Li W. (2006). Dependence of the cytotoxicity of multiwalled carbon nanotubes on the culture medium. *Nanotechnology* 17: 4668-4674.

Zhu L, Chang WD, Dai L, Hong Y. (2007). DNA damage induced by multi walled carbon nanotubes in mouse embryonic stem cells. *Nanoletters* Vol. 7, No. 12: 3592-3597.

Appendix

Appendix I

A table of some of the surfactants and solvents used or tested in order to solubilise carbon nanotubes. The aqueous solubility of CNT depends on the type of functional groups or molecules attached or associated with its surface, the water solubility of the functional groups, the extent of functionalisation or modification of the tubes surface and the strength of interaction between the functional groups and the CNT. The strength of interactions also determines the stability of the nanotube dispersion. It is worth noting however that there is no definition or standard for CNT solubility. Some methodologies achieve dispersion without sedimentation by using a limited amount of CNT whilst other procedures separate insoluble from soluble CNT by means of centrifugation or filtration. Differences in the speed and duration of centrifugation result in variations in CNT solubility's. Solubility's and solution concentrations of CNT have to be considered within the context of the conditions applied to achieve them and the application requirements (Lin et al 2004).

Authors	Journal	Dispersent
Zhao & Johnson		12 base pair DNA segment
Lin et al	**J. Mater. Chem.** 2004, 14: 527-541 (Review)	Aqueous buffers pH 3-12 foroxidised CNT
Lin et al, Moore et al, Islam et al	**J. Mater. Chem.** 2004, 14: 527-541 (Review), **Nano letters** 2003, Vol. 3, No. 10: 1379-1382, **Nano letters 2003**, Vol. 3, No. 2: 269-273.	Sodium dodecyl sulphate
Lin et al, Wenseleers et al	**J. Mater. Chem.** 2004, 14: 527-541 (Review), **Adv. Funct. Mater.** 2004, 14, No. 11: 1105-1112	Triton X-100
Lin et al, Wenseleers et al, Moore et al, Paredes & Burghard, Islam et al	**J. Mater. Chem.** 2004, 14: 527-541 (Review), **Adv. Funct. Mater.** 2004, 14, No. 11: 1105-1112, **Nano letters** 2003, Vol. 3, No. 10: 1379-1382, **Langmuir** 2004, 20: 5149-5152, **Nano letters** 2003, Vol. 3, No. 2: 269-273	Sodium dodecyl benzene sulphate
Lin et al, Moore et al, Islam et al	**J. Mater. Chem.** 2004. 14: 527-541 (Review), **Nano letters** 2003, Vol. 3, No. 10: 1379-1382, **Nano letters 2003**, Vol. 3, No. 2: 269-273	Dodecyltrimethyammonium bromide
Lin et al, Wenseleers et al, O' Connell et al	**J. Mater. Chem.** 2004, 14: 527-541 (Review), **Adv. Funct. Mater.** 2004, 14, No. 11: 1105-1112, **Chem. Phys. Lett. 2001**, 342: 265-271	poly(vinylpyrrolidone
Lin et al, O'Connell et al	**J. Mater. Chem.** 2004. 14: 527-541 (Review), **Chem. Phys. Lett.** 2001, 342: 265-271.	Poly styrene sufonate
		Nafion
Lin et al, Islam et al	**J. Mater. Chem** 2004, 14: 527-541 (Review), **Nano letters** 2003, Vol. 3, No. 2: 269-273	Dextrin
Lin et al, Dodziuk et al	**J. Mater. Chem.** 2004, 14: 527-541 (Review), **Chem. Commun** 2003: 986-987	γ-Cyclodextrin
		Starch
Lin et al, Furtado et al, Bandyopadhyaya et al	**J. Mater. Chem.** 2004, 14: 527-541 (Review), **J. AM. Chem Soc.** 2004, 14: 14850-14857, **Nano letters** 2002, Vol. 2, No. 1: 25-28	Gum Arabic
Lin et al	J. Mater. Chem. 2004. 14: 527-541 (Review)	nano-1
		poly(T) (30 mer)
		PSS-PAA
		$H_2N(CH_2)_2\ SO_3H$
Lin et al, Pompeo & Resasco	**J. Mater. Chem.** 2004, 14: 527-541 (Review), **Nano letters** 2002	Glucosamine
		2-Aminomethyl-18-crown-6 ether
		PEG_{1500N} Thermal reaction
		PEG_{1500N} Diimide coupling
		PEG_{1500N} Acylation-amidation
		PVA Diamide coupling
		KOH
Furtado et al, Ausman et al 2000	**J. Am. Chem. Soc.** 2004, 126: 6095-6105, **J. Phys. Chem B** 2000, Vol. 104, No. 38: 8911-8915	N,N-diethylformamide
Furtado et al, Ausmann et al 2001	**J. Am. Chem. Soc.** 2004, 126: 6095-6105, **J. Phys. Chem B** 2000, Vol. 104, No. 38: 8911-8916	N-methyl-2-pyrrolidone
Shvartzman-Cohen et al	**J. Am. Chem. Soc.** 2004, 126: 14850-14857	Pluronic diblock copolymers
		Pluronic triblock copolymers
		Mn Polystyrene 1900 acrylate

Authors	Journal	Dispersent
Huang et al, Jiang et al	**Nano Letters** 2002, Vol.2, No. 4: 311-312, **J. Mater. Chem** 2004, 14: 27-39	Bovine serum albumin by diimide activated amidation
		deoxycholic acid
		taurdeoxycholic acid sodium salt
		cetyltrimethylammonium bromide
		cetylpyridinium chloride monohydrate
		Brij 35
		Tween-20
		Tween-40
		Tween-60
		Tween-80
		Tween-85
		Dioctyl sulfosuccinate sodium salt
		d-BIGCHAP
		Sodium pyrenebutyrate
Kim et al	**J. Am. Chem. Soc.** 2003, 125: 4426-4427	Amylose
Moore et al	**Nano letters** 2003, Vol. 3, No. 10: 1379-1382	Sodium dodecyl sulfonate
		Sarkosyl
		TREM
		PSS-70
		CTAB
		Brij 78
		Brij 700
		Triton X-405
		PVP-1300
		EBE
		Pluronic P103, 104 & 105
		Pluronic F 108, 98, 68, 127, 87, 77 & 85
Ausman et al 2000	**J. Phys. Chem. B** 2000, Vol. 104, No. 38: 8911-8915	Hexamethylphosphoramide
		Cyclopentanone
		Tetramethylenesulfoxide
		ε-caprolactone
Zheng et al, Nakashima et al	**Nat. Mater.** 2003, Vol. 2: 338-342, **Chem. Lett.** 2003, Vol. 32, No. 5: 456-457.	DNA
Islam et al	**Nano letters** 2003, Vol. 3, No. 2: 269-273	Sodium octylbenzene sulfonate
		Sodium benzoate
		Sodium butyl benzene sulfponate
		Polystyrene-Poly ethylene oxide diblock polymer
Jiang et al	**J. Mater. Chem.** 2004, 14: 37-39	Ferritin by diimide activation

Appendix II

The unique properties of carbon nanotubes in particular their electrical and mechanical properties make these molecules attractive candidates in diverse nano-technological applications. This is hampered by their lack of solubility and difficulty of manipulation in both aqueous and organic solvents. Through chemical reactions of carbon nanotubes it is possible to make them more soluble for integration into aqueous, organic, biological or composite systems. The principal methods of modification can be grouped into covalent attachment of functional groups, non-covalent adsorption to or wrapping molecules around the nanotube or endohedral filling of their cores (Tasis et al 2006). Collated below are some of the chemical reactions that result in covalent functionalisation of CNT taken and summarised from the review of carbon nanotube chemistry by Tasis et al (2006). Broad reaction categories are given in bold type with specific examples written beside pictorial reaction mechanisms.

Fluorination

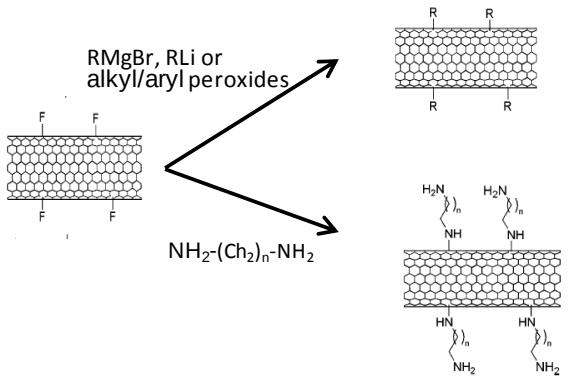

Cyclo-addition reactions

Dichlorocarbene

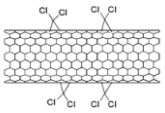

Carbene addition

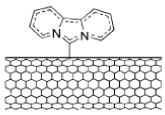

Nitrene addition

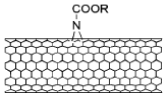

Fluoroalkyl radical addition

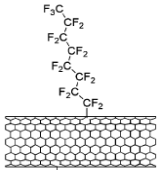

Nitrene addition

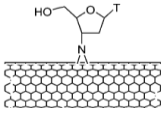

1,4-Dipolar cycloaddition of azomethine ylides

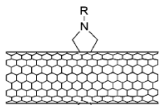

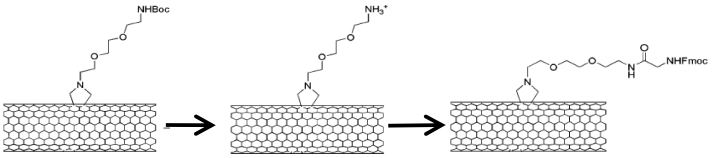

Addition of ammonium groups

1,3-Dipolar cycloaddition of nitrile imines

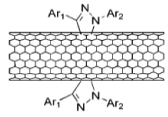

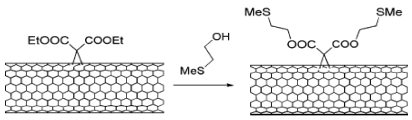

Bingel reaction (cyclopropanation) reaction resulting in a thiolated product

Radical Additions

Derivation by reduction of aryl diazonium salts

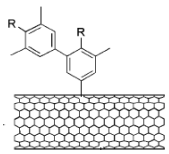

Reductive coupling of aryl diazonium salts

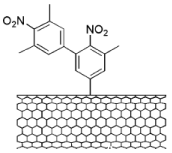

Oxidative coupling of aromatic amines

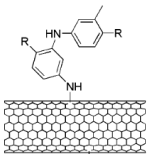

Addition of carboxyalkyl radicals

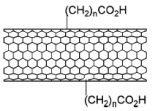

Hydrogenation – functionalisation of carbon nanotubes with hydrogen by reducing pristine CNT with Li and methanol in liquid ammonia or by proton bombardment.

Electrophilic addition reactions – Functionalisation of CNT with chloroform was reported in the presence of a Lewis acid.

Addition of inorganic compounds – reaction of CNT side walls with osmium tetraoxide under UV irradiation. Nanotube metal complexes have been formed following the reaction of CNT with trans-$IrCl(CO)(PPh_3)_2$. Metal coordination with CNT side walls appears mainly to occur at defect sites .

Ozonolysis – SWCNT have been subjected to ozonolysis resulting in the formation of CNT-ozonides.

Mechanochmical functionalisation – Ball milling MWCNT in reactive atmospheres produces short tubes functionalised with various groups. In a similar process milling SWCNT with potassium hydroxide resulted in CNT covered in hydroxyl groups.

Plasma activation – Treatment of CNT with aldehyde plasma followed by attachment of aminodextran linkages to the attached functional groups.

Nucleophilic addition – Solvent free amination of five membered rings of the graphitic network.

Polymer grafting – Polymer attachment to CNT surfaces provides one method for solubilising CNT into a wide range of solvents even at low levels of functionalisation. In the "grafting to" process a polymer with a specific molecular weight is synthesised followed by end group modification and attachment to the CNT surface. In the "grafting from" methodology polymer precursors are immobilised on the surface of nanotubes followed by growth of the polymer in the presence of monomeric species.

Grafting to approach for attachment of polystyrene to the surface of a CNT

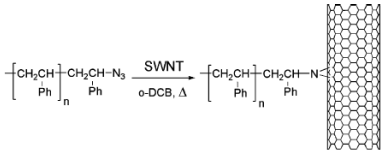

The grafting from process of polymer attachment to CNT surfaces, polystyrene chains are attached to CNT by anionic polymerisation.

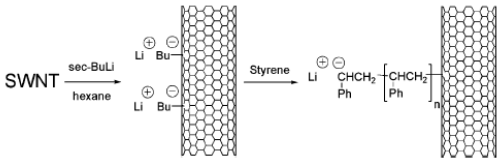

Defect site chemistry – Amidation & Esterification reactions

Acid purification of carbon nanotubes decorates the side walls and ends with oxygenated functionalities largely consisting of carboxylic acid and carbonyl groups. These act as anchoring sites for the attachment of other functional groups e.g. Attachment of alkylamines through acylation reactions.

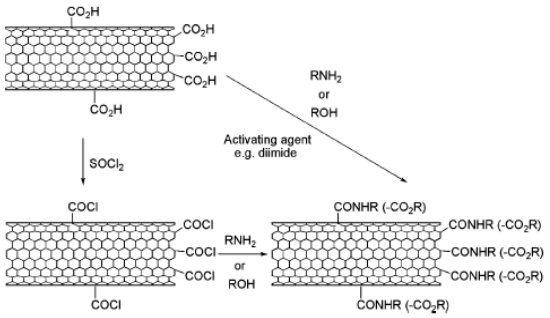

Appendix III

(A) The concentration of metals in particle and fibre samples determined by ICP-AES given in micrograms per gram of sample analysed. **(B)** The concentration of soluble metals extracted from particle and fibre samples given in micrograms per gram of sample analysed.

A

Metal Concentration (µg/g)										
Sample	Cd	Co	Cr	Cu	Fe	Mn	Ni	Ti	V	Zn
Carbon black	<0.1	<0.1	0.8	16.2	58.6	0.7	<0.1	0.8	0.3	23.7
Nano long	<0.1	44.1	<0.1	69.4	11600	12.6	<0.1	3.9	<0.1	30.3
Nano short	<0.1	5.7	23.4	105.2	17600	20.8	53.2	4.4	<0.1	32.2
Japanese MWCNT	<0.1	114.5	10	27.7	3426.9	9.2	<0.1	5.4	5.2	19.6
Diesel exhaust particles	<0.1	1.4	3.2	20.2	430	4	<0.1	4.3	0.6	359.5
Long Amosite	0.1	1.2	2.8	25.3	354.7	5.6	<0.1	35.4	0.1	21.7
Short Amosite	0.8	203.6	52.1	81.8	18140	1369	<0.1	181.1	1	118
DQ12	2	1	29.6	55.2	27910	2496	2.8	73.9	<0.1	39.3
Rutile TiO_2	0.2	<0.1	3	27	120.7	<0.1	<0.1	18770	23.1	365.3
Anatase TiO_2	0.1	<0.1	3.2	22.2	106.4	0.7	<0.1	11810	14.2	246.8

B

Metal Concentration (µg/g)										
Sample	Cd	Co	Cr	Cu	Fe	Mn	Ni	Ti	V	Zn
Carbon black	<0.1	0.3	<0.1	0.2	0.1	<0.1	2.6	0.2	0.1	0.1
Long MWCNT	<0.1	<0.1	<0.1	1	13.4	<0.1	5	0.7	<0.1	7.5
Short MWCNT	<0.1	3.7	0.2	5.1	7.9	0.4	9.7	0.7	<0.1	5.5
Japanese MWCNT	<0.1	1.9	0.1	1.2	<0.1	<0.1	6.2	0.4	0.8	0.7
Diesel exhaust particles	<0.1	0.5	<0.1	1	3.1	<0.1	4.2	<0.1	<0.1	8.8
Long Amosite	<0.1	1.4	3.4	5.2	853.7	104.8	5.1	2	<0.1	27.3
Short Amosite	<0.1	2.1	<0.1	3.1	574	36.3	18.4	31.5	3.1	10.5
DQ12	<0.1	0.7	0.3	1	2.7	0.2	4.8	2	<0.1	5.7
Rutile TiO_2	<0.1	0.6	0.1	1.8	0.9	<0.1	<0.1	2943.2	3.8	23.8
Anatase TiO_2	<0.1	0.3	<0.1	<0.1	<0.1	<0.1	2.4	6.7	<0.1	3.1

Transition metals analysed for by ICP-AES in a panel of particles and fibres

Cd – cadmium

Co – Cobalt

Cr – Chromium

Cu – Copper

Fe – Iron

Mn – Manganese

Ni – Nickel

Ti – Titanium

V – Vanadium

Zn – Zinc

Appendix IV - Reagents and buffers

RT-PCR

All reagents for RT-PCR were supplied by either Sigma-Aldrich UK or Promega, southhampton, UK.

Sterile Rnase free water (DRPC)

0.2% (w/v) diethyl pyricarbonate (DEPC) in distilled/de-ionised water. Solution prepared then autoclaved to inactivate DEPC.

RT-Buffer	PCR mix	GoTaq PCR* mix	5 x loading dye
10µl 5x M-MLV reaction buffer	100µl 10x storage buffer	200µl Go-taq 5x buffer	10mM Tris-HCL (pH 7.5)
5µl 100mM DTT	100µl $MgCl_2$ (final conc. 2.5mM)	100µl $MgCl_2$ (final conc. 2.5mM)	15% Fiscoll® 400
5µl 100µg/ml oligo(dT) primer	20µl dNTPs	20µl dNTPs	0.03% bromophenol blue
4µl 10mM dNTPs	20µl primer up	3µl primer up	0.03% xylene cyanol FF
0.5µl Rnasin	20µl primer reverse	3µl primer reverse	0.4% orange G
0.5µl M-MLV reverse transcriptase	740µl sterile H_2O	674µl sterile H_2O	

Preparation of cDNA

2µg RNA made up to a final volume of 25µl DEPC-ddH_2O and mixed with 25µl of the RT-Buffer reaction mix (number of volumes listed below multiplied by the number of samples). Samples incubated for 60-90 minutes at 37°C to allow cDNA synthesis then reaction stopped by heating to 90°C for 10 minutes.

Preparation for PCR

40µl PCR reaction mix (or Go-Taq PCR reaction mix) mixed with 5µl cDNA (3µl cDNA for housekeeping gene) and 2µl *Taq* DNA polymerase (0.25µl GoTaq polymerase).

* GoTaq PCR products supplied by Promega (UK) to replace previous Taq DNA polymerase (M1865).

Resolution of PCR products

5X Tris buffered EDTA, pH 8.3 (TBE):

0.45M Trizma Base

0.45M Boric acid

10mM EDTA

1.5% Agarose gel in 1x TBE:

1.5% seaKen LE agarose (Bio-Whittaker molecular applications, UK) in 1X TBE with 0.5µg ml^{-1} Ethidium bromide or 1:10000 dilution of ethidium bromide nucleic acid alternative Gel Red Nucleic acid stain. SeaKem agarose and TBE mixed and microwaved together (without ethidium bromide) for abount four minutes until agarose completely dissolved. Gel mix allowed to cool (but still liquid) and then ethidium bormide added. Gel red stain could be added whilst Gel mixture still molten.

ELISA

Substrate buffer (NIBSC)

Citric acid 3.65g

$Na_2HPO_4.7H_2O$ 8.94g

Reagent diluents

1x TBS (Tris buffered saline)

0.05% Tween 20

0.1% BSA

Glutathione Assay

0.1M phosphate buffer with 5mM EDTA (pH 7.5) (KPE buffer):

Solution A: 6.8g KH_2PO_4 (BDH) in 500ml dH2O

Solution B: 8.5g K_2HPO_4 (BDH) or 11.4g $K_2HPO_4.3H_2O$ (BDH) in 500ml dH2)

KPE Buffer: 16ml solution A added to 84ml solution B, adjusted to pH 7.5 prior to 0.327g EDTA added.

Extraction buffer – 0.1% Triton X-100 (Sigma)/0.6% sulfosalicylic acid (SSA) (Sigma):

20µl triton X100 and 120mg SSA to 20ml KPE buffer. Extraction buffer prepared immediately prior to use and made fresh each time.

NF-κB Staining

Formalin (Sigma):

3% formalin solution prepared by mixing 1.5ml 40% formalin to 18.5ml PBS

Ammonium Chloride (NH_4Cl) (Sigma):

50mM Ammonium chloride prepared by dissolving 0.5349g in 100ml, 0.1M ammonium chloride solution then diluted with dH_2O to 50mM.

Bovine serum albumin (Sigma):

0.2% solution prepared by dissolving 0.2g BSA in 100ml PBS

Antibodies:

Primary antibody: Rabbit polyclonal anti NFκB p50 subunit diluted 1:200 to working concentration in 0.2% BSA.

Secondary antibody: Anti-rabbit FITC labelled IgG diluted 1:500 in 0.2% BSA.

Mowiol mounting medium:

Mowiol 4-88 (clabiochem 475904) 4.8g

Glycerol 12g

dH2O 12ml

0.2M Tris pH 8.5 24ml

Glycerol place in 50ml centrifuge tube and mowiol added. Mixture stirred thoroughly before distilled water added and solution left to stand for two hours at room temperature. Tris (pH 8.5) added and solution mixture incubated at 53°C until mowiol dissolved with occasional stirring. Solution then centrifuged at 4000-5000rpm for 20 minutes to clarify with the supernatant transferred to 15ml centrifuge tubes. Mounting medium stored at -20°C, at this temperature it would remain viable for up to one year, once defrosted medium is stable for up to one month at room temperature.

Appendix V

A549 cells exposed for four hours to a panel of particles, including LMWCNT and SMWCNT at 10 and 100µg/ml. Cells were cultured on autoclaved glass cover-slips until 70% confluent, serum staved and then exposed to particles for the requisite time. Following exposure cells were washed in pre-warmed PBS to remove particles then stained with Eosin and haematoxalin. Images were captured using Pro-captureQ software at a magnification of x20.

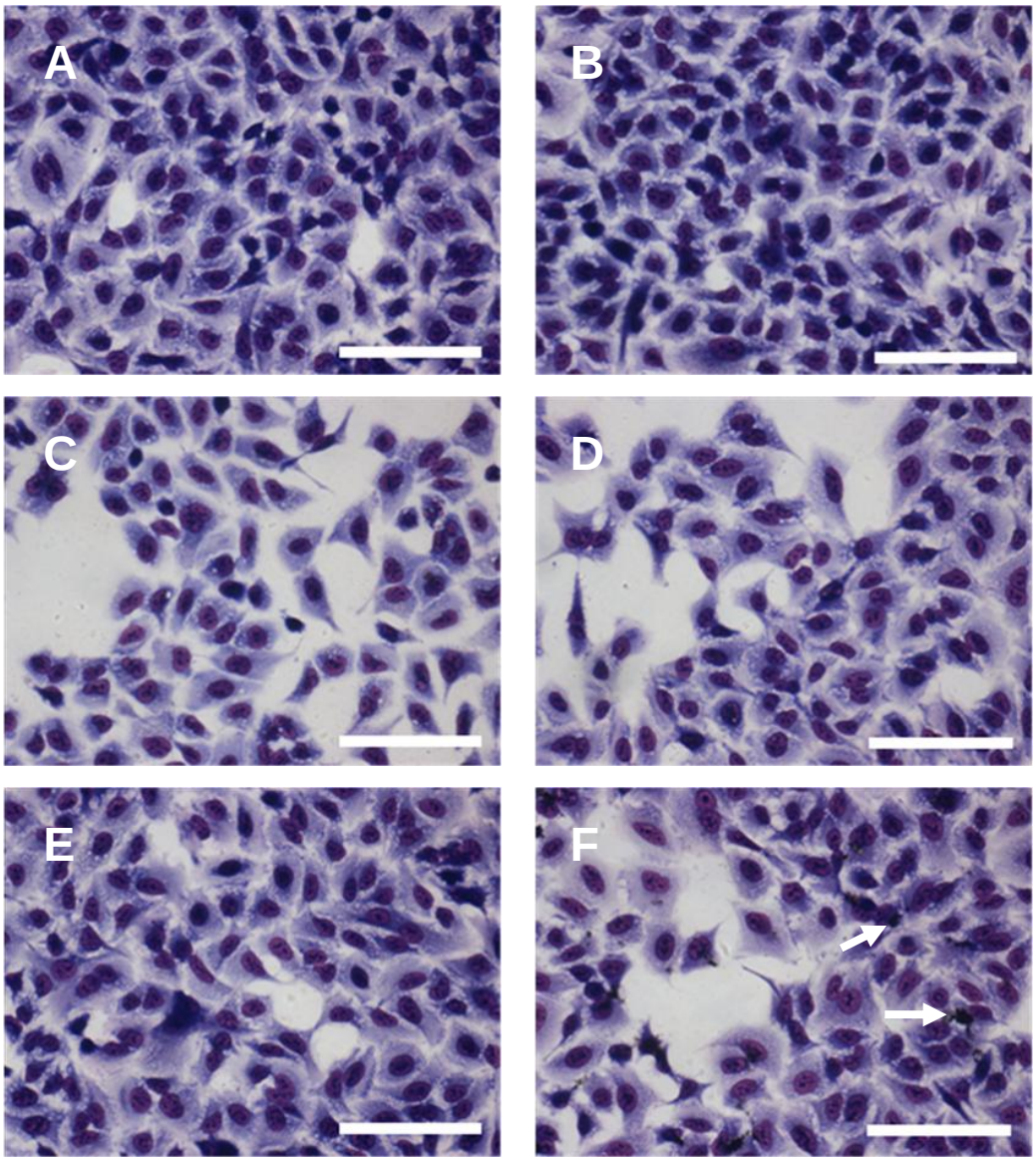

A549 cells stained with Eosin and haematoxalin fours after treatment with a range of particles including MWCNT at a concentration of 10 or 100µg/ml. (A) Untreated A549 cells. **(B)** A549 cells four hours after treatment with TNFα. **(C)** A549 cells after four hours treatment with 10µg/ml DQ12. **(D)** A549 cells following exposure to 100µ/ml DQ12. **(E)** A549 cells after treatment with 10µg/ml LMWCNT. **(F)** A549 cells following treatment with 100µg/ml. White arrows indicate examples of larger LMWCNT aggregates. Scale bars represent 100µm.

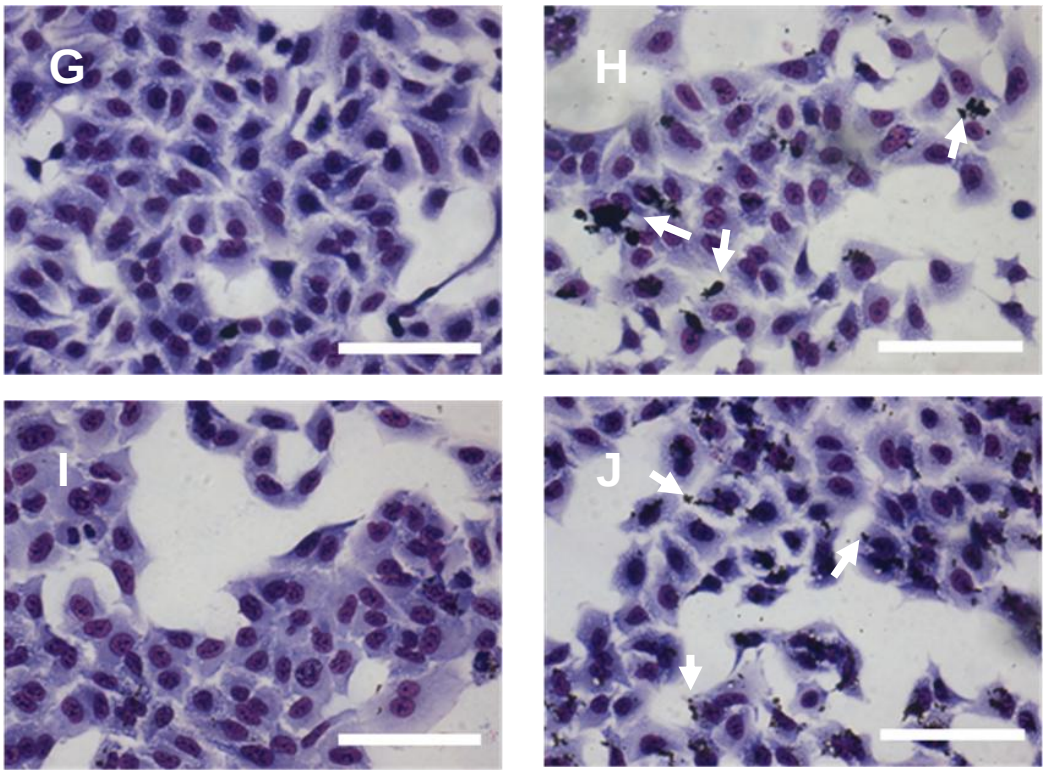

A549 cells stained with Eosin and haematoxalin fours after treatment with a range of particles including MWCNT at a concentration of 10 or 100µg/ml. (G) A549 cells treated with 10µg/ml SMWCNT. **(H)** A549 cells following four hours treatment with 100µg/ml SMWCNT, white arrows indicate representatives of bigger MWCNT aggregates. **(I)** A549 cells following treatment with 10µg/ml TiO_2. **(J)** A549 cells after treatment with 100µg/ml TiO_2, white arrows point to examples larger TiO_2aggregates. Scale bars represent 100µm.

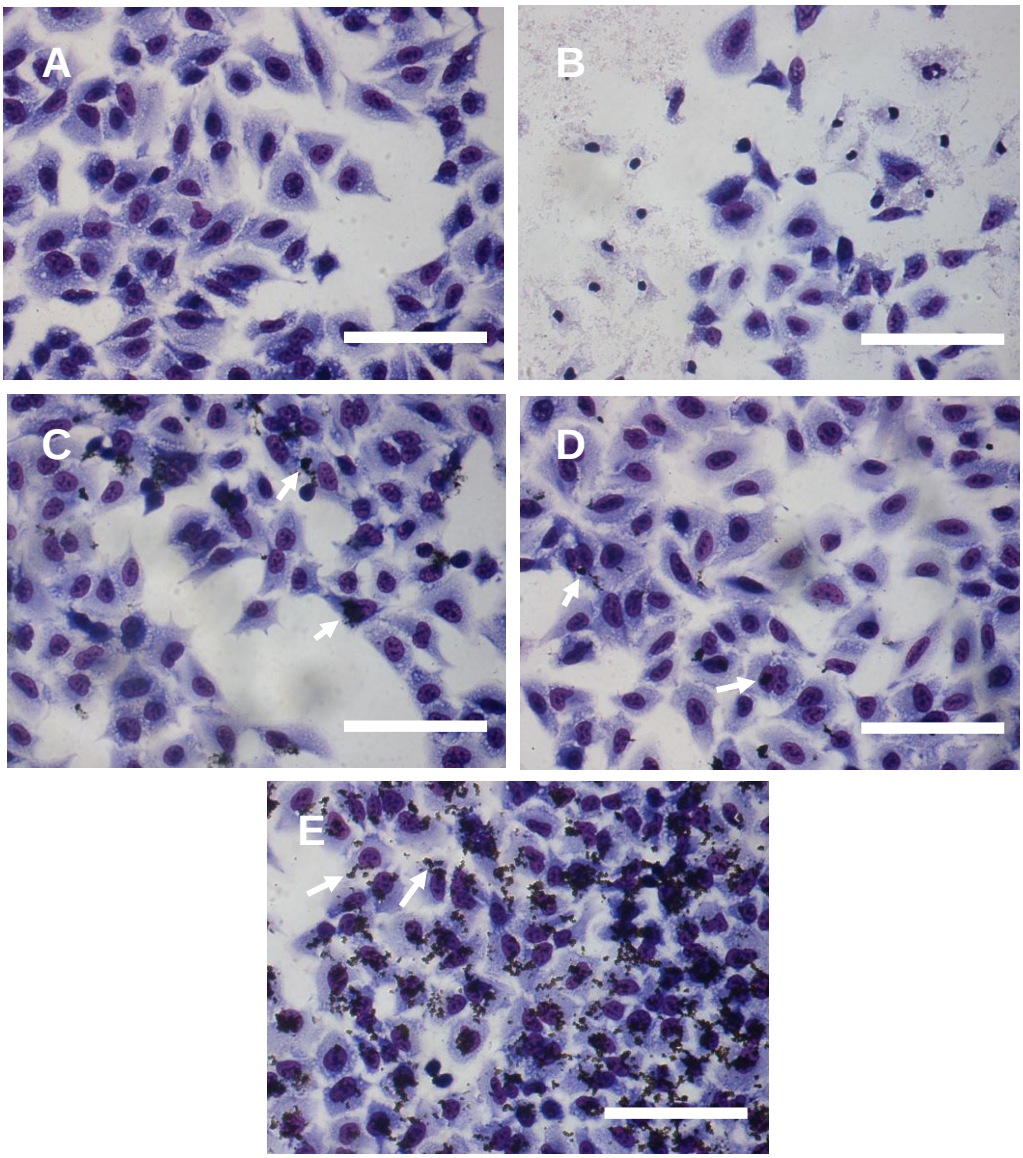

A549 cells stained with Eosin and haematoxalin fours after treatment with a range of particles including MWCNT at a concentration of 50.6 or 505µg/ml. (A) A549 cells treated with 50.5µg/ml DQ12. **(B)** A549 cells following four hours treatment with 505µg/ml DQ12. **(C)** A549 cells following treatment with 505µg/ml LMWCNT, white arrows indicate the presence of MWCNT aggregates. **(D)** A549 cells after treatment with 505µg/ml SMWCNT, white arrows point to examples larger aggregates. (**E**) A549 treated with 505µg/ml TiO_2, white arrows indicate representative aggregates. Scale bars represent 100µm.

Appendix VI

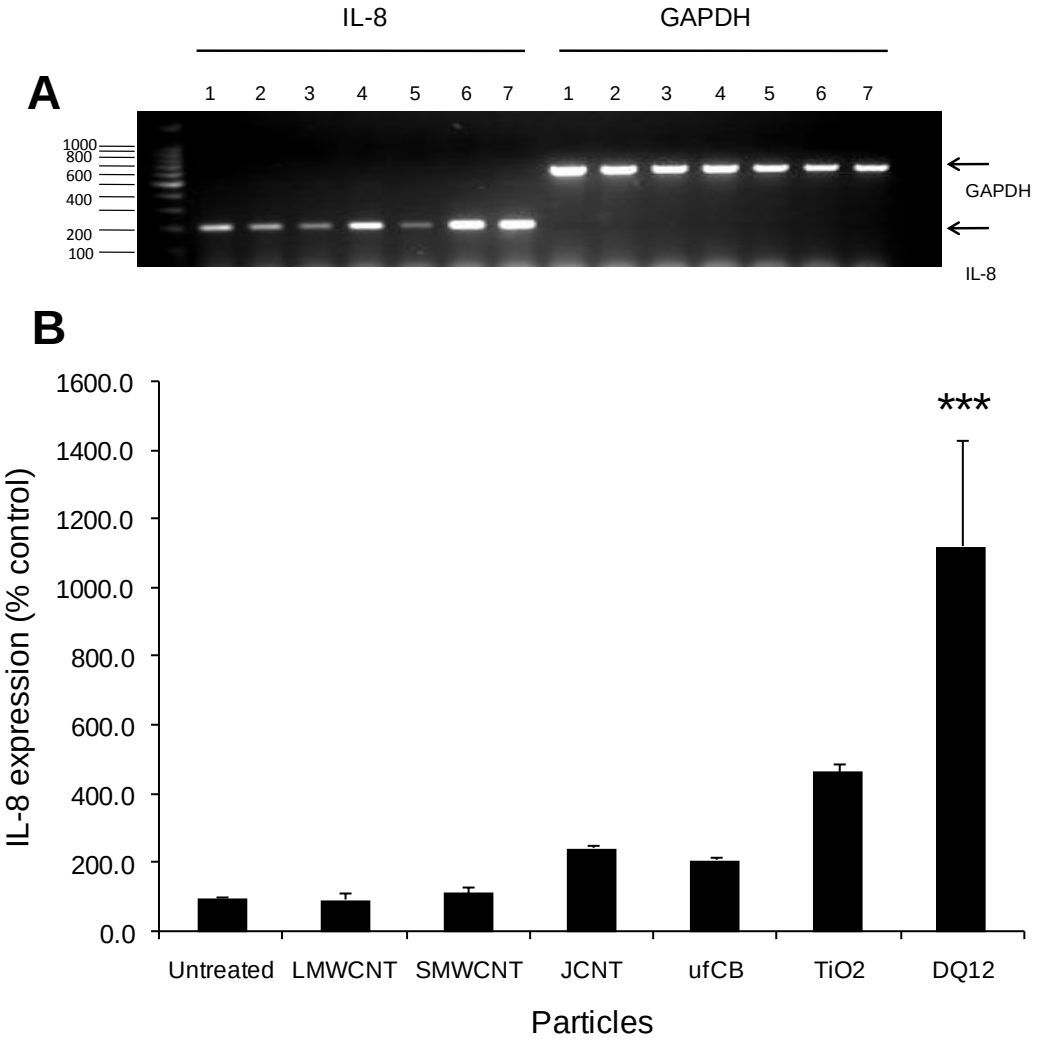

Figure 4.10 IL-8 gene expression profiles for A549 cells exposed for 24 hours to 52.6µg/cm^2 of MWCNT and control particles (10.5µg/cm^2 for DQ12). Cells were exposed to 24 hours to each particle in serum free medium, RNA was extracted and isolated and IL-8 mRNA quantified by RT-PCR **A. Representative PCR gel showing IL-8 and GAPDH IL-8 (1)** Untreated **(2)** LMWCNT **(3)** SMWCNT **(4)** JMWCNT **(5)** ufCB **(6)** TiO_2 **(7)** DQ12. **B. Histogram of IL-8 gene expression expressed as a percent of the negative (untreated) control.** The histogram represents the mean of three experiments conducted on pooled triplicate samples. IL-8 expression was quantified from the gels by densitometry and values expressed as a ratio of IL-8: GAPDH as a percent of the untreated control. The bars represent the S.E.M. **p< 0.001.

METAL & METALLOID PARTICULATES IN WORKPLACE ATMOSPHERES (ATOMIC ABSORPTION)

Method Number:	ID-121
Matrix:	Air, Wipes, or Bulks
OSHA Permissible Exposure Limits:	See Table 1
Collection Procedure:	Personal air samples are collected on mixed-cellulose ester filters using a calibrated sampling pump. Wipe or bulk samples are collected using grab sampling techniques.
Recommended Sampling Rate:	2 L/min
Recommended Air Volumes	
Time Weighted Average Samples:	480 to 960 L
Short-Term Exposure Limit Samples:	30 L
Ceiling Samples:	10 L*
Analytical Procedure:	Samples are desorbed or digested using water extractions or mineral acid digestions. Elemental analysis of the prepared sample solutions is performed by atomic absorption or emission spectroscopy.
Detection Limits:	See Table 2
Precision and Accuracy:	See Table 3
Method Classification:	Validated Analytical Method
Date:	1985
Date Revised:	February 2002

* Alternate air volumes may be necessary to achieve good analytical sensitivity.

Division of Physical Measurements and Inorganic Analyses
OSHA Technical Center
Salt Lake City, Utah

1. Introduction

This method can determine the amount of specific metal and metalloid particulates in the workplace atmosphere. The airborne particulates are collected on filters using calibrated sampling pumps. These samples are then analyzed using flame atomic absorption or emission spectrometry. This method can also determine specific metals and metalloids contained in wipe and bulk samples. The identification and quantification of the particulate is directly determined as the element. The elements are:

Aluminum (Al)	Silver (Ag)	Lithium (Li)	Cobalt (Co)
Gold (Au)	Bismuth (Bi)	Thallium (Tl)	Molybdenum (Mo)
Potassium (K)	Iron (Fe)	Cesium (Cs)	Yttrium (Y)
Antimony (Sb)	Sodium (Na)	Magnesium (Mg)	Copper (Cu)
Hafnium (Hf)	Cadmium (Cd)	Tin (Sn)	Nickel (Ni)
Selenium (Se)	Lead (Pb)	Chromium (Cr)	Zinc (Zn)
Barium (Ba)	Tellurium (Te)	Manganese (Mn)	Platinum (Pt)
Indium (In)	Calcium (Ca)	Titanium (Ti)	Zirconium (Zr)

For some analytes, there are alternate methods or procedures which may be more sensitive, accurate, or specific. When a separate OSHA method or procedure exists, that method shall take precedence over this method unless special circumstances render it inapplicable. Elements or compounds having alternate methods or stopgap procedures are:

Element or Compound	OSHA Method No.
Aluminum oxide	ID-198SG or ID-109SG
Barium sulfate	ID-204
Cadmium	ID-189
Chromic acid/chromates	ID-103
Ferrovanadium	ID-125G
Vapors (i.e. $Ni(CO)_4$, H_2Se, TeF_6, $C_5H_4Mn(CO)_3$]	In-House Methods
Organic tin compounds	ID-102SG
Platinum (soluble)	ID-130SG
Selenium	ID-133SG
Solders	ID-206
Stibine	NIOSH 6008, In House
Tetraethyl lead and tetramethyl lead	In-House Method
Titanium dioxide	ID-204
Welding fumes	ID-125G
Zinc oxide	ID-143

Depending on advances in technology or changes in exposure limits, substances may be added or deleted from the above lists.

1.1 History

Air and wipe samples containing metal and metalloid particulate have always been analyzed at the OSHA Salt Lake City Analytical Laboratory using atomic absorption or emission spectrometry (8.1). Constituents in bulk samples have been determined semi-quantitatively using this technique.

1.2 Principle

Air samples of the workplace are taken using calibrated sampling pumps with cassettes containing either mixed cellulose ester (MCE) or polyvinyl chloride (PVC) filters. These samples are prepared in the laboratory using concentrated (concd) acids or extracted with deionized water if a soluble fraction is required. The sample solution is diluted to a known volume after any necessary matrix modifiers are added. The sample is then aspirated into the flame of an atomic absorption or emission spectrophotometer (AAS or AES) and the molecules in the sample solution are subjected to the following processes:

1) nebulization
2) desolvation
3) liquefaction
4) vaporization
5) atomization
6) excitation (atoms converted from "ground" to excited state)
7) ionization

The absorption or emission of light occurring during processes 5 and 6 is then measured at the characteristic wavelength for the element of interest.

For absorption, a hollow cathode lamp or an electrodeless discharge lamp (EDL) is used as the light source. A double beam spectrophotometer is normally used where the lamp radiation alternately passes through and around a flame into which the sample is being aspirated. The sample is atomized and the metal or metalloid atoms absorb light from the source at their characteristic wavelengths. This absorption is proportional to the concentration of the element present in the sample solution. A monochromator isolates the characteristic radiation of the element being analyzed. A photosensitive device then measures the intensity of the transmitted radiation from the two light paths to determine the amount of absorbance occurring in the flame.

For emission, a light source is not used. The sample is introduced into the flame, atomized and excited, and then the light emission from excitation is isolated and measured. The intensity of the light emitted is proportional to the concentration of the element present.

The following flames are used in this method for absorption or emission:

a) Air/Acetylene mixture (Air/C_2H_2)
b) Nitrous oxide/Acetylene mixture (N_2O/C_2H_2)
c) Air/Hydrogen mixture (Air/H_2)

The use of a specific flame is dependent on the respective element's analytical stability, sensitivity, and interferences.

1.3 Advantages and Disadvantages

1.3.1 This analytical method is specific for the element to be determined and does not distinguish different compounds. When an analysis for a compound is requested, an elemental analysis is performed on the sample. A gravimetric factor is then applied to calculate the compound value (Note: For some compounds, additional analytical procedures (i.e. ion chromatography or X-ray diffraction) can be used to confirm the presence of the particular compound.

1.3.2 The analysis will also not differentiate between different particle size ranges, such as dusts and fumes.

1.3.3 Metallic analytes having Permissible Exposure Limits (PELs) designated as the soluble form (i.e., iron soluble salts, nickel, etc.) can be analyzed using this method. Samples for soluble analytes are extracted with deionized water and an elemental analysis is performed on the extract.

1.3.4 Some compounds may not dissolve using the digestion procedures described herein. In these cases, an alternative digestion method should be used.

1.3.5 Several elements can be determined from the same filter sample using this method; however, digestion procedures may solubilize only certain metals. If a combination of metals is requested on the same filter, all of the metals must be soluble in the digestion procedure used.

1.3.6 The equipment used is inexpensive and does not require specialized training.

1.4 Use of Metal and Metalloid Compounds in Industry

Metals, their alloys, and compounds are used in a wide variety of industries. In certain operations (e.g., welding, smelting, grinding, etc.), particulate matter containing metals and their compounds may be released into the workplace atmosphere. These substances pose a potential health hazard to workers exposed to them (8.2-8.4). Further documentation regarding industrial use, toxicity, and physical properties may be found in NIOSH criteria documents for the particular substance.

2. Analytical Range and Sensitivity

This method uses detection limit, linearity, and sensitivity terms which are characteristic of atomic absorption. These terms are further defined in Appendix A. Any detection limits, linear ranges, and sensitivities mentioned in this method are for analyses using the primary analytical wavelength, a flow spoiler, an Air/C_2H_2 flame, and a hollow cathode lamp unless otherwise noted.

2.1 The qualitative detection limits listed in Table 2 were taken from reference 8.5. The analytical detection limits (8.1) listed were determined from routine laboratory analyses using the definition listed in Appendix A. These limits are approximate since they are dependent on instrument performance and optimization, sample characteristics, and the range of standards analyzed.

2.2 The upper linear range for each element is also given in Table 2. These ranges were taken from reference 8.6. Instrument response is linear to greater concentrations if an alternate wavelength is used; however, the detection limit may also increase. Samples can be diluted to bring the concentration of the element(s) within the linear range. The upper linear range for most elements is usually found near 0.25 to 0.30 absorbance units (ABS).

2.3 The sensitivity for each element is also listed in Table 2. These values are for a nebulizer which has been optimized to give an ABS of 0.25 for an aqueous solution containing 5 µg/mL Cu (8.6). The actual sensitivity obtained will depend on the particular instrument and flame used, the sample matrix, and instrument operating parameters.

3. Method Performance - Precision and Recoveries

Listed in Table 3 are data compiled from quality control (QC) samples which were spiked with aqueous solutions of various analytes and then analyzed in single blind tests. Each analyte was spiked onto an individual MCE filter, allowed to dry, and then prepared and analyzed along with survey samples previously taken by industrial hygienists. These samples were analyzed from 1986 to 1989. Due to the limited number of survey samples received for a few substances, QC samples were not prepared and analyzed for all analytes included in this method.

4. Interferences

Interferences occur at the analytical level and can be characterized as chemical, matrix, ionization, spectral, or as background absorption.

4.1 Chemical or condensed phase interferences occur when the element of interest combines with another species in the flame, thus altering the number of atoms available for emission or absorption. This can result in either a positive or negative bias (usually negative) in the results obtained. Chemical interferences can be controlled by using a hotter flame, or by the addition of a releasing agent which inhibits the reaction between the metal and the interfering species.

4.2 Matrix interferences occur when the physical characteristics (viscosity, surface tension, etc.) of the sample and standard solutions differ considerably. This may occur when samples contain large amounts of dissolved salts or acid, when different solvents are used for samples and standards, or when the temperatures of samples and standards are appreciably different. To control this, samples

and standards must be matrix matched, or the sample must be diluted until any matrix effect becomes insignificant.

4.3 Ionization interferences occur when the flame temperature is sufficiently high to ionize the atoms of interest. This changes the absorption spectrum of the analyte and effectively removes atoms from the flame, causing a loss of sensitivity. Ionization interferences are controlled by adding large amounts (usually >0.1%) of an easily ionized metal such as Na, K, Cs, or rubidium (Rb). The excess electrons released in the flame greatly reduces the degree of ionization of the metal being determined.

4.4 Spectral interferences occur when an element other than the one analyzed absorbs at the same wavelength. This causes a positive bias in the results obtained when the interfering element is present in the samples. In this case, an alternate line should be used. Spectral interferences also occur when a multielement hollow cathode lamp is used which contains elements with absorbing wavelengths close to one another and the analytical slit width used is wide enough to allow the wavelengths of more than one element to pass. If the sample contains two or more of these elements, a positive bias will occur. To resolve this, a single element lamp, an alternate wavelength, or in certain cases, a narrower slit width can be used.

4.5 Background absorption interferences include flame absorption, molecular absorption, and light scattering:

a) Flame absorption is most severe below 250 nm. This absorption can be controlled by careful optimization of fuel and oxidant flow rates. Other mechanisms of control are: Use of flames which are more transparent at these wavelengths (i.e. Air/H_2 or argon/hydrogen flames), or deuterium arc background correction (DABC).

b) Molecular absorption is controlled by using hotter flames to break down molecular species or by DABC.

c) Light scattering occurs at shorter wavelengths when samples have a large salt content; this is controlled using DABC.

4.6 Large amounts of silicates or other particulates may interfere and may also cause aspiration problems (8.7). If present, they should be removed by filtration. The particulate should then be re-digested and analyzed to ensure the analyte(s) of interest have been completely extracted.

4.7 This analytical method is normally not compound-specific. Compounds are only determined as the element, and a significant positive bias can occur when any sample has additional analytes containing the same element. Other analytical procedures may be necessary to identify a specific compound. An assessment of the industrial operation sampled may also provide information regarding the potential existence of other analytes that could cause a positive bias.

4.8 Potential interferences for several of the elements determined by this method are listed in Appendix B.

5. Sampling

5.1 Equipment - Air Filter Samples

5.1.1 Mixed cellulose ester (MCE) filters (0.8 µm pore size), cellulose backup pads, and cassettes, 37-mm diameter (part no. MAWP 037 A0, Millipore Corp., Bedford, MA). Filters and cassettes having a 25-mm diameter can also be used.

5.1.2 Gel bands (Omega Specialty Instrument Co., Chelmsford, MA) for sealing cassettes.

5.1.3 Sampling pumps capable of sampling at 2 liters per minute (L/min).

5.1.4 Assorted flexible tubing.

5.1.5 Stopwatch and bubble tube or meter for pump calibration.

5.2 Equipment - Wipe Samples

5.2.1 Smear tabs (part no. 225-24, SKC Inc., Eighty Four, PA), or wipe filters (Whatman no. 41 or no. 42 filters, Whatman Labsales Inc., Hillsboro, OR).

5.2.2 Deionized water.

5.2.3 Scintillation vials, 20-mL (part no. 74515 or 58515, Kimble, Div. of Owens-Illinois Inc., Toledo, OH) with polypropylene or Teflon cap liners. Metal cap liners should not be used.

5.3 Equipment - Bulk Samples

5.3.1 High-volume sampling pump with appropriate sized MCE collection filters.

5.3.2 Scintillation vials, 20-mL (same as Section 5.2.3).

5.4 Sampling Procedure - Air Filter Samples

5.4.1 Place a MCE filter and a cellulose backup pad in each two- or three-piece cassette. Seal each cassette with a gel band.

5.4.2 Calibrate each personal sampling pump with a prepared cassette in-line to approximately 2 L/min.

5.4.3 Attach prepared cassettes to calibrated sampling pumps (the backup pad should face the pump) and place in appropriate positions on the employee or workplace area.

5.4.4 Collect the samples at approximately 2 L/min for the recommended sampling times (unless otherwise noted):

TWA	240 to 480 min
STEL Samples	15 min
Ceiling Samples	5 min*

The analytical sensitivity of a specific analyte may dictate the use of a different sampling time.

* When determining compliance with the Ceiling PEL for sodium hydroxide, take 15-min samples.

5.4.5 Place plastic end caps on each cassette after sampling. Attach an OSHA-21 seal around each cassette in such a way as to secure the end caps.

5.5 Sampling Procedure - Wipe Samples

Certain analytes may have a skin designation (See Table 1).

5.5.1 Wear clean, impervious, disposable gloves when taking each wipe sample.

5.5.2 Moisten the wipe filters with deionized water prior to use.

5.5.3 If possible, wipe a surface area covering 100 cm^2.

5.5.4 Fold the wipe sample with the exposed side in.

5.5.5 Transfer the wipe sample into a 20-mL scintillation vial and seal with vinyl or electrical tape. Securely wrap an OSHA-21 seal length-wise from vial top to bottom.

5.6 Sampling Procedure - Bulk Samples

5.6.1 In order of laboratory preference, bulk samples may be one of the following:

1) a high-volume (>1,000 L) filter sample of the workplace area,
2) a representative settled dust (rafter) sample,
3) a sample of the bulk material in the workplace.

5.6.2 If possible, transfer the bulk material or filter into a 20-mL scintillation vial and seal with vinyl or electrical tape. Securely wrap an OSHA-21 seal length-wise from vial top to bottom.

5.7 Shipment

5.7.1 Submit at least one blank sample with each set of air or wipe samples. Blank filter samples should be handled in the same manner as other samples, except that an air or wipe sample is not taken.

5.7.2 The type of bulk sample should be stated on the OSHA 91A and cross-referenced to the appropriate air sample(s). Bulk samples should be shipped with Material Safety Data Sheets (if available) and should be sent separately from air samples. Check current mailing restrictions and ship bulks to the laboratory by an appropriate method.

5.7.3 Send all samples to the laboratory with the OSHA 91A paperwork requesting the specific analyte(s) of interest. If analysis of a mixture of different elements or compounds is necessary, contact the lab to ascertain which analytes can be analyzed together.

6. Analysis

6.1 Safety Precautions

6.1.1 Care should be exercised when handling any acidic solutions. Acid solution contact with work surfaces should be avoided. If any acid contacts the eyes, skin, or clothes, flush the area immediately with copious amounts of water. Medical treatment may be necessary.

6.1.2 All work with concentrated acids is potentially hazardous. Always wear safety glasses and protective clothing. Prepare all mixtures, samples, or dilutions in an exhaust hood. To avoid exposure to acid vapors, do not remove any beakers from the hoods until they have returned to room temperature.

6.1.3 **Extra care** should be used when handling perchloric acid ($HClO_4$). Perchloric acid should only be used in a hood that has been approved for $HClO_4$ use. In this hood:

a) Organic reagents should not be used or stored near $HClO_4$.

b) A water wash down system for the ducts and work surface must be installed and periodically used.

c) Precautions should be taken to ensure that explosions or spontaneous ignition of sample material from $HClO_4$ is prevented.

Working with $HClO_4$ is very hazardous. Be sure to wear safety glasses, a laboratory coat, and gloves. Always add nitric acid (HNO_3) with $HClO_4$. When digesting backup pads or other samples with $HClO_4$, watch them carefully since there is a chance they

could ignite. Always keep HNO_3 nearby when using $HClO_4$. In the event of sample media ignition, quickly douse the sample with a small portion of HNO_3.

6.1.4 Care should be exercised when using laboratory glassware. Chipped pipettes, volumetric flasks, beakers, or any glassware with sharp edges exposed should not be used.

6.1.5 Pipetting is always performed using an automatic pipet or pipette bulb, never by mouth.

6.1.6 Before using any instrument, the operator should consult the Standard Operating Procedure (SOP) (8.8) and any instrument manuals.

6.1.7 Since metallic elements and other toxic substances are vaporized during flame operation, it is imperative that an exhaust hood is installed and used directly above the burner chamber of the spectrometer. Always ensure the exhaust system is operating before proceeding with the analysis.

6.2 Equipment

6.2.1 Atomic absorption spectrophotometer consisting of a(an):

Nebulizer and burner head.
Pressure-regulating devices capable of maintaining constant oxidant and fuel pressures.
Optical system capable of isolating the desired wavelength of radiation.
Adjustable slit.
Light measuring and amplifying device.
Display, strip chart, or computer interface for indicating the amount of absorbed or emitted radiation.
Deuterium Arc Background Corrector. This is usually required for determinations at short (<250 nm) wavelengths.

Light source for absorption:

a) Hollow cathode lamp for the specific element or multielement (Note: Please see specific limitations of multielement lamps in Appendix B)

b) Electrodeless Discharge Lamp (EDL) for the specific element. This type of lamp may provide better sensitivity and detection limits for some elements, especially Se, Sn, and Sb. If used, a separate EDL power supply is usually necessary.

6.2.2 Oxidant: Compressed, filtered air free from water, oils and other contaminants.

6.2.3 Nitrous oxide (N_2O).

6.2.4 Fuel (Use flash arrestors when using flammable gases. Consult with the manufacturer for appropriate use.):

a) Acetylene, commercially available acetylene dissolved in acetone. CAUTION: Do not use grades of acetylene that contain solvents other than acetone. These solvents may damage PVC tubing in some instruments. Do not use acetylene when the tank pressure drops below 520 kPa (75 psi).

b) Hydrogen is used as the fuel in the determination of certain elements.

6.2.5 Pressure regulators, Two-stage.

6.2.6 Flash arrestors (model 6103, Matheson Gas Products, East Rutherford, NJ).

6.2.7 Glassware

a) Conical beakers, 125- and 250-mL

b) Volumetric flasks, Class A: 10-, 25-, 50- and 100-mL

c) Pipettes, Class A: Assorted sizes

6.2.8 Forceps.

6.2.9 Exhaust hood and hotplate, or microwave digestion system (model no. MDS-81, CEM Corp., Matthews, NC).

6.2.10 Filtering apparatus consisting of MCE filters, 0.45-µm pore size, 47-mm diameter (cat. no. HAWP 047 00, Millipore Corp., Bedford, MA) and filtering apparatus (cat. no. XX15 047 00, Millipore).

6.2.11 Analytical balance (0.01 mg).

6.3 Reagents (All chemicals should be reagent grade or better. Many of the chemicals listed below are only used in specific instances. Specific reagents are listed within the additional procedures in Table 4 and also in Table 5.)

6.3.1 Deionized water (DI H_2O) with a specific conductance of less than 10 µS.

6.3.2 Ammonium fluoride (NH_4F) solutions (used for specific insoluble compounds, see AP 6, Table 4).

a) Ammonium fluoride, 1 M: Dissolve 37.04 g NH_4F and dilute to 1 L in DI H_2O. Store in a polyethylene bottle.

b) Ammonium fluoride, 0.1 M in 4% HNO_3: Carefully add 40 mL concd HNO_3 and 100 mL of the 1 M NH_4F solution to 500 mL DI H_2O and dilute to 1 L in a polyethylene volumetric flask. Store in a polyethylene bottle since acidic solutions of NH_4F may form small amounts of HF and etch glass containers.

6.3.3 Hydrogen peroxide (H_2O_2), 30% (used for digestions of Cr, see AP 5, Table 4).

6.3.4 Mineral acids (used for digestions) CAUTION: Refer to Section 6.1.2 before using acids.

a) Hydrochloric acid (HCl), concd (36.5 to 38%).

b) Hydrofluoric acid (HF), concd (49%).

c) Nitric acid (HNO_3), concd (69 to 71%).

d) Perchloric acid ($HClO_4$), concd (69 to 72%). Please see Section 6.1.3 before using $HClO_4$.

e) Sulfuric acid (H_2SO_4), concd (95 to 98%).

f) Acid mixture for platinum digestions: Prepare a mixture of HCl/HNO_3 by slowly and carefully adding 82 mL concd HCl to 18 mL concd HNO_3 (CAUTION: Do not store this solution; dispose of properly after use).

6.3.5 Mineral acids (used for dilutions or cleaning glassware) CAUTION: Refer to Section 6.1.2 before using acids.

a) Nitric acid, 1:1 HNO_3/DI H_2O mixture: Carefully add a measured volume of concd HNO_3 to an equal volume of DI H_2O.

b) Nitric acid, 4% v/v: Carefully add 40 mL concd HNO_3 to 500 mL DI H_2O and dilute to 1 L.

c) Nitric acid 10% v/v: Carefully add 100 mL of concd HNO_3 to 500 mL of DI H_2O and then dilute to 1 L.

d) Nitric and hydrochloric acid v/v mixture (4% HNO_3/X% HCl, where X% is listed below): Carefully add the appropriate amount of concd HCl to 500 mL of DI H_2O:

4% HCl 40 mL
16% HCl 160 mL
32% HCl 320 mL

Then carefully add 40 mL concd HNO_3 and dilute to 1 L with DI H_2O.

6.3.6 Chemical or ionization interference suppressants

a) Aluminum ion, 5,000 µg/mL: Dissolve 69.52 g aluminum nitrate ($Al(NO_3)_3 \bullet 9H_2O$) and dilute to 1 L in DI H_2O.

b) Potassium ion, 5,000 µg/mL: Dissolve 9.54 g potassium chloride (KCl) in DI H_2O and dilute to 1 L.

c) Sodium ion, 5,000 µg/mL: Dissolve 12.71 g sodium chloride (NaCl) in DI H_2O and dilute to 1 L.

6.3.7 Stock standard solutions

Commercially available aqueous standards are used. Expiration dates for standards should be followed. If there is no expiration date, dispose of after 1 year. As an alternative, standards can be prepared using the procedures described in the SOP (8.8) or instrument manufacturer manuals (i.e., 8.6, 8.9, 8.10).

6.4 Glassware Preparation

6.4.1 Place the conical beakers in an exhaust hood and add approximately 10 mL of a 1:1 HNO_3/DI H_2O mixture in each 125- or 250-mL conical beaker. Apply moderate heat until refluxing occurs. Decant the acid mixture into a waste container and allow the beakers to cool before removing from the hood. Rinse the beakers thoroughly with DI H_2O.

6.4.2 Rinse all volumetric flasks with 10% v/v HNO_3 and then rinse thoroughly with DI H_2O.

6.5 Working Standards

6.5.1 Dilute stock standard solutions to the appropriate ranges using a diluent that will match the sample matrix. Use information in Tables 1 and 2 as guides for the ranges; use Table 5 for matrices. The standard concentrations should bracket the expected sample concentrations and the standard/sample matrices should match.

6.5.2 Store standards in appropriate containers. Protect Ag standards from light by storing them in actinic or brown plastic bottles. Store standards containing NH_4F in polyethylene containers.

6.6 Sample Preparation

Note: Always prepare blank samples with every sample set. Prepare an additional blank media sample any time an extra procedure is used (i.e., wiping out the particulate contained inside a cassette with an MCE filter or preparing a contaminated backup pad). This blank media should be from the same manufactured lot as the prepared filter or backup pad.

6.6.1 Preparation of air and wipe samples

Use 125-mL conical beakers for air samples and smear tabs; use 250-mL beakers for large wipe samples. Carefully transfer any loose dust from the cassette into a labeled beaker. Using forceps transfer the sample filter into the same digestion beaker. If the backup pad appears contaminated, include it with the sample filter. If there is loose dust present, rinse the cassette top (and ring, if present) with a small amount of DI H_2O and pour the water into the beaker with the sample filter. Wipe out the cassette top (and ring, if present) interior surface with a clean Smear Tab (or 1×2 inch section of Ghost Wipe) that has been moistened with DI H_2O and place it in the same digestion beaker with the rinse and sample filter. Similarly wipe out the cassette bottom interior surface if the cassette contains loose dust or if the backup pad is contaminated. Ensure that blank samples are prepared and analyzed using the same materials and procedures as used for air samples.

If the backup pad appears to be discolored, it may be due to leakage of air around the filter during sampling.

6.6.2 Preparation of bulk samples

Review any available material safety data sheets to determine safe bulk handling. The safety data may also offer a clue as to the aliquot amount needed for adequate detection of the element(s) of interest.

Measure by volume or weight an appropriate aliquot of any liquid bulk sample.

Weigh the appropriate amount of any solid bulk sample.

Note: Aliquot amounts of bulks are dependent on the analytical sensitivity, detection limit, and solubility of the material used. If uncertain, a 20- to 50-mg aliquot of a solid material can be taken as a starting point. Make sure the aliquot taken is representative of the entire bulk sample. If necessary, use a mortar and pestle to grind any nonhomogenous particulate bulk samples in an exhaust hood.

After measuring, transfer the aliquot to a 250-mL conical beaker.

6.6.3 Extraction or digestion - all samples

Consult Tables 4 and 5 to determine the reagents used during extraction or digestion for each element to be analyzed. Some elements (Ba, Sn, etc.) or compounds are not digested with concd HNO_3, but are prepared using alternate procedures (APs) listed in Table 4. These elements or compounds and their AP numbers are:

Ag	AP 1	LiH	AP 7	Te	AP 1
Al (soluble)	AP 2	MgO	AP 3	TiO_2	AP 8
Al (pyro powders)	AP 3	Na cmpds	AP 7	Tl (soluble)	AP 2
Au	AP 4	Ni (soluble)	AP 2	Y	AP 3
Ba (soluble)	AP 2	Mo (soluble)	AP 2	Zr	AP 6
Ca cmpds	AP 3	Mo (insoluble)	AP 3	Cr (II or III)	AP 2
Pb	AP 1	Cr (metal)	AP 5	Pt (metal)	AP 4
CsOH	AP 7	Sb	AP 1	Fe (soluble)	AP 2
Se	AP 1	Hf	AP 6	Sn (inorganic)	AP 4
KOH	AP 7	SnO	AP 4		

For the element or compounds listed above, follow the APs recommended and then proceed with Section 6.6.4. For other elements or compounds, follow the procedures a, b, or c listed below:

a) <u>All MCE air filters and smear tabs requiring HNO_3 digestion</u>

Place the beakers in an exhaust hood and add 3 to 5 mL concd HNO_3 to cover the filter. Place the beakers on a hot plate and heat the samples until about 1 mL remains. Add a second portion of approximately 1 to 2 mL of concd HNO_3. Apply heat until the appropriate amount of HNO_3 remains in the beaker (1 mL of HNO_3 will give a 4% HNO_3 matrix when diluted to 25 mL final volume).

b) <u>Large wipe, PVC filters, or backup pads</u>

Place the beakers in an exhaust hood and add the following amount of concd HNO_3 to the beakers:

Large wipes and backup pads - 10 to 15 mL
PVC filters - 3 to 5 mL

Place the beakers on a hot plate and heat the samples until about 1 mL remains. Add 2 mL of concd $HClO_4$ along with a second portion of 2 mL HNO_3, heat the sample, and then remove when about 1 mL remains. (Note: Please see Section 6.1.3 before using $HClO_4$.)

As an alternative, an extraction of the backup pad or wipe sample using only HNO_3 may be used. Add HNO_3 to the media, digest on a hotplate, and continue to add HNO_3 until the solution becomes clear. Remove the beaker from the hotplate when the appropriate amount of HNO_3 remains.

c) <u>Bulk samples</u>

Add 10 to 30 mL HNO_3, place the beaker on a hot plate, and digest the bulk sample until the material dissolves and the appropriate amount of solution remains (about 1 mL if diluting samples to 25 mL, 2 mL if 50 mL final volume, etc. After dilution this will give a final volume of 4% HNO_3). If necessary, use other acids, or use a microwave digestion system to facilitate digestion [For further information regarding microwave digestion, see the Standard Operating Procedure (8.11)].

6.6.4 <u>Filtration - all samples</u>

1) Samples Previously Extracted:

Samples extracted with DI H_2O should normally be filtered. If particulate is present, filter the extract through a 0.45-µm MCE filter. Save the extract as the soluble portion. If necessary, digest the particulate on both filters using procedure (a) above or the

applicable AP to prepare the remaining insoluble material for additional analyses. To control for potential contamination, prepare blank samples in the same fashion as the filtered samples.

2) Samples Previously Digested:

If particulate matter is present after digesting, cool the sample, add approximately 10 mL DI H_2O, then filter the solution through a 0.45-µm MCE filter. Save the filtrate. Repeat digestion procedure (a) above for the filter containing the particulate.

6.6.5 Dilution - all samples

Allow all digested samples to cool to room temperature in an exhaust hood before proceeding. Additional sample or filtrate treatment may be required for certain elements. Perform any special sample treatments recommended in Table 5, and then quantitatively transfer each sample and each filtrate solution to individual volumetric flasks. Add any reagents necessary to achieve the final solution concentrations listed in Table 5 for specific analytes. Dilute to volume with DI H_2O and then mix well. Solution volumes are dependent on the following factors:

a) The amount of sample the industrial hygienist has collected (air volume and/or filter loading).

b) The detection limit of the analytical method.

c) The PEL of the analyte.

d) The number of analytes requested.

Air samples are normally diluted to 25 mL unless one or more of the above factors suggests an alternate volume should be used. For routine analysis, at least 1/10 of the OSHA PEL should be detectable. Final solution volumes can be estimated using the following equation:

$$\text{FV Factor} = \frac{0.1 \times \text{PEL} \times \text{Air Vol}}{\text{QnDL} \times \text{GF}}$$

where:
PEL is Permissible Exposure Limit (mg/m³)
Air Vol is Air Volume taken (L)
QnDL = Quantitative Detection Limit (µg/mL)
GF = Gravimetric Factor (if required - some factors are listed in Table 6)

Quantitative detection limits are listed in Table 2. The FV factor assists in determining the final volume. Sample solution volumes normally used are: 5-, 10-, 25-, 50-, or 100-mL. Final volumes of 50- and 100-mL are normally reserved for wipe or bulk samples. If possible, FV should always be larger than the final solution volume. For example, if a sample has a 200-L air volume, a PEL of 0.05 mg/m³, a GF of 1, and a QnDL of 0.09 µg/mL, then:

FV Factor = 11.1

and a final volume should be 10-mL. Due to the limited amount of solution available for analysis and the potential for sample loss during transfer, 5-mL solution volumes are only used when absolutely necessary.

6.7 Instrument Setup and Analysis

6.7.1 Set up the AAS or AES according to the SOP (8.8) or the manufacturer's instructions. Use the flame and wavelength recommended in Table 7. If alternate conditions are necessary, consult the instrument manufacturer's manual for other settings and operating procedures. Install an EDL or hollow cathode lamp for the element of interest and allow it to warm up for 10-20 min or until the energy output stabilizes. Optimize conditions such as lamp position, burner head alignment, fuel and oxidant flow rates, etc. See the SOP (8.8) or specific instrument manuals for details.

6.7.2 Aspirate and measure the ABS of a standard solution for the element of interest. The standard concentration should be within the linear range for the element. Compare the ABS to an expected sensitivity value (Note: Some values are listed in Table 7; these were adapted from reference 8.6 or obtained at the OSHA laboratory). Then aspirate the smallest standard to be used and assure the ABS reading is above the background level of the instrument.

6.7.3 Make any adjustments necessary for the particular analysis, such as: scale expansion, burner head rotation, background correction, or alternate wavelength.

6.7.4 Aspirate and measure the ABS of a prepared standard solution, then determine the baseline by aspirating DI H_2O and measuring the ABS.

6.7.5 Analyze standards, samples, and blanks. Repeat the baseline determination after each solution is analyzed. The baseline readings will assist in correcting any instrument drift. If more than one solution has been prepared for a sample (i.e. filtrate and sample, or soluble and insoluble portions), analyze each for all requested elements. Standards must bracket the sample concentrations. Analyze a standard after every four or five samples. Standard readings should be within 10 to 15% of the readings obtained at the beginning of the analysis.

6.7.6 If any samples exceed the linear range, they should be diluted. When diluting a sample, be sure that the diluted sample has the same matrix as the original sample and standards. If a number of samples must be diluted, it may be more advantageous to use a less sensitive wavelength.

6.8 Analytical Recommendations

6.8.1 When a fresh standard is prepared, analyze the old and new standards and compare results to verify the new standard is correct. If two or more stock solutions are available for working standard preparations, rotate the preparation from one stock solution to the next to verify the quality.

6.8.2 Keep a permanent record of all standard preparation and comparison data. Assign and follow expiration dates for all standards.

6.8.3 Always analyze blank samples along with the other samples. Treat blanks in the same fashion as samples, including any filtration steps.

6.8.4 When analyzing for Ag, carry-over from a large concentration sample or standard to the next sample can occur, causing erroneous readings. To remedy this, aspirate 4% HNO_3 instead of water between samples.

6.8.5 In this method, many different matrices are used to digest and keep analytes in solution. Occasionally, during multiple element analysis of the same sample, matrix effects can occur if standards are not matrix-matched with samples. Also, it is sometimes necessary to prepare samples in a matrix substantially different from recommendations. If these conditions occur, one or two standards should be prepared in the same matrix to determine

any matrix effects. A reagent blank should also be prepared and analyzed to determine any effect on the background signal. If a significant difference is noted in the analytical signals for the two different matrices, a full set of standards should always be prepared in the sample matrix and analyzed with the samples.

7. Calculations

7.1 Subtract each baseline ABS from the corresponding standard ABS, and plot the net ABS versus the standard concentrations. Using a least squares method, determine the equation for the best curve fit.

7.2 Subtract each baseline ABS from the corresponding sample or blank ABS, and use the standard curve to calculate the concentration of each analyte in µg/mL.

7.3 Calculate the concentration for each air sample as:

$$C = \frac{[(A \times SA \times D \times GF) - (B \times SB \times GF)]}{\text{Air Vol}}$$

where:
C is analyte (mg/m³)
A is concn of analyte in the sample solution (µg/mL)
B = concn of analyte in the blank solution (µg/mL)
SA = sample solution volume (mL)
SB = blank solution volume (mL)
D = dilution factor (if any)
GF = gravimetric factor (if any; see Table 6)
Air Vol = air volume sampled (L)

7.4 For wipe or bulk samples, calculate the total amount (in µg) of analyte in each sample using the equation above. An air volume is not used. Convert bulk sample analytes to % composition using:

$$\text{Analyte \%(w/w)} = \frac{(C)(100\%)}{(\text{Sample wt})(1000\ \mu g/mg)}\ \text{(Bulk Samples)}$$

where:
C is analyte amount (µg)
Sample wt aliquot (in mg) of bulk taken in Section 6.6

7.5 Reporting Results to the Industrial Hygienist

For those samples only extracted with DI H_2O, report the sample results as the soluble fraction of the sample. If more than one solution exists for a sample, and it is not necessary to report results separately, then combine these results. An example is a sample that was filtered due to insoluble particulate. The results from the filtrate plus results from the second particulate digestion are added together.

7.5.1 Report air sample results as mg/m³ analyte.

7.5.2 Report wipe sample concentrations as total micrograms or milligrams analyte.

7.5.3 Report bulk sample results as approximate percent by weight analyte (note: Sample results for bulk liquids may be reported as approximate percent by volume if volumetric aliquots were taken during sample preparation.) Due to differences in sample matrices between bulks and standards, bulk results are approximate.

8. References

8.1 Occupational Safety and Health Administration Analytical Laboratory: OSHA Manual of Analytical Methods edited by R.G. Adler (Method No. I-1). Salt Lake City, UT. 1977.

8.2 Clayton, G.D. and F.E. Clayton, ed.: Patty's Industrial Hygiene and Toxicology. 3rd ed. New York: John Wiley and Sons, 1978.

8.3 American Conference of Governmental Industrial Hygienists: Documentation of the Threshold Limit Values and Biological Exposure Indices. 5th Ed. Cincinnati, OH: American Conference of Governmental Industrial Hygienists, 1986.

8.4 National Institute for Occupational Safety and Health: The Industrial Environment--Its Evaluation and Control. Washington, DC: Government Printing Office, 1973.

8.5 Slavin, S., W.B. Barnett, and H.L. Kahn: The Determination of Atomic Absorption Detection Limits by Direct Measurement. Atomic Absorption Newsletter 11: 37-41 (1972).

8.6 Perkin-Elmer Corp.: Analytical Methods for Atomic Absorption Spectrophotometry. Norwalk, CT: Perkin-Elmer Corp., 1973 and revised edition, 1982.

8.7 National Institute for Occupational Safety and Health: NIOSH Manual of Analytical Methods. 2nd ed. (Method no. 173) Cincinnati, OH: National Institute for Occupational Safety and Health, 1977.

8.8 Occupational Safety and Health Administration, Salt Lake Technical Center: Standard Operating Procedure for Atomic Absorption. Salt Lake City, UT. In progress (unpublished).

8.9 Fisher Scientific Company: Atomic Absorption Methods Manual. Waltham, MA: Fisher Scientific Co., 1977.

8.10 Instrumentation Laboratory Inc.: Atomic Absorption Methods Manual. Wilmington, MA: Instrumentation Laboratory Inc., 1975.

8.11 Occupational Safety and Health Administration, Salt Lake Analytical Laboratory: Standard Operating Procedure for Microwave Digestions by D. Cook. Salt Lake City, UT. 1989 (unpublished).

8.12 "Air Contaminants; Final Rule": Federal Register 54:12 (19 Jan. 1989). pp. 2923-2960 and also 54:127 (5 July 1989). pp. 28054-28061.

8.13 Occupational Safety and Health Administration, Salt Lake Analytical Laboratory: OSHA Laboratory Quality Control Division Data by B. Babcock, Salt Lake City, UT, 1989 (unpublished).

8.14 Slavin, Walter: Atomic Absorption Spectroscopy. New York: Interscience Publishers, 1968.

8.15 Ediger, R.D.: Atomic Absorption Analysis with the Graphite Furnace using Matrix Modification. Atomic Absorption Newsletter. 14(5): 127-130 (1975).

Table 1
Air Contaminants - OSHA Permissible Exposure Limits*

Element	Substance Exposed to	Transitional PEL (mg/m^3)		Final Rule PEL (mg/m^3)		
		TWA	Ceiling	TWA	STEL	Ceiling
Ag	Metal and soluble cmpds (as Ag)	0.01		0.01		
Al	Soluble salts (as Al)			2		
	Pyro powders			5		
Ba	Soluble compounds (as Ba)	0.5		0.5		
Bi	Bismuth telluride (SE doped)**			5		
Ca	Calcium oxide	5		5		

Element	Substance Exposed to	Transitional PEL (mg/m^3)		Final Rule PEL (mg/m^3)		
		TWA	Ceiling	TWA	STEL	Ceiling
Cd	Calcium cyanamide	0.1	0.3	0.5		0.3
Co	Fume	0.2	0.6	0.1		0.6
	Dust	0.1		0.2		
	Metal dust and fume (as Co)			0.05		
Cr	Cobalt Carbonyl or hydrocarbonyl (as Co)	0.5		0.1		
Cs	Cr (II or III) compounds (as Cr)	1		0.5		
	Cr metal (as Cr)			1		
Cu	Cesium hydroxide	0.1		2		
	Fumes (as Cu)	1		0.1		
Fe	Dusts and mists (as Cu)	15		1		
	Dicyclopentadienyl iron total dust	10		10		
	Iron oxide fume (as Fe_2O_3)			10		
Hf	Iron salts (soluble) (as Fe)	0.5		1		
In	Hafnium			0.5		
K	Indium and compounds (as In)			0.1		2
Li	Potassium hydroxide	0.025				
Mg	Lithium hydride	15		0.025		
Mn	Magnesium oxide fume total particulate		5	10		5
	Mn compounds (as Mn)		5		3	
	Mn fume (as Mn)			1		
Mo	Manganese tetraoxide (as Mn)	5		1		
	Soluble compounds (as Mo)	15		5		
Na	Insoluble compounds (as Mo) total dust			10		
	Sodium bisulfite			5	0.15	
	Sodium fluoroacetate	2		0.5		2
	Sodium hydroxide					
	Sodium metabisulfaite			5		
Ni	Tetrasodium pyrophosphate***	1		5		
	Metal and insoluble compounds (as Ni)	1		1		
Pb	Soluble compounds (as Ni)			0.1		
Pt	Inorganic (see 29 CFR 1910.1025)					
Sb	Pt metal	0.5		1		
Se	Sb and compounds (as Sb)	0.2		0.5		
Sn	Se and compounds (as Se)	2		0.2		
	Inorganic compounds except oxides (as Sn)			2		
Te	Tin oxide (as Sn)	0.1		2		
Ti	Te and compounds (as Te)	15		0.1		
Tl	Titanium dioxide total dust	0.1		10		
Y	+Soluble compounds (as Tl)	1		0.1		
Zn	Yttrium	1		1	2	
	Zinc chloride fume	5		1	10	
	Zinc oxide fume	15		5		
	Zinc oxide total dust	15		10		
Zr	Zinc stearate	5		10	10	
	Zr compounds (as Zr)			5		

* From reference 8.12 - Final rule PELs were voided by court ruling and are not applicable.
** Sample is also analyzed for Te and Se content
*** Also can be analyzed for total phosphate content by ion chromatography
+Skin Designation

Note: Compounds having total and respirable dust PELs of 15 and 5 mg/m^3, respectively, are normally analyzed gravimetrically. Elements contained in these dust samples can be identified by this or other methods, if necessary.

Table 2
Detection Limits, Sensitivities, and Ranges

Element	Qualitative DL* (µg/mL)	Analytical DL* (µg/mL)	Sensitivity* (µg/mL)	Upper Linear Range* (µg/mL)
Ag	0.002	0.005	0.06	4
Al+	0.02	0.3	1	50
Au	0.01	0.05	0.25	20
Ba+	0.008	0.5	0.4	25

Element	Qualitative DL* (µg/mL)	Analytical DL* (µg/mL)	Sensitivity* (µg/mL)	Upper Linear Range* (µg/mL)
Bi	0.025	0.2	0.5	30
Ca	<0.0005	0.03+	0.08 (0.029)+	7
Cd	0.0002	0.004	0.025	2
Co	0.01	0.04	0.15	5
Cr	0.003	0.04 (0.04)+	0.1 (0.31)+	5 (10)+
Cs	0.005++		0.2	15
Cu	0.001	0.005	0.09	5
Fe	0.005	0.03	0.12	5
Hf+	2.0		15	500
In	0.02	0.1	0.7	50
K	<0.002	0.02	0.04	2
Li	0.0003	0.004	0.035	2
Mg	<0.0001	0.01	0.007	0.5
Mn	0.002	0.01	0.055	3
Mo+	0.02	0.04	0.5	60
Na	<0.0002	0.009	0.015	1
Ni	0.002	0.1	0.15	5
Pb	0.01	0.05	0.5	20
Pt		2.0	13	
Sb**	(0.08)	0.1	1.0	50
Se***	(0.05)	0.3	0.25	25
Sn***	(0.01)	0.1	0.6	40
Te	0.05	0.2	1.0	25
Ti	0.04		1.8	
Tl	0.03	0.05	0.5	20
Y	0.05	0.7	1.8	200
Zn	<0.01	0.01	0.018	1
Zr+	1.0	8	10.0	800

* DL = Detection Limit. See Appendix A for more information regarding definitions or calculations. Analytical DLs are approximate.
** Alternate line of 231.2 nm was used with one exception: The qualitative detection limit value is for the primary line (217.6 nm).
*** Air/H_2 flame used with the exception of the qualitative detection limit determination. This value is for Air/C_2H_2 flame.
\+ N_2O/C_2H_2 flame used.
++ Flame emission used to determine qualitative detection limit.

Table 3
Precision and Accuracy*

Element	CV	% Ave Recovery	Range**	N
Ag	0.083	97.8	1-4	270
Al	0.076	94.5	100-500	27
Au				
Ba	0.10	104.7	50-75	45
Bi				
Ca	0.162	98.3	100-500	51
Cd	0.087	99.5	10-15	93
Co	0.052	99.3	10-15	39
Cr (Soluable)				
Cr (Insoluble)	0.052	95.7	45-75	72
Cs				
Cu	0.043	96.8	100-150	45
Fe	0.084	98.2	300-400	69
Hf				
In				
K	0.063	93.3	125-200	30
Li				
Mg	0.073	112.1	100-300	24
Mn	0.044	100.2	100-150	60
Mo (Soluble)				
Mo (Insoluble)	0.075	91.2	100-250	27
Na	0.058	97.5	100-250	68
Ni	0.065	99.1	100-150	18
Pb	0.047	99.3	20-40	300
Pt	0.055	98.1	80-1800	24+

Element	CV	% Ave Recovery	Range**	N
Sb	0.081	98.4	50-75	36
Se	0.122	104.9	20-100	30
Sn	0.079	97.4	100-150	63
Te				
Ti				
Tl				
Y				
Zn	0.039	101.2	100-150	69
Zr				

CV Coefficient of Variation
* Table updated January, 1990 (8.13)
** Range (in µg) of analyte spiked onto MCE filters. Samples were spiked with aqueous solutions of dissolved metals or their salts. All samples were prepared and analyzed using conditions stated in the method.
\+ These samples were prepared by weighing the metal on filters. A single blind study was not performed.

Table 4
Alternate Procedures

AP 1: Ag, Pb, Sb, Se, Te

1) Digest samples with HNO_3. Heat until the liquid is nearly gone. Allow the samples to cool to room temperature.
2) For 25 mL final sample solution volumes, add the following amount of concd HCl (Adjust accordingly for alternate solution volumes):

Analyte Suspected to be Present	Amount of HCl
Sb	8 mL
Pb or Ag	4 mL
Se or Te	1 mL

3) Warm gently and swirl to dissolve the analyte. Allow samples to cool and dilute to a 25-mL volume with DI H_2O.

AP 2: Soluble Compounds of Al, Ba, Cr (II or III), Fe, Ni, Mo, Tl, Zn

1) Place the sample in a beaker and add an aliquot of room-temperature DI H_2O into the beaker (15 mL is typically used for a full-shift sample).
2) Place the beaker in an ultrasonic bath for approximately 10 min.
3) Filter the sample through a 0.45 µm MCE filter and transfer the filtrate to a 25-mL volumetric flask. If an insoluble fraction is also requested, digest both sample filters according to the appropriate procedure.
4) Add reagents to achieve the final solution concentrations listed:

Analyte Suspected t be Present	Final Concentration
Cr(II or III), Fe, Ni, Tl, Zn (as $ZnCl_2$)	4% HNO_3
Al, Ba	4% HNO_3/1000 µg/mL Potassium ion
Mo	4% HNO_3/1000 µg/mL Aluminum ion

AP 3: Al (pyro powders), Ca, Mg, Mo (insoluble), Y

1) Digest the sample using the procedure described in Section 6.6.3.a.
2) Transfer the sample to a volumetric flask.
3) Dilute the samples and add ionization suppressants to achieve the final solution concentrations listed:

Analyte Suspected to be Present	Final Concentration
Al (pyro powders), Ca, Mg, Y	4% HNO_3/1000 µg/mL Potassium ion
Mo (insoluble)	4% HNO_3/1000 µg/mL Aluminum ion

AP 4: Au, Pt (metal), Sn, or Tin Oxide (SnO)

1) For Au, Sn, or SnO, add 9 mL HCl to each beaker, swirl, and then add 2 mL HNO_3. CAUTION: Make sure the entire filter or sample is wetted with HCl and allow the filter/HCl solution to sit for a period of at least 2 to 3 min before adding the HNO_3.
2) Digest the sample on a hot plate until nearly dry.
3) Allow the samples to cool and then quantitatively transfer the sample, using a small amount of DI H_2O to rinse the beaker, to a clean volumetric flask. Dilute to volume, making the final solution 10% HCl. For example, add 2.5 mL concd HCl to a sample if the total solution volume is 25 mL.
4) Results for either Sn or SnO are reported as total Sn.

Table 4
Alternate Procedures

AP 5: Cr [Samples which potentially contain Cr(VI)]

For samples requiring analysis of total Cr, the following procedure should be used. This procedure avoids the loss of any Cr(VI) as chromyl chloride(CrO_2Cl_2). For chromate or chromic acid analysis, see OSHA Method ID-215.

1) Digest the samples collected on MCE filters with HNO_3 and then allow to cool to room temperature. If PVC filters were used, digest with HNO_3 plus 2 mL of $HClO_4$ and then allow to cool.
2) Add 1 or 2 mL of 30% H_2O_2 to the cooled solution to reduce any Cr(VI) that may be present. Let the sample sit for several minutes.
3) Heat approximately 5 min to boil off the H_2O_2 and then allow to cool. At this stage HCl may be added if needed to dissolve other metals.
4) Dilute to volume with DI H_2O and analyze.

NOTE: Do not add $HClO_4$ to the sample solution if a large amount of HCl is already present [any Cr(VI) in the sample would be lost as CrO_2Cl_2]. Add concd HNO_3, boil off the HCl, and then add the $HClO_4$.

AP 6: Elements or Compounds* which are Insoluble in Nitric Acid Digestions

1) For compounds such as zirconium dioxide or hafnium dioxide, place the sample filter in a platinum crucible, char at 300 ˚C, then heat the residue at 800 ˚C in a muffle furnace. [As an alternative, the digestion can be performed using a microwave digestion system (8.11).]
2) Add 1 to 2 mL of HF, swirl the solution, and then heat on a hot plate to dissolve the residue.
3) Evaporate the solution to approximately 0.4 mL and then transfer to a 10-mL polyethylene volumetric flask. Dilute to volume with a solution of 0.1 M ammonium fluoride in 4% HNO_3.

Another procedure can be used for elements which do not need to be converted to their fluoride salts:

1) Heat the HF solution on the hot plate until the liquid is nearly gone.
2) Add 2 to 3 mL HCl, and warm the solution until about 1 mL remains.
3) Quantitatively transfer the solution to a 10 mL volumetric flask and dilute to volume with the appropriate diluents mentioned in Table 5.
4) It is recommended to prepare quality control samples of the substance of concern. Digest the samples and analyze by the same procedure to check the recovery efficiency.

For platinum:

1) Place the sample filter in a Teflon microwave digestion vessel and add 5 mL of the "acid mixture (HCl/HNO_3) for platinum digestions" prepared in Section 6.3.4, part f).
2) Digest the sample according to Microwave Digestion Standard Operating Procedure (8.11) or manufacturer guidelines.
3) Allow the sample to cool and then transfer to a 25-mL volumetric flask. Dilute to volume with DI H_2O.

*Some Zr compounds, such as the oxide and sulfate, may be insoluble when using the HNO_3 digestion (8.6, 8.7). Hafnium dioxide may also be insoluble.

AP 7: CsOH, KOH, LiH, and Na Compounds

1) Place the sample filter in a beaker and desorb with 15 mL of DI H_2O for approximately 5 min.
2) Decant the sample solution into a 25-mL volumetric flask and add any reagents to achieve the final solution concentrations:

Analyte Suspected to be Present	Final Concentration
CsOH	DI H_2O/1000 µg/mL potassium ion
LiH, Na cmpds	DI H_2O
KOH	DI H_2O/1000 µg/mL sodium ion

For example, add 5 mL of 5,000 µg/mL potassium ion for Cs analysis and dilute to volume with DI H_2O. Add 5 mL of 5,000 µg/mL sodium ion for KOH analysis.

3) Analyze by flame emission or atomic absorption.

AP 8: Titanium Dioxide

1) Digest the filter with 1 mL HNO_3 and 2 mL H_2SO_4 in a conical beaker and heat until about 1 mL remains.
2) Quantitatively transfer the solution to a 25-mL volumetric flask, add 5 mL of 5,000 µg/mL potassium ion, then dilute to volume with DI H_2O.

Table 5
Digestion or Extraction Reagents

Substance	Reagents Used	Final Volume Concentration+
Ag	HNO_3/HCl	4% HNO_3/16% HCl
Al (soluble cmpds)	DI H_2O	4% HNO_3/1000 µg/mL K^+
Al (pyro powders)	HNO_3	4% HNO_3/1000 µg/mL K^+
Au	HCl/HNO_3	10% HCl
Ba (soluble cmpds)	DI H_2O	4% HNO_3/1000 µg/mL K^+
Bi_2Te_3	HNO_3	4% HNO_3
Ca & cmpds	HNO_3/HCl*	4% HNO_3/1000 µg/mL K^+
Cd	HNO_3	4% HNO_3
Co & cmpds	HNO_3/HCl*	4% HNO_3
Cr(III or III) soluble cmpds	DI H_2O	4% HNO_3
Cr metal	HNO_3/H_2O_2/HCl	4% HNO_3
CsOH	DI H_2O	DI H_2O/1000 µg/mL K^+
Cu	HNO_3	4% HNO_3
Fe & cmpds	HNO_3/HCl*	4% HNO_3
Fe (soluble salts)	DI H_2O	4% HNO_3
Hf	HF	4% HF/4% HNO_3/0.1 M NH_4F
In & cmpds	HNO_3	4% HNO_3
KOH	DI H_2O	4% HNO_3/1000 µg/mL Na^+
LiH	DI H_2O	DI H_2O
MgO	HNO_3/HCl*	4% HNO_3/1000 µg/mL K^+
Mn & cmpds	HNO_3/HCl*	4% HNO_3
Mo (soluble cmpds)	DI H_2O	4% HNO_3/1000 µg/mL Al
Mo (insoluble cmpds)	HNO_3	4% HNO_3/1000 µg/mL Al
Na & cmpds	DI H_2O	DI H_2O
Ni metal & insoluble cmpds	HNO_3/HCl*	4% HNO_3
Ni (soluble cmpds)	DI H_2O	4% HNO_3
Pb	HNO_3/HCl	4% HNO_3/16% HCl
Pt metal	HCl/HNO_3	4% HNO_3/16% HCl
Sb & cmpds	HNO_3/HCl	4% HNO_3/32% HCl
Se & cmpds	HNO_3/HCl	4% HNO_3/4% HCl
Sn (and SnO)	HCl/HNO_3	10% HCl
Te & cmpds	HNO_3/HCl	4% HNO_3/4% HCl
TiO_2	HNO_3/H_2SO_4	4% H_2SO_4/1000 µg/mL K^+
Tl (soluble cmpds)	DI H_2O	4% HNO_3
Y	HNO_3	4% HNO_3/1000 µg/mL K^+
$ZnCl_2$	DI H_2O	4% HNO_3
Zn & cmpds	HNO_3	4% HNO_3
Zr & cmpds	HF	4% HF/4% HNO_3/0.1 M NH_4F

+ Standards should be prepared in this matrix.
* After completing the digestion with HNO_3, add 1 or 2 drops of concd HCl to facilitate particulate dissolution.

Table 6
Gravimetric Factors

Element	Compound	Gravimetric Factor
Bi	Bismuth telluride (Bi_2Te_3)	1.916
Ca	Calcium cyanamide ($CaCN_2$)	1.998
Ca	Calcium hydroxide [$Ca(OH)_2$]	1.849
Ca	Calcium oxide (CaO)	1.399
Cr	Chromic acid (CrO_3)	1.923
Cs	Cesium hydroxide (CsOH)	1.128
Fe	Dicyclopentadienyl iron [$(C_5H_5)_2Fe$]	3.331
Fe	Iron oxide (Fe_2O_3)	1.430
Li	Lithium hydride (LiH)	1.145
Mg	Magnesium oxide (MgO)	1.658
Na	Sodium bisulfite ($NaHSO_3$)	4.525
Na	Sodium fluoroacetate (FCH_2COONa)	4.351
Na	Sodium hydroxide (NaOH)	1.740
Na	Sodium metabisulfite ($Na_2S_2O_5$)	4.134
Na	Tetrasodium pyrophosphate ($Na_4P_2O_7$)	2.891

Element	Compound	Gravimetric Factor
Ti	Titanium oxide (TiO_2)	1.668
Zn	Zinc chloride ($ZnCl_2$)	2.085
Zn	Zinc oxide (ZnO)	1.245
Zn	Zinc stearate [$Zn(C_{18}H_{35}O_2)_2$]	9.671

Table 7
Analytical Parameters

Element	λ (nm)	Slit (nm)	Optimization*	Flame Used	Comments
Ag	328.1	0.7	4 µg/mL=0.3 ABS	1	For multielement lamps containing Cu, use 0.2 nm slit
Al	309.3	0.7	50 µg/mL=0.22 ABS	3	
Au	242.8	0.7	15 µg/mL=0.26 ABS	1	
Ba	553.6	0.4	15 µg/mL=0.16 ABS	3	
Bi	223.1	0.2	20 µg/mL=0.18 ABS	1	
Ca**	442.7	0.7	4 µg/mL=0.22 ABS	4	
Cd**	228.8	0.7	2 µg/mL=0.35 ABS	1	
Co	240.7	0.2	5 µg/mL=0.015 ABS	2	
Cr**	357.9	0.7	2 µg/mL=0.05 ABS	3	
Cs	852.1	1.4	10 µg/mL=0.22 ABS	1	
Cu**	324.7	0.7	5 µg/mL=0.25 ABS	1	For multielement lamps containing Ni or Fe, use 0.2 nm slit
Fe**	248.3	0.2	5 µg/mL=0.18 ABS	2	In the presence of Co, do not use a multielement lamp containing Co at 248.3 nm. Use 248.8 or 72.0 nm
	248.8	0.2	5 µg/mL=0.11 ABS	2	
Hf	286.6	0.2	300 µg/mL=0.2 ABS	3	
In	303.9	0.7	25 µg/mL=0.15 ABS	1	
K	766.5	1.4	2 µg/mL=0.3 ABS	1	
Li	670.8	1.4	1 µg/mL=0.13 ABS	1	
Mg**	285.2	0.7	0.3 µg/mL=0.19 ABS	3	
Mn**	279.5	0.2	2 µg/mL=0.16 ABS	1	
Mo**	313.5	0.7	2 µg/mL=0.20 ABS	3	
Na	589.6	0.4	0.8 µg/mL=0.2 ABS	1	
Ni**	232.0	0.2	5 µg/mL=0.15 ABS	1	For multielement lamps containing Fe, use the secondary Ni line, 352.4 nm
Pb	283.3	0.7	20 µg/mL=0.18 ABS	1	
Pt	265.9	0.7	100 µg/mL=0.033 ABS	3	
Sb	217.6	0.2	20 µg/mL=0.18 ABS	1	For determination in the presence of Pb, use the 231.2 nm line
	231.2	0.7	20 µg/mL=0.07 ABS	1	
Se	196.0	2.0	20 µg/mL=0.18 ABS	5	Use an EDL
Sn	224.6	0.7	50 µg/mL=0.28 ABS	5	
Te	214.3	0.2	25 µg/mL=0.11 ABS	1	
Ti	365.3	0.2	120 µg/mL=0.3 ABS	3	
Tl	276.8	0.7	20 µg/mL=0.18 ABS	1	
Y	410.2	0.2	100 µg/mL=0.24 ABS	3	
Zn**	213.9	0.7	0.5 µg/mL=0.12 ABS	1	In the presence of Cu, do not use a multielement lamp containing Cu
Zr	360.1	0.2	400 µg/mL=0.17 ABS	3	

* Adapted from reference 8.6 or from laboratory determinations

** Due to the limited upper linear range, samples may have to be diluted, the burner head rotated, or an alternate wavelength used. The burner head is routinely rotated for Fe and Mg before analysis.

Flame Types:
1 Air/Acetylene mixture, lean, blue flame
2 Air/Acetylene mixture, very lean, blue flame
3 Nitrous oxide/Acetylene mixture, rich, red flame
4 Nitrous oxide/Acetylene mixture, slightly rich, red flame
5 Air/Hydrogen mixture

Appendix A
Terminology

For the purposes of this method, the following definitions are used:

Qualitative detection limit

The concentration (µg/mL) of an element which would yield an absorbance (ABS) equal to twice the standard deviation of a series of measurements of an aqueous solution containing the element. The signal obtained from the aqueous solution must be distinctly greater than the baseline (8.10). These detection limits were taken from reference 8.5.

Analytical detection limit

The lowest concentration (µg/mL) of an element that can be reliably quantitated. This limit is the largest value obtained from any of the three calculations:

a) Three times the smallest possible non-zero instrument reading,

b) Two times the average baseline variation, or

c) The lowest standard used to construct a concentration-response curve. One-tenth the concentration of this standard is considered to be the detection limit if:

   The average reading for this standard is within 20% of it's linear response. The linearity is determined by the other standards used to construct the least-squares curve fit.

   If the lowest standard ABS reading is more than 20% in error, then an algorithm is used and the concentration value is increased in 10% increments until a concentration is achieved that would display less than 20% error or until the lowest standard concentration is reached.

Sensitivity

The concentration (µg/mL) of an element in aqueous solution which will produce an ABS of 0.0044 (8.6).

Linear Range

The working range of a specific analyte. The range is considered linear if doubling the concentration of a standard results in at least a 75% increase in ABS.

Appendix B
Potential Interferences

Ag If a multielement lamp containing Cu is used, a spectral interference may occur when determining Ag in a sample containing Cu. A narrow slit should be used in this instance (8.6).

Thorium (Th) is a reported chemical interference (8.14); however, this element is extremely rare in workplace environments. Analyze the sample for Th first if both are suspected to be present.

Al Acetic acid, fluoroborate, Fe, and Ti enhance the Al signal. Ionization should be controlled by adding an alkali salt (potassium or lanthanum) to samples and standards.

Au Spectral interferences from Fe have been observed. Palladium, platinum, and cyanide complexes are reported interferences (8.6).

Ba This element is partially ionized in the N_2O/C_2H_2 flame. To control this interference, the samples and standards should contain 1,000 µg/mL potassium ion (8.6).

When analyzing using the primary Ba line (553.6 nm), background correction should be used if a large amount of Ca is present. The Ca can cause molecular absorption at this line.

Ca Sulfate, aluminate, phosphate, and silicate decrease sensitivity (8.14). Silicon (Si), Ti, Al, and Zr have also been reported as interferences (8.6). Using a N_2O/C_2H_2 flame will control these interferences; however, samples and standards should contain 1,000 µg/mL potassium ion to control any ionization.

Acetone from acetylene tanks has been reported to decrease sensitivity. Tanks should be changed when the pressure drops below 75 to 85 psig to prevent acetone from entering the flame (8.9).

Cd A possible interference is Si; however, Si is not significantly soluble using the mentioned digestion procedures.

Co A reported interference is Ni in concentrations greater than 1,500 µg/mL (8.10). Such levels of Ni are unusual in industrial environments. If a large amount is expected, samples should be analyzed for Ni first and then analyzed using an alternate Co line if Ni concentrations exceed 1,500 µg/mL.

Cr Co, Fe, Ni, Cu, Ba, Al, Mg, Ca, Na, and other metals have been reported as chemical interferences (8.6, 8.9, 8.10). Determining Cr in a lean flame will control these interferences, but with a decrease in sensitivity (8.9, 8.10). The instrument should be optimized using a mixed standard containing Fe and Ni in addition to the Cr when using the Air/C_2H_2 flame. The above interferences are not noticed when a N_2O/C_2H_2 flame is used.

Cs Solutions should contain 1,000 µg/mL potassium ion to control ionization.

Strong acids may suppress the signal; therefore, samples and standards should be matrix-matched.

Cu Spectral interferences may occur when Ni or Fe is contained in the multielement lamp and in the sample solution. Use a single element Cu lamp or a narrow slit to circumvent this problem.

A large amount of Zn in the sample may interfere but can be controlled by using a lean flame (8.10).

Fe A spectral interference may be observed if the multielement lamp and the sample solution contain Co. An alternate line for Fe should be used (8.6).

Citric acid, Ni, and HNO_3 may interfere but can be controlled by using a lean flame and by carefully optimizing burner height (8.6, 8.10). Silica may also interfere (8.14), but is not appreciably soluble in the acid digestion procedures mentioned.

Hf The presence of fluoride greatly enhances the sensitivity in the determination of Hf. Samples and standards should contain 0.1 M NH_4F to control this effect and to obtain the best sensitivity (8.6).

In A 100-fold or greater excess of Al, Mg, Cu, Zn, or phosphate will suppress the signal.

Mg Al, H_2SO_4, HNO_3, Si, Ti, and HF are reported to interfere. Addition of a suppressant (lanthanum or potassium) will control these interferences (8.6, 8.14). Interferences can also be controlled using a N_2O/C_2H_2 flame.

Mn Phosphate, perchlorate, Fe, Ni, and Co may interfere but can be controlled by using a lean flame (8.10). Tungsten (W), Mo, and Si have been reported to interfere when the pressure in the acetylene tanks is low (8.14).

Mo Many interferences have been reported for Mo including Fe, Mn, Ni, Cr, Si, and strontium (Sr). Addition of Al controls these interferences (8.9, 8.10, 8.14).

Na Ionization in the flame can occur; an ionization suppressant should be added to the standards and samples (8.6).

Ni A spectral interference from Fe will result when determining Ni in a sample containing Fe with a multielement lamp containing Fe. An alternate line should be used.

Cr, Co, and Fe (8.9), or HCl and $HClO_4$ in the presence of these metals (8.10) have been reported as interferences. They are controlled by using a lean Air/C_2H_2 flame (8.10, 8.14).

Pb Al, Be, Th, and Zr in a 1,000-fold molar excess over the Pb concentration decrease sensitivity (8.14). The digestion procedure used for Pb does not solubilize a significant amount of Al, Be, or Zr for them to be a problem in the analysis. Workplace environments rarely contain significant amounts of Th along with Pb; however, if suspected to be present, the sample should also be analyzed for Th since it is very toxic.

Phosphate, carbonate, iodide, fluoride, and acetate at a 10-fold excess may also interfere (8.10). Sulfate and Ca in excess have also been reported as interferences (8.7).

Pt A number of elements interfere with the determination when using an Air/C_2H_2 flame (8.6). These interferences are minimized when using a N_2O/C_2H_2 flame.

Sb A spectral interference occurs when Sb is determined at 217.6 nm in the presence of large amounts of Pb, which has an adjacent line at 217.0 nm. It has been reported that large concentrations of Cu also absorb at 217.6 nm. In either situation, the alternate 231.2 nm line for Sb should be used (8.6, 8.7)

Cu and Ni have been reported to suppress Sb sensitivity, but can be controlled by using a lean flame (8.9, 8.10).

Se Background absorption is severe at the wavelengths used to determine Se. Background correction should be used (8.6).

Large amounts of Ni, Co, Fe, Cu, Mn, Pb, and other metals, if present in the sample may form selenides in the flame, decreasing sensitivity (8.9).

Increased sensitivity is noted when using an Air/H_2 flame as compared to an Air/C_2H_2 flame. For greatly enhanced sensitivity, analyze Se by graphite furnace atomic absorption using a modified matrix containing Ni (8.15).

Sn Alkali metals and alkaline earths, Cu, Co, Zn, Al, Ti, phosphoric acid (H_3PO_4), and H_2SO_4 have been reported as interferences when Air/H_2 flames are used. Interferences are reduced or eliminated in hotter flames, but sensitivity is greatly reduced (8.6, 8.10).

Te A spectral interference may occur when Cu is contained in the multielement lamp and in the sample (8.14).

Enhanced sensitivity can be obtained for this element using graphite furnace atomic absorption analysis of sample solutions modified to contain a Ni matrix (8.15).

Ti Samples and standards should contain 1,000 µg/mL potassium ion to control ionization.

The Ti signal is enhanced by many other metals (8.6).

Y Samples and standards should contain 1,000 µg/mL potassium ion to control ionization.

Strong acids may suppress the signal; therefore, samples and standards should be matrix-matched.

Zn A spectral interference may occur if the multielement lamp and the sample contain Cu (8.14).

Zr Fluoride, chloride, and ammonium enhance Zr sensitivity. Sulfate, nitrate, and nickel bromide decrease sensitivity. Addition of NH_4F will control these interferences (8.6).